DANISH SOCIETY OF HYDRAULIC ENGINEERING

SEMINAR

ISLAST PÅ OFFSHORE VINDMØLLER OG ANDRE OFFSHORE KONSTRUKTIONER

Torsdag den 31 marts 2005

På ENERGI E2

DANSK VANDBYGNINGSTEKNISK SELSKAB

DANISH SOCIETY OF HYDRAULIC ENGINEERING

v/ Helge Gravesen, Carl Bro as, Granskoven 8, 2600 GlostrupTlf. +45 4348 6328, Fax +45 4363 6567, email: hlg@carlbro.dk + hgx@e2.dk

Seminar om islast på offshore vindmøller og andre offshore konstruktioner

(se www.dansk-vandbygning.dk)

Sted: Energi E2, Teglholmen, A.C.Meyers Vænge 9, 2450 København SV, Auditoriet.

Tidspunkt: Torsdag den 31 marts 2005. Kl. 13:00-17:30

Program

13:00: Velkomst

13:10 – 14:30 Helge Gravesen (Carl Bro/DTU): Grundlæggende gennemgang af islaster (Basic on design ice forces)

14:30 – 15:00 Helge Gravesen (Carl Bro/DTU): Ismodelforsøg med havmøllefundamenter (Ice model tests with offshore wind turbine foundations)

15:00 – 15:20 Kaffepause

15:20 – 16:10 Bjarke Petersen (LicEngineering) Laster fra isrygge (loads from ice ridges)

16:10 – 17.30 Toumo Kärna: Status of ice standards and state of the art on design ice loads. (Toumo Kärna from VTT Finland is a leading ice expert, chairman of the working committee for new offshore ice load standard)

Seminaret repræsenterer en ny type seminar, hvor der indledes med en mere grundlæggende undervisningspræget del og fortsættes med nyere viden.

Praktiske bemærkninger:

Pris for deltagelse: 300 kr . Betaling sker til giro 8 24 46 69 eller ved indsendelse af check til nedenstående adresse.

Tilmelding skal ske snarest og senest fredag d. 18 marts, 2005 ved indsendelse af nedenstående blanket til: c/o Kystdirektoratet

Højbovej 17620 Lemvig

Att. Per Sørensen Tlf.: 99 63 63 63 Fax.: 99 63 63 99 Email: PSo@kyst.dk

Seminar : Islaster

Energi E2, Teglholmen torsdag d. 31/3 kl 13-17.30

Nr	Fornavn	Efternavn	Company	Speaker	Email
1	Hans-Jørgen	Riber	DNV Global Wind Energy		Hans.Joergen.Riber@dnv.com
2	Kristian Bendix	Nielsen	DNV Global Wind Energy		Kristian.Bendix.Nielsen@dnv.co
2	Tuomo	Kärnä	VTT Bulilding and Transport	Yes	
3	Henrik Lund	Rasmussen	Per Aarsleff		hlr@aarsleff.com
4	Gerner Juhl	Petersen	COWI A/S		gjp@cowi.dk
5	Andreas G	Jensen	DNV - Global Wind Energy		Andreas.Gregersen.Jensen@dr
6	Andreas	Roulund	Niras		aro@niras.dk
7	Jørgen	Lisby	Per Aarsleff		
8	Søren Viborg	Kristensen	Per Aarsleff		
9	Stig Balduin	Andersen	COWI A/S		sia@cowi.dk
10	Lotte Meldgaard	Pedersen	COWI A/S		lmp@cowi.dk
11	Dorte	Gadebjerg	COWI A/S		
12	Tommy	Carlsen	COWI A/S		
13	Torben	Søndergaard	Det Norske Veritas		Torben.Soendergaard@dnv.con
14	Helge	Gravesen	Carl Bro	Yes	
15	Niles Kjær	Lauritsen	Vestas		nkl@vestas.com
16	Hanne	Grindsted	Moe og Brødsgaard A/S		hgr@moe.dk
17	Stephan	Østergaard	LICEngineering		
18	Bjarke	Petersen	LICEngineering	Yes	
19	Christian	LeBlanc Bakmar	Energi E2		
20	Søren Thorbjørn	Larsen	Energi E2		
21	Klaus	Mortensen	Energi E2		
22	Per	Vølund	Energi E2		

LIST OF CONTENTS

DETERMINATION OF EXTREME ICE FORCES
LECTURE NOTES

by Flemming Thunbo Christensen and Helge Gravesen

2003

27.02.03

LIST OF CONTENTS

1. INTRODUCTION

This note describes ways to determine extreme ice forces on offshore structures. The aim is to guide engineers in desk studies of ice forces on structures. The note has been logically structured in the following parts:

- Ice properties
- Driving forces
- Interaction formulas
- Selection of design forces
- Codes and standards
- Relevant literature

The present material was originally prepared for a short-course at University of Salford, England in 1989 by Flemming Thunbo Christensen. They have later been extended with certain sections translated from Per Tryde's danish lecture notes plus some supplementary sections by Helge Gravesen. It is only natural that there are many interesting aspects within ice -structure interaction, which are not covered, or only superficially covered, herein. Among subjects which are not covered are local ice pressures, multi-legged structures, ride-up and pile-up phenomena, rafting, rubble fields, remote sensing, sea ice dynamics simulation, fracture toughness of ice, friction between ice and various materials, icebreaking ships, physical and computational modelling of ice structure interaction, etc. It is the authors hope, however, that these notes will aid readers in acquiring a first insight into the problems associated with the determination of design ice loads on offshore structures.

2. ICE PROPERTIES

2.1 Crystal Structure

Ice is a polycrystaline material. The crystal lattice is formed by the oxygen atoms joined by hydrogen bonds. In the basic lattice, each oxygen is surrounded by four other oxygens to form an almost perfect tetrahedron with one hydrogen (really only a proton) between each set of oxygens. The molecules are organized in a near hexagonal pattern with an axis of symmetry called the c-axis or the optic plane. The plane perpendicular to the c-axis is called the basal plane. The lattice is illustrated in Figure 2.1.1. It is clear from the illustration that the pure (mono) crystal of ice is anisotropic with respect to most physical and mechanical parameters.

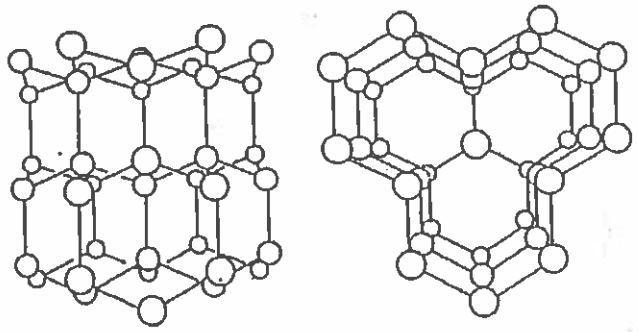

Figure 2.1.1 Crystal lattice of ice: a) View perpendicular to c-axis, b) View parallel to c-axis

The basic crystal lattice is the same for all types of ice normally encountered by offshore structures. But the macroscopic structure of ice varies significantly with its growth history. Most ice types contain pockets of air, and sea ice also contains pockets of entrapped high salinity water called brine. The brine content is the major reason for the pronounced differences between fresh water ice and sea ice.

Typical sizes of grains in ice range from 2 mm to 50 mm, but crystals in excess of one metre have been observed. If an ice cover has reasonably uniform crystal sizes throughout the cover and a random orientation of the individual c-axes, it is referred to as isotropic. It is important to note that this term can be justified only on a macroscopic scale. Under freezing conditions, the basic crystal lattice will grow faster in the directions of the basal plane than in the direction of the c-axis. This preferred growth results in a selective mechanism favouring crystals with their c-axis in the horizontal plane because they grow faster in the vertical direction than other crystals.

Ice formed in still water has often been found to have all horizontal c-axes of the grains more than a few centimeters below the surface, although this is far from always the case.

In sea ice the transition (with depth) to all horizontal c-axes is often very distinct but located slightly deeper, typically 10-20 cm below the surface. The preferred vertical growth results in vertically elongated crystals, and the ice is consequently referred to as columnar. Impurities, typically air and salt, are trapped at the grain boundaries as well as in the middle of grains while the crystals grow, and the columnar appearance of the polycrystalline material is thereby enhanced. Note that salt is also entrapped within each crystal. (The two terms "grain" and "crystal" are synonomous).

Because of the columnar structure, sea ice is normally anisotropic on the macroscopic scale also. Since the c-axis distribution within the horizontal plane is almost always random, the material is transversely isotropic, though.

In the remainder of these notes, all properties are related to the horizontal plane in the ice. Compressive strength" is to be understood as "compressive strength in the horizontal direction" unless something else is specifically stated. This simplifies the analyses considerably. Imagine for example the complexity arising from using six different moduli for just a monocrystal instead of using simply one Young's modulus.

Because of the temperature variation with depth and because of the strong temperature dependence of most of the mechanical properties of ice, floating ice covers are normally inhomogeneous, especially with respect to the vertical direction.

In many calculations, sea ice is still considered a homogeneous and isotropic material. For the purpose of load calculation, cf. section 4, these assumptions are adopted here.

2.2 Ice Growth

The growth of ice in nature is affected by a multitude of factors, and so an ice thickness calculated entirely on the basis of theoretical considerations cannot be used for design purposes. It is mandatory to compare with measurements from the area of concern. If such measurements do not exist, they must be carried out.

Ice Growth in Fresh and Saline Water

Take a column of a lake consisting of *fresh water* at a temperature of +10° C. As fall moves on, the surface water is cooled, drops down, and leaves warmer water exposed to the colder atmosphere. The water is mixed and maintains an (ideally) uniform temperature profile. This continues until the lake is at +4° C, where fresh water has its maximum of density. When cooling is continued, the colder water becomes lighter than the warmer water and forms a top layer, which eventually begins to freeze into an ice cover.

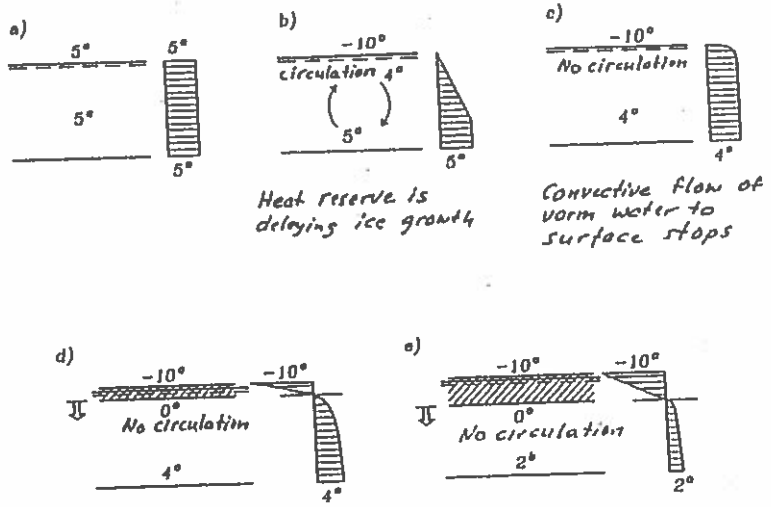

Figure 2.2.1 Ice growth in a fresh water lake. Temperatures in °C

In the *seas* with a salinity S > 24.7‰, this scenario is quite different because the temperature at which sea water has its maximum density is lower than the freezing point. This means that the mixing process will continue until the entire water column has reached the freezing point. The oceans, however, have too much heat stored in them for the atmosphere to remove it all in one winter. This is the reason why the oceans do not freeze over in winter, except of course the polar ocean.

The difference between lakes and seas is the content of dissolved salts in the sea. The oceans contain roughly 35 per thousand or 3.5 per cent salt. The freezing point of water (at atmospheric pressure) as a function of salinity is:

$$\theta_f = 0°C - 1.3°C \; S/(24.7‰) \qquad (2.2.1)$$

where S is inserted in per thousand corresponding to the constant in the denominator. The temperature at which the density maximum occurs is:

$$\theta_{md} = 4°C - 5.3°C \; S/(24.7‰) \qquad (2.2.2)$$

Note that the two expressions coincide at θ = -1.3° C and S = 24.7 ‰. Seas with a salinity above 25 ‰ will thus continue mixing all the way to the freezing point.

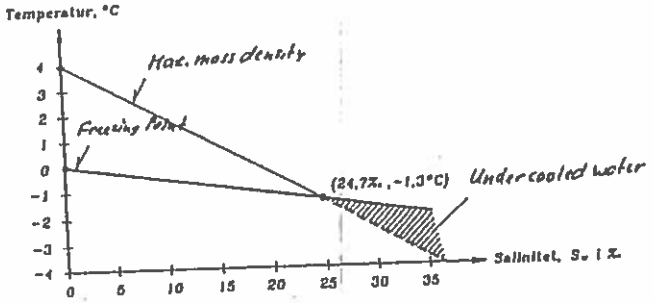

Figure 2.2.2 Maximum Mass Density and Freezing Temperature for Water

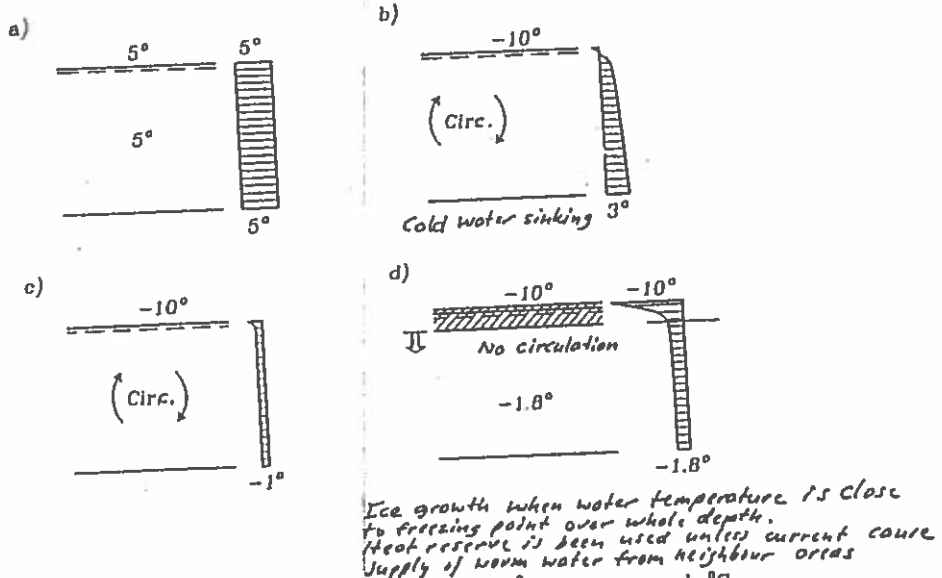

Figure 2.2.3 Ice growth in Seas with Salinity S > 24.7‰. Temperatures in °C

Formula for Ice Thickness Development

One of the simplest and most common formulae forcalculating ice thicknesses can be derived directly from the linear differential equation of heat conduction by using constant values of the thermal properties of the ice and of the sea temperature. The formula becomes:

$$h = K^{1/2} \cdot 0.032 \text{ m/(°C-days)}^{1/2} \qquad (2.2.3)$$

where K is the accumulated freezing degree-days and h the thickness. Ideally, K represents the integral of the air temperature with time, but in most practical situations each day is assigned a mean temperature, and K is increased by this amount:

$$K = \sum_{days} |\theta_{mean}\,(day)| \text{ , } \theta_{mean} > 0 \text{ not counted} \qquad (2.2.4)$$

Experienced K values are presented in Annex A1.

Note that positive temperatures are not added. If a layer of snow is present, ice growth is slowed substantially because of the insulating effect. This would change the constant 0.032 in eq. (2.2.3), which is likely to overpredict actual ice hicknesses.

In fact, a coefficient of 0.024 m/(°C-day)$^{1/2}$ is used by the U.S. Army Corps of Engineers for some inland waterways in the USA.

The thermal properties applied in order to arrive at eq. (2.2.3) were:
Latent heat of freezing of ice: $L_i = 334 \cdot 10^3$ J/kg
thermal conductivity of ice: $k_i = 2.24$ W/(m °C)
density of ice: $\rho_i = 920$ kg/m^3

These values of course change as a function of temperature and salinity. The listed values apply to near 0°C and very low salinity conditions. The purpose of showing eq. (2.2.3) is to give the reader a feel for the order of magnitudes of ice thicknesses. A scientific calculation would also account for solar radiation, reflection, wind and currents etc.

Formula (2.2.3) may be developed as described below:

A unit of 1 m^2 ice is considered:

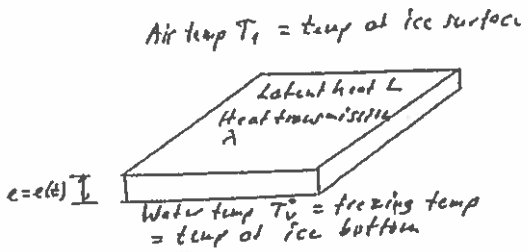

Fig.2.2.4 1 m^2 floe

Heat transmitted through ice:

$$dq = \lambda \frac{\Delta T}{h} dt \ (W/m^2) \qquad (2.2.5)$$

This is equal to the released heat from freezing:

$$L \rho \, de \ (W/m^2) \qquad (2.2.6)$$

This results in Stefan's law:

$$\lambda \frac{\Delta T}{h} dt = L \cdot \rho \, dh \qquad (2.2.7)$$

Integration over time/depth is carried out:

$$\lambda \Delta T \int_{t_0}^{t} dt = L\rho \cdot \int h \, dh$$

$$h^2 = \frac{2\lambda}{L\rho} \int_{t_0}^{t} \Delta T \, dt = \frac{2\lambda}{L\rho} \Delta T (t - t_0) = \frac{2\lambda}{L\rho} K_t$$

$$h = \sqrt{\frac{2\lambda}{L\rho}} \sqrt{K} \qquad (2.2.8)$$

The factor $\sqrt{\frac{2\lambda}{L\rho}} = \sqrt{\frac{2 \ 2.24}{334 \cdot 10^3 \cdot 920}} = 1.208 \cdot 10^{-4}$

$1.208 10^{-4} \sqrt{3600 \cdot 24} = 0.0355 \ m(^\circ C \ døgn)^{-1/2}$

$h = 0.036 \sqrt{K}$ (m) (2.2.9)

$L = 334 \cdot 10^3$ (joule/kg) = Latent heat

ρ (ice) = 920 (kg/m^3)

Coefficient $\beta = \beta$ (T gradient in air, snow depth)

$h = \beta \cdot 0.036 \sqrt{K}$

$\beta \cong 0{,}89 (0{,}5 \text{ to } 0{,}9) \Rightarrow$

$h = 0.032 \sqrt{K}$ (m) (2.2.10)

Account to periods with $T > 0^\circ \Rightarrow$

$h = 0.032. \sqrt{K - 50}$ (m)

Thermodynamic calculation of ice thickness

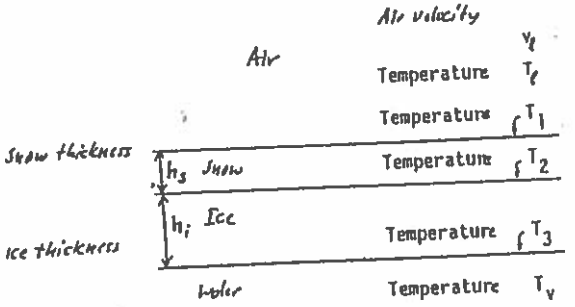

Fig. 2.2.5 System considered

Transfer from air to snow:

$q_1 = h_a (T_a - T_1)$ (2.2.11)

where h_1 = boundary layer thickness

Transfer through snow:

$q_2 = \frac{\lambda_s}{h} (T_1 - T_2)$ (2.2.12)

Transfer through ice:

$q_3 = \frac{\lambda_i}{h_i} (T_2 - T_3)$ (2.2.13)

Transfer from water to ice:

$q_4 = h_w (T_3 - T_w)$ (2.2.14)

$q = q_1 = q_2 = q_3 = q_4$

This results in:

$$T_i - T_v = q \left(\frac{1}{h_a} + \frac{h_s}{\lambda_s} + \frac{h_i}{\lambda_i} + \frac{1}{h_w} \right) \qquad (2.2.15)$$

Heat flow through the ice:

$$q = \frac{T_f - T_v}{\frac{1}{h_f} + \frac{e_s}{\lambda_s} + \frac{e_i}{\lambda_i} + \frac{1}{h_v}} \qquad (2.2.16)$$

Stefans's law:

$$q\,dt = L\rho_i\,dh_i \qquad (2.2.17)$$

This results in:

$$(T_a - T_w)\,dt = L\rho_i\left(\frac{1}{h_a} + \frac{h_s}{\lambda_s} + \frac{h_i}{\lambda_i} + \frac{1}{h_w}\right)dh_i \qquad (2.2.18)$$

Integration:

$$(T_f - T_v)\int_0^t dt = L\rho_i\left(\int_0^M \frac{1}{h}\,dh_i + \int_0^M \frac{h_s}{\lambda_s}\,dh_i + \int_0^M \frac{h_i}{\lambda_i}\,dh_i + \int_0^M \frac{1}{h_v}\,dh_i\right)$$

$$(T_f - T_v \cdot t = L\rho_i\left(\frac{h_i}{h_a} + \frac{h_s h_i}{\lambda_s} + \frac{h^2 i}{2\lambda_i} + \frac{h_i}{h_w}\right)$$

Solution:

$$\frac{L\rho_i}{2\lambda i}e^2_i + (1/h_a + h_s/\lambda_s + 1/h_w)L\rho_i h_i - \Delta T\ t = 0$$

$$T_a - T_w = \Delta T$$

$$A = \frac{L\rho_i}{2\lambda_i};\ B = (1/h_a + h_s/\lambda_s + 1/h_w)L\rho_i \qquad (2.2.19)$$

$$C = -\Delta T\ t = K$$

$$h_i = -\frac{B}{2A} + \sqrt{\frac{B^2 - 4AC}{4A^2}}$$

Examples:

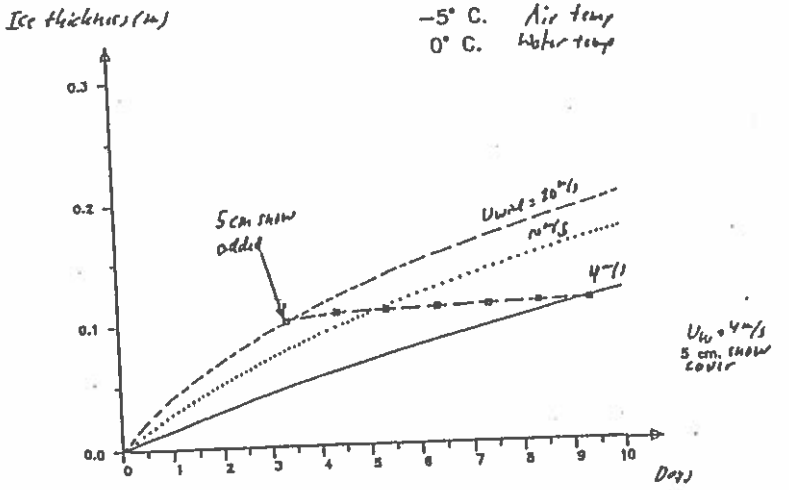

Fig. 2.2.6 Ice thickness growth for average air temperature θ = - 5° C

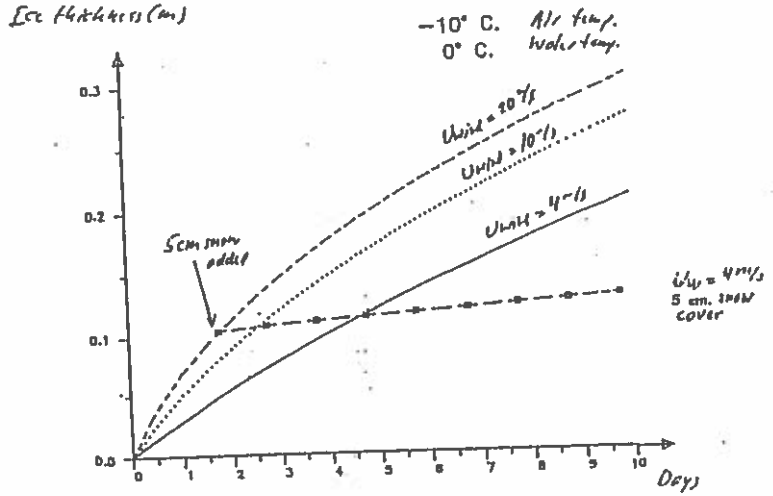

Fig. 2.2.7 Ice thickness growth for average air temperature θ = - 10° C

The processes of ice decay and melting are highly complex and outside the scope of these notes. The reader is referred to specialized literature, e.g. Ashton (1985).

2.3 Ice Salinities and Temperature

Ice from frozen sea water includes pockets with water at a high salt concentration. Immidialely after freezing the salt content is been drained out of the ice through the vertical channels in the ice. Even in case of sea water salinity 33‰ the ice salinity never exceeds 15‰ and the latter occour only in newly frozen ice. Figure 2.3.1 shows a typical example of the salinity variation of sea ice during freezing to various thicknesses, Weeks & Asssur (1967):

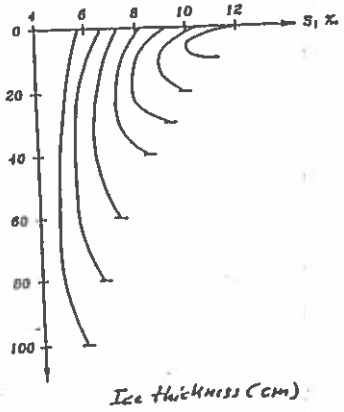

Figure 2.3.1 Series of typical salinity profiles for new sea ice

The average ice salinity (S_i) of thin first year sea ice may be calculated from:

$$S_i = 14.2 - 19.4\ h\ ‰ \quad \text{for } 0 < h < 0.5 \text{ m} \tag{2.3.1}$$

where h is entered in m

The average ice salinity (S_i) of thick first year ice and multi year sea ice may be calculated from:

$$S_i = 7.9 - 1.6\ h\ ‰ \quad \text{for } 0.5 < h < 4 \text{ m} \tag{2.3.2}$$

where h is entered in m

Above numbers corresponds to a sea water salinity of 31-34 ‰. As discussed by Kovacs (1997) the ice salinity seems to be nearly proportional to the water salinity, S_w, so above estimates may be scaled down by means of the local water salinity. Another estimate is that the final salinity at the end of the growth season may be approximted by:

$$S_i = 0.16\ (0.13 \text{ á } 0.18)\ S_w \tag{2.3.3}$$

Table 2.3.1 shows typical salinities of ice samples from inner Danish waters and the Botnic Sea :

Location	Av[illegible]	Standard deviation	Minimum	Maximu[illegible]
Inner Danish Waters	1.7 ‰	1.0 ‰	0.8 ‰	3.5 ‰
Botnic Sea	1.9 ‰	1.0 ‰	0.0 ‰	3.8 ‰

Table 2.3.1 Typical salinities of ice in Scandinavian

Table 2.3.2 show ice temperatures (average over ice thickness) of ice samples from inner Danish waters and the Botnic Sea:

Location	Average	Standard deviation	Minimum	Maximum
Inner Danish Waters	- 1.9 °C	0.8 °C	-4.1°C	-0.9 °C
Botnic Sea	-4.0 °C	1.9 °C	-10.0 °C	-1.0 °C

Table 2.3.2 Typical ice temperatures (average over ice thickness) of ice samples from inner Danish waters and the Botnic Sea

2.4 Ice Density

The density of pure ice is 916.6 kg/m^3 at 0°C and increases linearly with decreasing temperature to 920.7 kg/m^3 at -30°C, see e.g. Ashton (1986) p. 32. In most practical calculations the value 920 kg/m^3 is used. The density of natural ice is found as a weighted average of the pure ice density and the densities of impurities contained in the ice, primarily air and salt. The basic formula for sea ice density, given e.g. by Schwerdtfeger (1963), reads:

$$\rho_i = \rho_{i0}\,(1 - v_a)/(1 - (1 - 4.56/\theta_i)S_i/1000) \quad \text{for } -8\ °C < \theta_i < 0_f \tag{2.4.1}$$

ρ_{i0} = 916.6 kg/m , density of pure ice
v_a = relative volume of air bubbles in the ice (typically 0.02 for sea ice)
S_i = ice salinity in parts per thousand
θ_i = ice temperature in (negative) Celcius degrees
θ_f = freezing point (see eq. (2.2.1))

As an example, consider an ice with a relative air content of v_a = 0.02 by volume and a salinity of 3 ‰ at a mean temperature of θ_i = - 4°C. The above equation then leads to a density of ρ_i = 898 kg/m^3.

2.5 Thermal Properties of Ice

The most commonly used thermal properties of ice are the latent heat, the specific heat, and the thermal conductivity. Simple formulas for the values of these parameters are given without a thorough explanation of the physics behind the formulas. Such explanations are outside the scope of these notes.

Latent Heat

The latent heat of sea ice is determined from:

$$L_i = L_{i0}\,(1 - S_i/S_w) \qquad (2.5.1)$$

$L_{i0} = 334 \times 10^3$ J/kg, the latent heat of freshwater ice
S_i = sea ice salinity ($S_i < S_w$)
S_w = sea water salinity

This formula is repeated from Schwerdtfeger (1963).

Specific Heat

For fresh water ice the specific heat, c_{i0}, varies only little with the temperature. At –2°C it is , $c_{i0}(-2) = 2.09 \times 10^3$ J/kg°C and at –20°C the value is $c_{i0}(-20) = 1.97 \times 10^3$ J/kg°C.

Saline ice, however, shows a substantial variation in specific heat near the freezing point.

For $S_i = 2\ ^0/_{00}$ it is:

$$c_i = 1/(0.20\ \ln(-\theta_i) - 0.049) \text{ for } -12°C \le \theta_i \le -2°C \qquad (2.5.2)$$

and for $S_i = 4\ ^0/_{00}$ it is:

$$c_i = 1/(0.19\ \ln(-\theta_i) - 0.084) \text{ for } -12°C \le \theta_i \le -2°C \qquad (2.5.3)$$

where θ_i is in Celsius degrees and c_i in 10^3 Joule/kg °C.

Heat Conductivity

The thermal conductivity of sea ice is found from:

$$\lambda_i = \lambda_{i0}\,(1 - v_i) \qquad (2.5.4)$$

$\lambda_{i0} = 2.24$ W/m°C, conductivity of freshwater ice
v_i = relative brine volume of sea ice
$v_i = (0.532 - 49.185/\theta_i)\, S_i/1000$ for $-22.9°C \le \theta_i \le -0.5°$ C

The variation in conductivity with salinity and temperature is modest.

Thermal-Expansion-Coefficient

The last parameter of interest is the expansion coefficient. For practical reasons it is described in section 3.3.

2.6 Young's Modulus of Ice

Young's modulus, also called the elastic modulus, and Poisson's ratio are apparently not true material parameters. Researchers have attempted to measure them and describe their dependence on various other parameters since they are quite useful in simple calculations.

Estimates of the values of E and v should be based on general experience with ice in the field and in the laboratory. It is important to realize how difficult these parameters are to measure. The values recommended here should be seen as rough estimates only. A certain amount of conservativeness should be applied when choosing a value in a design calculation.

When deforming metals at room temperature it is customary to find the elastic modulus as a constant factor of proportionality between the applied stress and the resulting strain. With ice, things become considerably more difficult. In nature ice mostly occurs at high homologuous temperatures, i.e. close to its melting point. It behaves somewhat like metals near their melting point. It has pronounced viscoelastic properties and exhibits creep for relatively small stresses. This makes it difficult to measure the elastic modulus in a simple static test.

To overcome this problem, seismic methods can be used to measure the modulus. (They are sometimes referred to as dynamic methods or ultrasonic methods also). The advantage is obviously that creep is minimized.

Monocrystals of ice seem to be temperature independent in terms of elastic modulus (Gold, 1958). On the other hand, Young's modulus of polycrystalline ice i's clearly temperature dependent (Nadreau and Michel, 1984),and a general form like:

$$E = E_m(1 - c\cdot\theta_i) \qquad (2.6.1)$$

E = elastic modulus
E_m = elastic modulus immediately below the melting point
c = constant (unit 1/celsius degree)
θ_i = ice temperature in celcius degree (negative)

can be used to describe the relationship. Because of the pronounced creep properties, the measured elastic modulus becomes rather sensitive to the strain rate during measurement, with the highest values occurring at high strain rates (Trætteberg et al., 1975) .

The elastic modulus of saline (sea) ice is lower than that of freshwater ice. Weeks and Assur (1967) show the dynamic modulus to be dependent on both brine volume and temperature. The general form of the relationship is:

$$E = E_0(1 - c/c_0) \qquad (2.6.2)$$

E = elastic modulus

E_0 = elastic modulus of pure ice

e = porosity, i.e. sum of air and brine ($v_a + v_b$)

e_0 = reference porosity (≈ 0.2)

Pure freshwater ice typically has an elastic modulus in the order of 9 GPa (GigaPascals).

For sea ice it is recommended to use the expression:

$$E = 5.7(1 - 0.011\theta_i) \text{ GPa} \qquad (2.6.3)$$

with the inherent assumption that the ice is columnar.

For a mean ice temperature of –5°C the modulus becomes $E(-5°C) = 5.7(1 - 0.011(-5)) = 6.0$ GPa. More detailed information can be found in the literature, e.g. Lainey and Tinawi (1984). It should be remembered that both temperature, salinity, i.e. porosity, and loading rate affect the modulus. As a comparison, a typical elastic modulus for steel is in the order of 200 GPa.

It must be emphasized that sea ice is an anisotropic material essentially having six different moduli depending on which axes are considered. The values given in this section apply only to strains occurring in the direction of loading (stress).

Poisson's ratio is defined as the ratio of transverse strain (relative to loading direction) to longitudinal strain. It is often assumed to equal 0.33 and then left without attention. The anisotropy of some ice types leads to a variety of measured values. The mean value of 0.33 ,appears reasonable, but for columnar sea ice values up to 0.5 may apply, cf. Nadreau and Michel (1984). It is recommended to use the most conservative value.

2.7 Compressive Strength of Ice

The compressive strength of sea ice is dependent on a number of parameters. The most important ones are:

- ice type
- grain size and crystallographic orientation
- air content
- brine volume (i.e. salinity)
- loading rate
- confinement conditions
- temperature

In fact, all of these parameters must be known in order to make a strength value have any meaning. A scientist would like to know the value of each of these parameters. The designer, on the other hand, primarily wants to know what liability he has, as this may influence his judgement.

There is some disagreement among researchers whether the sample size has an effect or not. Sanderson (1986) shows a pronounced size effect of the effective contact pressure. On the other hand, Lee et al. (1986) and Petrie and Poplin (1986) found no size effect in their careful investigations.

In these notes, the effect of the ice type, grain size, and crystallographic orientation will not be described in any detail. Sea ice is normally of the S2 type in the classification system by Michel and Ramseier (1971). It has the columnar structure described in section 2.1. The effect of the latter five parameters in the list is described in the following.

Weeks and Assur (1967) developed a theory relating the ice strength to the brine volume in the ice. The brine volume, in turn, is dependent on the (gross) salinity of the ice and on the temperature. The colder the temperature, the smaller the brine volume and vice versa. Frankenstein and Garner (1967) developed an expression for the relative brine volume, v_b as a function of (gross) salinity and temperature:

$$v_b = (0.532 + 49.185/|\theta_i|)\, S_i/1000 \quad -22.9°C < \theta_i < -0.5°C \qquad (2.7.1)$$

where θ_i must be inserted in (negative) celcius degrees and S_i in per thousand. At a temperature of -22.9°C the NaCl salts precipitate and the relationship changes substantially. The strength of the ice was described on the form:

$$\sigma_u = \sigma_0 (1 - (v_b / v_0)^{1/2}) \qquad (2.7.2)$$

where σ_0 and v_0 are reference values of strength and relative brine volume. For first estimates $v = 0.275$ is often used. The underlying model explains the strength variations with variations in "contact area" because of the brine pockets, and by failure planes following "weak contacts" joining the pockets. A more refined model was presented by Cox and Weeks (1983) taking into account the porosity caused by air bubbles also.

Formula				2.7.2	2.8.2
Reference strength	Ice salinity	Ice temperature	Brine content	Compressive strength	Flexural strength Form.(2.8.2)
σ_0	S_i	θ_i	v_b	σ_u	σ_f
MPa	‰	°C	%	MPa	MPa
2.4	2	-2	5.0	1.4	0.38
2.4	2	-5	2.1	1.7	0.51
2.4	2	-10	1.1	1.9	0.58

Table 2.7.1 Examples of Sea ice Strength Parameters

The loading rate, whether expressed in terms of strain or stress, has a very pronounced effect on the strength of ice. For low strain rates, ice fails in ductile yield, while for high strain rates it fails in a brittle manner. The overall relationship is shown in Figure 2.7.1.
For strain rates lower than approximately 10^{-3} sec^{-1} there is a nearly linear relationship between the applied strain rate and the resulting strength. For strain rates above approximately 10^{-2} sec^{-1} there is not much variation in strength. In the intermediate range of strain rates from 10^{-3} to 10^{-2} sec^{-1} there is a peak strength. This is normally explained by the fact that cracks, which initially propagate in a brittle manner, do not penetrate the test sample but comes to a stop after which plastic deformation of a zone around the crack tip takes place. The "extra" peak stength is thus mobilized by the combined load requirements of crack initiation and plastic deformation. The maximum strength, and its corresponding strain rate, are found to be scale dependent by Sanderson (1984a). Against this stands the arguments of Lee et al. (1986) and Petrie and Poplin (1986) .

As a comparison of compressive strengths, typical values are 2-3 MPa for sea ice, 3-5 MPa for freshwater ice, 5-10 MPa for iceberg ice, 30-60 MPa for concrete, 300-600 MPa for steel and 600-1400 MPa for high strength steel.

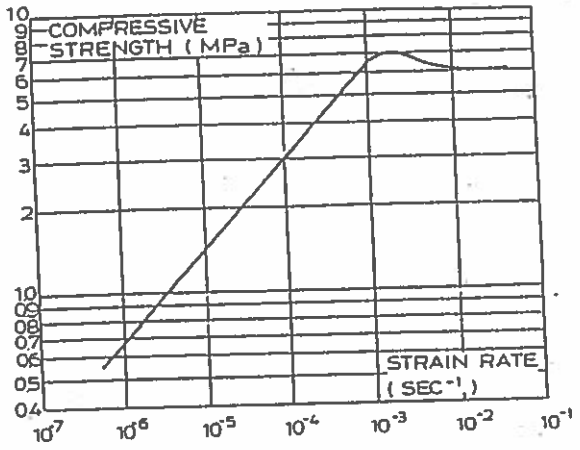

Figure 2.7.1 Examples of compressive ice strength as a function of strain rate for freshwater ice without air and salt.

One of the most recent formulas for predicting the in-plane (horizontal) unconfined compressive strength of S2 ice at low strain rates is that proposed by Timco and Frederking (1990):

$$\sigma = 37\,(\dot{\varepsilon})^{0.22}\,(1-(v_t/0.270)^{1/2}) \qquad 10^{-7} \le \dot{\varepsilon} \le 10^{-4}\ (10^{-3}*) \tag{2.7.3}$$

* not valid for brittle failue

here $\dot{\varepsilon}$ is the strain rate in sec^{-1} and v_t is the <u>total</u> relative porosity, $v_t = v_a + v_b$, i.e. the sum of the relative air volume and the relative brine volume. The strength is then in MPa (MegaPascals).

$\frac{d\varepsilon}{dt} = \frac{V}{2D}$, where V = ice velocity and D = diameter of structure.

In confined configurations, increased strength can be found for certain types of confinements. The main types of interest for S2 sea ice are:

Type A: horizontal loading with vertical confining plates

Type B: horizontal loading with horizontal confining plates

Type D: vertical loading with vertical confining plates

The confinement types are illustrated in Figure 2.7.2. The B and D types of confinement appear to have very little effect on the measured strenghts. The A type of confinement, however, can result in strength increases by as much as a factor of four.

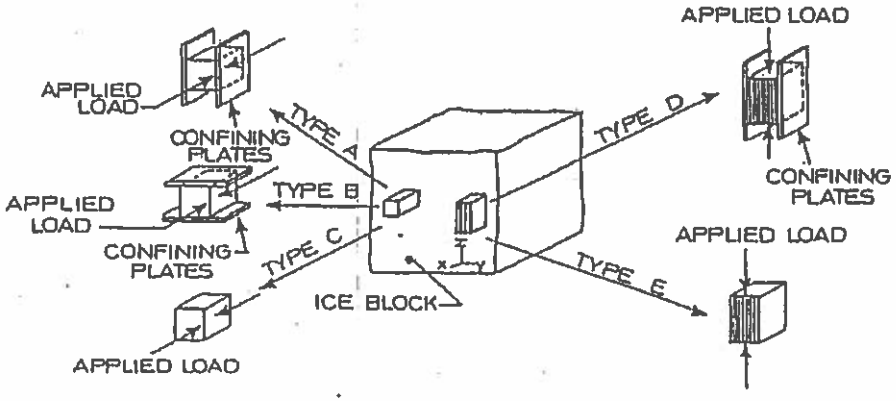

Figure 2.7.2 Types of confinement in ice strength testing.

2.8 Flexural Strength of Ice

The flexural strength of ice is most commonly determined from the breaking of beams and calculating:

$$\sigma_f = 6M/bh^2 \quad (2.8.1)$$

where M is the breaking moment, b the beam width, and h the ice beam thickness.

The underlying assumptions, elastic behaviour and a linear stress distribution, are very coarse. Simplicity has made this formula the most widely used one, though. Flexural strength is normally expressed on the same form as compressive strength. Nadreau and Michel (1984) used:

$$\sigma_f = 0.75(1-(\upsilon_b/0.202)^{1/2}) \text{ Mpa} \quad (2.8.2)$$

where υ_b is determined as described in the previous section. The data supporting this formula were measured in salinity ranges from 5 to 19 $^0/_{00}$, temperature ranges from -1.7°C to -12° C and with sample lengths ranging from 0.14 to 27 metres.

Other authors have presented different formulas:

Vaudrey (1977):

$$\sigma_f = 0.96 - 1.92(\upsilon_b)^{1/2}) \text{ Mpa} \quad (2.8.3)$$

Timco & O'Brien (1994) have based on 1000 beam tests of sea ice proposed

$$\sigma_f = 1.76 \exp(-5.88(\upsilon_b)^{1/2}) \text{ Mpa} \quad (2.8.4)$$

2.9 Adhesion Strength of Ice

Missing

2.10 Friction Coefficient

The friction coefficient is usually describe as static friction coefficient μ_s and dynamic friction coefficient μ_d. The dynamic friction coefficient has usually been considered to be a constants but newer investigations, Nakazawa et al (1993) and Frederking & Barker (2002), have shown that μ_d is strongly dependent upon the relative velocity between the structure and the ice.

The following estimate may be proposed:

$$\mu_d = 2\,\mu_{d0},\ 1 \text{ m/s} < V_i$$
$$\mu_d = \mu_{d0}\,(2 - \log V_i),\ 10^{-3} \text{ m/s} < V_i < 1 \text{ m/s} \quad (2.10.1)$$

where μ_{d0} is a constant depending upon the structure surface, see Table 2.10.1

Surface of structure	Static friction coefficient μ_s	Dynamic friction factor μ_{d0}	Dynamic friction coefficient μ_d		
Ice velocity (m/s)	0		0.01	0.1	1
Concrete	0.3	0.05	0.20	0.15	0.1
New uncoated steel	0.3	0.03	0.12	0.09	0.06
Painted steel	0.25	0.02	0.08	0.06	0.04
Corroded steel	0.45	0.05	0.20	0.15	0.1

Table 2.10.1 Friction coefficients between ice and structures

Ice to ice friction:

Missing

3. DRIVING FORCES

The driving forces, which cause movement of the ice, are wind drag, current drag, and thermal expansion forces. Each of these are briefly described in the following three sections. If these forces act simultaneously, they must obviously be added vectorially.

3.1 Wind Drag Forces

Wind over an ice surface can develop a static pressure on structures frozen into the ice cover, or impact loads in the case of moving ice sheets and floes. In large lakes, open estuaries, and oceans, wind forces are usually sufficient to cause the ice to fail against the structure, and the design ice forces are then governed by ice failure criteria. In some environments, however, the area of ice on which the wind acts may be sufficiently small that forces may be limited by the available wind drag force. Wind shear stress can be estimated from:

$$\tau_{wi} = 0.5\ \rho_a\ C_{dw}\ V_{10}^2 \qquad (3.1.1)$$

where ρ_a = density of air = 1.3 kg/m^3 at 0°C

V_{10} =Wind velocity 10 metres above the surface

C_{dw} = drag coefficient (dependent on the height at which V is determined)

The total wind drag force, F_{wi} is found from:

$$F_{wi} = \tau_{wi}\ A \qquad (3.1.2)$$

where τ_{wi} = wind shear stress

A = surface area of ice

The drag coefficient C_{dw} is a function of surface roughness. Values varying from 2.8 to 5.2 x 10^{-3} have been reported for ice sheets in the Gulf of St. Lawrence, and a mean value of 4 x 10^{-3} seems to be reasonable for calculations based on V_{10}. As a rule of thumb, it has been shown that the steady-state velocity of floating ice sheets moving under the influence of a steady wind is approximately 3% of the wind speed, when no currents are present.

3.2 Current Drag Forces

The current drag is calculated in a manner similar to that used for wind drag. The current shear stress can be estimated from:

$$\tau_{cu} = 0.5\ \rho_w\ C_{du}\ U^2 \qquad (3.2.1)$$

where
ρ_w = density of water = 1000-1020 kg/m^3

U = current velocity at a specific depth below the ice, usually 1.0 metre

C_{du} = drag coefficient (dependent on the depth at which U is determined)

The total current drag force F_{cu}, is found from:

$$F_{cu} = \tau_{cu}\ A \qquad (3.2.2)$$

where

τ_{cu} = current shear stress

A = (bottom) surface area of ice

The drag coefficient C_{du}, is a function of the undersurface roughness of the ice, which may vary substantially. A reasonable mean for calculations is C_{du} = 0.006, when U is measured 1 m below the ice. If an ice floe moves with the current, the relative velocity must be used, and this is normally very small. The above calculation of current drag is intended for a stationary ice cover, e.g. at rest against a structure.

3.3 Drifting Ice Floe

Current forces on ice floe edges

For thicker ice floes there should be added a current (drag) force determined by the thickness (h) and the width (d) of the ice floe:

$$F_d = C\ (0.9\ h)\ d\ 0.5\ \rho_w\ U^2 \qquad (3.3.1)$$

where C is a form factor varying between 0.4 to 1.2 (the low value for thin floes and the high value for thich floes on shallow water).

Hydrodynamic mass

For a circular ice floe the hydrodynamic mass is equal to:

$$M_e = M\ (1 + 1.4\ h/d) \qquad (3.3.2)$$

where h = ice floe thickness and d = ice floe diameter.

Determination of drifting velocity for ice floe in stagnant water

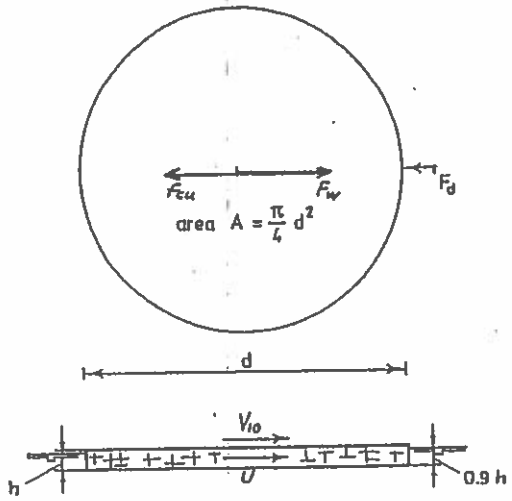

Figure 3.3.1 Driftting Ice Floe

Forces from wind:

$F_w = \tau_{wi} \pi d^2/4$

Forces from stagnant water (shear to ice area):

$F_{cu} = \tau_{cu} \pi d^2/4$

Forces to ice edges:

$F_d = C\ (0.9\ h)\ d\ 0.5\ \rho_w U^2$

Because $F_w = F_{cu} + F_d$

$0.5\ \rho_a C_{dw} V_{10}^2 \pi d^2/4 = 0.5\ \rho_w C_{du} U^2 \pi d^2/4 + C\ d\ (0.9\ h)\ 0.5\ \rho_w U^2$

$U = ((0.5\ \rho_a C_{dw} V_{10}^2 \pi d^2/4)/(0.5\ \rho_w C_{du} \pi d^2/4 + C\ d\ (0.9\ h)\ 0.5\ \rho_w))^{0.5}$ (3.3.3)

Example:

With $V_{10} = 20$ m/s, h = 0.6 m, d = 300 m, $C_{dw} = 0.004$, $C_{du} = 0.006$ and C = 0.6, $\rho_a = 1.3$ kg/m^3 and $\rho_w = 1020$ kg/m^3 :

$U = ((0.5\ 1.3\ 0.004\ 20^2\ \pi\ 300^2/4)/(0.5\ 1020\ 0.006\ \pi\ 300^2/4 + 0.6\ 300\ (0.9\ 0.6)\ 0.5\ 1020))^{0.5}$

U = 0.53 m/s = 2.6 % of wind velocity

3.4 Thermal Expansion Forces

Forces arising from thermal expansion and contraction of ice are very complicated to calculate in detail. This is mainly due to the complex mechanical properties of the ice. Two different scenarios are envisaged: Expansion of an ice sheet between two adjecent bridge piers (limited ice movement) and the expansion of a fast ice cover between a shore and,a structure.

The latter type can cause significant ice movement at the structure. An ice sheet restricted between two piers will instead of actually expanding generate a force sufficient to induce a creep rate in the ice equal to the expansion rate. The net movement rate thereby becomes zero. The following discussion.is based on studies by Bergdahl (1977), by Bergdahl and Wernersson (1978) and by Sanderson (1984b).

Salinity (o/oo)	0	2	4	6	8	10
θ_i = -2°C	1.69	-22.10	-45.89	-69.67	-93.46	-117.25
θ_i = -4°C	1.69	-4.12	-9.92	-15.73	-21.53	-27.34
θ_i = -6°C	1.69	-1.06	-3.81	-6.55	-9.30	-12.05
θ_i = -8°C	1.69	0.16	-1.37	-2.90	-4.43	-5.95
θ_i = -10°C	1.69	0.83	-0.02	-0.88	-1.73	-2.59
θ_i = -12°C	1.69	1.13	0.57	0.00	-0.57	-1.13
θ_i = -14°C	1.69	1.23	0.78	0.33	-0.13	-0.59
θ_i = -16°C	1.69	1.27	0.85	0.43	0.02	-0.40
θ_i = -18°C	1.69	1.33	0.96	0.60	0.23	-0.13
θ_i = -20°C	1.69	1.38	1.07	0.76	0.45	0.14
θ_i = -22°C	1.69	1.44	1.18	0.93	0.70	0.42

Table 3.4.1 Volumetric expansion coefficient for sea ice as a function of temperature and salinity. All values must be multiplied by 10^{-4}. A positive value indicates expansion with increasing (warmer) temperature and vice versa.

The coefficient of expansion depends strongly on both salinity and temperature. Values of the volumetric expansion coefficient,, α_v, is given in Table 3.4.1. The coefficient of linear expansion, α_l, can be found from these values as:

$\alpha_l = (1+\alpha_v)^{1/3} - 1$ (3.4.1)

or for small values and quick computations the relationship $\alpha_l = \alpha_v / 3$ can be used. Note that for fresh water ice the expansion coefficient does not depend on temperature. It is interesting that the coefficients can take both positive and negative values, but the sign does not have any implications for the design forces, because both temperature increases and decreases must normally be expected.

Following the calculations of Bergdahl and Wernersson (1978) the equations become:

$$d\varepsilon = \alpha_t \, d\theta \quad (3.4.2)$$

$$d\varepsilon/dt = \alpha_t \, d\theta/dt \quad (3.4.3)$$

For the linear expansion, and for the constitutive equation they use:

$$d\varepsilon/dt = (d\sigma/dt / E) + K D \sigma^n \quad (3.4.4)$$

ε = strain
$d\varepsilon/dt$ = strain rate
θ = temperature
t = time
σ = stress in the ice
$d\sigma/dt$ = stress change rate
E = elastic modules of ice
$n = 3.651$
$K = 4.40\ 10^{-26}\ m^{-2}(N/m^2)^{-n}$
D = coefficient of self diffusion i.e. $D_0 \exp(-Q_s/RT)$
$D_0 = 9.13\ 10^{-4}\ m^2/s$
$Q_s = 59.8$ KJ/mol (=activation energy for self diffusion)
$R = 8.31$ J/mol (=universal gas constant)
T = absolute temperature in Kelvin degrees

The idea is then to set the two strain rates equal to each other. The only unknowns are then $d\sigma/dt$ and σ.

$$\alpha \, d\sigma/dt = (d\sigma/dt /E) + K D \sigma^n \quad (3.4.5)$$

This non-linear relationship can be solved by iteration on a computer. Stresses can be computed for different depths and the pressure evaluated by integration over the depth.

Calculated extreme pressures with 1000 year return periods are less than 400 kN per meter structure (Bergdahl and Wernersson, 1978), and as such the forces are substantially smaller than those resulting from impact of drifting ice floes. The extreme pressure with a 100 year return period found for a Swedish lake at 57° 1' northern latitude was 330 kN/m.

In the case of expansion of a fast ice cover of several kilometer in size between a shore and a structure, the expansion rate is determined from a simulation of the thermal changes in the ice. The load on the structure is then determined from suitable ice failure theories with the appropriate ice movement rate.

4. INTERACTION FORMULAS

Offshore structures in ice-infested waters may be exposed to a number of different loading scenarios. Furthermore, different types of structures will cause different responses of the ice -structure system to the loading. The primary factors affecting the interaction are the structure configuration, the mechanical properties of the approaching ice and the velocity of the ice. The type of ice feature is of course also of major importance.

Ice loading on offshore structures can be divided into groups corresponding to forces from:

- landfast ice
- packice (also called drifting sheet ice)
- first-year pressure ridges
- multi-year pressure ridges
- rubble fields and blocking features
- icebergs

Structures have so far been divided into vertical and inclined structures, but with the growing activity in polar regions the list must be expanded to include some further distinctions:

- vertical vs. inclined structures
- rigid vs. flexible structures
- (bottom)fixed vs. floating structures
- narrow vs. wide structures

Only fixed rigid structures are included in the main scope of these notes. That leaves four categories, vertical and inclined, being narrow or wide.

4.1 Sheet Ice Forces on Vertical Structures

The seemingly simple problem of ice indentation forces is far from easy to solve, that is to predict the forces. This is primarily because of the complicated material behaviour of sea ice, although other factors also contribute to complicate the problem. In this chapter we shall assume that the necessary driving forces to cause ice failure are always present.

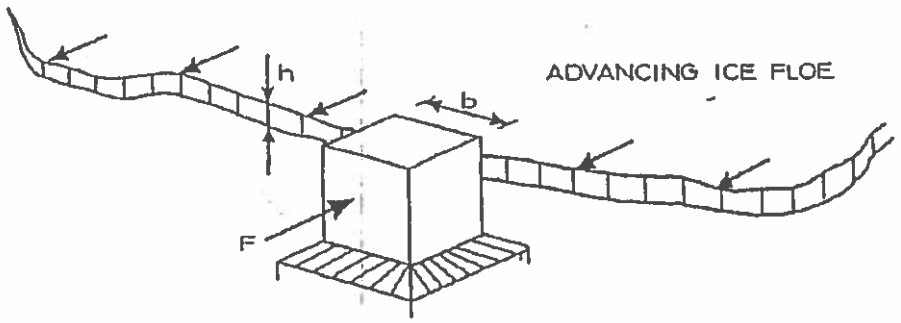

Fig. 4.1.1 Ice indentation (Type I)

Ice may fail against structures in a number of different failure modes:

- crushing
- fracture
- buckling
- creep
- bending (mostly against inclined structures)
- spalling
- cleavage
- splitting

which are mentioned here without further descriptions of each individual process. The most common failure mode against narrow vertical structures is that of crushing. Narrow structures include light-houses, bridge piers, and structures supported on columns. Early experience with offshore structures in ice has been described by Peyton (1968) and by Blenkarn (1970).

The force exerted on a structure due to ice crushing is:

$$F_c = p_e\, b\, h \qquad (4.1.1)$$

where p_e is the effective pressure over the contact area, b the structure width and h the ice sheet thickness. Naturally, p_e must depend of the ice crushing strength and the interaction conditions.

Drifting ice floes impact structures from a range of directions and within a range of different speeds. After the impact, an ice floe will fail locally as the structure "penetrates" the floe. Failure usually occurs in the form of crushing. The compressive strength of ice is very sensitive to the loading rate. For low strain rates ice behaves as a ductile material and fails by yielding. For high strain rates, say above approximately $5 \cdot 10^{-4}$ s^{-1}, it behaves in a brittle manner.

Formulas that predict loads on vertical structures from moving level ice have been presented by:

- Korzhavin (1962)
- Afanas'yev et al. (1971)
- Schwarz et al. (1974)
- Saeki et al. (1977)
- Croasdale, Morgenstern and Nuttall (1977)
- Ralston (1978)

and by a variety of authorities in the form of design codes. Most of these formulas give the horizontal force as the product of the projected contact area and the ice strength multiplied by some coefficient(s) dependent on interaction speed, geometry etc. They apply to bridge piers, lighthouses, and similar narrow structures. In the early seventies, when the first artificial islands for oil exploration were built in the Beaufort Sea, the same formulas were initially used. It was quickly realized, however, that they predicted highly conservative values for the very wide structures (50-100 metres).

In the following the formulas for narrow structures are first reviewed. Next the wide artificial islands about which much has been learned since the mid-seventies are discussed.

Korzhavin (1962)

Korzhavin (1962) proposed the following empirical formula:

$$p_e = I\, m\, k\, (V/V_0)^{-1/3}\, \sigma_u \qquad (4.1.2)$$

where the coefficients I, m, and k have physical justifications. The last factor, σ_u, is the unconfined compressive ice. strength at a strain rate in the range of 10^{-3} to 10^{-2} sec^{-1}. I is an indentation coefficient accounting for confining effects as a function of the ratio of ice floe width, B, to structure width, b. The contact factor, k, accounts for the non-simultaneous contact failures occurring during continuous crushing, and the shape factor, m, accounts for the shape of the upstream face of the structure (e.g. a bridge pier). The coefficients are given as:

$I = (B/b)^{1/3}$	for $B/b < 15$	(4.1.3)
$I = 2.5$	for $B/b > 15$	(4.1.4)
$m = 1.0$	for flat (rectangular) indentors	(4.1.5)
$m = 0.9$	for semicircular indentors	(4.1.6)
$m = 0.85\ (\sin\alpha)^{1/2}$	for wedge-shaped piers with wedge angles of 2α between 60° and 120°	(4.1.7)
$0.4 \le k \le 0.7$	with low values for high velocities and wide structures	(4.1.8)
$V_0 = 1$ m/s	is a reference velocity	(4.1.9)

The velocity function was included in the empirical formula by Korzhavin (1962) to account for the fact that he fitted measured forces using compressive ice strengths measured in the range of strain rates from 10^{-2} to 10^{-3} sec^{-1}. The formula is sometimes presented without the term $(V/Vo)^{-1/3}$, and in this case σ_u should be taken as the strain rate dependent unconfined compressive ice strength.

Afanas'yev et al.'s (1971)

Afanas'yev et al.'s (1971) formula for crushing reads:

$$F_c = m\, C\, \sigma_u\, b\, h \qquad (4.1.10)$$

m = dimensionless shape coefficient

m = 1.0 for flat upstream face

m = 0.9 for a semicircular upstream face

C = dimensionless function of aspect ratio:

$$C = (5\,(h/b)+1)^{1/2} \text{ for } 1 < b/h < 6 \qquad (4.1.11)$$

C is obtained from a linear interpolation between 4 (at b/h = 0.1) and 2.5 (at b/h = 1) for $0.1 < b/h < 1$

This formula is based on model tests with saline ice of small thickness, and it is not applicable for b/h > 6.

Schwarz et al.'s (1974)

Schwarz et al.'s (1974) formula, which is sometimes called the Iowa-formula (it was developed partly at the University of Iowa) is based on cleavage failure. The authors saw a horizontal cleavage crack forming in the midplane of the ice in front of the pile.

Their formula can be written:

$$F = 0.564\, m^{0.4}\, \sigma_u\, b^{0.5}\, h^{1.1} \qquad (4.1.12)$$

where m is the unit meter, σ_u the uniaxial compressive strength, b the pile diameter, and h the ice thickness. The formula is supported by full-scale measurements on a b = 0.60 metre bridge pile in the Eider river in Germany and small-scale laboratory tests at the University of Iowa in the USA. The formula pertains to cleavage failure of ice within a few degrees of the freezing point against a vertical, circular structure. It should not be used for diameters in excess of two metres.

Saeki et al.'s (1977)

Saeki et al.'s (1977) formula is rather similar to that by Schwarz et al. It reads:

$$F = C\ \sigma_u\, b^{0.5}\, h \qquad (4.1.13)$$

where again the constant (C) must be given a dimension in order to make the equation dimensionally correct. Besides the values of C, the only other difference is in the power of h. The C values are:

$C = 5.0\ m^{0.5}$ for a circula... (4.1.14)

$C = 6.8\ m^{0.5}$ for a rectangular pile (4.1.15)

and the failure is by cleavage as described earlier. The formula represents an upper-bound empirical fit to a combination of model test results and full-scale measurements.

Croasdale, Morgenstern and Nuttall (1977)

Croasdale, Morgenstern and Nuttall (1977) presented the formula normally referred to as *Morgenstern and Nuttall's formula*. They assume an ideal elastoplastic and homogeneous ice and use a Tresca yield criterion to postulate:

$$\tau = \sigma_u / 2 \qquad (4.1.16)$$

where τ is the shear strength. A truly homogeneous ice would then fail in 45° wedges as shown in Figure 4.1.2. The formula for the corresponding force is:

$$F = (1/\cos\varphi)\,(h/(4b) + 1/(2\sin\varphi))\,\sigma_u\, b\, h \qquad (4.1.17)$$

when the indenting structure is considered frictionless. The angle φ, shown in Fig. 4.1.2., is close to 45°, and using $\tau = \sigma_u/2$ the formula can also be written:

$$F = ((2^{0.5}/4)\, h/b + 1)\, 2\, \tau\, b\, h = (0.354\, h/b + 1)\, \sigma_u\, b\, h \qquad (4.1.18)$$

The formula is an upper bound solution based on plastic limit theory.

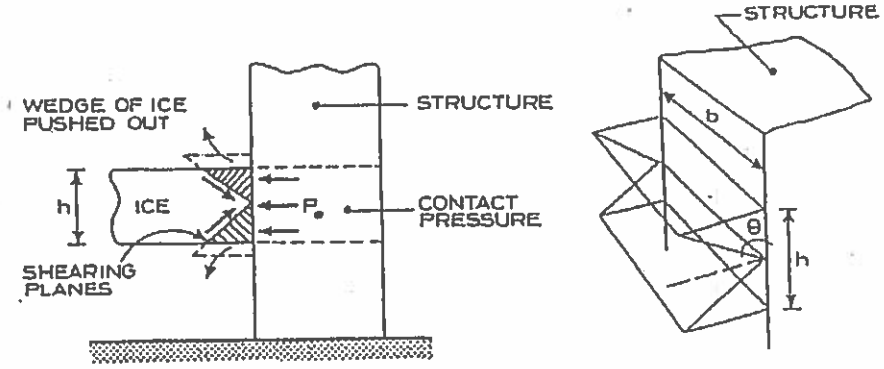

Fig. 4.1.2 Failure pattern assumed in Morgenstern and Nuttall's formula.

Ralston (1978)

Ralston (1978) among others applied plastic limit analysis to the indentation problem for ice. This type of analysis is based on two theorems, viz.:

The lower bound theorem:
The loads determined from a distribution of stress alone that satisfies a) the equilibrium conditions, b) stress boundary conditions, and c) nowhere violates the yield criterion are not greater than the actual collapse load.

The upper bound-theorem:
The loads determined by equating the external rate of work to the internal rate of dissipation in an assumed deformation mode (or velocity field) that satisfies a) velocity boundary conditions and b) strain and velocity compatibility conditions, are not less than the actual collapse load. By suitable choice of stress and velocity fields, the above two theorems enable the required collapse load to be bracketed as closely as seems necessary for the problem under consideration.

The particular advantage of limit analysis is that it is not necessary to have a correct solution before having an answer. The correct answer, however, is revealed by identical upper and lower bounds. Thus one can start by making rough estimates that can be improved successively. The reader is referred to the literature for a more detailed presentation of the application of plastic limit analysis to ice indentation.

Ice Forces on Wedge Shaped Structures (with vertical faces)

Wedge shaped structures with vertical faces are usually designed as other vertical structures with due account to the actual width of the structure. In certain cases with smaller ice floe it is possible that a splitting type of failure may exist instead of crushing. A wedge typemay be favourable if b/h >3. When the floe is been stopped after a certain penetration with a structure width b_l at maximum penetration the force is been calculated from the previous mentioned formula's or DS 410, see section 6.1.
Below is used the DS 410 formula:

$$F_c = k \sigma_u b h \qquad (4.1.19)$$

$$k = 1+3/(1+b/h) \qquad 0 < b/h < 9$$

The following scenario is considered:

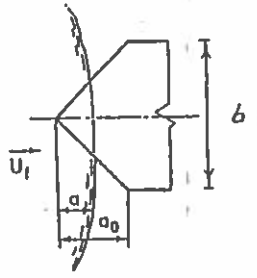

Figure 4.1.3 Ice Floe Impact to a Wedge Shaped Structure

$$F_c = (1+3/(1 + (a\ b)/(a_0\ h))\ \sigma_u\ b\ h\ a/a_0 \qquad (4.1.21)$$

Non-dimensionalised:

$$F_c /(\sigma_u\ b\ h) = (1+3/(1 + (a\ b)/(a_0\ h))\ a/a_0 \qquad (4.1.22)$$

This function is shown on Figure 4.1.4

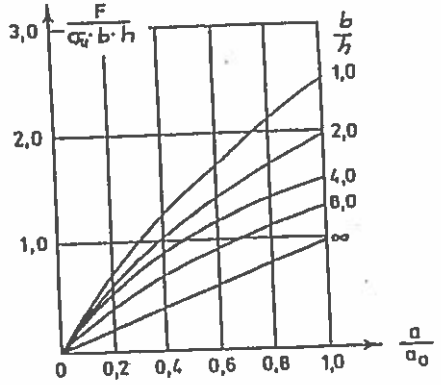

Figure 4.1.4 Dimensionless Force on Vertical Wedge

The penetration may be calculated from equalising the impacting kinetic energy with the crushing energy E_c:

$$E_c = \int F_c(a)da \qquad (4.1.23)$$

$$C(a) = (a\ b)/(a_0\ h) \qquad (4.1.24)$$

$$E_c = \sigma_u\ b\ h\ (a^2/a_0 + 3\ a_0\ (h/b)^2\ (C - \ln(1 + C)) \qquad (4.1.25)$$

The actual value for a may be determined by iteration.

Dynamic Ice Forces
The continuous crushing of ice against a bridge pier is a highly dynamic process which is both cyclic and irregular. Stresses in the ice build up in front of the pier, and microcracks beginto expand. As stresses increase the microcracks join and the ice separates into individual pieces. This pulverizing of the ice is what is usually referred to as crushing. But the formation and joining of microcracks and the possible formation and propagation of shear cracks are also part of the crushing process. At present, the ice crushing process is not fully understood (Timco and Jordaan, 1987).

Permanent deformations of a structure experiencing large loads are created over an interval of time rather than instantly. The time necessary to produce permanent deformations can be in the order of

milliseconds or it can be as high as tens of seconds depending on structure material, on structure stiffness, and on foundation conditions.

The variation in load with time has been measured at high sampling rates by a number of researchers. A time series plot basically shows a number of peaks separated by drop-offs to minimum values in the range from 10% to 50% of the peak load. The duration of a peak depends on the interaction speed and the ice type among other things.

If a peak load is larger than the static design load of the structure, it may still pass without causing permanent deformations, provided that the duration of the peak is sufficiently short. The required magnitude and duration of a peak to cause permanent deformations can only be determined when a detailed structure design is available.

The stiffness and natural frequency of a structure must be determined first, and then the time necessary to cause permanent deformation for the foundation is found. This normally requires detailed geotechnical investigations of the seabed material.

It is not unlikely that loads increase due to dynamic amplification if the natural frequency of the structure coincides with the typical frequency in the ice failure process. A first estimate of the typical crushing frequency, f_c, is:

$$f_c = \xi V/F_c \qquad (4.1.19)$$

where F_c is the peak crushing force, V the velocity of the ice floe, and ξ the spring constant of the system. Amplification can also occur for buckling loads, see e.g. Christensen et al. (1989b) .

Ice Forces on Wide Structures

As I mentioned earlier, the formulas presented above overestimate the forces on wide structures such as the artificial islands in the Beaufort Sea. Small scale ice strength tests and indentation theory resulted in global design ice pressures near 8 MPa. Even with various factors the pressure could not be lowered below approximately 4 MPa in the early island designs.

The first artificial island built in the Beaufort Sea was "Immerk" in the Canadian Beaufort Sea. It was a fill island in 3 metres of water depth. Nowadays caisson-retained-islands (CRI's) are used in water depths in excess of 30 metres. Caisson-type structures often have vertical sides.

At the time of the design of the first islands, reductions in ice forces were attempted because of:

- limited ice movement rates for the landfast ice near the coast,
- the possibility of a size effect in effective ice strength, and
- the possibility of alleviating measures in landfast ice zones.

The first limitation, that of movement rate, has been explored more over the last 16 years, [illegible]oday a design ice pressure would definitely be limited by the rate-dependent ice strength if a maximum strain rate less than about 10^{-3} sec^{-1} can be ensured.

The second point, that of size effect, has been a major point of discussion among ice researchers for a number of years now. The foremost arguments are those by:

- Sanderson (1986) for the existence of a size effect, and
- Lee et al. (1986) and Petrie and Poplin (1986) against the existence of a size effect.

Sanderson (1986) uses a large number of experimental data from laboratory and field tests, full-scale measurements, and computer models of meso-scale ice mechanics to support proportionality of the upper bound indentation pressure and the contact area to the power -0.5.

Lee et al. (1986) and Petrie and Poplin (1986) carried out full-scale ice strength measurements with a very carefully controlled test set-up and were unable to identify any size effects. The size effects observed by Sanderson could instead reflect other causes such as non-simultaneous failures, imperfect contact, etc. In any case, wide structures are designed for a lower global pressure than narrow structures. The reader is warned that this treatment of the ice-structure interaction problem for wide structures is very simplified. You are encouraged to study specialty literature on your own, e.g. on non-simultaneous failure (Ashby et al 1986, Kry 1981, Eranti 1990).

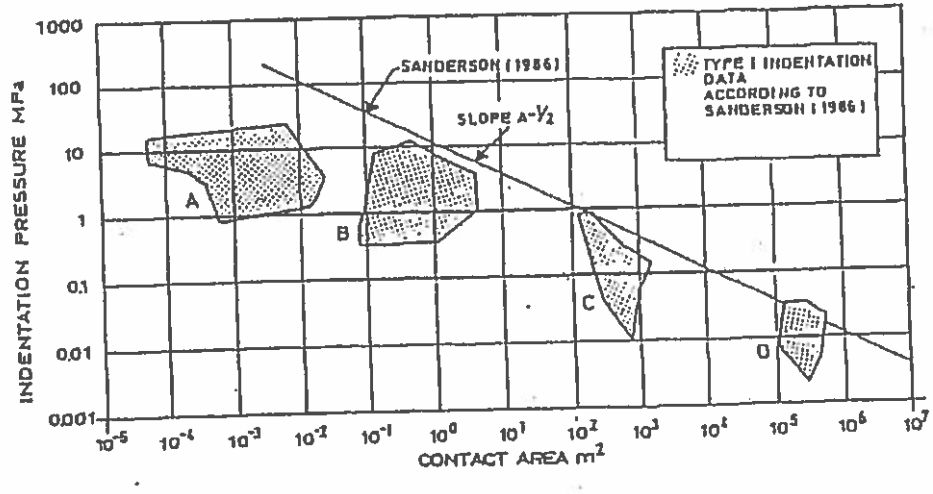

Figure 4.1.3 Pressure-Area Curve for Ice after Sanderson (1986). The four Data Groups are: A: Laboratory Tests, B: Medium-Scale Field Tests, C: Large-Scale Arctic Island Measurements, D: Theoretical Mesoscale Models

Sanderson's (1986) graph is shown in Figure 4.1.3. Other relationships than $\sigma \sim A^{-0.5}$ have been suggested for design, e.g. Vivatrat and Slomski (1984) and by Christensen et al. (1989a).

The determination of ice loads on wide vertical structures is currently being based on three different approaches (see e.g. Croasdale (1988)), and they are:

- the indentation equation,
- the reference stress method, and
- the cut-oft stress method

each of which is briefly commented on below.

Indentation equation

The indentation equation is used with indentation factors determined from plastic limit analysis. The strength would be strain -rate dependent. Frozen-in structures subjected to ice pressure from a gradually increasing wind drag on the ice will experience "perfect contact", but a low strain rate. At higher strain rates the peak strength of the ice is used, but a contact factor less than one will apply (typically in the range from 0.3 to 0.7). The method still appears to be conservative for the widest structures.

Reference stress method

The reference stress method described by Ponter et al. (1983) is for the creep regime, i.e. low strain rates. The results from this method are relatively close to those from the indentation equation when a rate-dependent strength and perfect contact are used. The validity of both methods ceases when fracturing begins. It appears that the onset of fracturing occurs for lower strain rates and at lower stress levels the larger the contact area becomes.

Cut-off stress method

The cut-off stress method described by Walden et al. (1987b) considers the above finding, and suggests that the ice pressure has a maximum associated with the transition from ductile yield to brittle fracture. They suggested that the transition point is scale-dependent, like Sanderson (1984a) also did, and show how to determine it from full-scale data (Walden et al.; 1987a). Croasdale (1988) showed this last approach to give the best results which is natural since it is empirical.

The global ice pressure on wide arctic offshore structures (100 metres) rarely exceeds 1.0-1.5 MPa, but higher stresses cannot be excluded, Sanderson and Child (1986) for higher strain rates.

Local Ice Pressure

The ice pressure can locally rise to values far higher than the unconfined compressive ice strength. This is in agreement with the observation of high confined compressive ice strengths for horizontal loading with vertical confining plates, cf. section 2.6, and also with the general plot by Sanderson in Figure 4.1.3. Local pressures are of importance to local structural stability and to abrasion etc. For a ...st estimate, it is recommended to use upper bound values from Figure 4.1.3. in special cases, however, values of twice those shown for very small areas can be achieved. The reader is referred to Cammaert and Muggeridge (1988) for a discussion of local ice pressures.

Multilegged Structures

Ice loads on multi-legged structures are not described in these notes. This is solely in order to limit the length of the manuscript. The reader is referred to Sodhi and Kato (1983), to Timco (1986), and to Christensen et al. (1989a).

4.2 Sheet Ice Forces on Inclined Structures

Typical structures classified as "narrow" and "inclined" are bridge piers with inclined noses often used in rivers where the direction of the ice floes is constant, and conical structures for lighthouses etc., which experience ice floe impact from all directions. The "philosophy" behind inclined structures is to promote bending as the dominant failure type and thereby reduce the ice forces.

Commonly appearing formulas for ice forces on inclined structures include those by:

Croasdale (1978), simple 2D theory
Croasdale (1978), adjusted 2D theory
Ralston (1977, 1979), plastic limit analysis
Edwards and Croasdale (1976), empirical
Tryde (1975), elastic
Afanas'yev et al. (1971), elastic and empirical
Korzhavin (1962), empirical

These formulas are briefly presented in the following. Figure 4.2.1 illustrates a conical structure in ice.

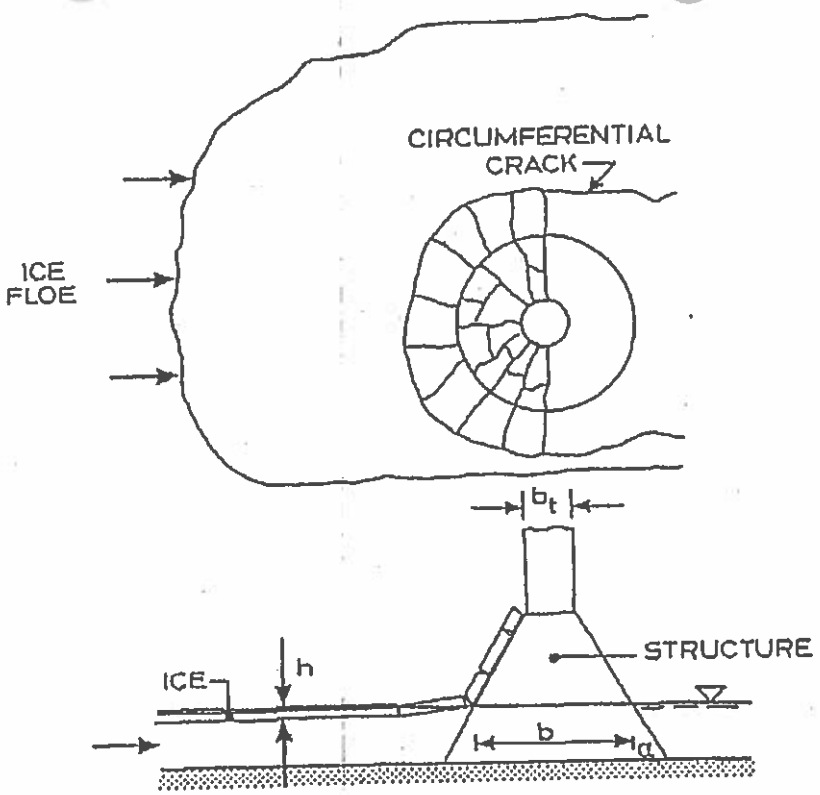

Figure 4.2.1 Sheet ice being pushed against a conical structure.

Croasdale (1978)

Croasdale (1978) presented two formulas for the horizontal ice force on a conical structure. They are normally referred to as the simple 2D theory and the adjusted 2D theory. The former theory gives the expression:

$$F = 0.68\, C_1\, \sigma_f\, b\, (\gamma_w\, h^5/E)^{1/4} + C_2\, \gamma_i\, Z\, b\, h \qquad (4.2.1)$$

where the first term represents the ice breaking force and the second term the ride-up force. The flexural ice strength is denoted σ_f, and γ_w and γ_i are the specific weights of water and ice, respectively. Z is the vertical height reached by the ice on the slope and C_1 and C_2 are functions of the surface slope, α, and the friction coefficient, μ, given by:

$$C_1 = (\sin\alpha + \mu\cos\alpha) / (\cos\alpha - \mu\sin\alpha) \qquad (4.2.2)$$

$$C_2 = (\sin\alpha + \mu\cos\alpha)^2/(\cos\alpha - \mu\sin\alpha) + (\sin\alpha + \mu\cos\alpha) / \tan\alpha \qquad (4.2.3)$$

Remember that cos > sinα

In the adjusted 2D theory an ice failure zone slightly wider than the structure is taken into account. The resulting difference is that the structure width (at the water line), b, in the ice-breaking term is replaced by a function, l', of the characteristic length, l, of the ice sheet given by:

$$l = (Eh^3/(12\,\gamma_w\,(1-\upsilon^2))^{0.25} \qquad (4.2.4)$$

$$l' = (\pi^2/4)\, l \approx 2.47\, l \qquad (4.2.5)$$

The function l' is the approximate length of the circumferential crack in front of the structure. Since it depends only on the ice properties and not on the structure width, one should expect this theory to overestimate the breaking force on narrow structures and underestimate it on wide structures.

Ralston (1977, 1979)

Ralston (1977, 1979) used plastic limit analysis for inclined structures also. Determination of ice loads on conical structures is in most cases carried out by using his theories, which have also been adopted as the recommended practice for offshore structures by the American Petroleum Institute (1982). Ralston's theory is known to be the most conservative among those predicting forces on conical structures. There is, however, no evidence that it should be too conservative. It includes both ice breaking and ice ride-up forces.

The inclination angle (with horizontal) should not exceed approximately 65° in order for the theories to be applicable. This limit is given different values by various researchers, but 65° is felt to be safe. It can be increased if the friction coefficient is lowered, e.g. by surface coating.

Ralston's (1977) method is based on plastic limit analysis, and the main result can be expressed as:

$$R_H = (A_1\,\sigma_f\,h^2 + A_2\,\gamma_w\,h\,b^2 + A_3\,\gamma_w\,h\,(b^2 - b_t^2)A_4 \qquad (4.2.6)$$

$$R_V = B_1\,R_H + B_2\,\gamma_w\,h\,(b^2 - b_t^2) \qquad (4.2.7)$$

R_H = horizontal force on cone
R_V = vertical force on cone
σ_f = flexural stength of ice
γ_w = specific weight of sea water
h = ice sheet thickness
b = cone diameter at the water line bt = cone diameter at its top

$A_1, A_2, A_3, A_4, B_1, B_2$ - dimensionless coefficients which are functions of the ice-to-cone friction coefficient, μ, and the cone inclination angle, α.

Graphs for determining the coefficients are given in Fig. 4.2.2.

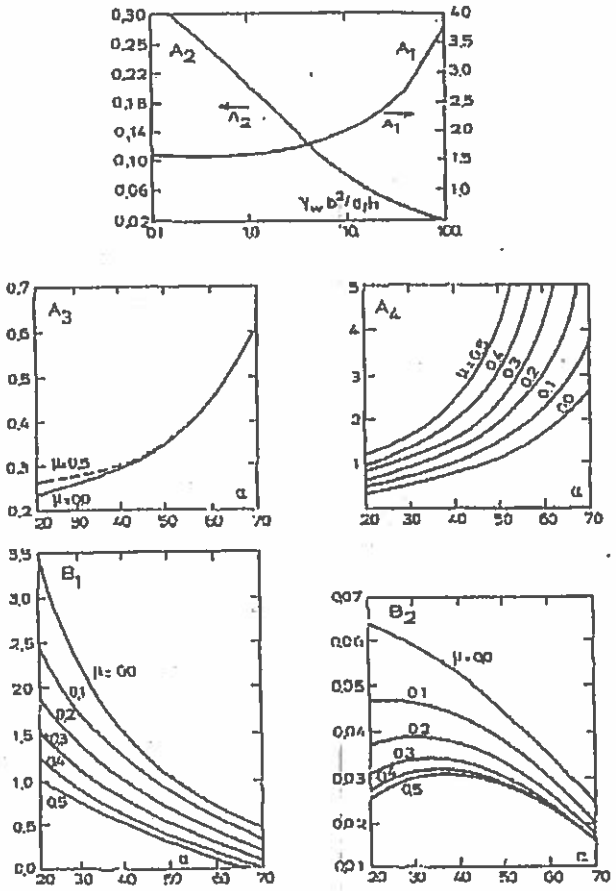

Figure 4.2.2 Ice force coefficients for plastic limit analysis. From Ralston (1977)

The above formulas may be used when the length of the slope from the water line to the top exceeds the size of the broken floes. It is assumed that the largest ice pieces broken off the ice sheet have a length of $l/2_{,,}$ where l is the characteristic length of the ice. The criterion becomes:

$$S \geq 0.5\,(E\,h^3/12\gamma_w(1-\upsilon^2))^{0.25} \qquad (4.2.8)$$

S = length of slope above water

E = elastic modulus of ice

υ = Poisson's ratio

If this condition is not satisfied considerable forces may be exerted on the vertical part of the structure, and the advantage of the conical shape is partly lost. In a situation with E = 6.0 GPa, h = 0.965 m, γ_w = 10 kN/m^3 and υ = 0.5 the characteristic length becomes 15.6 m. The length of the conical surface from the water line to the top (transition to vertical pier) must therefore be about 8 m unless a. more refined (dynamic) analysis is carried out. This applies to rotationally symmetric piers only. This estimate is very conservative. Refined analyses will normally show 3-4 meters to be sufficient, depending also on the tidal range at the structure.

In the above calculation it has been assumed that the cone would lift the ice sheet upon contact. A configuration with a cone inducing downwards bending of the ice is also possible, and it is actually preferable because it causes smaller vertical forces. Instead of the gravity of the ice, the bouyancy becomes the source of the vertical force.

The specific weight of the ice was taken as 90% of the specific weight of the sea water (0.9 γ_w) for the calculation of the dimensionless coefficients. The buoyancy acting on depressed ice will correspond to 10% of the specific weight of the sea water (0.1 γ_w). As such, the theory may be applied to downward breaking cones by replacing γ_w with γ_w /9 and changing the sign on R_V.

The dimensionless coefficients given in the graphs can be determined semi-analytically. The procedure was described e.g. by Christensen (1988).

Example

For an example assume that the following values apply:

σ_f = 700 kPa h = 0.965 m μ = 0.15
γ_w = 10 kN/m3 α = 45°
b = 17.0 m b_t = 5.0 m

The dimensionless parameter ($\gamma_w\,b^2/\sigma_f h$) then amounts to 4.28 and the resulting values of the constants become A_1 = 1.81, A_2 = 0.12, A_3 = 0.32, A_4 = 1.40, B_1 = 0.92, and B_2 = 0.037. The horizontal and vertical forces are then found as:

R_H = 3.3 MN
R_V = 3.1 MN

These forces are substantially smaller than those for vertical piers of similar overall dimensions. Note that the vertical force introduces a stabilizing moment on the structure.

Edwards and Croasdale (1976)

Edwards and Croasdale (1976) derived their formula on the basis of model test data. They used a surface slope angle of 45° and a friction coefficient of about 0.1. Their formula for the horizontal force reads:

$$F = 1.6\ \sigma_f h^2 + 6.0\ \gamma_w\ b\ h^2$$

where b is the structure width at the water line. The two terms allegedly represent breaking and ride-up contributions to the total force. Note that the breaking term is independent of the structure width. The formula should be seen as an expression of test results rather than a tool for design.

Tryde (1975)

Tryde (1975) gives a formula for the ice force on a wedge shaped structure, e.g. an upstream bridge pier face. His formula is based on a specific assumed crack pattern. Let S be half the apex angle of the wedge in the horizontal plane, and let α be the angle between the horizontal and the upstream edge of the wedge, see Figure 4.2.3. The coefficient of friction between the ice and the pier is denoted μ. Typical friction coefficients for ice on concrete piers are in the range of 0.1 to 0.2. The ice thickness is denoted h and the pier width b.

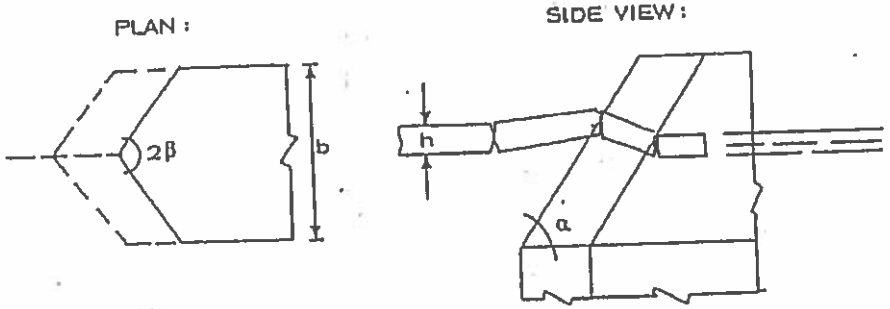

Figure 4.2.3 Definition sketch for inclined wedge piers.

The first step is to calculate the three dimensionless coefficients:

$$C_1 = 1 - \mu\ (\tan\alpha / \sin\beta) \qquad (4.2.10)$$

$$C_2 = \mu + (\tan\alpha / \sin\beta) \qquad (4.2.11)$$

$$C_3 = 6\ (h / b)\ \cos\beta + 6\ (C_1 / C_2) \qquad (4.2.12)$$

Let furthermore E denote the elastic modulus of the ice, ρ the density of the ice, and v the velocity of the ice floe. The next step is then to calculate the combined dimensionless coefficient

$$C = 0.16\ (E / \rho\ v^2 \sin^2\beta)^{1/2}\ (C_1 / C_2)\ C_3^2 \qquad (4.2.13)$$

Finally, let the ratio of the bending strength to the compression strength be denoted ε ($=\sigma_f / \sigma_u$), and calculate the coefficient:

$$k = 5.2\ \varepsilon^{1/3}\ C^{-1/2} \qquad (4.2.14)$$

The maxium horizontal force on the bridge pier may then be found by the formula:

$$F = k\ \sigma_u\ b\ h \quad 3.3 < b/h < 20 \qquad (4.2.15)$$

which is identical to the one for vertical piers, except that the coefficient k is calculated in an entirely different way. Remark that Tryde's formula include the effect of ice velocity.

Example

For an example assume that the following parameters apply:

Pier:	Ice:	
b = 5.0 m	μ = 0.15	v = 0.7 m/s
α = 60°	E = 6.0 GPa	σ_f = 500 kPa
β = 30°	h = 0.60 m	σ_u = 1500 kPa
	ρ = 910 kg/m3	

This leads to the following coefficients:

$C_1 = 0.48$ $C_2 = 3.61$ $C_3 = 1.42$ $C = 315$ $k = 0.203$

and eventually the horizontal force:

$F = 0.203 \cdot 1500 \cdot 5 \cdot 0.60$ kN = 0.914 MN

Note that the compression strength is used in the final formula. The ice actually fails in flexure, and this is accounted for through the parameter ε.

Piers with inclined wedges as upstream faces have been successfully used in rivers where the ice floes impact largely in the longitudinal direction of the pier. An inclined upstream face will only be effective for a limited range of directions. Consequently, it can be of interest to consider piers with a conical shape in the zone around the water line, if a range of impact directions is expected.

Afanas'yev et al.'s (1971)

Afanas'yev et al.'s (1971) formula is based on small-scale model tests with conical structures interpreted through elastic plate theory. Their formula reads:

$$F = (S_c \tan\alpha\, \sigma_f h^2)/(1.93\, l) \qquad (4.2.16)$$

where α is the surface slope, l the characteristic length of the ice sheet, and S_c the length of the circumferential crack given by:

$$S_c = 0.62\, b + 1.38\, l \qquad (4.2.17)$$

where b is the structure width at the water level. The test data were obtained in ice of 3 to 3.5 cm thickness and with α-values of 30°, 45°, and 60°.

Korzhavin (1962)

Korzhavin (1962) states that the ice force is the lowest of the three forces calculated for failure in crushing, bending, and shear. His crushing formula is presented in section 4.1. The bending and shear formulas are:

$$F = C_0 \tan\alpha\, \sigma_f\, b\, h \quad \text{(for bending)} \qquad (4.2.18)$$

$$F = 1.1\, k \tan\alpha\, \tau\, b\, h / \sin\beta \quad \text{(for shear)} \qquad (4.2.19)$$

where τ is the shear strength (a Tresca criterion would give $\tau = \sigma_u/2$, albeit the Tresca criterion is simplified here), $2\beta = 80°$ is recommended), k is a contact coefficient, and C_0 is a function of the angles α and β as follows:

α 2β =	45°	60°	75°	90°	120°
45°	0.20	0.17	0.16	0.16	0.15
60°	0.24	0.20	0.19	0.18	0.17
70°	0.38	0.27	0.23	0.21	0.19
75°	0.79	0.38	0.29	0.26	0.22

Table 4.2.1 Values of Korzhavin's (1962) coefficient, C_0

A decrease in apex angle (2β) results in an increase of C_0 and thus in effective ice pressure. This is explained by the fact that a narrower structure is likely to penetrate further into an ice floe before breaking it. This means that larger pieces will break off. C_0 increases with surface slope (α). This might be because of combined bending and compression failures on the steep structures.

4.3 Ice Ridge Forces on Vertical Structures

An ice ridge or pressure ridge is an accumulation of ice pieces caused by compressive ice forces in an ice cover. Pressure ridges can in arctic areas exceed drafts of 50 metres, and they are frequently a governing factor in arctic design and operations. Typical ridges have drafts in the range of 2-15 metres. The under water accumulation is referred to as the keel, and the above water part of the accumulation is called the sail. There is often a solid zone between the keel and the sail.

Pressure ridges that r have not (yet) undergone a melting season are called first-year ridge. opposed to multi-year ridges which are more consolidated features with a larger solid zone. Loads from first-year ridges are predicted mainly by three models, viz.:

- Croasdale (1980), plug shear
- Prodanovic (1981) ,spiral shear
- Rojansky and Gerwick (1981), beam bending

while loads from multi-year ridges will be substantially larger than those from first-year ridges with similar dimensions.

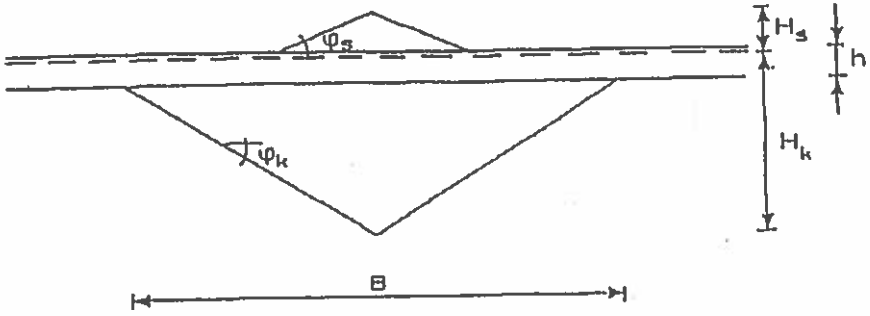

Figure 4.3.1. Definition sketch for ice pressure ridges.

Typical keel depth to sail height ratios are in the range of $H_k:H_s = 3:1$ to 5:1 depending on how deteriorated the ridge is. Newly formed ridges can have ratios near 8:1, but then the keel has almost no structural integrity. Typical angles of repose are $\varphi_s = 20°\text{-}30°$ and $\varphi_k = 30°\text{-}40°$.

Croasdale (1980)

Croasdale (1980) assumed two plane shear failures to create a plug type shear failure stopping a section of the ridge in front of the structure. His formula reads:

$$F = F_r + F_s \qquad (4.3.1)$$

where F_r and F_s are the forces required to fail the rubble (keel and sail) and the solid zone, respectively. He suggests:

$$F_r = 2/3\ BH_k^2\ (\gamma_w - \gamma_i)\ \tan \varphi_k \qquad (4.3.2)$$

where B is the ridge width, γ_w the specific weight of water, and γ_i that of the ice. He furthermore suggests determining F_r by the usual crushing formulas setting the solid zone thickness equal to the ice sheet thickness.

Prodanovic (1981)

Prodanovic (1981) also suggests two independent terms. The rubble is assumed to fail in accordance with a Mohr-Coulomb failure criterion. This results in two spiral curved cracks, see Figure 4.3.2. The resulting rubble force, F_r, is shown graphically in Figure 4.3.3., as a function of the aspect ratio (structure width to ice thickness).

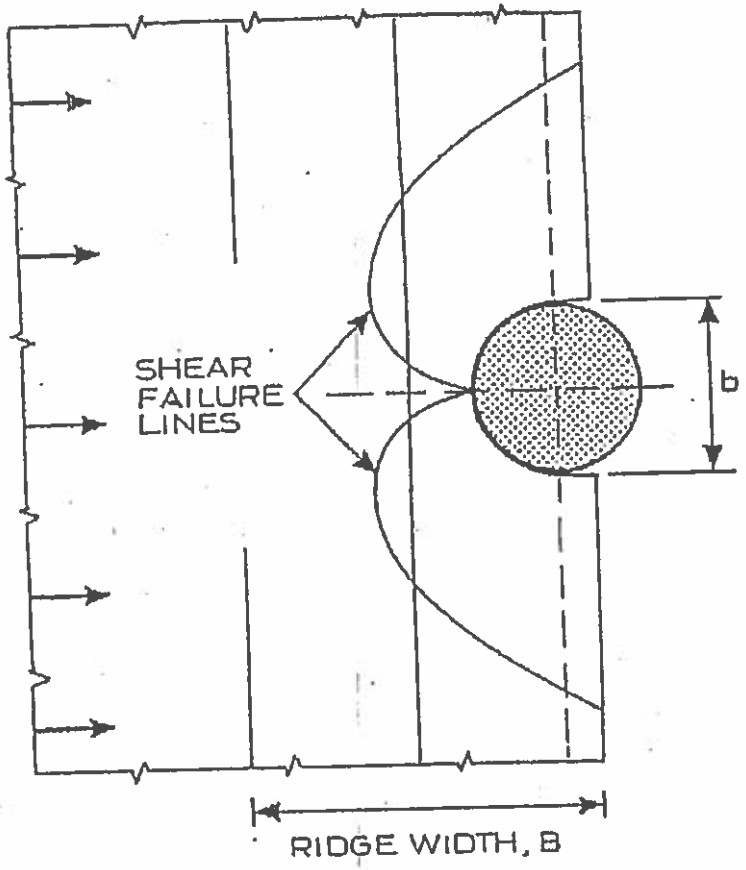

Figure 4.3.2 Failure planes from Prodanovic's model.

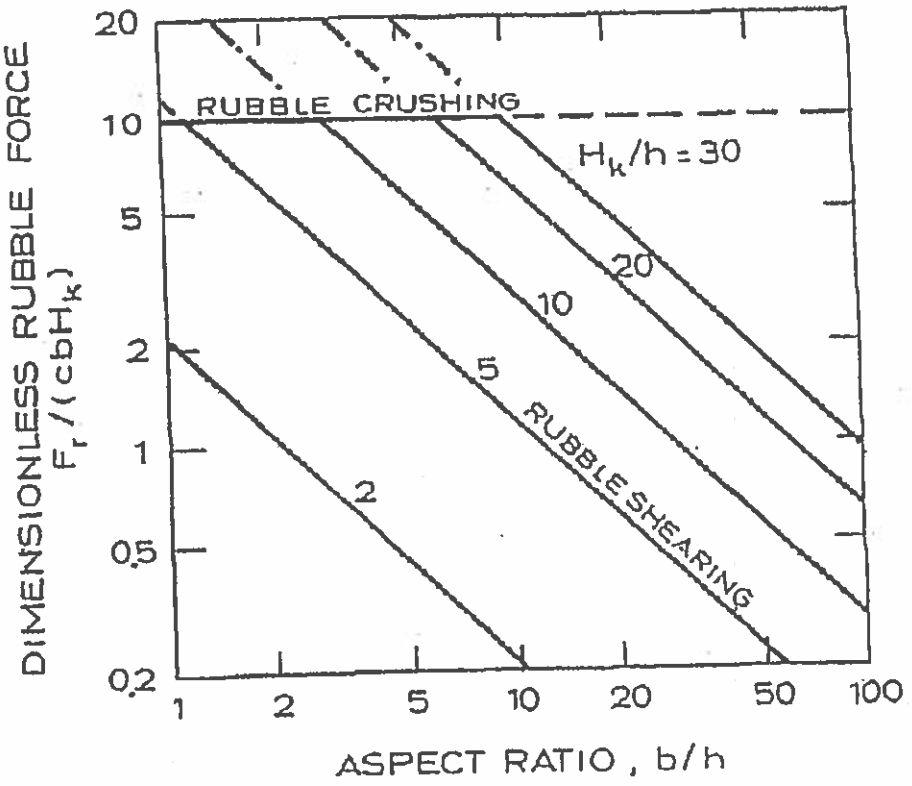

Figure 4.3.3 Rubble force as a function of aspect ration according to Prodanovic (1981)

Multi-year ridges, which are normally stronger than first-year ridges, are also handled by Prodanovic (1981) who uses an anisotropic, pressure-sensitive yield function to predict failure of the large solid zone in the ridge. His result for multi-year ridges are illustrated in Figure 4.3.4, which shows the total ridge force as a function of aspect ratio.

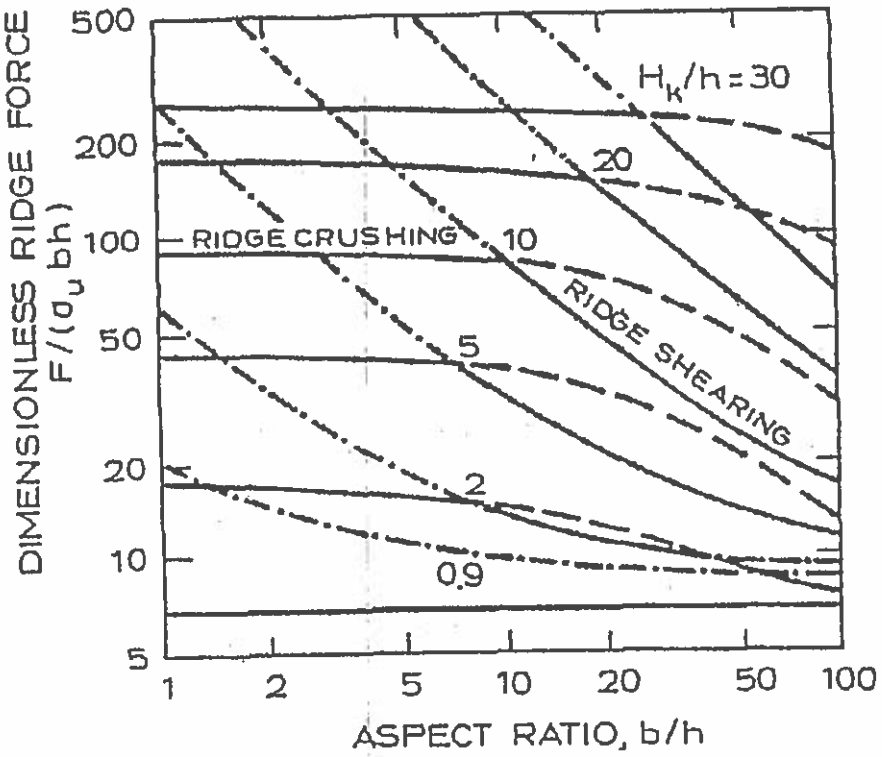

Figure 4.3.4 Multi-year ice ridge force as a function of aspect ratio according to Prodanovic (1981).

Rojansky and Gerwick (1981)

Rojansky and Gerwick's (1981) model is based on in-plane beam type bending of the ridge, and therefore likely to be better at multi-year ridge forces than at first-year ridge forces.

4.4 Ice Ridge Forces on Inclined Structures

For first-year ridges impacting inclined offshore structures, it is suggested to calculate the rubble force in the same way as for vertical structures. The solid zone (ice sheet) force, however, should be calculated according to Ralston's (1977, 1979) theories.

Multi-year ridges fail against conical structures in crushing, bending, shearing, or twisting. The preferred mode seems to be a vertical bending as the part of the ridge hitting the structure is being lifted.

Two typical bending failures have been frequently observed in model tests: initial crack formation and hinge crack formation, cf. Figure 4.4.1. Through an analogy with a floating ice beam (an elastic beam on an elastic foundation) the corresponding vertical forces on the conical structure from an infinitely long ridge become:

$$R_V = 4\sigma_f I /(y_t l) \text{ for the initial crack, and} \quad (4.4.1)$$

$$R_V = 6.17\sigma_f I /(y_b l) \text{ for the hinge crack} \quad (4.4.2)$$

where I is the moment of inertia of the ridge cross-section, y_t and y_b the distances from the top and bottom, respectively, to the neutral axis, and l the ridge characteristic length given by:

$$l = (4EI/\gamma_w B)^{0.25} \quad (4.4.3)$$

where E is the elastic modulus of the ridge (ice blocks plus porosity). The horizontal force is simply determined as:

$$R_H = R_V (\sin\alpha + \mu \cos\alpha)/(\cos\alpha - \mu \sin\alpha) \quad (4.4.4)$$

where α is the surface angle and μ the coefficient of friction.

For ridges of finite length, the reader is referred to Ralston (1977). For failure in the (probably rare) twisting mode, the reader is referred to Gershunov (1987).

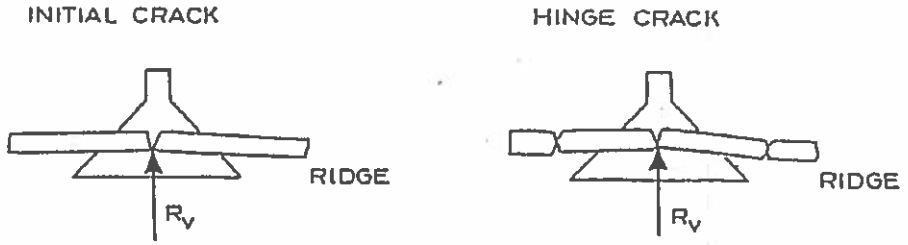

Figure 4.4.1 Initial and hinge crack formation in ridge impacting inclined structure.

4.5 Iceberg Impact Forces

Johnson and Nevel (1985) proposed a simple model for calculation of the force exerted by an impacting iceberg on an offshore structure. A vertical cylindrical structure was considered, and the iceberg was assumed to have a trapezoidal shape with a vertical front $h_0 = 5$ m high and an angle of $\alpha = 56°$ between the horizontal and the slant sides of the iceberg. These values are also suggested by Johnson and Nevel (1985).

The impact force is calculated on the basis of a simple energy based model. The kinetic energy is dissipated by crushing of the ice, and the force can be calculated under the following conservative assumptions:

- the impact is head-on,
- the structure is rigid and immovable,
- the ice fails in crushing only,
- the ice strength is a constant,
- the structure stops the iceberg.

The structure has vertical sides and a circular cross-section with a diameter of D. For an indentation of length Δ, the width and height of the projected contact area becomes:

$$W(\Delta) = 2\,(\Delta\,(D - \Delta))^{1/2}\,,\ \Delta \le D/2 \qquad (4.5.1)$$

$$h(\Delta) = h_0 + 2\,\Delta\,\tan\alpha \qquad (4.5.2)$$

The force is calculated as the crushing strength multiplied by the projected contact area:

$$F_c(\Delta) = 2\sigma_c\,(\Delta\,(D - \Delta))^{1/2}\,(h_0 + 2\,\Delta\,\tan\alpha) \qquad (4.5.3)$$

The energy dissipated during the impact is expressed by:.

$$E_c(\Delta) = \int_0^{\Delta} F_c(\Delta)\,d\Delta \qquad (4.5.4)$$

For $\Delta \ll D$ the expressions for F_c and E_c reduce to:

$$F_c(\Delta) = 2\,\sigma_c\,(\Delta D)^{1/2}\,(h_0 + 2\,\Delta\,\tan\alpha) \qquad (4.5.5)$$

$$E_c(\Delta) = 2\,\sigma_c\,D^{1/2}\int_0^{\Delta}(h_0 + 2\,\Delta\,\tan\alpha)\,\Delta^{1/2}\,d\Delta \qquad (4.5.6)$$

$$E_c(\Delta) = \sigma_c\,D^{1/2}\,(1.33\,h_0\,\Delta^{1.5} + 1.60\,\tan\alpha\,\Delta^{2.5}) \qquad (4.5.7)$$

When the impacting kinetic energy is known, A can thus be found and the characteristic maximum force estimated.

A more refined calculation was presented by Nevel (1986), who considered rotation of the impacting iceberg. If a collision is eccentric, rotational energy may be left in the iceberg, and the largest force during the indentation will be reduced. Methods of determining probabilities associated with iceberg impact have been presented by Christensen (1989).

Note that icebergs consist of snow-ice, which is normally fine -grained, fresh and stronger than the saline sea ice.

4.6 Lifting Forces

Long vertical wall

$$P_{max} = 0.6\,h\,(\sigma_f\,h_o\,\gamma_w)^{1/2} \qquad (4.6.1)$$

where h_o = water level increase

No account is gtiven to the velocity of water level change, because small plasticity occurs together with small velocity and high plasticity occurs together with high velocity.

Fig. 4.6.1 illustrates the conditions for various ice thickness for σ_f = 500 kPa

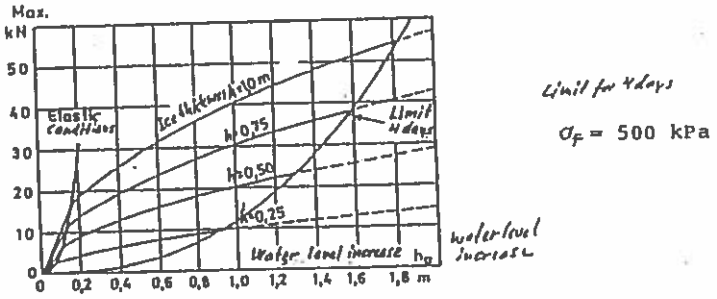

Fig. 4.6.1 Ice Lifting Forces at Vertical Wall

Piles

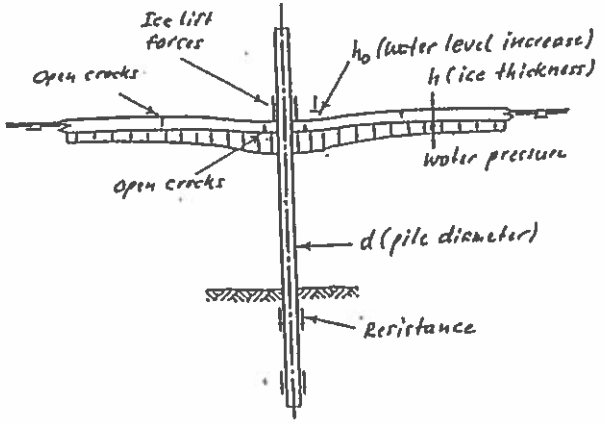

Fig. 4.6.2 Ice Lifting of Piles

Limited driving depths of piles in yachting harbours limit the lifting resistance (specialy in sand).

Minimum force to result in bending failure in ice:

$$P_{min} = \frac{\pi}{3} r_b h^2 \frac{a}{\ell} F(a/\ell) \quad \text{when } a/\ell = \alpha \tag{4.6.2}$$

$$F(\alpha) = \frac{(\text{kei}'\alpha)^2 + (\text{ker}'\alpha)^2}{\text{kei}\,\alpha\,\text{kei}'\alpha + \text{ker}\,\alpha\,\text{ker}'\alpha} \tag{4.6.3}$$

Characteristic length l:

$$\ell = \sqrt[4]{\frac{E h^3}{12\gamma(1-\nu^2)}} \tag{4.6.4}$$

Maximum lifting force (radial and tangential cracks)

$$P_{max} = 1.154\, r_b \cdot h^2 \cdot (1.05 + 2\alpha + 0.5\alpha^3) \tag{4.6.5}$$

In practice a probability. Estimate for median value (p_m = 50%):

$$P_m = 0.8\, \sigma_f\, h^{1.75} \cdot d^{0.25} \text{ (in kN when } \sigma_f \text{ in kPa, h and d in m)} \tag{4.6.6}$$

Example:

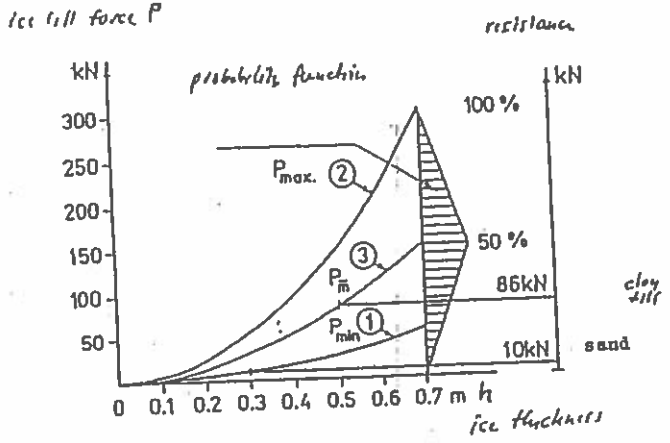

Fig.4.6.3 Ice-Lifting Force to Pile

Influence from soil conditions:

Soil type	Number of piles	Mean driving depth (m)	No. of piles lifted	% lifted
Sand	≅ 5000	3.50	1200	24
Clay till	≅ 9300	2.75	800	9

Table 4.6.1 Piles in Yachting Harbours Lifted

Lifting resistance versus driving depth l and pile diameter d:

Sand:

$$Q = \pi\, d\, l^2 \text{ (kN)} \tag{4.6.7}$$

Clay till:

$$Q = 1.25\, c_u\, d\, l \text{ (kN)} \tag{4.6.8}$$

c_u = undrained shear strength

For d = 0.25 m, l_{sand} = 3.5 m, l_{clay} = 2.75 m, c_u = 100 kPa results in
Q_{sand} = 9.6 kN
Q_{clay} = 86 kN

4.7 Ice Bearing Capacity

Both short term and long term capacity are to be considered, when the bearing capacity of ice is calculated.

Below is given a simple (short term) bearing capacity analysis:

For a concentrated unit load:

$$w = -\frac{P\ell^2}{2\pi D} \cdot \text{kei}\,(r/\ell) \tag{4.7.1}$$

w = deformation
P = load
r = radius
w = w(r)
D = bending stiffness
ν = Poissons ratio

Characteristic length l:

$$\ell = \sqrt[4]{\frac{E h^3}{12\gamma(1-\nu^2)}} = \sqrt[4]{\frac{D}{\gamma}} \tag{4.7.2}$$

Maximum deformation:

$$w_{max} = \frac{P\ell^2}{8D} \text{ because kei}\,(r/\ell) = -\pi/4 \tag{4.7.3}$$

For a load distributed over a circle with radius a, the maximum deformation is:

$$w_{max} = \frac{P(1 + \alpha\,\text{ker}'\alpha}{\pi\rho\alpha^2\ell^2} \text{ when } \alpha = a/\ell \tag{4.7.4}$$

The load may be determined from:

$$P = \frac{\pi\alpha\, r_b h^2}{3\,(1+\nu)\,\text{kei}\,'\alpha} \qquad (4.7.5)$$

when r_b = bending strength of ice

The analysis is based on infinite thin ice.

The conditions for finite ice thickness, h, is illustrated in Fig. 4.7.1 (versus h/l)

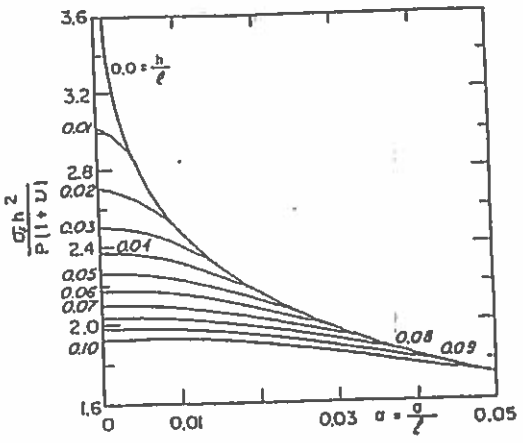

Figure 4.7.1 Dimensionless Force versus α for various h/l ratios (in the figure is used $\sigma = r_b$)

Example:
h = 0.5 m
r_b = 0.2 MPa
E = 5 x 10^9 Pa
γ = 10 kN/m^3
ν = 0.3

results in:

$$\ell = \sqrt[4]{\frac{5\;10^6\;0.5^3}{12\;10.0\,(1-0.3^2)}} = 8.70\,(\text{m})$$

$$D = \ell^4 \gamma_v = 5.7 \cdot 10^3 \cdot 10.0 = 5.72 \cdot 10^4$$

With a = 1.5 m, α = 1.5/8.7 = 0.17, kei'α = 0.2:

$$P = \frac{\pi\, 0.17\, 200\, 0.5^2}{3\,(1+0.3)\,0.2} = 34.2\ \text{kN}$$

5. DESIGN ICE FORCES

The choice of design forces from sheet ice must be based on the extreme strength and thickness together with interaction formulas, e.g. some of those described in chapter 4.

When ice floes are pushed against a structure, there are three basic limitations which may limit the load on the structure, viz.:

- limited ice strength (i.e. ice failure),
- limited driving force, and
- limited momemtum

each of which is addressed in this chapter. In order to calculate the ice loads, it is necessary to first determine the extreme (design) ice properties.

5.1 Design Ice Properties

Design criteria are normally based on the average recurrence time of a given situation, or if you will, the risk of exceeding a given situation in any one year. The first task of the (ice) design process is then to establish a relation between recurrence time and ice properties such as strength and thickness.

By looking at the formulas (2.2.3), (2.6.1), and (2.6.2) it becomes evident that both the strength and the thickness in some way increase when it becomes colder. The two parameters are not fully uncorrelated and cannot be combined if analysed separately unless the correlation is known. For this reason, the statistical analyses should be carried out of for the recurrence times of the products $\sigma_u h$ and $\sigma_i h^2$ instead. These products enter most formulas pertaining to crushing and/or bending failure of ice.

The recurrence time of the load due to ice crushing is determined by the recurrence time of the product $\sigma_u h$. In order to find this quantity the statistical distribution of $\sigma_u h$ must be known. If no combined values of σ_u and h exist for the area of interest, the statistical distribution of the product can be obtained as described below.

First the crushing strength is assumed to be given by the product of a reference strength and a function dependent on the salinity and temperature of the ice:

$$\sigma_u = \sigma_0\,(1-(\nu/0.275)^{1/2}) \qquad (5.1.1)$$

This formula is essentially eq. (2.6.2) with ν_0 = 0.275 as a first estimate except for the reference strength σ_0 which is introduced as a stochastic variable (rather than a constant) in this derivation. By use of the equation together with available test data, the value of σ_0 is calculated for each individual test and e.g. plotted in probability paper. A simple example is shown in Figure 5.1.1. It appears that ao tends to a Gaussian distribution having the probability density function:

$$f_1(\sigma_0) = (1 / (2\pi\lambda)^{0.5}) \exp(-0.5((\sigma_0 - \mu)/\lambda)^2)) \quad (5.1.2)$$

where λ is the standard deviation and μ the mean value. The following values were determined with the data in Figure 5.1.1:

$$\mu = 2.11 \text{ MPa} \quad (5.1.3)$$
$$\lambda = 0.528 \text{ MPa} \quad (5.1.4)$$

Hence, if combined values of temperature, salinity, and thickness of the ice are known the product $\sigma_u h$ can be determined.

In many cases such data sets do not exist, and instead some conservative assumptions are necessary. They could e.g. be:

- A constant ice salinity, S_{io}.
- The mean ice temperature is lowest at the end of the winter taking a value of half the mean air temperature of the coldest week in the winter.
- The ice thickness at the end of the winter is given by equation (2.2.3).

Based on these assumptions auh takes its maximum value at the end of the winter as both the strength and the thickness take their maximum values at that time. Evidently, the lowest air temperature in the winter is lower than the air temperature mentioned in the second assumption, but since it takes in the order of days for temperature waves to propagate to an appreciable depth, the crushing strength is determined by the mean temperature over a few days rather than the lowest temperature. The assumption that the coldest week is at the end of the winter is a conservative assumption.

The product of the maximum ice thickness and the temperature dependent part of equation (5.1.1) i.e.:

$$x = (1-(v/0.275)^{1/2})\ 0.032\ (K-50)^{1/2} \quad (5.1.5)$$

is determined for as many winters as possible. These values can e.g. be plotted in a Weibull paper in order to obtain a distribution for x. An example is shown in Figure 5.1.2. The Weibull distribution is expressed as:

$$F_2(x) = P(X < x) = 1 - \exp(-(x/\beta)^n) \quad (5.1.6)$$

The probability distribution for the product of thickness and crushing strength can now be expressed by:

$$P(Y < y) = \int_0^\infty F_2(y/\sigma_0)\, f_1(\sigma_0)\, d\sigma_0 \quad (5.1.7)$$

where

$$y = \sigma_0 (1-(v/0.275)^{1/2})\ 0.032\ (K-50)^{1/2} \quad (5.1.8)$$
$$y = \sigma_u h$$

This integral can be carried out, e.g. by means of a computer, and values of $\sigma_u h$ corresponding to various recurrence times can be determined.

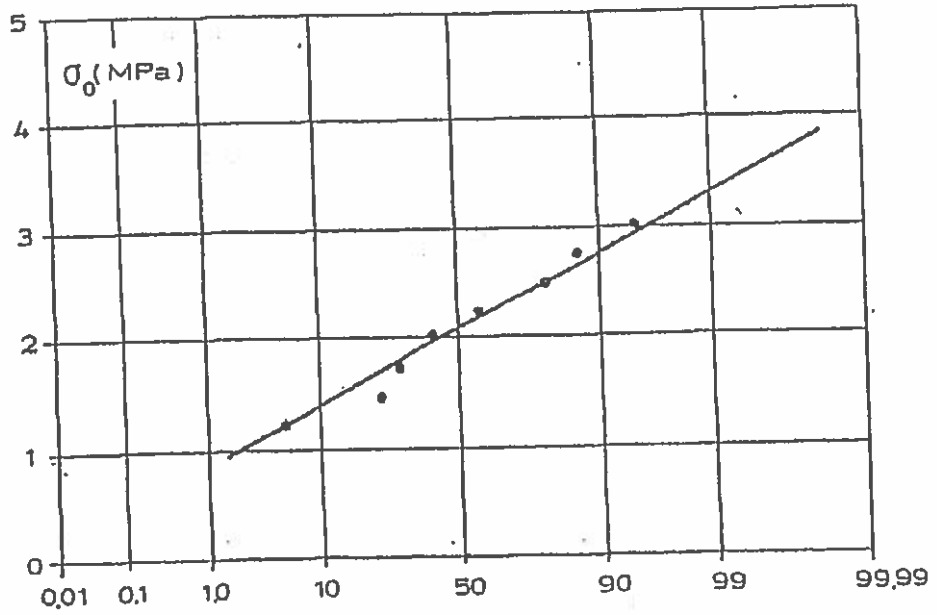

Figure 5.1.1 Gauss-plot of probability distribution of compressive~reference strength of ice. (Example).

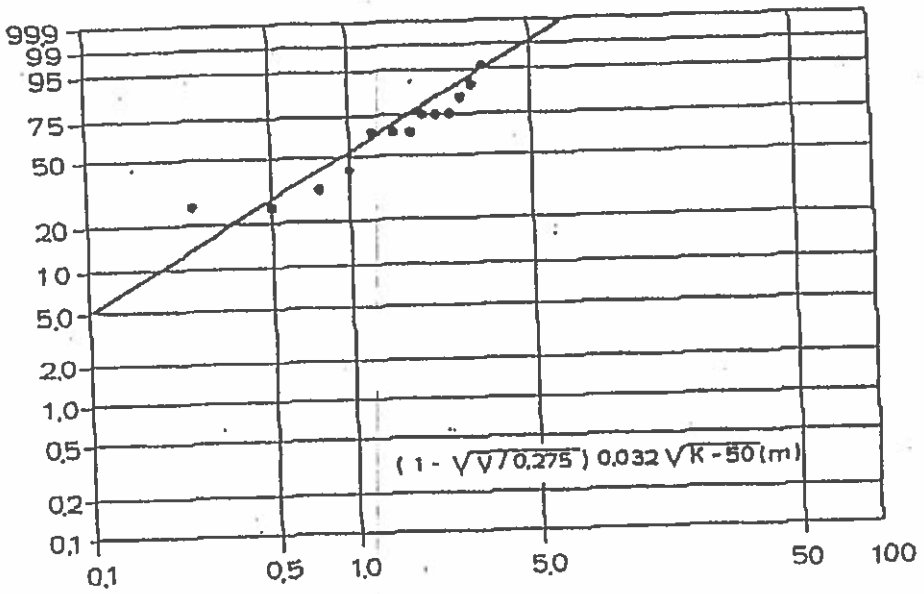

Figure 5.1.2 Weibull-plot of Non-exceedance probabilities for the temperature-dependent part of $\sigma_u h$. (Example).

The remaining problem is then to break the design value of the product $\sigma_u h$ down into a strength and a thickness. A simple way of doing this is to estimate the extreme thickness from the distribution of accumulated (over the entire winter) freezing degree-days, K. In most areas of the world it is possible to obtain an estimate of the distribution of K. A simple exponential distribution often suffice:

$$K = K_m(\ln(A)+a) \qquad (5.1.9)$$

where K_m is the average value of K, A is the average recurrence time in years and a is a constant determined by fitting the expression to available data. (Since in theory h is proportional to the square-root of K, the use of a Weibull distribution for thicknesses is a natural result of using an exponential distribution, which is a Weibull distribution with the power one, for K). The value of K corresponding to the prescribed recurrence time is then used to determine the extreme thickness through equation (2.2.3). Finally, the strength is determined by dividing the product $\sigma_u h$ with the extreme thickness, h. A similar analysis can be used for the flexural strength.

It should be emphasized that the choice of distribution of the product will influence the resulting values significantly, especially for extreme recurrence times. For low return periods the density of data points is normally relatively high. These points sdo not reflect extreme winter conditions, however. For the long; return periods, the density of data points normally is small.

This is unfortunate, because these points reflect the extreme winters which produce severe ice conditions. In extrapolation to extreme values the large number of less severe data will bias the extrapolation. It appears that the bias will be in the conservative direction in mild seasonal ice climates and in the non-conservative direction in severe arctic climates.

Finally, it is pointed out that in an improved extreme value analysis, the variability within the ice sheet under given conditions and the variability of environmental conditions should preferably be separated.

5.2 Ice Loads Limited by Stress

Technically, ice loads limited by stress, i.e. failure of the ice, can be determined with design properties as described in section 5.1 and interaction formulas as described in chapter 4. The thing to remember, though, is that these notes have only covered ice forces from sheet ice, to some extent from ridges, and in a very simplifed form from iceberg impact. Furthermore, not all loading scenarios and failure types have been considered/described.

To mention but a few, the "blocking" scenario and the "rubble field" -scenario have not been dealt with in these notes. Blocking occurs when a massive ice feature, e.g. a multi-year ice floe, comes to rest against a structure under conditions where failure of the multi-year floe does not occur. The limiting force may then correspond to failure of the advancing first-year ice sheet against the thicker and stronger multi-year floe. The massive multi-year floe has thereby increased the "effective diameter" of the structure. This increase can be substantial e.g. in the Beaufort Sea.

The "rubble field" scenario is a common situation around artificial islands in the Beaufort Sea, particularly in shallow waters. A field of ice rubble accumulates in front of an island, especially wide islands which make it difficult for the ice to clear around the sides. Often, though not always, the rubble pile will be grounded even in 15-20 metres of water. The rubble pile can form a vertical side against the advancing sheet ice, and in this way a wide sloping structure can become loaded by the same forces which apply to vertical structures. In most cases, however, the rubble field is believed to reduce the total force on the island, because the grounded rubble transmits some of the external force to the seabed. Attempts to quantify force transmission through rubble fields are in progress, see e.g. Sayed (1988).

5.3 Ice Loads Limited by Driving Forces

In some cases it is possible to prove that the driving forces are limited, e.g. by the floe size combined with extreme winds and currents. Physical features such as coasts or structures in some areas limit the maximum floe size. In other areas wave action might limit the floe size. Satellite data can be used to obtain floe size distributions, and maximum sizes of limited magnitude can sometimes be found. It is important, however, to consider the possibility of several floes pushing against a structure simultaneously, one behind the other.

In general, the load on the structure cannot exceed the driving forces on the ice except for cases where the ice possesses considerable momentum. If the calculated load exceeds the driving force, the limitation must be by momentum, or a mistake must be present.

When a limitation because of driving forces applies, it is very important to calculate whether the ice has sufficient momentum to cause a load larger than the driving force, or not.

5.4 Ice Loads Limited by Momentum

Ice floes with considerable kinetic energy can cause impact loads larger than the driving force on the ice itself. Icebergs are good examples of this.

The momentum limitation can be expressed by equating the kinetic energy of the ice floe, E_k, and the energy dissipated in ice crushing, E_c, and it reads:

$$E_k = 2\,MV^2\,(1+C_m) = \int_0^x F(x)\,dx = E_c \qquad (5.4.1)$$

where (1+Cm) accounts for the added mass of the ice feature, x is the indentation length (= ice movement after initial contact) and F is the interaction force which normally depends on the indentation length. From equation (5.4.1) plus the geometries of the ice feature and the structure, F(x) can be determined. If the kinetic energy is sufficient to cause development of an interaction width equal to the structure width, the force is no longer limited by the momentum, but by the failure stress.

5.5. Basic Design Rules for Ice Engineers

When you are faced with the challenge of selecting a design ice load, make sure that you always:

- calculate an upper bound design ice load, which you can thoroughly prove to be conservative. Use advanced methods and all your skills to provide the lowest possible upper bound force.
- calculate a central estimate (or even a lower bound) of the design ice force. Realistic estimates can e.g. be based on published measurements. Have a colleague review your calculation, and see if he/she also finds it realistic.
- compare the two calculated loads. If the difference is too large, search for an explanation. Your upper bound might be too conservative, or your central estimate might be unrealistic.
- repeat the process for all relevant failure types and/or limitations which are likely to occur. (This note has not given formulas for all failure types).
- have your design checked by someone with up-to-date experience in ice engineering. Being a developing field, new understandings are continuously gained, and you should naturally exploit the most recent results available from research.

6. CODES AND STANDARDS

Many countries and/or authorities have established design codes in the field of ice forces. Many of them are young codes, which are quickly outdated as new research yields new insight. Some of the ice codes and recommendations, which the author knows of, are listed below.

USA, American Petroleum Institute, American Petroleum Institute (1982)

USA, American Association of State, American Association of State Highway and Transportation Highway and Transportation Officials, Officials (1978)

Canada, Gulf, Esso and Dome Petroleum, Beaufort Sea-Mackenzie Delta Environmental Impact Statement, ,Vol. 3A (1982)

Canada, Canadian Standards Association, Canadian Standards Association, Bridge Code (1978) Lighthouse practice

Canada, Canadian Standards Association, Canadian Standards Association Preliminary Standard 5471, (1988) Part 1

USSR, State Committee of the Council of Ministers for Construction, SN-76-66 (1967)

Norway, Norwegian Petroleum Directorate, Norwegian Petroleum Directorate (1987)

Denmark, Danish Engineering Association, Danish Engineering Association, Danish Standard, DS410, (1999)

Sweden, Vägverket (Eng.: The Road Directorate), Löfquist,(1987) Istryck mot bropelare (Eng.: Ice pressure on bridge piers)

The various codes are briefly reviewed and compared in the following:

6.1 Codes for Vertical Structures

The Danish Code of Practice, DS410 (published by the Danish Engineering Association (1999)), is based on the same idea as the formula by Afanas'yev et al. The horizontal force is given in DS410 as:

(6.1.1)

$F_e = k\,\sigma_u\,b\,h$

$k = 1+3/(1+b/h)$ $\quad 0 < b/h < 9$

$k = 1.75-0.05b/h$ $\quad 9 < b/h < 15$

$k = 1$ $\quad 15 < b/h$

where k is a dimensionless factor which is a function of the aspect ratio, b/h, as shown. It does not depend on the shape of the vertical pier.

In typical design situations the aspect ratio (projected structure width to ice thickness) will not fall below approximately 1, and it will probably not exceed say about 40.

This leads to coefficients from about 2.5 down to 1.0. In comparison the Swedish recommendation by Löfquist (1987) , gives a coefficient of 0.8 for aspect ratios larger than four and a coefficient of 1.3 for an aspect ratio of one.

The presented formulas are reasonable for an impact parallel to the long axes of a rectangular structure, but for oblique impacts the use of a projected width will probably lead to an overestimation of the forces, as argued by Neill (1981), who states that the upstream end (nose) of e.g. bridge piers will tend to cut through the ice floe while it rotates to pass along the exposed side of the pier. Thus the failure mode (in Neill's view) is not a simultaneous crushing over the entire (projected) contact area. Correct determination of longitudinal and transverse forces resulting from an oblique impact of an ice floe requires special analyses.

Various other design codes exist, notably by the American Petroleum Institute (1982), the Canadian Standards Association (1978) and the Swedish Vagverket (Löfquist, 1987). The American Petroleum Institute recommends using $F = C\,\sigma_u\,b\,h$ where C is in the range from 0.3 to 0.7. For the Cook Inlet in Alaska which is characterized by a tidal flow that never leaves the ice at rest, a factor of 0.55 is recommended specifically. An application of the API code was presented by Utt et al. (1987)

The Canadian Standards Association (1978) recommends using $F = p_e\,b\,h$ where p_e is an effective ice pressure. Prior to 1974 this was given as 2.76 MPa, and after 1974 a range from 0.69 to 2.76 MPa has been suggested. The CSA has not given limits to the applicability of the formula. A new Canadian Standard is very close to being. published.

The ice crushing strength is strongly dependent on salinity, temperature, and loading rate, as already mentioned. Korzhavin and Afanas'yev et al. have analysed their experiments but not suggested design values for strength. Various design codes suggest strengths in the range from as low as 0.7 MPa to as high as 3.5 MPa.

The coefficient of proportionality between F and $\sigma_u\,b\,h$ has often been split into a series of factors such as:

- an indentation coefficient taking into account the biaxial stress state in the ice in front of the structure,
- a shape factor taking into account the upstream shape of the structure,
- a contact coefficient taking into account non-simultaneous failure along the structure, and
- a correction coefficient taking into account the velocity of the ice in the interaction process.

Most design codes are in some way based on the two original formulas by Korzhavin and by Afanas'yev et al. For large ice floes with sizes exceeding say 15 times the structure width, Korzhavin's coefficient of proportionality equals 2.5 regardless of aspect ratio, b/h. Afanas'yev et al.'s coefficent, $C = 5(h/b+1)^{1/2}$ is approximately equal to Korzhavin's indentation coefficient when the aspect ratio equals unity. If the effect of the biaxial stress pattern on the force is assumed to be independent of the structure size itself, Korzhavin's formula must underestimate forces for small aspect ratios and overestimate forces for large aspect ratios. All in all, Afanas'yev et al.'s coefficient appears far more reasonable than Korzhavin's.

For aspect ratios less than approximately 11 the Danish Code of Practice, DS410, is slightly more conservative than the formula by Afanas'yev et al. For aspect ratios larger than 11 Afanas'yev et al.'s formula is the,most conservative of the two, especially for aspect ratios above 15. It should be remembered, though, that Afanas'yev et al. gave $b/h < 6$ as an upper limit for applicability of their formula. The tests on which the formula is based did not cover aspect ratios higher than 6.

The more up-to-date recommendation for wide structures is contained in the Canadian "Beaufort Sea-Mackenzie Delta Environmetal Impact Statement" (1982), Vol. 3A. The EIS (which it is called for a shortname) was prepared by Dome Petroleum, Esso Resources Canada, and Gulf Canada. It expresses their experience with operations in the Canadian arctic with special emphasis on the impact on the environment. A part of it (Vol. 3A) deals with ice loads on structures. Figure 6.1.1 shows their recommendation for global ice pressure on offshore structures as a function of the aspect ratio, structure width to ice thickness. Note that the y-axis values are not dimensionless, and consequently cannot be used directly elsewhere.

This curve and the data that support it are likely to support the new Canadian Standard which is due to be published very soon, (Canadian Standards Association, 1988).

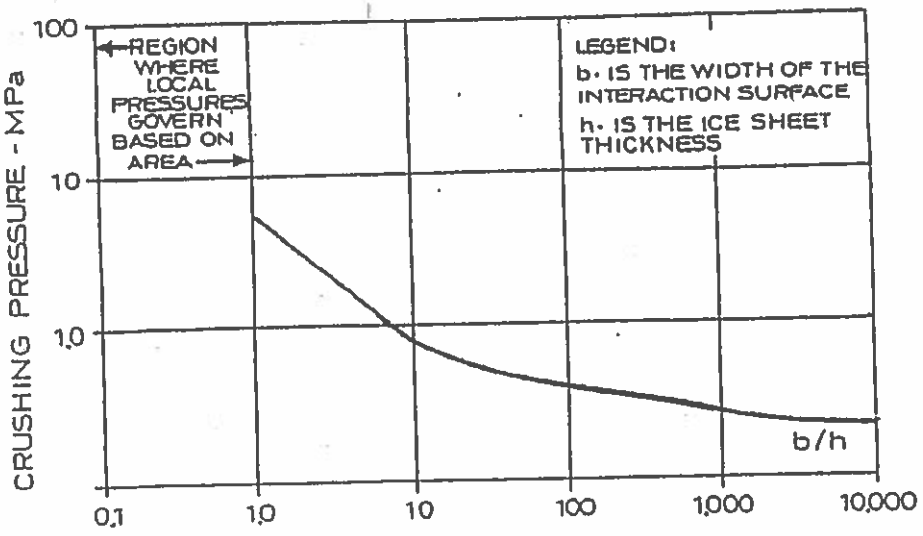

Figure 6.1.1 Pressure-aspect ratio diagram according to the Canadian Beaufort Sea-Mackenzie Delta Environmental Impact Statement (1982).

6.2 Codes for Inclined Structures

Four of the mentioned codes give formulas for ice forces on inclined structures. The Soviet code, SN-76-66 (1967) gives for the horizontal force on inclined bridge piers:

$$F = A \tan\alpha \, \sigma_f \, h^2 \qquad (6.2.1)$$

where α is the surface slope angle, and A is a regional climate coefficient varying between 0.75 and 2.25. The formula is independent of pier width and should only be applied where it was meant. It need not be correct under different climatic conditions.

The Canadian Standards Association in their 1974 code (CSA S6 1974) recommended reduction factors:

$$C_n = 1.00 \text{ for } 75^\circ < \alpha < 90^\circ \qquad (6.2.2)$$

$$C_n = 0.75 \text{ for } 60^\circ < \alpha < 75^\circ \qquad (6.2.3)$$

$$C_n = 0.5 \text{ for } 45^\circ < \alpha < 60^\circ \qquad (6.2.4)$$

to be multiplied with the force recommended for the corresponding vertical pier. The angle α is the angle between the upstream face and the horizontal.

The Canadian Lighthouse Practice recommends the formula:

$$F = m \sin^2\alpha \, \sigma_f \, b \, h \qquad (6.2.5)$$

where m is a combined shape and contact coefficient (dimensionless) varying between 0.4 and 0.9, see Iyer (1978).

Finally, the American Petroleum Institute (1982) recommends using Ralston's plastic limit analysis as described in section 4.2.

The wider the structure, the more important the ride-up part of the force is. The formulas considering ride-up forces are Ralstons, Edwards and Croasdale's and the 2D theories, cf. section 4.2. The other reviewed formulas were meant for bridge piers. For the very wide structures it will be necessary to consider the formation of an ice rubble field.

The formulas based on bending failure should show proportionality with h^2 and with the length of the circumferential crack. The 2D theories and Korzhavin's formula do not agree with this. They show proportionality with $h^{5/4}$ and h, respectively, making these formulas less sensitive to variations in ice thickness. The simple 2D theory and Korzhavin's formulas suggest proportionality with the structure width. This appears sensible for wide structures, but will lead to underestimation of forces on narrow structures. The adjusted 2D theory with its lack of a structure i width dependence in the ice-breaking term, on the other hand, will overestimate the force on narrow structures and underestimate the force on wide structures.

The Soviet code and Edwards and Croasdale's formula lack dependence on both structure width and characteristic length of the ice. These two formulas should consequently be used only for narrow structures.

Afanas'yev et al.'s formula can be rewritten:

$$F = (0.41 + 0.46\, b/l) \tan\alpha \, \sigma_f \, b \, h^2 \qquad (6.2.6)$$

where b is the diameter of the conical structure at the water line and l the characteristic length. This illustrates the two proportionalities, one with h^2 and one with bh^2/l or $bh^{5/4}$. It is then seen that for narrow structures ($b/l \rightarrow 0$) the formula approaches the ice-breaking term of Edwards and Croasdale's formula. On the other hand an increasing width, b, results in an increased force, which makes sense.

Ralston's formula is also split in two terms, but it is far more sensitive to variations in structure width because the second term includes b^2.

Some numerical examples are given for two conical structures. Bear in mind that the formulas by Tryde and Korzhavin and the Codes, except the API recommendation, were intended for bridge piers with inclined upstream faces and vertical sides.

The following data are applied:

Narrow cone diameter at water level, b	3.0 m
Wide cone diameter at water level, b	20.0 m
Surface slope angle, α	45°
Ice thickness, h	1.0 m
Uniaxial crushing strength, σ_u	2.76 MPa
Flexural strength, σ_f	1.38 MPa
Shear strength, τ	0.69 MPa
Young's modulus, E	7.0 GPa
Poisson's ratio,v	0.33
Gravitational acceleration, g	9.81 m/sec^2
Friction coefficient, μ	0.1

The resulting horizontal forces are shown in the tables below:

Formula	Breaking (MN)	Ride-up (MN)	Total (MN)
Simple 2D theory	0.120	0.045	0.165
Adjusted 2D theory	1.565	0.045	1.610
Ralston	2.710	0.035	2.745
Edwards & Croasdale	2.210	0.175	2.385
Afanas'yev et al.	1.072	-	1.072
Tryde	0.900	-	0.900
Korzhavin	0.660	-	0.660
SN-76-66	0.845	-	0.845
CSA S6 1974	4.140	-	4.140
Can. Lighthouse	3.726	-	3.726

Table 6.2.1 Forces on a narrow conical structure with b = 3.0 metres.

Note how small the ride-up portion is on a narrow structure. This changes for a wide structure as seen from the other example. Of the formulas above the dashed line, Ralston's is consistently the most conservative.

Formula	Breaking (MN)	Ride-up (MN)	Total (MN)
Simple 2D theory	0.800	1.860	2.660
Adjusted 2D theory	1.565	1.860	3.425
Ralston	3.755	1.360	5.115
Edwards & Croasdale	2.210	1.175	3.385
Afanas'yev et al.	1.545	-	1.545
Tryde	7.650	-	7.650
Korzhavin	4.420	-	4.420
SN-76-66	0.845	-	0.845
CSA S6 1974	27.600	-	27.600
Can. Lighthouse	24.840	-	24.840

Table 6.2.2 Forces on a wide conical structure with b = 20.0 metres

In both examples, the Canadian codes (which were not developed for conical structures) overestimate the force.

In conclusion for inclined structures, it is suggested to use:

- simple 2D theory for wide structures when ice clearing can take place,
- formulas for vertical structures when the inclined structure is so wide that ice clearing is hindered,
- Ralston's formula for conical structures,
- the largest force of Tryde's, Korzhavin's and the one by SN-76-66 for narrow bridge piers with inclined upstream faces, and
- formulas for vertical structures when the surface slope angle exceeds 70°

unless model experiments are carried out.

7. A SHORT GUIDE TO RELEVANT LITERATURE

7.1 Books

Books on ice engineering are scarce, but several good manuscripts have been published very recently. Below five major references are mentioned:

A.B. Cammaert and D.B. Muggeridge (1988)"Ice Interaction with Offshore Structures" Van Nostrand Reinhold, 11 New Fetter Lane, London EC4 P4EE,England

This book is written specifically with offshore structures in mind, which gives it a well-limited scope and a clear and logical presentation. It goes relatively deep into ice properties, which is necessary for the understanding of the limitations of theories and practices. The ice-structure interaction chapters are well written, and the authors avoid too much detail where unnecessary. A more comprehensive chapter on selection of design forces would have improved it greatly, but that is strictly speaking more statistics than ice engineering.

The topic of dynamic ice loads will receive more attention in the future. This book is one of the first to address these problems. Finally, some brief chapters on physical modelling, laboratories, and on "special topics" such as uncertainty, icing, monitoring, forecasting, and ice control are included. Unfortunately, the book is brief on what concerns remote sensing, computational modelling, and forecasting. Overall, this book presents an excellent description on ice-structure interaction.

T.J.O. Sanderson (1988) "Ice Mechanics; Risks to Offshore Structures" Graham and Troman Limited, Sterling House, 66 Wilton Road, London SW1V 1DE, England

In terms of quality this book levels with that of Cammaert and Muggeridge. Sanderson's chapters on ice types, ice occurrence, and morphology are particularly well written and very informative for newcomers in the field. The book concentrates on vertical-sided structures for the arctic environment, especially the wide structures in the shallow areas of the Beaufort Sea. An excellent chapter on selection of design loads completes the book.

This book is a very good reference together with the first one described. They do overlap in considerable areas, but each have their strong points. The first is written by engineers, which you can sense from the logical presentation. The second one, Sanderson's, is written by a talented designer, who had to deal with real ice (which does not always look like you draw it on paper), and who had to make some very real design decisions. The combination of these two books offers a very comprehensive understanding of ice-structure interaction.

G.D. Ashton, editor (1986) "River and Lake Ice Engineering" Water Resources Publications, P.O. Box 2841, Littleton, Colorado 80161, USA

As the title says, this is not an offshore-related book. All the physics and mechanics of ice, however, are still relevant. The book has been put together from contributions by a long list of researchers in the field of ice engineering. It includes chapters on river ice problems and ice control in waterways. It has a brief chapter on remote sensing (which is these years becomes outdated rather quickly) and a chapter on icebreaking ships. It gives a somewhat broader view of ice engineering than the first two books mentioned before, and it does not address offshore structures as such.

B. Michel (1978) "Ice Mechanics" Les Presses de l'.Universite Laval, Quebec, Canada

This book seems to be available in many university libraries because it was the only textbook on ice for many years. Anyhow, it lacks many of the newer developments. It is a good book on the mechanics of ice, but unfortunately it contains quite a few printer's errors, so be careful with its equations. And if you are determining design ice loads, you should acquire a more up-to-date reference.

E. Eranti and G.C. Lee (1986) "Cold Region Structural Engineering" McGraw-Hill

If you are dealing with a project that involves onshore operations in cold regions you will find this book of assistance. It also includes chapters on ice-structure interaction although less comprehensive than those described above. The book is written from a contractor's point of view. If you are interested in earth works, machinery, utility lines, etc. in cold regions this book is worth looking at.

Paperbacks published by the Technical Council on Cold Regions Engineering

Finally, the paperbacks published occasionally by the Technical Council on Cold Regions Engineering under the ASCE must be mentioned. They are usually advertised in "Civil Engineering" Magazine (US version).

7.2 Journals

Problems related to ice loads on offshore structures may appear in "Ice" journals as well as in offshore journals. The "ice" journals which should be reviewed by anyone interested in this field are:

- Journal of Cold Regions Engineering, ASCE
- Cold Regions Science and Technology, Elsevier
- Journal of Offshore Mechanics and Arctic Engineering, ASME
- Journal of Hydraulic Research, IAHR
- Journal of Glaciology, Int. Glaciological Society

Also of interest with occasional ice-related articles are:

- Journal of Waterway, Port, Coastal and Ocean Eng., ASCE
- Canadian Geotechnical Journal (especially for ice mechanics)
- Journal of Energy Resources Technology, ASME

Finally to be mentioned is:

- Iceberg Research, Scott Polar Research Institute, England.

7.3 Conference Proceedings

The following conferences result in proceedings with good quality material on ice-structure interaction:

- Offshore Mechanics and Arctic Engineering, OMAE
- Port and Ocean Engineering under Arctic Conditions, POAC
- Int. Assoc. of Hydr. Res. Symposia on Ice, IAHR
- Offshore Technology Conference, OTC
- Polartech

and there are always regional conferences of interest, such as Canadian Coastal Conference, ASCE Specialty Conferences, etc.

REFERENCES

Afanas'yev, V.P., I.V. Dologopolov and Z.I. Shvayshten (1971): "Ice Pressure on separate supporting Structures in the Sea". U.S. Army Cold Regions Research and Engineering Laboratory, Draft Translation 346.

American Association of State Highway and Transportation Officials (1978): "Interim Specifications for Highway Bridges", AASHTO, Washington DC, USA.

American Petroleum Institute (1982). "Planning, Designing and Constructing Fixed Offshore Structures in Ice Environments", Bulletin 2N, American Petroleum Institute, Washington D.C.

Ashton, G.D. (1985): "Deterioration of floating ice covers", Journal of Energy Resources Technology, 107 (June): 177-182.

Ashton, G.D., (1986): "River and Lake Ice Engineering", Water Resources Publications, Colorado, USA.

Beaufort Sea - Mackenzie Delta Environmental Impact Statement (1982), Vol. 3A, Prepared by Dome Petroleum Ltd., Esso Resources Canada Ltd. and Gulf Canada Inc. Available from: Pallister Resource Management, Bay 105, 4116-64th Ave. SE., Calgary, Alberta, Canada T2C 2B3.

Bercha, F.G. and J.V. Danys (1975): "Prediction of ice forces on conical offshore structures", Marine Science Communications, 1(5): 365-380.

Bergdahl, L. (1977): "Physics of ice and snow as affects thermal pressure", Report Series A:1, Department of Hydraulics, Chalmers University of Technology, Gothenburg, Sweden.

Bergdahl, Lars (1978): "Thermal Ice Pressure in Lake Ice Covers". Report Series A:2, Department of Hydraulics, Chalmers University of Technology, Gothenburg,-Sweden.

Bergdahl, Lars and Lars Wernersson (1978): "Calculated and Expected Thermal Ice Pressures in five Swedish Lakes". Report Series B:7, Department of Hydraulics, Chalmers University of Technology, Gothenburg, Sweden.

Blenkarn, K.A. (1970): "Measurements and analysis of ice forces on Cook Inlet Structures", Proc. Offshore Technology Conference, Paper OTC 1261, Vol.2, pp. 365-378, Houston, Texas, USA.

Cammaert A.B. and D.B. Muggeridge (1988) : "Ice Interaction with Offshore Structures", Van Nostrand Reinhold, London, England.

Canadian Standards Association (1978): "Design of Highway Bridges", Standard CAN3-56-M78.

Canadian Standards Association (1988): "General requirements, design criteria, environment, and loads", Preliminary Standard S471, Part 1, CSA code for the design, construction and installation of fixed offshore structures. Draft. Rexdale, Ontario, Canada.

Christensen, F.T. (1988): "Calculation of optimal dimensionless coefficients for Ralston's plastic limit analysis approach to determination of sheet ice loads on conical structures". Progress Report 66, pp. 35-38 Institute of Hydrodynamics and Hydraulic Engineering (ISVA), Technical University of Denmark, February 1988.

Christensen, F.T. (1989): "Efficiency of Detachable Platforms in the Arctic", ASCE Journal of Cold Regions Engineering, Vol. 3, No. 1, pp. 37-54, March 1989.

Christensen, F.T., N.-E. Ottesen Hansen, K.-U. Evers, S. Spangenberg and L.J. Vincentsen (1989a): "Design of the Great Belt Western Bridge for Ice Forces", 8th int. conf. on Offshore Mechanics and Arctic Engineering (OMAE-89), Vol. 4, pp. 365-376, the Hague, the Netherlands.

Christensen, F.T., N.-E. Ottesen Hansen, S. Spangenberg and L.J. Vincentsen (1989b): "Dynamic ice loads on the Great Belt Western Bridge", 10th int. conf. on Port and Ocean engineering under Arctic Conditions (POAC-89), Luleaa, Sweden.

Cox, G.F.N. and W.F. Weeks (1983): "Equations for determining the gas and brine volume in sea ice samples", Journal of Glaciology, 29(102): 306-316.

Croasdale, K.R. (1978): "Ice forces on rigid structures". Report of the Working Group on ice interaction with hydraulic structures, International Association of Hydraulic Research.

Croasdale, K.R. (1980): "Some implications of ice ridges and rubble fields on the design of Arctic Offshore Structures", Proc. Nat. Res. Council of Canada Workshop on Sea Ice Ridging, Calgary, Technical Memo 134, pp. 157-180, NRC of Canada, Ottawa, Canada.

Croasdale, K.R. (1988): "Ice Forces : Current Practices", Proc. 7th int. conf. on offshore Mechanics and Arctic Enginering (OMAE-88), Vol. 4, pp. 133-151, Houston, Texas, USA.

Croasdale, K.R., N.R. Morgenstern and J.B. Nuttall (1977): "Indentation tests to investigate ice pressures on vertical piers", Journal of Glaciology, 19(81): 301-312.

Danish Engineering Association (1982): "Code of Practice for the Safety of Structures, DS 409 and DS 410.

Edwards, R.Y. and K.R. Croasdale (1976): "Model experiments to determine ice forces on conical structures", Preprint, Applied Glaciology Symposium, Cambridge, England.

Eranti, E. and G.C. Lee (1986): "Cold Region Structural Engineering", McGraw-Hill.

Frankenstein, G.E. and R. Garner (1967): "Linear Relationship of Brine Volume and Temperature from –0.5°C to –22°C for Sea Ice". Journal of Glaciology, 6(48): 943-944.

Gershunov, E.M. (1987): "Structure-ridge interaction", Cold Regions Science and Technology, 14(1): 85-94.

Gold, L.W. (1958): "Some observations on the dependence of strain on stress for ice", Canadian Journal of Physics, 36(10): 1265-1275.

Iyer, S.H. (1978): "Existing Ice Codes and suggested Criteria". Proc. 5'th Int. Assoc. of Hydr. Res. (IAHR) Ice Symposium, Luleaa, Sweden.

Johnson, R.C. and D.E. Nevel (1985): "Ice impact structural design loads", Proc. 8'th int. conf. on Port and Ocean engineering under Arctic Conditions (POAC-85), Vol. 2, pp. 569-578, Narssarssuaq, Greenland.

Korzhavin, K.M. (1962): "Action of Ice on Engineering Structures". U.S. Army Cold Regions Research and Engineering Laboratory, Draft Translation 260, 1971.

Lainey, L. and R. Tinawi (1984): "The mechanical Properties of Sea Ice - A Compilation of available Data", Canadian Journal of Civil Engineering, Vol. 11, No. 4, pp. 884-923.

Lee, J., T.D. Ralston and D.H. Petrie (1986): "Full-thickness sea ice strength tests". Proc. 8'th Int. Assoc. of H-dr. Res. (IAHR) Ice Symposium, Vol. 1, pp. 293-306, Iowa City, Iowa, USA.

Löfquist, Bertil (1987): "Istryck–mot Bropelare" (in Swedish). Dokument 1987:43, Vagverket, CentralforrAdet, Knivsta, Sweden.

Michel, B. and R.O. Ramseier (1971): "Classification of River and Lake Ice", Canadian Geotechnical Journal, 8(36): 36-45.

Michel, B. (1978): "Ice Mechanics", Les Presses de l'Universite Laval, Quebec, Canada.

Nadreau, J.P. and B. Michel (1984): "Ice Properties in relation to Ice Forces". Proc. 7'th Int. Assoc. of Hydr. Res. (IAHR) Ice Symposium, Vol. 4, pp. 63-115, Hamburg, West Germany.

Neill, C.R. (editor) (1981): "Ice Effects on Bridges". Published by Roads and Transportation Association of Canada, 1765 St. Laurent Blvd., Ottawa, Canada K1G 3V4.

Nevel, D.E. (1986): "Iceberg impact forces". Proc. 8'th Int. Assoc. Hydr. Res. (IAHR) Ice Symposium, Vol. 3, pp. 345-369, Iowa City, Iowa, USA.

Norwegian Petroleum Directorate (1987): "Guidelines for the determination of loads and load effects", Stavanger, Norway. This is an appendix to the "Regulation for the structural design of load bearing structures intended for exploitation of petroleum resources" published in 1984 by the Norwegian Petroleum Directorate.

Petrie, D.H. and J.P. Poplin (1986): "Comparison of small-scale and large-scale sea ice strengths", Proc. 8'th Int. Assoc. Hydr. Res. (IAHR) Ice Symposium, Vol. 1, pp. 265-276, Iowa City, Iowa, USA.

Peyton, H.R. (1968): "Ice and Marine Structures", Part 1 in Ocean Industry, March 1968, pp. 40-44, Part 2 in Ocean Industry, September 1968, pp. 59-65, Part 3 in Ocean Industry, December 1968, pp. 51-63.

Ponter, A.R.S. et al. (1983): "The force exerted by a moving ice sheet on an offshore structure, Part 1, he creep mode", Cold Regions Science and Technology, 8(2): 109-118.

Prodanovic, A. (1981): "Upper bounds of ridge pressure on structures", Proc. 6th Int. conf. on Port and Ocean Engineering under Arctic Conditions (POAC-81), Vol. 3, pp. 1288-1298, Quebec City, Quebec, Canada.

Ralston, T.D. (1977): "Ice force design considerations for conical offshore structures", Proc. 4'th int. conf. on Port and Ocean Engineering under Arctic Conditions (POAC-77), Vol. 2, pp. 741 -752, St. John's Newfoundland, Canada.

Ralston, T.D. (1978): "Analysis of ice sheet indentation", Proc. 5th Int. Assoc. of Hydr. Res. (IAHR) Ice Symposium, Vol. 1, pp. 13-31, Luleaa, Sweden.

Ralston, T.D. (1979): "Plastic limit analysis of sheet ice loads on conical structures". Proc. of IUTAM Symposium on Physics and Mechanics of Ice, pp. 289-308, Copenhagen, Denmark. (Edited by P. Tryde).

Rojansky, M. and B.C. Gerwick (1981): "Failure modes and forces of pressure ridges acting on cylindrical towers", Proc. 6th int. conf. on Port and Ocean engineering under Arctic Conditions (POAC-81), Vol. 2, pp. 663-673, Quebec City, Quebec, Canada..

Saeki, H., K. Hamanaka and A. Ozaki (1977): "Experimental study of the ice forces on a pile, Proc. 4th int. conf. on Port and Ocean engineering under Arctic Conditions (POAC -77), Vol. 2, pp. 695-706, St. John's, Newfoundland, Canada.

Sanderson, T.J.O. (1984a): "Theoretical and measured Ice Forces on wide Structures". Proc. 7'th Int. Assoc. of Hydr. Res. (IAHR) Ice Symposium, Vol. 4, pp. 151-207, Hamburg, W. Germany.

Sanderson, T.J.O. (1984b): "Thermal Ice Forces against isolated Structures". Proc. 7'th Int. Assoc. of Hydr. Res. (IAHR) Ice Symposium, Vol. 4, pp. 289-299, Hamburg, W. Germany.

Sanderson, T.J.O. (1986): "A pressure-area curve for ice". Proc. 8'th Int. Assoc. Hydr. Res. (IAHR) Ice Symposium, Vol. 2, pp. 361-384, Iowa City, Iowa, USA.

Sanderson, T.J.0. (1988): "Ice Mechanics, Risks to Offshore Structures", Graham and Trotman Limited, London, England.

Sanderson, T.J.O. and A.J. Child ,(1986) :"Ice loads on offshore structures. The transition from creep to fracture". Cold Regions Science and Technology, 12(2):157-162.

Sayed, M. (1988): "Transmission of loads through grounded ice rubble", Proc. 9th Int. Assoc. of Hydr. Res. (IAHR) Ice Sympo sium, pp. 692-707, Sapporo, Japan.

Schwarz, J., K. Hirayama and H.C. Wu (1974): "Effect of ice thickness on ice forces", Proc. 6th Offshore Technology Conference, Paper OTC 2048, Volume 2, pp. 145-155, Houston, Texas, USA.

Schwerdtfeger, P. (1963): "The thermal properties of sea ice", Journal of Glaciology, Vol. 4, No. 36, pp. 789-807.

SN-76-66 (1967): "Instructions for determining ice loads on riverstructures", State Committee of the Council of Ministers of Construction, Published in Russian by Izdatel'stvo Literatury PoStroitel'stvu in Moscow 1967, translated into English by the National Research Council of Canada as their technical translation TT-1663 in 1973.

Sodhi, D.S. and K. Kato (1983): "Ice action on pairs of cylindrical and conical structures", Report 83-25, Cold Regions Research and Engineering Laboratory, New Hampshire, USA.

Timco, G.W. (1986): "Ice forces on multi-legged structures", Proc. 8'th Int. Assoc. Hydr. Res. (IAHR) Ice Symposium, Vol. 2, pp. 321-337, Iowa City, Iowa, USA. .

Timco, G.W. and R.M.W. Frederking (1986): "Confined compression tests: Outlining the Failure Envelope of Columnar Sea Ice", Cold Regions Science and Technology, 12(1): 13-28.

Timco, G.W. and I.J. Jordaan (1987): "Time-series variations in ice crushing", Proc. 9'th int. conf. on Port and Ocean Engineering under Arctic Conditions (POAC-87), Fairbanks, Alaska, USA.Preprint.

Timco, G.W. and R.M.W. Frederking (1990): "Compressive strength of sea ice sheets", Cold Regions Science and Technology, 17(3): 227-240.

Tryde, P. (1975): "Intermittent ice forces acting on inclined wedges", Proc. 4th Int. Assoc. of Hydr. Res. (IAHR) Ice Symposium, pp. 339-343, Hanover, New Hampshire, USA.

Trætteberg, A., L.W. Gold and R. Frederking (1975): "The Strain Rateand Temperature Dependence of Young's Modulus of Ice", Proc. ; 4'th Int. Assoc. Hydr. Res. (IAHR) . Ice Symposium, pp. 479-486, Hanover, New Hampshire, USA.

Utt, M.E., K.D. Vaudrey and B.E. Turner (1987): "Design Sea Ice Load Examples using API Recommended Practice 2N" Proc. 9th int. conf. on Port and Ocean engineering under Arctic Conditions (POAC-87), Vol. 1, pp. 387-393, Fairbanks, Alaska, USA.

Vivatrat, V. and S. Slomski (1984): "Probabilistic selection of ice loads and pressures". ASCE, J. Waterway, Port Coastal and Ocean engineering, 110(4): 375-391.

Walden, J.T., J.T. Baldwin, S.D. Hallam and G.A.N. Thomas (1987a): "Prediction of Multi-year Ice Impact Loads utilizing Hans Island data", Proc. 9th int. conf. on Port and Ocean engineering under Arctic Conditions (POAC-87), Preprint, Fairbanks, Alaska, USA.

Walden, J.T., S.D. Hallam and J.T. Baldwin (1987b): "An explicit technique for calculating first-year ice loads on structures", Proc. 6th int. conf. on Offshore Mechanics and Arctic Engineering (OMAE-87), Vol. 4, pp. 267-272, Houston, Texas, USA.

Weeks, W.F. and A. Assur (1967): "The mechanical Properties of Sea Ice". Cold Regions Science and Engineering, Part II, Section C. (Old CRREL Monograph Series).

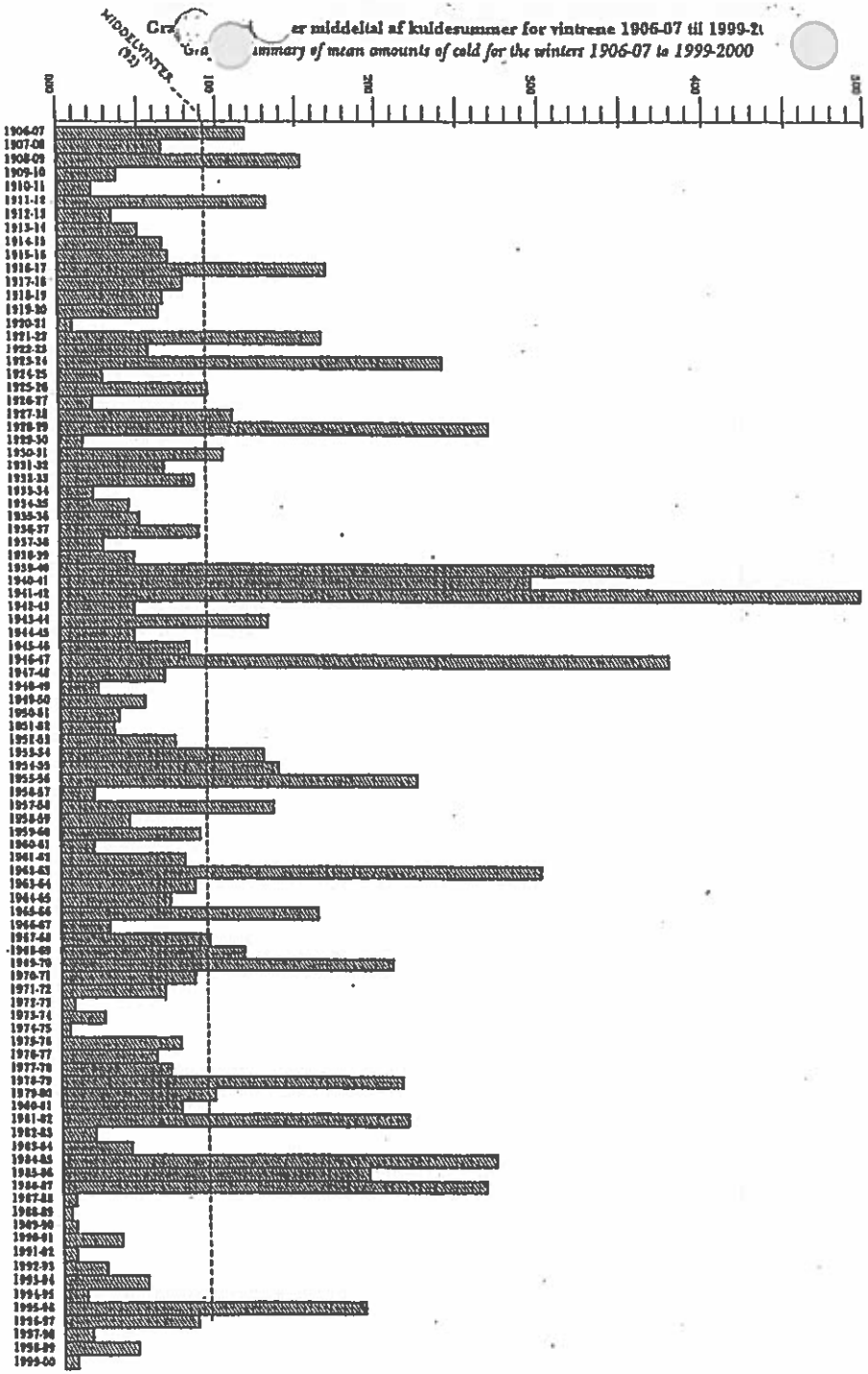

ANNEX A-1

ANNEX A2

Kelvinfunctions incl. derivatives

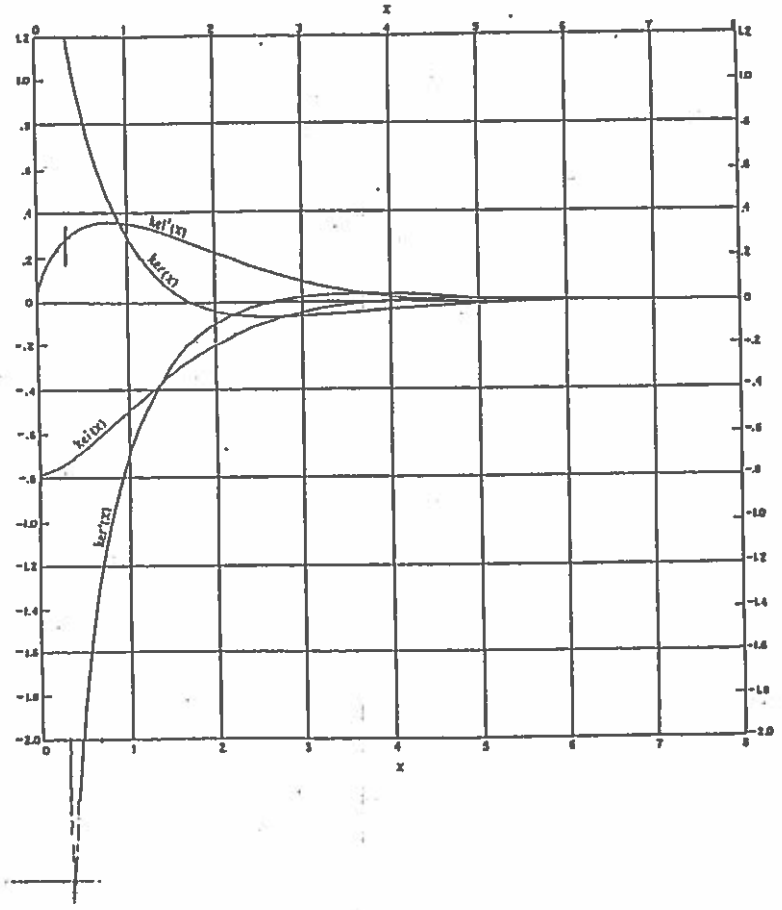

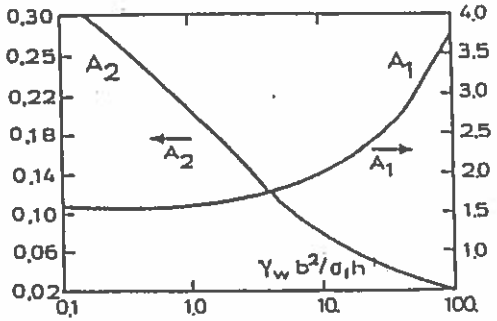

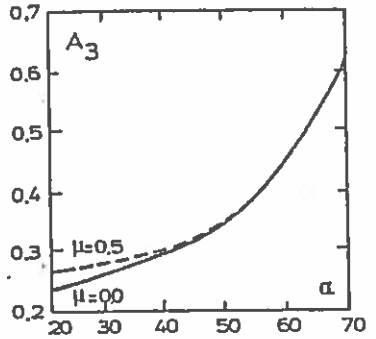

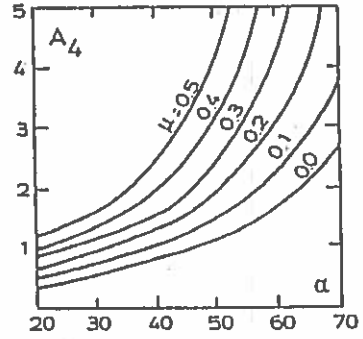

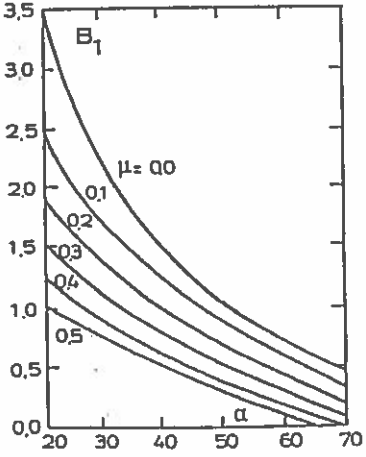

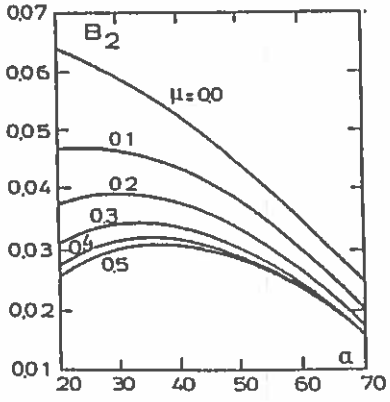

Ice force coefficients for plastic limit analysis.
From Ralston (1977).

Extreme Ice Properties

By Flemming Thunbo Christensen[1] and Jesper Skourup[2]

ABSTRACT: An extreme-value analysis is carried out for ice properties in the Great Belt in Denmark. The Great Belt is an 18-km-wide body of water that connects the Baltic Sea with Kattegat and the North Sea. It divides the country of Denmark into halves of nearly equal population. The design of a bridge and tunnel system across the Great Belt called for knowledge of extreme ice properties, because dynamic ice loading governs part of the design. Because of the extremely low exceedance probability of 2×10^{-3} per year accepted for ice loading, and because of the very limited amount of data available concerning ice at the location of interest, the analysis had to depend on air-temperature records. Statistical correlation between strength and thickness of the ice was handled effectively by splitting their product in temperature dependent and independent parts and joining distributions for these by simple integration. The effect of a snow cover on the ice was also analyzed.

Introduction

The result of a preliminary extreme value analysis of ice properties in the Great Belt in Denmark was briefly described by Christensen et al. (1989) as a basis for selection of parameters for model tests. The present analysis is the final version of that for the Great Belt West Bridge. It constitutes a substantial expansion of the preliminary analysis and leads to higher compressive ice strengths. For the West Bridge, dynamic ice loads govern the design of the bridge piers.

The recurrence time of the load resulting from ice crushing is determined by the recurrence time of the product $\sigma_u h$, where σ_u = the uniaxial compressive ice strength and h = the ice sheet thickness. To determine a design value of this product, the statistical distribution of $\sigma_u h$ must be known. However, no combined values of σ_u and h exist for the Danish waters, so distributions for each parameter must be combined. This leads to the question of statistical correlation between ice strength and ice thickness. The correlation must be known to properly combine the distributions. It is clear that they are not fully uncorrelated, since cold weather will increase both strength and thickness of the ice, but it is equally clear that they are not fully correlated either, since a warm spell of, say, −2° C will weaken the ice considerably without reducing its thickness. To circumvent this problem, the product of $\sigma_u h$ is split into temperature-dependent and temperature-independent parts. Distributions for these parts can be combined safely under an assumption of no correlation.

Compressive ice strength variations have been described [e.g., Weeks and Assur (1969)] in the form

$$\sigma_u = \sigma_0 f_u(S_i, T_i) \quad \ldots\ldots (1)$$

[1]Res. Hydr. Engr., Danish Hydr. Inst., Agern Allé 5, DK-2970 Hørsholm, Denmark.

[2]Res. Hydr. Engr., Danish Hydr. Inst., Agern Allé 5, DK-2970 Hørsholm, Denmark.

Note. Discussion open until November 1, 1991. To extend the closing date one month, a written request must be filed with the ASCE Manager of Journals. The manuscript for this paper was submitted for review and possible publication on July 30, 1990. This paper is part of the *Journal of Cold Regions Engineering*, Vol. 5, No. 2, June, 1991. ©ASCE, ISSN 0887-381X/91/0002-0051/$1.00 + $.15 per page. Paper No. 25856.

σ_0 = a constant reference strength and f_u = a [illegible] of the mean ice temperature, T_i, and the ice salinity, S_i. In the present analysis, it was decided to describe the reference strength as a stochastic parameter. Exponential, Weibull, Gumbel, and lognormal distributions were fitted to the reference strength data described later. Goodness of fit was determined for each of these by a χ^2 test, by a Kolmogorov-Smirnov test, and by visual observation. The Weibull and Gumbel distributions both describe the data well and are clearly superior to the other distributions. The goodness of fit is equal for the Weibull and Gumbel distributions, and the Weibull distribution was selected

$$\sigma_0 \in We(\beta, k) \quad (2)$$

$$f(\sigma_0) = \frac{k}{\beta}\left(\frac{\sigma_0}{\beta}\right)^{k-1} \exp\left[-\left(\frac{\sigma_0}{\beta}\right)^k\right] \quad (3)$$

$$F(\sigma_0) = 1 - \exp\left[-\left(\frac{\sigma_0}{\beta}\right)^k\right] \quad (4)$$

where f = the probability density function; F = the distribution function; and β and k distribution parameters.

The ice thickness was calculated from a simple linear differential equation for heat conduction. The resulting expression is of the general form

$$h = f_h\left(\int T_a dt\right) \quad (5)$$

i.e., a function of the accumulated freezing-degree-day (fdd) index. A commonly used formulation of the fdd index is

$$K = \Sigma(-\bar{T}_a) \qquad \text{for } \bar{T}_a < 0^\circ\text{ C} \quad (6)$$

where the index K = zero at the onset of winter; $\bar{T}_a$ = the daily average air temperature, and the summation is carried out daily. This index has many shortcomings (e.g., that the effect of thaw periods are not accounted for), but it is nevertheless widely used and reported. Wherever daily temperature records are available, the effects of thaw periods should be investigated. But the advantage of the simple index (6) is the availability of data for a larger number of years. An estimate of the thickness of the sea ice is

$$h = 0.032(K - 50)^{1/2} \text{ meter} \quad (7)$$

where K must be in Celsius degree-days. This formula is derived theoretically from an assumption of one-dimensional heat conduction, except for the subtraction of 50 degree-days, which is of empirical nature. It accounts for the freezing point being lower than 0° Celsius.

By rewriting (1) and (5) it follows that

$$\frac{\sigma_u h}{\sigma_0} = x = f_u(S_i, T_i) f_h[T_a(t), t] \quad (8)$$

$$\sigma_u h = \sigma_0 x \quad (9)$$

By defining the parameter x in (8) as the temperature-dependent part of the product $\sigma_u h$, and by letting σ_0 represent the temperature-independent part of the product, the previously mentioned split illustrated in (9) is achieved.

The methodology then entails determination of distributions for σ_0 and x, which are eventually combined into the probability distribution function for the product $\sigma_u h$ by integration

$$F(\sigma_u h) = \int_0^\infty F(x) f(\sigma_0) d\sigma_0 \quad (10)$$

The simple integration in (10) implies that σ_0 and x are statistically independent, which was precisely the reason for the applied split of the product. In the following statistical distributions are determined for the reference strength σ_0 and for annual maximum values of the parameter x.

The compressive ice strength of sea ice is known to be strongly dependent on strain rate. It would, therefore, be desirable to determine this functional relationship and include ice velocity in the probabilistic formulation of ice-loading conditions. Because of time constraints this was not included. Instead, compressive strength in this analysis is meant to be representative of the brittle range, in which the rate effects are moderate.

Reference Strength Distribution

The specific expression defining reference strength, suggested by Weeks and Assur (1969), read

$$\sigma_u = \sigma_0\left[1 - \left(\frac{\nu}{0.275}\right)^{1/2}\right] \quad (11)$$

where ν = the relative brine volume in the ice. This quantity may, according to Frankenstein and Garner (1967), be calculated as

$$\nu = \left(0.532 - \frac{49.185}{T_i}\right)\frac{S_i}{1{,}000} \quad (12)$$

where T_i is in negative degrees Celsius and S_i in parts per thousand. More accurate descriptions are available, e.g., Cox and Weeks (1982), but (11) and (12) give sufficient accuracy when fitted to experimental data.

It appears to be a simple matter to deterine a σ_0 distribution from a large amount of strength measurements in the area of interest. But in Danish domestic waters, only low-quality strength measurements are available. By low quality we refer to the fact that, for example, strain-rate and crystal structure have never been documented. The Danish data all stem from field programs carried out jointly by the Institute of Hydrodynamics and Hydraulic Engineering (ISVA), at the Technical University of Denmark, and by Danish Hydraulic Institute. The results have been reported by Tryde and Zorn (1979), Mortensen and Zorn (1982), and Christensen (1986). Because of the low quality of these measurements, it was decided to also use the data presented by Fransson and Elfgren (1987) from the Bay of Bothnia, provided that these data could be considered representative of reference strengths in the Great Belt some 1,000 km to the south.

The Swedish data were used as published. In the Danish data, measurements with mean ice temperatures of −0.5° or warmer were discarded, leading to omission of seven of 57 measurements. These seven were all from the same locality and showed unrealistic results, probably because of faulty

TABLE 1. Comparison of Danish and Swedish Measurements Regarding Reference Strength, Salinity, and Temperature

Ice parameters (1)	Mean value (2)	Standard deviation (3)	Minimum (4)	Maximum (5)
		(*a*) Reference strength		
Swedish σ_0 (MPa)	2.76	1.07	1.49	6.51
Danish σ_0 (MPa)	2.44	0.86	1.31	5.27
Joint σ_0 (MPa)	2.61	0.99	1.31	6.51
		(*b*) Salinity		
Swedish S_i (ppt)	1.85	1.00	0.00	3.78
Danish S_i (ppt)	1.69	0.95	0.8	3.5
		(*c*) Temperature		
Swedish T_i (°C)	−4.01	1.87	−10.0	−1.0
Danish T_i (°C)	−1.88	0.82	−4.1	−0.9

temperature measurements. The Danish tests were made with cubes of ice, and the resulting strength was multiplied by 0.67 to obtain the "cylinder strength." The factor 0.67 was adopted from concrete testing technology, where it varies between 0.67 and 0.80. The Swedish tests were made using cylindrical ice samples and a constant strain rate of 2×10^{-4} sec^{-1}.

The description of crystal structures in the Swedish samples offered by Fransson and Elfgren (1987) correspond well with what is expected in the Great Belt, namely, mostly columnar ice with some granular and mixed ice types as well. In Table 1 the two data sets are compared in terms of both reference strength, temperature, and salinity. The reference strengths are very close. It is tempting to raise the cylinder-to-cube-strength ratio to 0.75, and thereby achieve identical mean values in the two data sets. Because the strain rate is unknown, although brittle, in the Danish tests, it cannot be argued that the two mean values should be equal. The ratio of 0.67 remains the most commonly used value.

The salinities appear identical except perhaps for the minimum values, which is less significant. This is somewhat surprising since the water bodies have distinctly different salinities, namely, 16–20 ppt in the Great Belt versus 2–4 ppt in the Bay of Bothnia. Part of the explanation lies in the growth process. While growing, the ice rejects salt from its underside and only traps a limited amount when neighboring fingers of the skeleton layer join to form a brine pocket. Thus, as long as the water salinity exceeds typical ice salinities of, say, 2 ppt, the ice will filter out the excess salt in the growth process. According to Cox and Weeks (1988), salt entrapment during ice growth is proportional to the growth rate. In the present case, this may be balanced by the difference in water salinities. Brine drainage will also cause salinities to be similar.

The temperatures clearly show the difference in latitude, with the Bay of Bothnia having lower temperatures. This difference in ice temperatures need not be a problem if the expressions (11) and (12) are capable of extracting the effects of the temperature correctly. This is investigated in a (σ_0, T_i) bias plot (see Fig. 1). A salinity (σ_0, S_i) bias plot is also made (see Fig. 2).

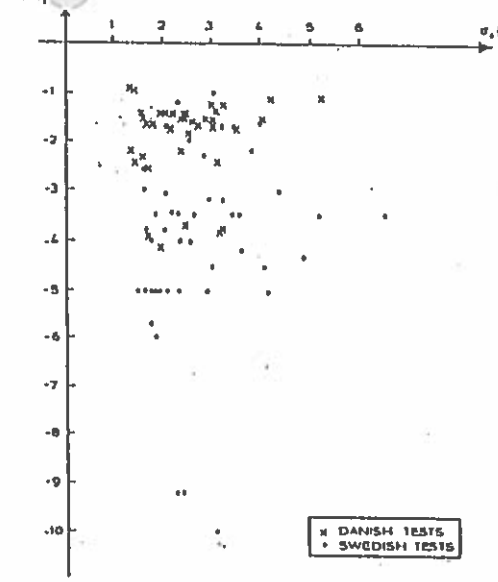

FIG. 1. Temperature T_i versus Reference Strength σ_0 for Danish and Swedish Tests

There are no visible differences in the distributions of σ_0 between the two data sets shown in the bias plots. Although the temperatures of the Swedish test samples are generally lower than the temperatures of the Danish test samples, (compare Table 1 and Fig. 1), there is no indication of differing distributions. The same holds true for the salinity plot. Note furthermore that extreme values of T_i and S_i do not coincide with extreme values of σ_0, and vice versa.

The agreement between the data sets is good for mean values. The Swedish standard deviation is slightly larger than the Danish one. This can be related to the strain rate as well as the choice of multiplication by 0.67 to obtain cylinder strengths. Because of the good agreement, it was decided to base the σ_0 distribution on the joint data set. It would be desirable to include even more data, but none were accessible within the available time frame.

The present ensemble of Danish and Swedish tests is a compromise. From a purely scientific point of view, the Danish measurements should be discarded, because the strain rates are unknown. Ideally, all scientific measurements of compressive ice strengths (meaning those with fully documented test conditions) from anywhere in the world should be included as long as they were made with appropriate ice types. The Swedish data give some confidence that the Danish measurements are reasonable. The Danish tests are included because they represent waters relatively close to the Great Belt. Through the comparisons in Table 1, they give some confidence that the Swedish data set is applicable, because of the nearly identical parameters. The agreement between the two sets of data is shown in Figs. 1 and 2.

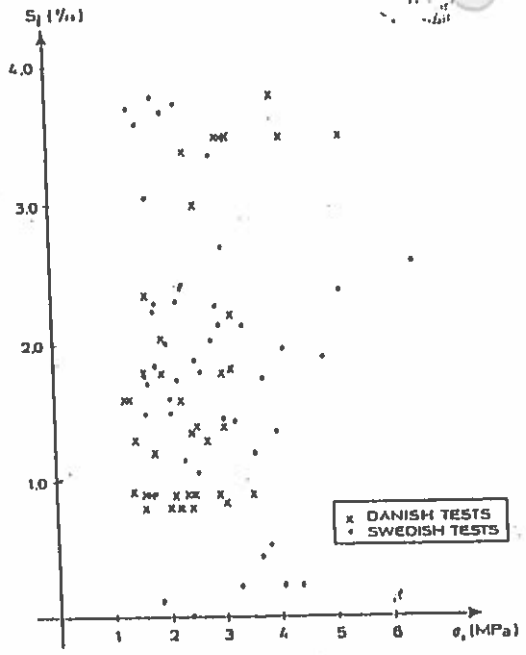

FIG. 2. Ice Salinity, S_i versus Reference Strength σ_c for Danish and Swedish Tests

When two data sets are used to validate each other, the validation is of limited value. It is, therefore, desirable to compare with a broader spectrum of values obtained in scientific measurements. One of the best references for that purpose is an article by Timco and Frederking (1990), published shortly after the completion of this extreme value analysis. The article analyzes 283 small-scale measurements of compressive strength of first-year sea ice to formulate an empirical model that gives good results when compared with large-scale measurements. The final results of this extreme value analysis are in good agreement with the large ensemble of scientific measurements analyzed by Timco and Frederking (1990). By agreement, we mean that thicknesses, temperatures, strain rates, and strengths relate well to each other. The absolute values of extreme ice strengths in the Great Belt need obviously not equal the average values of these 283 tests.

A Weibull distribution was fitted to the joint set of data on reference strengths. Through a least-squares fit, distribution parameters of $\beta = 2.844$ and $k = 2.749$ [compare with (4)], were determined. Statistical model uncertainty has not been included in the present investigation. Only central estimates have been calculated. Distributions have been fitted by the least-squares method. This is assumed to be permissible. A comparison with maximum likelihood estimation and moment estimation results would be interesting, but the effects are assumed to be moderate, and the comparisons have therefore not been carried out.

Ice Thickness and x-Distribution

The specific expression for the x parameter corresponding to the general expression (8) becomes

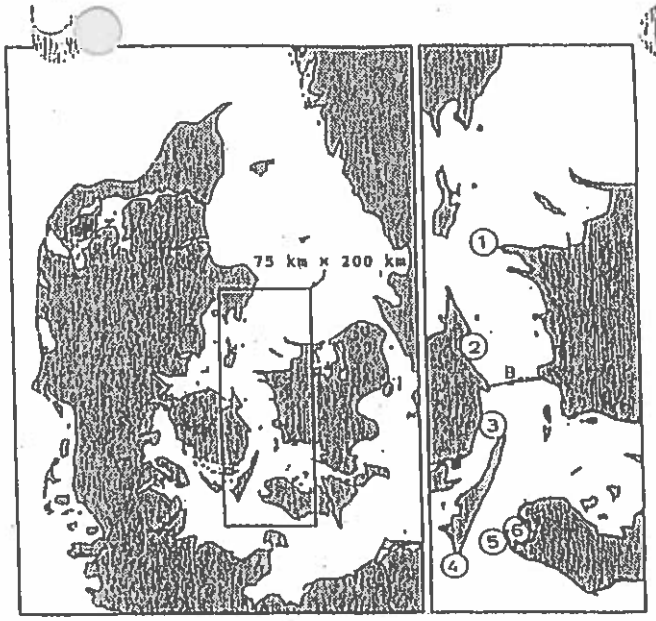

FIG. 3. Locations for Ice Thickness Observations in Entire Great Belt: (1) Rønnæs Lighthouse; (2) Kerteminde Bay; (3) Lohals; (4) Keldsnor; (5) West of Albuen; (6) Nakskov Outer Fiord; and (B) Bridge

$$x = \left(1 - \left\{\frac{\left[0.532 - \left(\frac{49.185}{T_i}\right)\right]S_i}{275}\right\}^{1/2}\right) 0.032(K - 50)^{1/2} \quad \text{..... (13)}$$

where T_i is in degrees Celsius and negative; S_i is in ppt, K is in accordance with (6); and x comes out in meters. This expression can easily be calculated day by day once $\Sigma(-\bar{T}_a)$ exceeds 50. The latter part representing thickness of the ice obviously has a direct effect on the values of x, and it consequently is important to check whether or not this theoretical expression describes nature well. This is investigated in two ways: By comparing with extreme observations from the past 80 years and by comparing with a larger amount of observations near the site of the future bridge.

Annual maximum observations of ice thickness at various locations have been reported in annual bilingual (Danish and English) publications by Statens Istjeneste in the period 1907–86. Locations of interest are shown in Fig. 3 for the entire Great Belt and in Fig. 4 for the immediate vicinity of the bridge. Observations from the five coldest winters in the 80 winters surveyed are shown in Table 2 together with theoretical thicknesses calculated from (7). A reasonable agreement is found. In the coldest winter, 1941–42, the agreement is excellent. In the other three winters, (7) appears to slightly overpredict the thickness, but since there is no guarantee of all ice thicknesses being smaller than the largest thickness observed, this has not resulted in modifications to the expression for x in (13).

Observations near the site of the future bridge have been plotted against

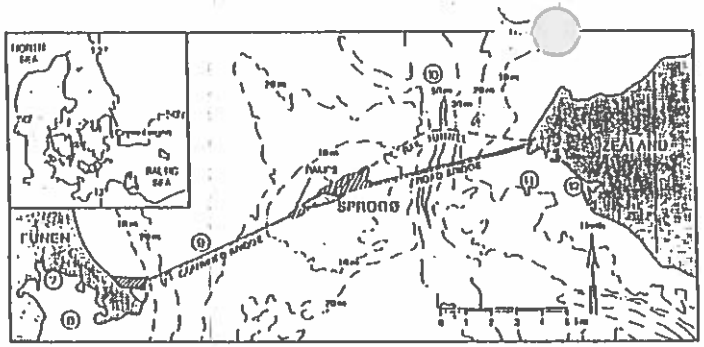

FIG. 4. Locations for Ice Thickness Observations near Site of Future Bridge: (7) Nyborg Harbour; (8) Nyborg Fiord; (9) Western Channel; (10) Eastern Channel; (11) Access to Korsør Harbour; (12) Korsør Harbour

the total amount of freezing degree-days for the relevant winters in Fig. 5. As indicated in the figure, (7) yields ice thicknesses above the best fit to the data, especially for shorter recurrence times. For longer recurrence times the difference vanishes, and this general trend may also be seen in Table 3. Furthermore, the figure shows that the best-fit curve is nonconservative with respect to the data from the Western Channel. Consequently, (7) was maintained as a reasonable estimate of the ice thickness. It is worth noting that the factor 0.032 in (7) is larger than corresponding factors used in the Arctic.

The problem is then reduced to determining the x-distribution. The development of x through the winter is of limited interest for design. The maximum value from each winter is used to determine design values. The maximum x typically occurs when K has reached about 90% of its final value for the winter. The end of the winter tends to be warmer and thus the maximum x occurs slightly before the maximum or final K.

One of the most serious shortcomings of the preliminary analysis (Christensen et al. 1989) was that the temperature records only covered 19 winters. Therefore, it was decided to use as many data as possible from nearby measurement stations in the final analysis. From the nearby Røsnæs lighthouse (see Fig. 3), eight temperature readings per day are available from 1960 on.

TABLE 2. Measured Ice Thicknesses (in cm) at Locations in Vicinity of Future Bridge during Five Coldest Winters in Period 1907–86 Compared with Results from (7)

Year (1)	K_{max} (°C-days) (2)	Location: Kerteminde Bay (3)	Nyborg Harbour (4)	Nyborg Fiord (5)	Lohals (6)	Keldsnor (7)	West of Albuen (8)	Nakskov outer Fiord (9)	Eq. (7) (10)
1941–42	497.5	65	60	—	—	—	65	67	64
1946–47	378.0	45	50	50	40	44	—	48	55
1939–40	368.5	—	35	50	—	—	—	30	54
1962–63	300.3	—	—	—	—	—	—	—	47
1940–41	290.7	40	35	45	—	—	25	37	47

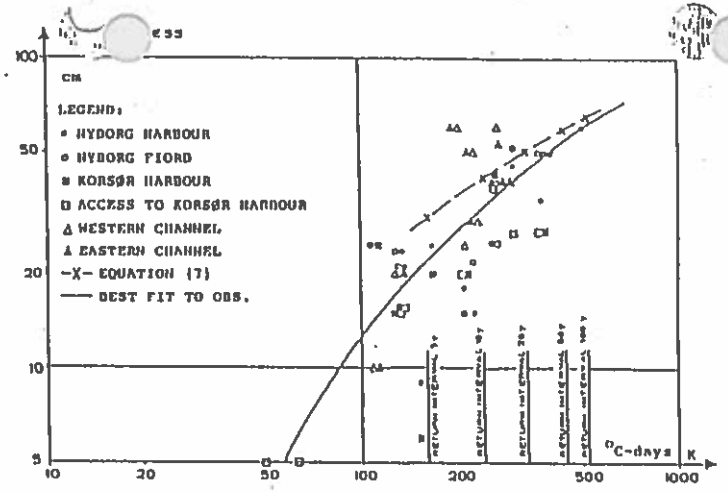

FIG. 5. Maximum Observed Ice Thicknesses (Annually) versus Number of Freezing Degree-Days, According to Statens Istjeneste

Additional data from Bogø were used for the period 1875–1960. The Bogø station is about 60 km east-southeast of the future bridge, but it is considered representative of temperature conditions at the bridge. The Bogø data contain three daily readings, plus minimum and maximum readings. The average of the latter two was used as a daily mean value.

The national mean air temperature for each of the winters 1875–1989, defined as December 1 through March 31, is shown in Fig. 6. The figure reveals a relatively mild winter climate and significant interannual variations. These variations were indeed the reason for the preliminary analysis giving unrealistically low design values. It is assumed that the temperature variations can be considered stochastic realizations of a stationary process. Hence, no trend toward a different climate is taken into account.

A 114-year temperature record may seem excessively long, but with design probabilities of exceedance in the range 2×10^{-3} to 4×10^{-3} per year this is not the case. Furthermore, calculations to obtain design values based on two different 30-year periods resulted in extreme values a factor of two

TABLE 3. Design Values of $\sigma_u h$ from POT Analysis with Weibull and Gumbel Distributions. Product $\sigma_u h$ is in MN/m

x_{th} (m) (1)	Number of data (2)	Weibull $\sigma_u h$ (MN/m) (3)	Gumbel $\sigma_u h$ (MN/m) (4)	P_W (5)	P_G (6)
0.22	29	2.60	3.32	0.0095	0.0063
0.23	26	2.66	3.35	0.0075	0.0058
0.24	23	2.80	3.42	0.0031	0.0035
0.25	17	2.71	3.33	0.0051	0.0051
0.26	14	2.65	3.21	0.0095	0.0071
0.27	12	2.60	3.04	0.0208	0.0111
0.28	11	2.65	3.08	0.0205	0.0138

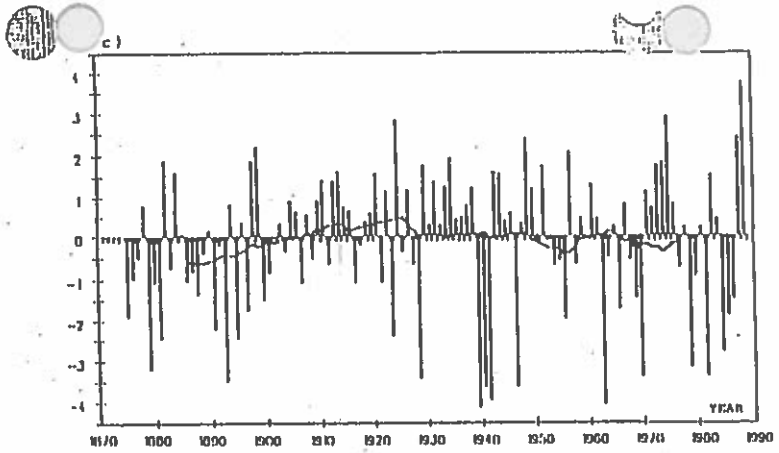

FIG. 6. Mean Air Temperature in Each Winter from 1874/75–1988/89. Solid Curve Shows Centered 30-year Average Winter Temperature (Figure Courtesy of Danish Meteorological Institute)

apart. Those calculations are not shown here. In the more severe ice winters with relatively thick ice, it normally takes about three to four days of low temperatures for the temperature profile in the ice to adjust so that the mean value corresponds to the mean of the surface and bottom temperatures of ice. Therefore, the x values were computed by using average temperatures of the last three days. This reduces the final result by about 10% compared with an analysis using individual day averages. It was decided to use a constant salinity of 1.5 ppt for the ice in the Great Belt. Timco and Frederking (1990) found decreasing gross salinities with increasing thickness. This is not taken into account in the present analysis.

Accurate temperature simulations could have been carried out, e.g., as suggested by Schwarz and Miloh (1972), but because of lack of time it was decided to use the three-day average temperatures and add a sensitivity analysis. More complex thermodynamic models of ice growth could have been used, e.g., as suggested by Maykut and Untersteiner (1971), Miller (1981), or Cox and Weeks (1988). However, the lack of the necessary data precluded use of these models.

The 114 maximum values of x were divided into groups and averaged within each group such that only about 20 points remain for determination of the distribution, as shown in Fig. 7. The grouping procedure was introduced to give equal weight to the information at either end of the curve. Without the grouping, the lower end would have a dominant effect on the best-fit distribution. In addition, Fig. 7 shows that the extreme maximum values follow another distribution than the maximum values at the lower end. The dashed line indicates the differing lower end distribution. It was also found that the extreme values of maximum x occur at low temperatures and not for temperatures close to the freezing point. Fig. 7 is a Weibull plot, but the Gumbel distribution may be just as relevant for describing the variations. The distribution functions are

$$F_W(x) = 1 - \exp\left[-\left(\frac{x}{\beta}\right)^k\right] \quad \ldots\ldots (14)$$

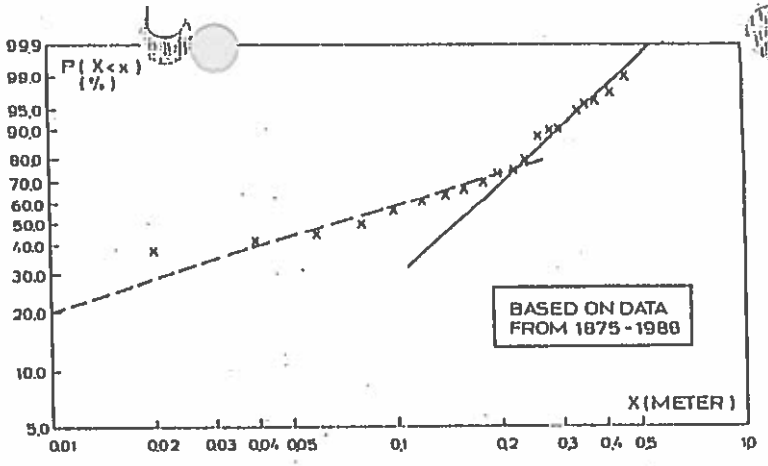

FIG. 7. Annual Exceedance Probability for x Based on Temperature Data from 1875–1988. Data Points Correspond to Upper Limits of Division Intervals

$$F_G(x) = \exp\{-\exp[-a(x-b)]\} \quad \ldots\ldots (15)$$

where the subscripts refer to the distribution names and (β, k, a, b) are distribution parameters to be determined from, for example, least-squares fit to the data. A χ^2-test is performed to determine which of the two distributions best fit the data. This means calculating a verification parameter, P, for each distribution as

$$P = \frac{1}{n-1}\sum_{i=1}^{n}(P_i - P_a)^2 \quad \ldots\ldots (16)$$

where P_i = the theoretical value according to the distribution function and P_a = the actual value based on the data. The count parameter i runs over the number of points to be fitted to. Because of the interest in extreme values, the χ^2-test is performed in conjunction with the peaks-over-threshold (POT) analysis instead of over all data points.

POT Analysis

A POT analysis is performed for the parameter x, being the standard statistic method for extreme statistics. The idea behind this analysis is that only extreme events belonging to the same family are considered. All nonextreme data are excluded.

The POT-analysis result is a function of the threshold chosen, and it is, therefore, performed with different thresholds both by use of the Weibull distribution function $F_W(x)$, and by use of the Gumbel distribution function $F_G(x)$. If the variation of the extreme values is small and nonsystematic for different thresholds, then the confidence in the results from the POT analysis will be good.

In the present analysis, the value with an exceedance probability of 2×10^{-4} per year was the one to be determined. [It was later shifted to 4×10^{-5} per year and mi[illegible] even shift again. The reasons behind the use of such

nc exceedance probabilities were explained by Chri... et al. (1989).] The 2×10^{-5} per year corresponds to an average recurrence time of 50,000 years, and a distribution function value $F(\sigma_u h) = 0.99998$. This design value of $\sigma_u h$ was computed using all data points in Fig. 7 above a threshold, x_{th}, and the results are shown in Table 3 for different thresholds. Both the Weibull and the Gumbel distribution functions are used, and the χ^2-test [according to (16)] is performed to decide which of the two distribution functions are modeling the x-variation with highest accuracy.

From Table 3, it is seen that the Gumbel distribution gives results that are 10–20% larger than the results from the Weibull distribution. When the Weibull and Gumbel distribution functions are compared with the data for large values of x, it is found that the Gumbel distribution is below the actual data while the Weibull is above. It was therefore decided to base the design value of $\sigma_u h$ on a weighted average between the two distributions, and to use the values of the verification parameters as weights.

Table 3 is a good example of the importance of the theoretical expression of the distribution function when determining extreme values. At a threshold of $x_{th} = 0.28$, the two distributions give design values that are 16% apart, namely, 2.65 and 3.08 MN/m, based on the exact same data. Note also that both distributions yield $\sigma_u h$ design values that vary nonsystematically with x_{th}. This indicates that both distributions describe the general variation of the data well.

The weighted design value of $\sigma_u h$ was with $x_{th} = 0.28$ determined from

$$\frac{205}{343} F_G(\sigma_u h) + \frac{138}{343} F_W(\sigma_u h) = 2 \times 10^{-5} \quad \ldots\ldots (17)$$

where after a few iterations it was established that

$$\sigma_u h = 2.96 \text{ MN/m} \quad \ldots\ldots (18)$$

This is the central result of the extreme value analysis. It is, however, necessary to break the product into a strength and a thickness in order to continue with accurate load calculations. Eq. (7) was found to describe maximum ice thicknesses well (compare with Table 2). Christensen (1987) found that the K index for Danish domestic waters may be expressed as

$$K = 103.8[\ln(A) + 0.04]^\circ\text{C-days} \quad \ldots\ldots (19)$$

where A = the average recurrence time in years and K is in Celsius degree-days. For the design situation, (19) gives $K = 1{,}127$ °C-days. As mentioned earlier, the maximum x typically occurs when K has reached 90% of its final value for the winter. With $K = 0.9 \times 1{,}127 = 1{,}014$ °C-days, the thickness is calculated from (7) and the strength is determined by dividing the product $\sigma_u h$ with the thickness. The results are

$$h = 0.99 \text{ m} \quad \ldots\ldots (20)$$

$$\sigma_u = 3.0 \text{ MPa} \quad \ldots\ldots (21)$$

Other breakdowns of the product in (18) are possible. The selected one agrees well with, for example, Timco and Frederking (1990); see their Fig. 10, where a thickness of 1 m and a strain rate of 2×10^{-4} sec^{-1} gives a compressive ice strength close to 3.0 MPa.

TABLE 4. Res... r Various Recurrence Times, Excluding Effect of Snow... on Ice

Average return period (years) (1)	$\sigma_u h$ (MN/m) (2)	K (degree-days)* (3)	h (m) (4)	σ_u (MPa) (5)
50	1.26	410	0.57	2.21
100	1.48	482	0.63	2.35
1,000	2.05	721	0.78	2.63
10,000	2.58	960	0.91	2.84
25,000	2.82	1,055	0.96	2.94
50,000	2.96	1,127	0.99	2.99

*Degrees Celsius.

Results for various recurrence times are shown in Table 4. For a 10-year recurrence time, the POT-analysis method gives $\sigma_u h = 0.81$ MN/m, $h = 0.42$ m, $\sigma_u = 1.93$ MPa. The POT-analysis method, however, is suited for extreme recurrence times, and the 10-year value thus should be regarded with caution. Comparison with the preliminary results described by Christensen et al. (1989) shows that the extension of the temperature records to include 114 years resulted in a substantial increase of the design values.

Sensitivity Analyses

According to Frankenstein and Garner (1967), a more accurate estimate of the relative brine volume ν of the ice than the one given by (12) can be computed by

$$\nu = \left(1.189 - \frac{43.795}{T_i}\right)\frac{S_i}{1{,}000}, \qquad -22.9^\circ\text{C} \le T_i \le -8.2^\circ\text{C} \quad \ldots\ldots (22a)$$

$$\nu = \left(0.930 - \frac{45.917}{T_i}\right)\frac{S_i}{1{,}000}, \qquad -8.2^\circ\text{C} \le T_i \le -2.06^\circ\text{C} \quad \ldots\ldots (22b)$$

$$\nu = \left(-2.28 - \frac{52.56}{T_i}\right)\frac{S_i}{1{,}000}, \qquad -2.06^\circ\text{C} \le T_i \le -0.5^\circ\text{C} \quad \ldots\ldots (22c)$$

When (22) is used instead of (12) to evaluate ν when the σ_0 values are computed, the relative changes in the mean value and standard deviation of the σ_0 distribution are less than 1%. Hence, it is concluded that (12) is adequate for computing ν in this analysis.

To investigate the relative importance of the largest measured σ_0 values, computations were carried out with the upper integration limit in (10) lower than infinity (which, of course, is necessary when a numerical integration is performed). The upper integration limit is chosen to be so large that the truncation error from the numerical integration is immaterial. A numerical integration of the probability density function $f(\sigma_0)$, which was given as a Weibull distribution, from 0–8 gives a difference of $1.5 \cdot 10^{-9}$ from the exact value 1. In the computations performed in this paper, the upper integration

limit is chosen as large as 20, and the numerical quadrature is performed with 10,000 points between 0 and 20.

The maximum x-values have been computed using mean air temperatures for one-, three- and five-day intervals. This gives a variation of the largest value of x computed in the period 1874/75–1988/89 between 0.5149 m for one-day intervals, 0.5108 m for three-day intervals, and 0.4911 m for a five-day averaging interval.

If the data in Fig. 7 are considered a single population, then a POT analysis is sufficient to predict the extreme values. If, on the other hand, they are considered two populations, then the extreme occurrence in both populations must be calculated. If the division point is located at the 75% fractile, then the relevant extreme value of the lower distribution is the $0.75 \cdot 50{,}000 = 37{,}500$ years event in that distribution after integration as specified in (10). This value has been computed as

$$(\sigma_u h)^* = 1.96 \text{ MN/m} \quad \ldots\ldots (23)$$

and is thus smaller than that resulting from the POT analysis. Hence, it is concluded that the results from the POT analysis are conservative with regard to the distribution of the parameter x.

Snow Cover

The effect of a snow cover on the ice has not been included in the analysis until this point. Because of the good agreement between observed and calculated thicknesses demonstrated in Table 2, it was decided not to include the snow cover in the theoretical model for ice growth. An additional reason for this is the total lack of sufficient statistics for snow layer thickness, h_s, over sea ice in Danish waters. Instead only the warming effect is included.

The presence of a snow layer will raise the mean ice temperature somewhat. Denoting the thermal conductivities of ice and snow by λ_i and λ_s, respectively, enables expression of the heat flux as a function of the thickness and temperatures, and after some simple calculations the temperature T_i at the ice-snow interface can be expressed by

$$T_i = \frac{\lambda_s h T_a + \lambda_i h_s T_w}{\lambda_s h + \lambda_i h_s} \quad \ldots\ldots (24)$$

where T_w = the temperature of the ice-water interface. The thermal conductivities of ice and snow were taken as

$$\lambda_i = 2.24 \frac{\text{W}}{(\text{m °C})} \quad \ldots\ldots (25)$$

$$\lambda_s = 2.84 \cdot 10^{-6} \rho_s^2 \frac{\text{W}}{(\text{m °C})} \qquad 140 < \rho_s < 340 \frac{\text{kg}}{\text{m}^3} \quad \ldots\ldots (26)$$

where ρ_s = the density of snow, [compare with Bergdahl (1977)]. The density ρ_s and thickness h_s of the snow cover must be estimated. The density of snow varies over a broad range [from 50 kg/m³ (new snow in still air) to more than 400 kg/m³ (consolidated snow)]. In this analysis, a value of 280 kg/m³ is used. This is an average value for wind-toughened snow (Gray and Male 1981). Sensitivity calculations are carried out with a lower value (ρ_s = 200 kg/m³) and a higher value (ρ_s = 340 kg/m³) to investigate the effect of snow density. The thickness of the snow layer is estimated based on a mean value of the snow thicknesses from the 10 coldest winters in the period 1938–1988. Daily measurements of snow thicknesses (measured at 8 a.m.) are available from 1938 onward in "Meteorologisk Årbog" published by the Danish Meteorological Institute. Data from three different locations were used and a weighted mean value of the snow thicknesses was 9.7 cm.

This snow thickness was computed on the basis of measurements on open land. The retention coefficient relative to open land is for sea ice 0.4–0.5 (Gray and Male 1981), thus providing an estimate of the mean snow thickness on the ice sheet as

$$h_s = 4 \text{ cm} \quad \ldots\ldots (27)$$

This value was used in the computations. For sensitivity analyses snow thicknesses of 3 cm and 5 cm were also used as input for the computations.

The design value of $\sigma_u h$ is, as in the preceding analysis, found to be the weighted mean of the design values coming from POT analyses made with use of the Gumbel and the Weibull distributions, respectively. The results are shown in Table 5, with the central calculation giving a product of 2.82 MN/m.

TABLE 5. Design values of $\sigma_u h$ in MN/m for Various Values of Snow Density ρ_s and Snow Thickness h_s

ρ_s (kg/m³) (1)	h_s = 3.0 (cm) (2)	h_s = 4.0 (cm) (3)	h_s = 5.0 (cm) (4)
200	2.76	2.71	2.66
280	2.85	2.82	2.78
340	2.89	2.86	2.84

A similar calculation for the 25,000-year situation using h_s = 4 cm and ρ_s = 280 kg/m³ resulted in a product $\sigma_u h$ of 2.67 MN/m. With an ice thickness of 0.96 m (compare with Table 4), the compressive ice strength becomes 2.78 ≅ 2.8 MPa. This analysis of the effect of a snow cover on sea-ice strengths is fairly simple, and a number of questions have been left open. However, because of the complexity of the problem it is necessary to use professional judgment to some extent. Reductions in the area of 5% as indicated by Table 5 (relative to the $\sigma_u h$ = 2.96 MN/m found without snow) is seen as reasonable.

Eq. (7) gave a good estimate of ice thicknesses (compare with Table 2), even though it was based on a fairly simple model, i.e., one-dimensional heat conduction. The addition of a snow layer reduces ice growth significantly. The agreement therefore means either that there is very little snow or that other effects balance the insulating effect of the snow. Both are plausible explanations. A short warming can melt the snow or winds can deposit it in snow drifts, leaving large areas without snow. These snow-free areas would grow the largest ice thicknesses, and it is precisely those that are reported in Table 2. The bottom line, however, is that (7) gives good agreement with observations. Because of that, it was decided to only include the warming effect on strength and not on growth.

important question is the appropriateness of the m[illegible]ow thickness. Many arguments have been weighed: (1) Extreme winters have northeasterly dry winds with little precipitation; (2) extreme winters have few or no thaw periods and, thus allow a long continuous snow accumulation without intermittent melting; (3) local spatial variations of snow thickness will leave some areas without the insulating snow cover, or at least with a reduced snow depth; and (4) can snow data from the selected locations be used as representative? All of these have been weighed, and, in the light of lack of sufficient data for a scientific approach, professional judgment was used. This led to the use of $h_s = 4$ cm, with only the warming effect included.

Conclusion

An extreme value analysis of ice properties in the Great Belt in Denmark has been carried out. For an annual exceedance probability of 2×10^{-3}, an ice thickness of 0.99 m and a uniaxial compressive ice strength of 2.8 MPa was found, when a snow cover was included in the analysis. Results for larger exceedance probabilities were also given.

Certain conservative assumptions mean that these values should be considered a "best-conservative" estimate rather than a central estimate. Some of these conservative assumptions are the ignoring of thaw periods when accumulating K in (6) and the assumption of a stationary stochastic process, i.e., that climatic trends are disregarded.

A method of circumventing the problem of correlation between ice thickness and ice strength was introduced by splitting their product in temperature-dependent and independent parts. The distribution of reference strength proved similar for the Great Belt and the Bay of Bothnia, which are more than 1,000 km apart. The analysis relies heavily on air temperature records and is thus well suited for areas with scarce ice information.

The effects of the testing machines on the standard deviations in the reference strength distributions have not been analyzed.

Acknowledgment

The presented analysis was carried out on behalf of the Great Belt Link Ltd. The company's permission to publish the results is gratefully acknowledged.

Appendix I. References

Bergdahl, L. (1977). "Physics of ice and snow as affects thermal pressure." *Report Series A:1*, Dept. of Hydraulics, Chalmers Univ. of Tech., Gothenburg, Sweden.

Christensen, F. T. (1986). "Sea ice strength measurements from the inner Danish Waters in early 1985." *Proc.*, First Int. Ice Technology Conf. (ITC-86), 247–253, Massachusetts Inst. of Tech., Cambridge, Mass.

Christensen, F. T. (1987). "Temporal variations of freezing degree-days in Danish domestic waters." *Proc.*, Ninth Int. Conf. on Port and Ocean Engineering under Arctic Conditions (POAC-87), Vol. 3, 201–206, Fairbanks, Alaska.

Christensen, F. T., Ottesen Hansen, N. E., Evers, K.-U., Spangenberg, S., and Vincentsen, L. J. (1989). "Design of the Great Belt Western Bridge for ice forces." *Proc.*, Eighth Int. Conf. on Offshore Mechanics and Arctic Engineering (OMAE-89), Vol. 4, 365–376, the Hague, the Netherlands.

Cox, G. F. N., [illegible]Weeks, W. F. (1982). "Equations for determining the gas and brine volumes in sea ice samples." *Report 82-30*, Cold Regions Research and Engineering Laboratory, Hanover, N.H.

Cox, G. F. N., and Weeks, W. F. (1988). "Numerical simulations of the profile properties of undeformed first-year sea ice during the growth season." *J. Geophys. Res.*, 93(c10), 12449–12460.

Frankenstein, G. E., and Garner, R. (1967). "Equations for determining the brine volume of sea ice from −0.5° C to −22.9° C." *J. Glaciol.*, 6(48), 943–944.

Fransson, L., and Elfgren, L. (1987). "Horizontal uniaxial compressive strength of low-salinity sea ice in the Gulf of Bothnia." *Proc.*, Ninth Int. Conf. on Port and Ocean Engineering under Arctic Conditions (POAC-87), Vol. 3, 21–29, Fairbanks, Alaska.

Gray, D. M., and Male, D. H., eds. (1981). *Handbook of snow*. Pergamon Press, Elmsford, N.Y.

Maykut, G. A., and Untersteiner, N. (1971). "Some results of time-dependent thermodynamic model of sea ice." *J. Geophys. Res.*, 76(6), 1550–1575.

Miller, J. D. (1981). "A simple model of seasonal sea ice growth." *Trans.*, ASME, Vol. 103, 212–218.

Mortensen, P., and Zorn, R. (1982). "Ice investigations at Farø bridge in 1982." Danish Hydraulic Institute, Hørsholm, Denmark (in Danish).

Schwarz, J., and Miloh, T. (1972). "On the time dependent temperature variations within ice sheets." *Proc.*, Int. Assoc. of Hydraulic Research Ice Symposium, 262–269, Leningrad, the Soviet Union.

"Ice and navigational conditions in the Danish waters during the winter 1985–86." (1986). Statens Istjeneste, Copenhagen, Denmark.

Timco, G. W., and Frederking, R. M. W. (1990). "Compressive strength of sea ice sheets." *Cold Reg. Sci. Tech.*, 17(3), 227–240.

Tryde, P., and Zorn, R. (1979). "Ice strength measurements in inner Danish waters during the winter of 1978–79." Danish Technical Research Council, Copenhagen, Denmark (in Danish).

Weeks, W. F., and Assur, A. (1969). "The mechanical properties of sea ice." Cold Reg. Sci. Engrg., Part II, Section C, Cold Regions Research and Engineering Laboratory, Hanover, N.H.

Appendix II. Notation

The following symbols are used in this paper:

a = parameter in Gumbel distribution;
b = parameter in Gumbel distribution;
f = probability density function;
f_h = function expressing h by k;
f_w = function of T_i and S_i;
F = probability distribution function;
F_G = Gumbel distribution function;
F_W = Weibull distribution function;
h = ice sheet thickness;
h_s = snow layer thickness;
k = parameter in Weibull distribution;
K = freezing degree-days index;
P = verification parameter;
P_d = distribution function based on data;
P_t = distribution function based on theory;
P_G = verification parameter for Gumbel distribution;
P_W = verification parameter for Weibull distribution;
S_i = gross ice salinity;

t = time;
T_a = air temperature;
$\bar{T}_a$ = daily average air temperature;
T_i = mean ice temperature;
T_s = temperature at ice-snow interface;
T_w = temperature at ice-water interface;
x = temperature-dependent part of $\sigma_u h$;
x_{th} = threshold value in POT analysis;
β = parameter in Weibull distribution;
λ_i = thermal conductivity of ice;
λ_s = thermal conductivity of snow;
ν = relative brine volume in ice;
ρ_s = density of snow;
σ_u = uniaxial compressive ice strength; and
σ_0 = reference compressive ice strength.

RESEARCH MEMO FOR DESIGN BASIS FOR ICE FORCES AT THE MIDDELGRUNDEN

Non-authorised translation by Rambøll, January 2000

1. INTRODUCTION

On behalf of SEAS, Helge Gravesen of Carl Bro has initiated a research of ice forces concerning preparation of design basis for the project regarding wind turbines at the Middelgrunden.

The research group consists of:

Helge Gravesen, Carl Bro A/S
Carsten Sørensen, RAMBØLL
N.-E. Ottesen Hansen, LIC Engineering A/S.

The research memo has been prepared within a limited time based upon the research group's existing knowledge on the basis of a draft from Carl Bro at an initial meeting 26 August 1999. The memo contains both comments and recommendations. The memo is primarily based upon a draft prepared by N.-E. Ottesen Hansen. Supplements and corrections are incorporated by Helge Gravesen, partly on the basis of comments from Carsten Sørensen and partly on the basis of a union meeting held 15 September 1999 at the premises of Carl Bro with participation of the research group and the following:

Lars Jørgensen and Per Vølund, SEAS
Sten Frandsen and Morten Lybech Thøgersen, Risø
René Zorn, DHI
Jørgen Pinholt, Elsamprojekt
Simon Green and Claus Gormsen, Niras
Torben Arnbjerg Nielsen, RAMBØLL
Jeppe Blak Nielsen, Carl Bro.

To the largest possible extent general demands to wind turbines in inner Danish waters have been worded.

2. SYMBOLS

U_{is}	velocity of the ice floes (m/s)
τ	shear tension on ice floe from air or water (pa)
c_D	drag coefficient on ice floe (= 0,004 and 0,006 for air and water, respectively) (-)
ρ	density of water and air, respectively (kg/m^3)/auxiliary parameter for ice load evaluation
V	water velocity 1 m below water surface or wind velocity at a height of 10 m (m/s)
c_u	compressive strength of the ice (pa)
σ_f	bending strength og the ice (pa)
t	thickness of the ice (m)
K_{max}	the total of the 24-hour mean of the frost period (<0°C)
ρ_{is}	density of the ice (900 kg/m^3)
Y_{is}	bulk density of the ice (8.84 kN/m^3)
γ_w	bulk density of the water (=ρ_wg) (N/m^3)
g	acceleration due to gravity (9.81 m/m^2)
E	elasticity module of the ice (2 GPa)
μ	friction coefficient (-)
F	ice load (N)
k	dimensionless factor on the ice load depending on the D/t ratio
D	diameter of the structure at the attack height of the ice, respectively the diameter of the conic structure at the water level line (m)
D_T	diameter at the top of the conic structure (m)
α	the angle with horizontal on the conic structure (°)
f_n	the eigenfrequency of the structure (s^{-1})
L	length of fissures in the ice (m)
ν	Poisson's ratio (-)
$\sigma_{c,lokal}$	local ice load (pa) on small area A_{lokal}
A_{lokal}	small area on the structure exposed to local ice load (m^2)
f_{is}	the frequency of the ice load (s^{-1})

3. DIMENSIONING FACTORS

In connection with the establishment of a wind farm a design basis will be prepared for ice loads.

The wind turbines are expected to have foundations with either vertical sides or being issued with a cone (directed upwards or downwards). Design basis shall comprise all these types. Ice load is not defined for structures dominated by fatigue loads.

In the design basis rules are to be specified for the following:

- The strength of the ice
- The friction between ice and turbine foundation
- The static load on the turbine foundation from ice floes
- The dynamic load on the turbine foundation from ice floes
- The load from icing up.

4. ICE FLOES

Ice loads on a structure result from the ice bumping against the structure or by the ice being pressed against the structure as a result of influence from current and wind. Thus there is an upper limit for the amount of ice loads, which may arise in the Øresund depending on forces of nature and the geography. The upper limit for the influences depend on:

a) The kinetic energy of the ice floes
b) Current and wind in the area
c) The size of the ice floes

The limit for the ice forces are evaluated by:

1. Maximum size of ice floe 2 × 2 km

2. Maximum current velocities and distributions of current velocities determinated for the area. It is assumed that the current line at the Drogden course is approx. twice the size of the current over the Middelgrunden. In connection with bid U_{is} = 1.0 m/s is estimated, since no correlation with wind is assumed

3. Wind and current load on ice floes are calculated on the basis of the formula:

   $\tau = 0.5\, c_D\, \rho\, V^2$
   where c_D = 0.004 and 0.006 for air and water, respectively
   ρ = density of water and air, respectively
   V = water velocity 1 m below the water surface or wind velocity at a height of 10 m, respectively.

The ice floes are assumed to have a shape so that the force initially is transferred to one wind turbine. As the ice floe is broken by a wind turbine, this will eventually come into contact with others.

As the basis for the above it may be noted that floes with a diameter of 500-2000 m and a thickness of up to 50 cm were observed in the waters opposite the Prøvestenen on a few days during the winter 1995/96. During the winter 1996/97 ice floes with a diameter of up to 20 m and a thickness of up to 5 cm were observed. SOK (1996 and 1997).

5. THE STRENGTH AND THE THICKNESS OF THE ICE

In the Øresundskonsortiet's Contract No. 2, Dredging & Reclamation, the following dimensioning ice thickness is stated in Design Requirement:

Recurrence period	5 years	10 years	50 years
t(m)	0.33	0.42	0.57

It is suggested to use the same basis for the Middelgrunden.

In the Elsam Project EFP-96 report about wind turbine foundations at sea the following strength parameters for the ice at a 50 years' ice situation at Rødsand are stated:

Compressive strength of the ice, σ_u	1.65 MpPa
Bending strength of the ice, σ_f	0.36 Mpa

It is suggested to use values for ice parameters approx. corresponding to those used by the Øresundskonsortiet for foundations for wind turbines situated at the Belts or further down towards the Baltic Sea, as these values are the newest for the area:

Return period	5 years	10 years	50 years	100 years	10,000 years
K_{max} (-°C 24 hours)	170	245	410	480	960
σ_u (Mpa)	1.0	1.5	1.9	2.0	2.6
σ_f (Mpa)	0.25	0.39	0.50	0.53	0.69
t (m)	0.33	0.42	0.57	0.63	0.91

where
σ_u = the thickness of the ice
σ_f = the bending strength of the ice
t = thickness of the ice = $0.032\ (0.9\ K_{max} - 50)^{0.5}$
K_{max} = the total of the 24 hours mean degree in the frost period (<0°C)

Other ice parameters:

Density of the ice, ρ_{is}	900 kg/m^3
Unit weight, Y_{is}	8.84 kN/m^3
Elasticity module, E	2 GPa
Friction coefficient between ice and ice is estimated to, μ	0.1

The 10,000 years' situation is included in case the ice load is treated as an accident load (without partial coefficients) and not as a natural load with characteristic parameters and appurtenant partial coefficients.

6. STATIC ICE LOADS

6.1 Structure with vertical sides

For determination of the ice load (crushing) on the wind turbines the application formulas stated in DS 410 for vertical structures are suggested. Structures are assumed to have vertical sides, the angle of which is less than 20°.

$$F = k\sigma_u Dt \qquad (6.2)$$

F	:	Horizontal ice force
k	:	Dimensionless factor depending on the D/t ratio
σ_u	:	The compressive strength of the ice
D	:	Diameter of the structure at the attack height of the ice
t	:	Thickness of the ice

$k = 1 + 3/(1 + D/t)$ for wind turbine foundations (with $D/t < 9$).

The above-mentioned formula originates from Tryde (1983).

6.2 Conic structures

For determination of the ice force (upbending ice, incl. share from crushing and ride-up) on the wind turbines the Ralston's formula for conic structures is used (API, Bul. 2N, 1995).

For an upward structure, see figure 1, the following formulas are used:

$$F_H = [A_1\sigma ft^2 + A_2\rho_w g\, t\, D^2 + A_3\rho_w g\, t\, (D^2-D_T^2)]A_4 \qquad (6.2)$$

$$F_v = B_1F_H\ 0\ B_2\rho_w g\, t\, (D^2-D_T^2) \qquad (6.3)$$

F_H	:	Horizontal force on the conic structure
F_V	:	Vertical force on the conic structure
$\gamma_w=\rho_w g$	:	Unit weight of water
μ	:	Friction coefficient between ice and structure
σ_f	:	Bending strength of the ice
t	:	Thickness of the ice
D	:	Diameter of the conic structure in the water level line
D_T	:	Diameter at the top of the conic structure
α	:	Angle with horizontal on the conic structure

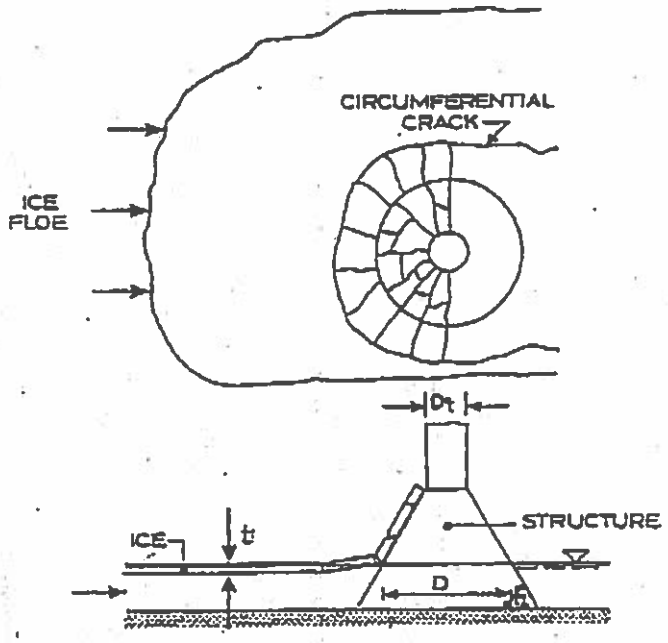

Figure 1. Ice floes pushed towards conic (upward) structure

The dimensionless coefficients, A_1, A_2, A_3, A_4, B_1, and B_2 are found from the figures in Enclosure 1. Often it will be more practical to use an auxiliary parameter ρ defined as a solution to the equation, cf. Thunbo Christensen (1988)

$$\rho - \ln(\rho) + 0.0830\,(2\rho + 1)\,(\rho - 1)^2\,(\gamma_w D^2/\sigma_f t) \tag{6.4}$$

Thus, A_1 and A_2 may be found analytically as

$$A_1 = (1 + 2.711\rho\,\ln(\rho))/(3(\rho - 1)) \tag{6.5}$$

$$A_2 = 0.075\,(\rho^2 + \rho - 2) \tag{6.6}$$

The correlation between ρ and $(\gamma_w D^2/\sigma_f t)$ is also shown on a figure in Enclosure 1.

If the conic structure is very steep ($\alpha > 70°$) the formulas (6.3) and (6.4) may be applied.

For a downward conic structure the formulas (6.3) and (6.4) may be applied with the correction that A_2, A_3, and B_2, read for an upward conic structure, are all multiplied by 1/9.

An attack point for the ice force is assumed between water level and 0.8 × ice thickness below the water level for a vertical construction. For an upward cone an attack point is estimated at the water level. For a downward cone an attack point 0.8 × ice thickness below the water level is estimated.

7. DYNAMIC LOADS

7.1 Vertical walls

It is suggested to use the method from LIC Engineering (1997).

By ice drift both dynamic and static influences arise. The natural vibrations of the structure will influence the breaking frequency of the ice, especially for structures with vertical sides, so that it is tuned to the eigenfrequency (lock-in). This means that the structure is influenced to vibrations in its eigenfrequency forms.

A conservative method for analysis of these vibrations is as follows.

The criterion for tuning is (cf. Singh et al (1990)):

$$U_{is}/t\, f_n > 0.3 \qquad (7.1)$$

U_{is} : The velocity of the ice floe
t : The thickness of the ice
f_n : The eigenfrequency of the structure

The load is applied as a serrate profile, see figure 2, where the maximum value is the static, horizontal ice load. After crushing of the ice the load is reduced to 20% of the maximum load. The load is applied with a frequency corresponding to the eigenfrequency of the structure. All eigenfrequencies fulfilling the tuning criterion shall be gone over.

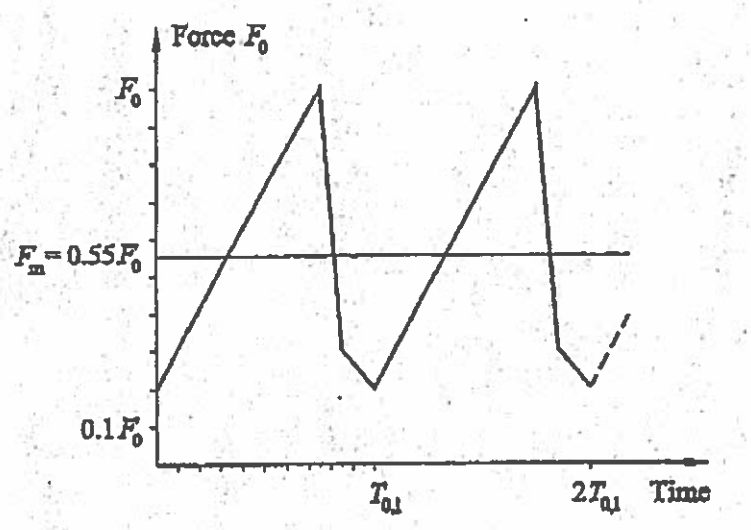

Figure 2. Serrate load profile

All subduing contributions in the structure are taken into account. Generalized contributions to be anticipated. Extra subduing as a consequence of the upfolding of the ice floes may be included if documentation therefore is available.

7.2 Conic structures

For conic structures the breaking frequency of the ice shall be calculated independent of the natural vibration of the structure. For all structures still applies that the frequency of

the ice load must not be close to the eigenfrequency of the structure / that the eigenfrequency of the structure must be minimum 20% outside the load frequency area for breaking ice.

The frequency from the ice load, f_{is}, may be determined as

$$f_{is} = U_{is}/L \tag{7.2}$$

where
U_{is} is the velocity of the ice floe
L is the length of fissures in the ice

L is determined as

$$L = \rho\, D/2 \tag{7.3}$$

where
D is the diameter of the cone at the water surface
ρ is determined from Enclosure 1, where ρ is given as function of $(Y_w D^2/\sigma_f t)$
σ_f = the bending strength of the ice
t = the thickness of the ice

The force is applied from the same assumed simplified model as shown in Figure 2 despite the breaking mechanism differs totally for conic structures compared to vertical structures.

The question regarding what is the best estimation for the length of the fissures and whether this changes from static to dynamic load case has been the subject of quite of few discussions.

Thunbo Christensen (1989) states

$$L = (0.5\, E\, t^3/(12\gamma_w(1-\nu^2)))^{0.25} \tag{7.4}$$

This is also stated by Clough & Vinson (199x). In Tsinker (1991) Blanchet et al (1989) are quoted for the fact that the block typically is 4-5 times t.

Izumiyama et al (1991) quotes Tatinclaux (1986) for the following expression:

$$L/t = 0.26 - 0.54\, (\sigma_t/\gamma_w t)^{0.5} \tag{7.5}$$

The fact that the velocity of the ice floe is included in the calculation expression for the length of the fissures is missing.

Carsten Sørensen has used a previous model for wedge-shaped structures (Sørensen, 1978), in which the velocity of the ice floe is included, for comparison of Ralston's (static) calculation with a wedge of approximately the same geometry, see Enclosure 2. It appears from the example that the dynamic calculation gives fissure lengths of 40% of Ralston's static calculation corresponding to a frequency of ice bumps of approx. 0.13 Hz.

It must be concluded that relatively wide limit of frequencies be assumed in order to give a safe design.

8. LOAD ON THE FOUNDATION FROM FROZEN ICE

In case the ice freezes on to the *foundation* a change of the water level will cause a vertical force on the pile.

The adhesion strength by shear breach for sea ice may be estimated to $\tau_0 < 0.1$ Mpa for structures of wood, steel, or concrete. The values correspond to an upper limit for the load.

Adhesion will appear only during quiet periods with neap tide.

It should be investigated whether the surrounding ice is able to absorb the force arisen in bending.

Values may be found in the literature Nakazawa et al (1994), Terashime et al (1999), and Tsinker (1991).

9. FRICTION ICE/WIND TURBINE FOUNDATION

The decisive factor for the friction between ice and wind turbines is the marine fouling on the wind turbines. A heavy fouling consisting of acorn barnacles and mussels increases the friction while a soft fouling consisting of plants does not increase the water resistance of the structure.

There will be sparse fouling of acorn barnacles below the ripple zone (lowest water level plus wave amplitude). Regarding ice forces the roughness from acorn barnacles is thus not taken into account. This means that normal roughness for concrete or steel will be used in the area where the ice attacks.

The value for friction coefficients is presented in for instance Nakazava et al, 1994.

By investigation of bridge piers and some of our own structures the hard marine fouling – acorn barnacles and mussels – appear below the ripple zone at low water. Some individuals may occur at the border but they will not contribute to a rough surface.

Besides, the few individuals that have settled at the water line are expected to be scoured off during building-up of an ice cover.

The following friction coefficients are used by calculation of ice forces.

Static: steel/ice: 0.2
concrete/ice: 0.3

Dynamic: steel/ice: 0.1
steel/concrete: 0.2

Marine fouling may be ignored.

The friction coefficients may be reduced if special covers are used, for which friction coefficients are given. The covers shall be of a nature so that at least they can be kept intact during an entire hard winter.

10. LOCAL ICE PRESSURE

The expression recommended by Thunbo Christensen et al (1995) is used:

$$\sigma_{c,lokal} = \sigma_c(5t^2/A_{lokal} + 1)^{0.5}$$

assuming that $\sigma_{c,lokal} < 20$ Mpa

At the same time the maximum load must be exceeded.

11. RAISING OF ICE

For a situation with a recurrence period of 50 years dimensioning for raising of ice to a minimum of level +7 m shall be used. Partial coefficient with earth pressure at rest from a large-grained mass with specific gravity 6 kN/m^3 should not be included.

12. ICING UP OF TURBINE TOWER

Norwegian standards state the following two load cases for icing up corresponding to 56° N latitude:

- spray from waves ice thickness max. 80 mm
- rain/snow ice thickness max. 10 mm

It is estimated that icing up is not a critical load case.

13. LITERATURE

Tryde, P. (1983): "Ice technique, the physical and mechanical properties of the sea ice. Ice forces on structures" (in Danish). Notes from 1983.

Nakazava, N., T. Terashima and H. Saeki, 1994: Ice Material Surface Interaction in Ice Friction and Ice-Adfreeze Bonding. Proceedings of the Fourth (1994) International Offshore and Polar Engineering Conference, Osaka, Japan, April 10-15, 1994.

Terashina, T., T. Kawai, A. Furya, K. Narita, N. Usani and H. Saeki, 1999: Experimental Study on Adfreeze Bound Strength between Ice and Pile Structures, Proceedings of the Ninth (1999) International Offshore and Polar Engineering Conference, Brest, France, May 40 – June 4, 1999.

SOK's Ice and navigation conditions in the Danish waters in winter 1995/96 and 1996/97, respectively (in Danish).

API (1995): "Recommended practice for planning, designing, and constructing structures and pipelines for arctic conditions", Bul. 2N, ed. 1995.

LIC Engineering (1997): "Mono-Pile Foundation. Wind turbine foundations at sea" (in Danish), EFP-96, J.nr. 1363/96-0006. Final report from 1997.

Thunbo Christensen (1988): "Calculation of Optimal Dimensionless Coefficients for Ralston's Plastic Limit Analysis Approach to Determination of Sheet Ice Loads on Conical Structures". Progress Report 66, ISVA, DTU, 1988.

Thunbo Christensen (1989): "Determination of extreme ice forces. Notes from a short course at University of Salford, with corrections from 1995.

Thunbo Christensen, F., Bruun, P. and sackinger, W.M. (1995): "Ice loading and pileup against vertical and inclined sea walls". ASCE task committee on inclined and vertical wall structures.

Ralston, T.D. (1977): "Ice force design considerations for conical offshore structures". Proc. 4th int. conf. on Port and Ocean Engng. under Arctic Conditions (POAC-77, vol. 2, pp. 13-31, Luleå, Sweden.

Ralston, T.D. (1979): "Plastic limit analyses of sheet ice load on conical structures". Physics and mechanics of ice. IUTAM symposium, Copenhagen, 1979.

Singh, S.K., Timeo, G.W., Frederking, R.M.W., and Jordan, L.J. (1990): "Test of ice crushing on a flexible structure". 9th Int. Conf. on Offshore Mechanics and Arctic Engng. Vol IV, pp. 89-94.

Clough & Vinson (199x): "Ice forces on fixed conical structures".

Tsinker (1995): "Marine structures engineering: Specialized applications". Chapman & Hall.

Blanchet, D., Churcher, A., Fitzpatrick, J., and Barda-Blanchet (1989): "An analysis of observed failure mechanics for laboratory first-year and multi-uear ice". In special report 89-5 by IAHR, edited by G.W. Timco.

Izumiyama, K., Kitagawa, H., Koyama, K., and Uto, S. (1991): "On the interaction between a conical structure and ice sheet". Proc. 11th int. conf. on Ports and Ocean Engng. under Arctic Cond., St. John's, Canada.

Tatinclaux (1986): Ice floe distribution in the wake of a simple wedge". Proc. OMAE'86, vol. 4.

Sørensen, C. (1978): Interaction between floating ice sheets and sloping structures. Series Paper 19, ISVA. DTU.

ENCLOSURE 1

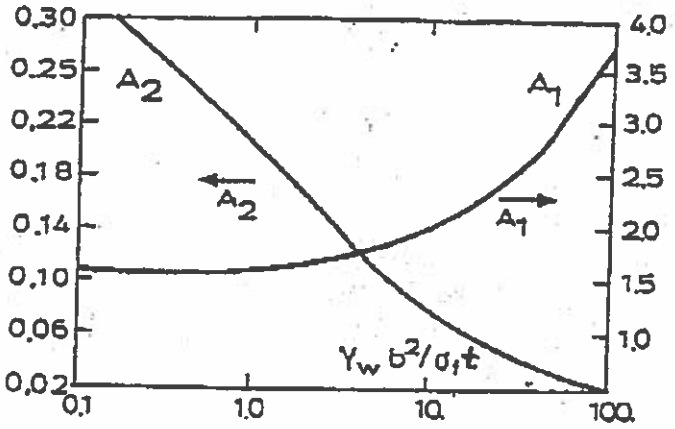
A2
A1
A2
A1
Yw b²/σit
0.30
0.25
0.22
0.18
0.14
0.10
0.06
0.02
4.0
3.5
3.0
2.5
2.0
1.5
1.0
0.1
1.0
10.
100.

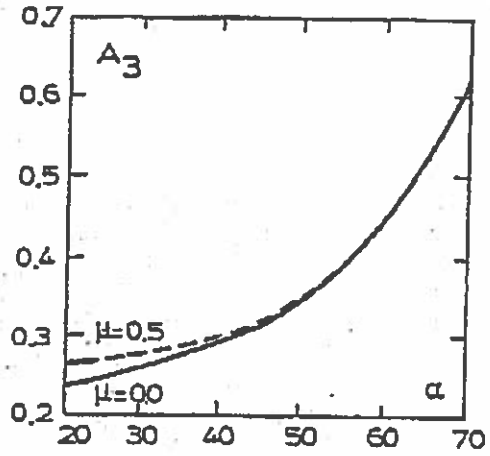
A3
μ=0.5
μ=0.0
α
0.7
0.6
0.5
0.4
0.3
0.2
20
30
40
50
60
70

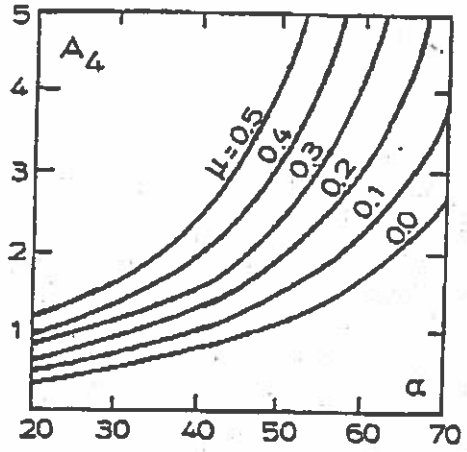
A4
μ=0.5
0.4
0.3
0.2
0.1
0.0
α
5
4
3
2
1
20
30
40
50
60
70

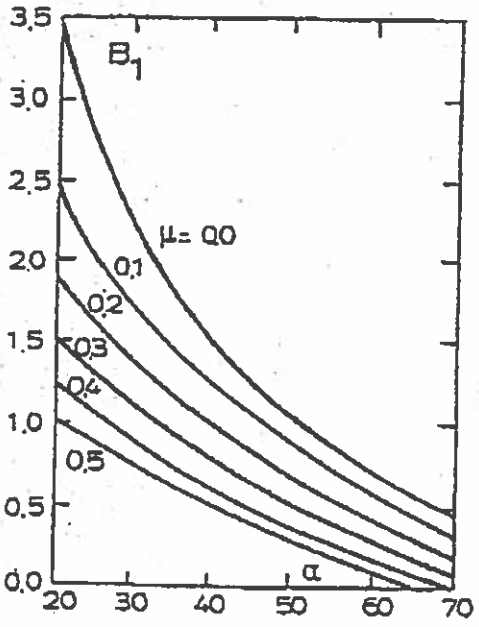
B1
μ= 0.0
0.1
0.2
0.3
0.4
0.5
α
3.5
3.0
2.5
2.0
1.5
1.0
0.5
0.0
20
30
40
50
60
70

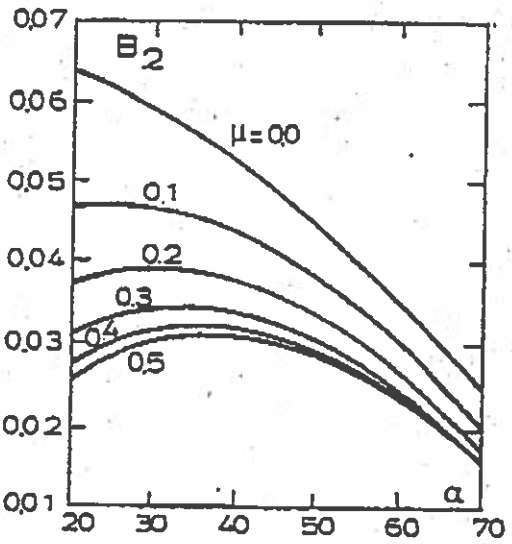
B2
μ=0.0
0.1
0.2
0.3
0.4
0.5
α
0.07
0.06
0.05
0.04
0.03
0.02
0.01
20
30
40
50
60
70

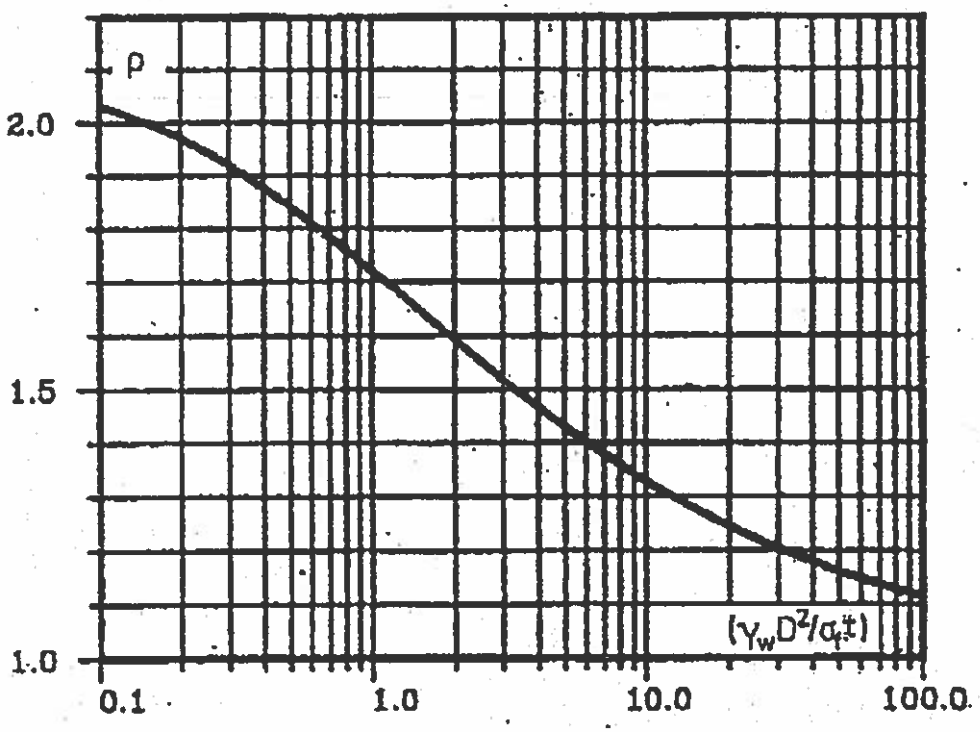
ρ
2.0
1.5
1.0
0.1
1.0
10.0
100.0
$(\gamma_w D^2/\sigma_t^{\ddagger})$

ENCLOSURE 2

Comparison of sundry formula expressions

A. CALCULATION ASSUMPTIONS

Structure with leaning front – Cone, cone angle = 45°, diameter = 8 m, tower diameter = 2 m.

Ice parameters: r_o = 1250 kN, r_f = 500 kN, h = 0.64m, velocity of floe u = 1 m/sec, friction factor = 0.2, crushing contact factor k = 0.7.

B. CALCULATION RESULTS

Load case	Horizontal ice movement				Vertical ice movement
Component	horizontal ice load (kN)	vertical ice load (kN)	ice breach, length (m)	ice bump frequency (Hz)	vertical ice load (kN)
method					
ref. 1	750	-680	7.9	0.13	
ref. 2	640	-520	3.1	0.32	

Annex E (Informative) Recommendations for design of offshore wind turbine support structures with respect to ice loads

Comment [Pu40]: Action 14.03 based on 10243_003

E.1 Introduction

Ice loading is a severe and decisive load case in waters with winter climate. The occurrence of ice must be assessed at offshore sites in lakes and sea waters in North America, northern Europe and northern Asia. Moving ice can induce extreme foundation loads and cause catastrophic failures for offshore wind turbines.

This annex is, to a large extent, based on [1] and [2].

The magnitude of the ice forces shall be estimated taking into account local ice conditions and water levels as well as ice movements, and to the size and form of the foundation. The following ice loads shall be assessed:

- horizontal load due to temperature fluctuation in a fast ice cover (thermal ice pressure)
- horizontal load from a fast ice cover subject to water level fluctuations and in terms of valve effect.
- horizontal load from moving ice floes
- pressure from hummocked ice and ice ridges due to both subduction and ridging processes
- vertical force from fast ice covers subject to water level fluctuations.

E.2 General

Ice loads are normally assumed to occur at an arbitrary water level between MHW and MLW if no specific statistical analysis has been carried out. For structures including cones sensitive to the water level, statistical data for water level fluctuations at winter conditions, should be collected in order to identify the design water level range determining the height of the cone. The foundations in this annex are assumed to be constructions with a cylindrical/rectangular waterline cross-section including vertical cylinders and cones constructed of concrete or steel.

In lakes or in the sea close to the coastline, the ice sheet is normally not moving after having grown to a certain thickness. Loads originating from moving ice shall be checked up to this thickness. Loads from thermal pressure, valve effect and vertical lift shall be checked for thicker ice covers due to later growth.

In areas where moving ice is expected, the loads from moving ice shall be calculated for all seasons and be considered to act in the directions of the prevailing current and wind vector. The possibility that the wind direction can be independent of the motion direction of the ice shall be considered. A dynamic time simulation of the load case is usually required. The possibility for dynamic locking of the ice breaking frequency to the wind turbine eigenfrequencies and to other turbines in a wind farm shall be considered. Model tests can be used as part of an assessment.

E.3 Choice of ice thickness

The ice thickness, h, shall be based on analysis of statistical data from a local ice atlas or similar document (see [7]). References to databases are given at the end of the annex. In most cases a combined analysis of ice thickness and crushing strength is to be carried out. For wind turbines in the open sea the thickness shall be chosen as a category corresponding to the 50 year recurrence period. For wind turbines in archipelagos and

inland seas, the thickness of moving ice shall be chosen to correspond to "Normal winters" and fast ice cover thickness corresponding to the 50 year recurrence period.

Below is an equation to estimate the ice thickness at the end of a frost period is given:

$$h = 0{,}032\sqrt{0{,}9K_{max} - 50} \quad (1)$$

where K_{max} is the absolute value of the total of those 24 hours mean temperatures that are less than 0°C in a frost period (degreedays)

E.4 Load Cases

The following load cases shall be applied if relevant for the site. The wind and wave conditions are given in Table 3 in the main document. Load cases E1, E2, E3, E5 and E6 are ultimate load cases while E4 and E7 are fatigue load case where interaction of wind is important. The implementation of dynamic loading is described in E.4.6.

E.4.1 Horizontal load from fast ice cover originating from temperature fluctuations (DLC E1)

Thermal ice pressure shall only be considered in lakes and in brackish seas. In the open sea with saline water like the North Sea the thermal ice pressure can be neglected.

Unilateral thermal ice pressure will be largest on the outer wind turbine foundations in a wind farm, and shall be assumed to act from land towards the open sea or from the centre of a windfarm, radially outwards. If an icebreaker makes a channel through a fast ice cover under thermal pressure the ice will expand towards the open channel and forces according to (2) can occur.

The thermal force can be written

$$H_t = f_t D \quad (2)$$

where D is the diameter of the foundation at the water line. D is set to 4 m if D < 4 m.

f_t unit force/width of foundation

f_t is set to 300 kN/m for stand-alone foundations or for peripherical foundations in a windfarm. For foundations behind the outer row or inside a windfarm f_t is given the value 100 kN/m.

E.4.2 Horizontal load from fast ice cover originating from water level fluctuations and valve effect (DLC E2)

Unilateral horizontal pressure from valve effect between wind turbine foundations or between foundations and the shore can be estimated as in (3).

$$H_v = f_v D \quad (3)$$

where D is the diameter of the foundation at the water line. D is set to 4 m if D < 4 m.

f_v = 200 kN/m

E.4.3 Horizontal load from moving ice (DLC E3, E4 and E7)

Forces from large moving ice floes shall be estimated according to the method described in E.4.3.1 or in E.4.3.2. The requirement for extrapolation of combined extreme wind and ice loads for DLC E3 is addressed in E.6. No wave condition or water level is stated for the load case but the water level shall be checked for the specific site during ice conditions, in order to find the relevant action point for the resulting pressure.

DLC E7 is a situation where the turbine is parked and moving ice can introduce fatigue loads on the support structure and the tower.

E.4.3.1 Vertical cylindrical shapes

This method is taken from [1] and [3]. It considers vertical structures with cylindrical shapes. The maximum static force due to crushing may be estimated from:

$$H_d = k_1 k_2 k_3 h D \sigma_c \qquad (4)$$

where k_1 shape factor for the shape of the foundation on the ice impact side,

k_2 contact factor for the ice contact against the foundation,

k_3 factor for the ratio between ice thickness and the foundation diameter,

D is the diameter of the foundation at the water line,

σ_c crushing strength of the ice

Ice crushing strength σ_c

The values should be determined from statistical data of crushing strength or of the product $\sigma_c h$. The available data shall be corrected for the actual temperature and brine content in order to carry out a statistical analysis of the reference crushing strength, see [7].

In case no local ice data are available the crushing strength can be chosen from below which are values typical for the Northern Baltic Sea and Arctic Canada[12]:

σ_c = 3,0 MPa for ice in motion from wind and current at the coldest time of the year

= 2,5 MPa for moving ice at a very slow motion caused by thermal expansion or shrinking.

= 1,5 MPa for ice during spring at temperatures near the melting point

= 1,0 MPa for partly deteriorated ice at temperatures near the melting point

= 0,5 MPa for saline first year ice in the open sea, as e.g. in the North Sea.

---

[12] The above referred values are in accordance with the Canadian bridge standard (1978) which gives values in the range of 0,7 – 2,8 MPa. The Soviet standard (1976) states a range of 0,44 – 1,47 MPa. The above given values can be seen as conservative.

Shape factor k_1

If the foundation can cut the ice floe instead of only crush it at the impact point, the shape factor k_1 is given values:

k_1 = 1 for rectangular shape

= 0,9 for circular shape

Contact factor k_2

The contact factor covers the fact that ice under continuous crushing is not in contact with the whole nominal foundation surface *Dh* except at the start of the movement when it is completely frozen to the foundation.

k_2 = 0,5 when the ice is continuously moving.

= 1 when the ice is frozen to the foundation surface at the time the ice is starting its movement.

= 1,5 when the frozen ice is locally increased in thickness around the foundation.

For the third case an alternative approach is to exchange the thickness *h* by the thickness of the ice in the immediate vicinity of the foundation instead of referring to the undisturbed ice field.

Aspect ratio factor, k_3

The aspect ratio factor takes the three-dimensional stress state in the contact point into consideration. If the pile or tower is slim in comparison with the ice cover thickness the stress state can be considered to be two-dimensional. Thus

$$k_3 = \sqrt{1 + 5h/D}$$

Height of load

If there is risk of ice piling up close to the foundation, the height of load action shall be increased with 0,2 times the water depth at depths less than 6 m.

Calibration with model tests

Model tests have shown that the force level and type are very dependent on whether continuous crushing takes place or if a non-stationary buckling pattern occurs, see [9]. No significant dependence on the peak force level from the ice velocity has been found. Model testing is further described in E.7.

E.4.3.2 Sloping Shapes

This equation by Ralston, 1977, is proposed in [2] and is valid for sloping structures, i.e. wind turbine towers with ice cones. This has also been adopted as recommended practice by API in [5]. The formula is quoted valid for slope $0° < \alpha < 70°$, where α is the slope measured from a horizontal level. Model tests referred in [9] have shown that Ralston's formula present a safe value for ice forces on cones up to ice floe velocities of 1 m/s.

Comment [Pu41]: Up-bended ??

The horizontal load for ice being up-bended is

$$H = A_4\left[A_1\sigma_b h^2 + A_2\rho_w ghD^2 + A_3\rho_w gh\left(D^2 - D_T^2\right)\right] \quad (5)$$

The vertical downward load is

$$V = B_1 H + B_2\rho_w gh\left(D^2 - D_T^2\right) \quad (6)$$

where A_1, A_2, A_3, A_4, B_1 and B_2 are dimensionless coefficients which are functions of the ice-to-cone friction coefficient μ, and the cone angle α. The coefficients are found in the graphs in fig. 1.

σ_b = bending strength of ice, not less than 0,26 σ_c

h = thickness of ice sheet

ρ_w = density of water

g = gravitational acceleration

D = water line cone diameter

D_T = cone top diameter (equal to tower diameter)

For cones down-bending the ice, the same formulas applied if ρ_w is changed to $\rho_w/9$ and the vertical force has an upward direction.

The above formulae may be used if the height of the cone exceeds one ice thickness from top of ice (up-bending cone) or bottom of ice (down-bending cone).

For double sided cones the forces may be estimated as described above except for forces directly on the tip. For a sharp tip the horizontal force shall be increased by a factor 2, and for a round tip the forces shall be increased by a factor 3, see [9].

Friction

The dynamic ice-to-cone friction coefficient μ may be set to:

μ = 0,15 for a cone of concrete/corroded steel

and

μ = 0,10 for a cone of new or painted steel.

E.4.3.3 Local ice pressures

The foundation shall be designed for the following local ice pressure:

$$\sigma_{c,local} = \sigma_c\,(5\,h^2/A_{local} - 1)^{0.5} < 20\ \text{MPa} \quad (7)$$

where

A_{local} = local area considered

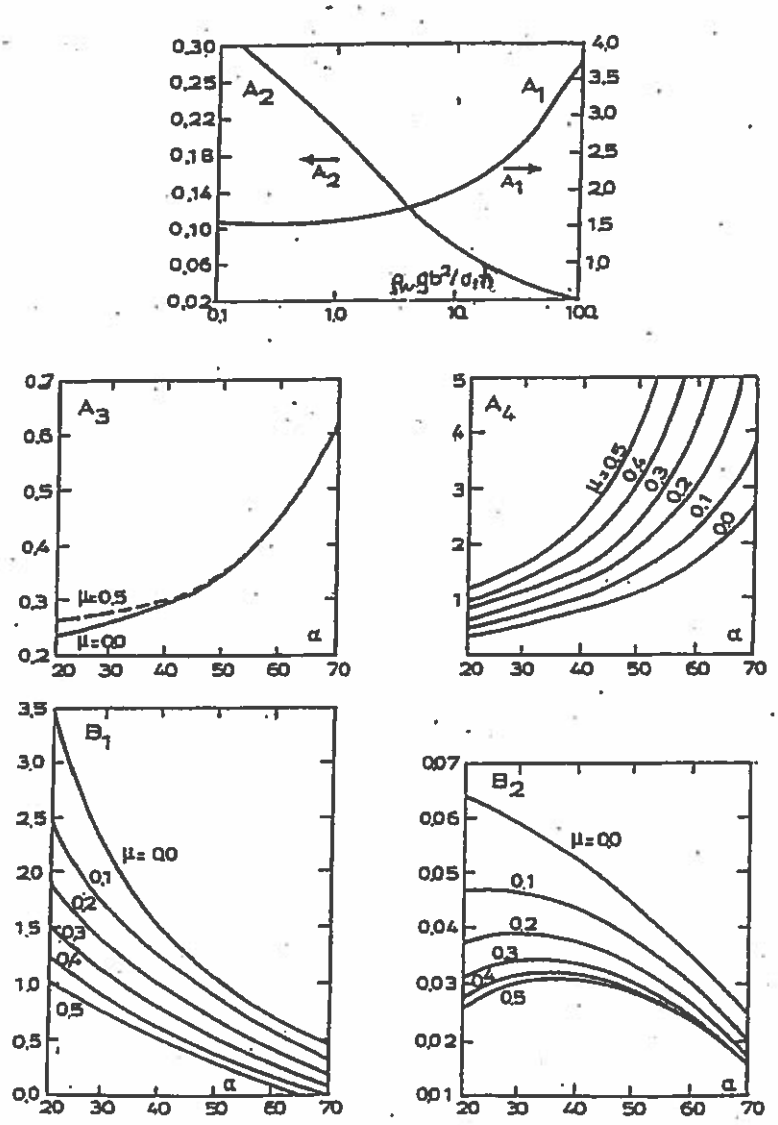

Fig. 1 Ice force coefficients for plastic limit analysis. From [6].

E.4.3.4 Wind and current induced load

The load from wind or current on an ice floe can be estimated with

$$H = C_d \rho \frac{U^2}{2} A \qquad (8)$$

where for wind

C_d = 0,004

ρ = 1,3 kg/m^3

U = free stream velocity at 10 m above ice surface

and for water

C_d = 0,006

ρ = 1000 kg/m^3

U = free stream velocity at 1 m below the ice lower surface

A = area of the ice floe.

The wind and/or current load is limited up to the crushing strength of the ice. The combined drift forces from wind and current should be based on a statistical analysis of the site data.

E.4.4 Vertical load from fast ice cover (DLC E5)

The vertical load in case of fluctuating water level with a fast ice cover frozen to the foundation is limited either by the shear strength at adhesion to the foundation surface, V_τ, or by the bending strength if the ice is broken in a ring around the foundation, V_b.

The lower of the two alternatives is decisive and shall be used.

$$V_\tau = A\tau \qquad (9)$$

where τ = adhesive shear strength

A = πDh is contact surface for a circular vertical foundation

The adhesive shear strength τ can be set to 0,8 MPa for steel – fresh water ice, to 0,3 MPa for steel – saline ice [12], and to 1 MPa for concrete – saline ice [8]

$$V_b = 0{,}6A\sqrt{\sigma_b \rho g \Delta z} \qquad (10)$$

where A = the contact surface,

σ_b = the bending strength of ice, not less than 0,26 σ_c

ρ = water density,

g = gravitational acceleration

Δz = water level difference

E.4.5 Pressure from ice ridges (DLC E6)

DLC E6 covers the situation with an extreme ice load combined with extreme wind conditions. At this situation wave loads are of no importance for the structure. The wind load which gives the highest shear loads on the support structure shall be applied.

Very large loads can appear if ice ridges enclosed in a moving ice sheet press on the foundations. Such an ice ridge consists of ice fragments and can contain consolidated ice fragments frozen together to 2–3 m thickness. Loose blocks below and above the consolidated ice give little contribution to the ice load.

The loads are roughly estimated either with the assumption that the ice is crushed or that the ice ridge is bent in the horizontal plane to failure. It is generally not recommended to install wind turbines in areas with the risk of ice ridging.

E.4.6 Dynamic loading

The wind turbines shall be checked for dynamic effects from ice loading. Below some simplified equations are given for dynamic load simulation which can be used if statistical data or measurements are not available.

The variation of loading from moving ice on vertical foundations may be approximated to be vertically shifted sinusoidal as

$$H_{dynv} = H_d\left(\frac{3}{4} + \frac{1}{4}\sin(f_N t/(2\pi))\right) \quad (11)$$

where H_d = the horizontal load from moving ice from (4)

t = time

f_N = the wind turbine structural eigenfrequency. Both 1st and 2nd modes should be checked.

The dynamic effects is strongest when a buckling type of failure occurs, which induces strong variations in the ice force, see [9] and [11].

Criteria for tuning is according to [10]

$$\frac{U}{(h \cdot f_N)} > 0{,}3 \quad (12)$$

where U = ice floe speed

The variation of loading from moving ice on conical foundations ($\alpha \geq 30°$) may be approximated to be vertically shifted sinusoidal as

$$H_{dynk} = H_d\left(\frac{3}{4} + \frac{1}{4}\sin(\frac{f_b}{2\pi}t)\right) \quad (13)$$

where H_d = the horizontal load from moving ice from (4)

t = time

$f_b = U / Kh$ where U is the actual speed of the ice floe and $4 \le K \le 7$. The value of K which gives highest load shall be chosen.

Alternatively a triangular shaped form, see Figure 2, may be assumed for the dynamic load (both vertical cylinders and cones).

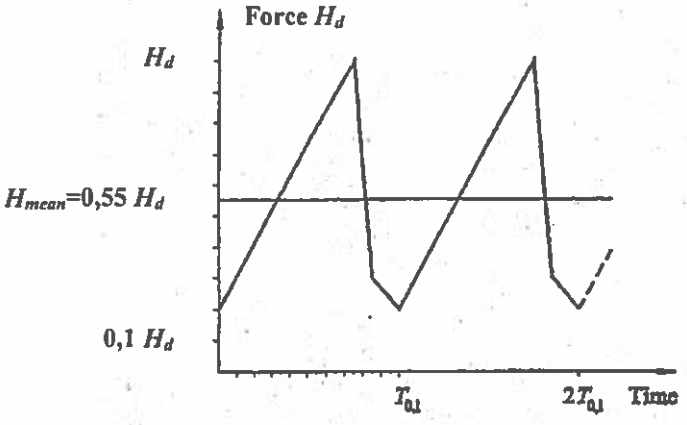

Fig. 2 Serrated load profile ($T_{0,1}$ = 1/f_N or 1/f_b)

Loads from shock impact of a large ice floe should be checked with a transient load approach as suggested below.

$$H(t) = kUt \quad for \quad t \le \frac{H_d}{kU}$$

$$H(t) = \begin{cases} 0 \\ or \\ H_d \end{cases} \quad for \quad t > \frac{H_d}{kU} \qquad (14)$$

where U = impact velocity

t = duration of shock impact

k = stiffness of the structure at waterline

E.6 Requirements on stochastic simulation

Due to limited access to quality ice field monitoring it is usually required to base response simulations primarily on ice model tests as described below in E.7. From such model tests time series describing the stochastic ice load may be available. As ice model tests usually only generate load time series corresponding to a few minutes prototype load it is required to extend the measured time series by methods as described in [9], in order to obtain a number of almost statistically independent 10 minutes simulations of the dynamic ice load.

Independent ice load time series and wind forces are then simulated in a dynamic turbine model. The number of 10 minutes events (N) with combined operational wind load and extreme ice load is estimated and the extrapolated extreme load may then be estimated as outlined in Annex F of IEC 61400-1 with the modification that it is not the inverse of the

number of 10 minute events in 50 years but the inverse of the number 10 minute events with operational wind speeds during the movement of the 50-year ice floes that shall be used in the Eq. (F-6).

E.7 Requirements on model testing

Model tests may be carried out with artificial ice. Usually the results are scaled on the basis of a Froude modelling law scaling the forces by λ^3, bending and crushing strengths with λ and time by $\lambda^{0.5}$.

In order to model dynamic interaction between the ice force and the structure it is required to model the resonance frequency, the damping and the stiffness of the structure exposed to ice loads correctly.

For cone structures limited dynamic interaction occurs, so stiff model test results may be used to generate the dynamic ice load input to the foundation. For vertical structures severe dynamic interaction between the ice load and the oscillations of the structure may occur and this aspect should be part of the modelling. For this case it is of special importance that relevant resonance frequency, damping and stiffness are being modelled so the ratio between the ice floe speed and the speed of the structural oscillation is correctly modelled. For a typical wind turbine foundation it is usually the 2nd mode of resonance which may give rise to dynamic interaction with the ice load.

Typical requirements for model tests, the associated results and a design procedure are illustrated in [9]

References

[1] Bergdahl, Lars: Islaster på vindkraftverk till havs, Dimensioneringsrekommendationer (in Swedish) Department of Water, Environment Transport, Chalmers, Rapport nr 2002:1. (Ice Loads on Wind Turbines at Sea, Recommendations for Design).

[2] Christensen, Flemming Thunbo and Gravesen, Helge: Determination of Extreme Ice Forces, Lecture Notes. 2003.

[3] Haapanen, E, Määttänen, M and Koskinen, P: Offshore Wind Turbine Foundations in Ice Infested Waters. Proceedings OWEMES conference 1997.

[4] Löfquist, Bertil: Istryck mot bropelare (in Swedish), Vägverket 1987. (Ice pressures at bridge columns.

[5] American Petroleum Institute, API: Planning, Designing and Constructing Fixed Offshore Structures in Ice Environments. Bulletin 2N, API, Second Edition, 1995.

[6] Ralston, T: Ice Force Design Considerations for Conical Offshore Structures. POAC 1977

[7] Christensen, F.T. and Skourup, J: Extreme ice properties, Journ. of Cold Regions Engineering, Vol. 5, No. 2, June, 1991, pp 51-68.

[8] Cammaert, A.B. and Muggeridge, D.B: Ice interaction with offshore structure. Van Nostrand Reinhold. New York, 1988

[9] Gravesen, H., Petersen, B., Sørensen, S.L., and Vølund, P: Ice forces to wind turbine foundations in Denmark. POAC'03, Trondheim. Norway, 2003.

[10] Singh, S.K., Timco, G.W., Frederking, R.M.W., and Jordam, L.J: Test of ice crushing on a flexible structure. 9th Int. Conf. on Offshore Mechanics and Arctic Engng, Vol. IV,pp 89-94, 1990.

[11] Yue, Q., & Bi, X.,: Ice-Induced Jacket Structure Vibrations in Bohai Sea, Journal of Cold Regions Engineering, Vol. 14, No. 2, June 2000, ASCE.

[12] Oksanen P: Adhesion strength of ice, VTT, Espoo, Finland 1982

Databases for ice conditions

Climatological Ice Atlas for the Baltic Sea, Kattegat, Skagerak and Lake Vänern. Sjöfartsverket , S-601 78 Norrköping, Sweden

The National Ice Center, USA (NATICE): www.natice.noaa.gov

The National Snow and Ice Data Center, USA (NSIDC): www.nsidc.org

Available online at www.sciencedirect.com
SCIENCE DIRECT
Cold Regions Science and Technology 41 (2005) 1–23
cold regions science and technology
www.elsevier.com/locate/coldregions

Ice loading on Danish wind turbines Part 1: Dynamic model tests

Anne Barker[a,*], Garry Timco[a], Helge Gravesen[b], Per Vølund[c]

[a] Canadian Hydraulics Centre, National Research Council of Canada, Ottawa, Ontario, Canada K1A 0R6
[b] Carl Bro, Granskoven 8, DK 2600 Glostrup, Denmark
[c] SEAS, Slagterivej 25, DK 4690 Haslev, Denmark

Received 14 July 2003; accepted 19 May 2004

Abstract

An extensive model test program has been carried out to investigate the key ice load issues on offshore wind turbines in Danish waters. Tests were performed using a compliant structure that had scaled structural characteristics. The test program investigated seven configurations of model structures and dynamic characteristics. Both first- and second-mode vibration issues were investigated. Forty-one ice sheets were used giving information on 144 different experimental set-ups. The parameters that were changed in the tests included the ice velocity, ice thickness, shape of the structure, water level on the structure, structure stiffness and the natural frequency of the structure. Measurements were made of forces, accelerations and displacement of the model during the interaction with ice.

Four different ice failure modes were identified—flexure, crushing, mixed mode, and lock-in. The results gave information on the anticipated ice loads and the likelihood of ice-induced vibrations for both the first-mode and second-mode vibration frequencies. They also provided guidance on the optimum angle and cone-size for a protective ice collar for the wind turbines. This paper provides the results of the model tests. A companion paper [Cold Reg. Sci. Technol., (2004)], provides information on the application of the results to the design of an offshore wind turbine farm.

Keywords: Offshore; Wind turbine; Model; Ice; Forces; Acceleration; Vibration

1. Introduction

SEAS, a Danish power production company, has been responsible for developing wind power utilisation through construction of large offshore wind farms (see Fig. 1). SEAS contracted the Canadian Hydraulics Centre (CHC) of the National Research Council of Canada (NRC) to perform a model test program to investigate ice loading on offshore wind turbines in Danish waters. The test program was designed to investigate the key ice engineering issues for the Rødsand site, as well as identify ice issues for other sites being considered in Danish waters. The model tests were designed to provide guidance on a number of key issues:

1. To define a load scenario (time series) corresponding to, respectively, a 2×10^{-2}/year and an 8×10^{-4}/year event with associated water level

* Corresponding author.
E-mail addresses: anne.barker@nrc-cnrc.gc.ca (A. Barker), garry.timco@nrc-cnrc.gc.ca (G. Timco), HIG@CARLBRO.DK (H. Gravesen), pvl@e2.dk (P. Vølund).

0165-232X/$ - see front matter © 2004 Elsevier B.V. All rights reserved.
doi:10.1016/j.coldregions.2004.05.002

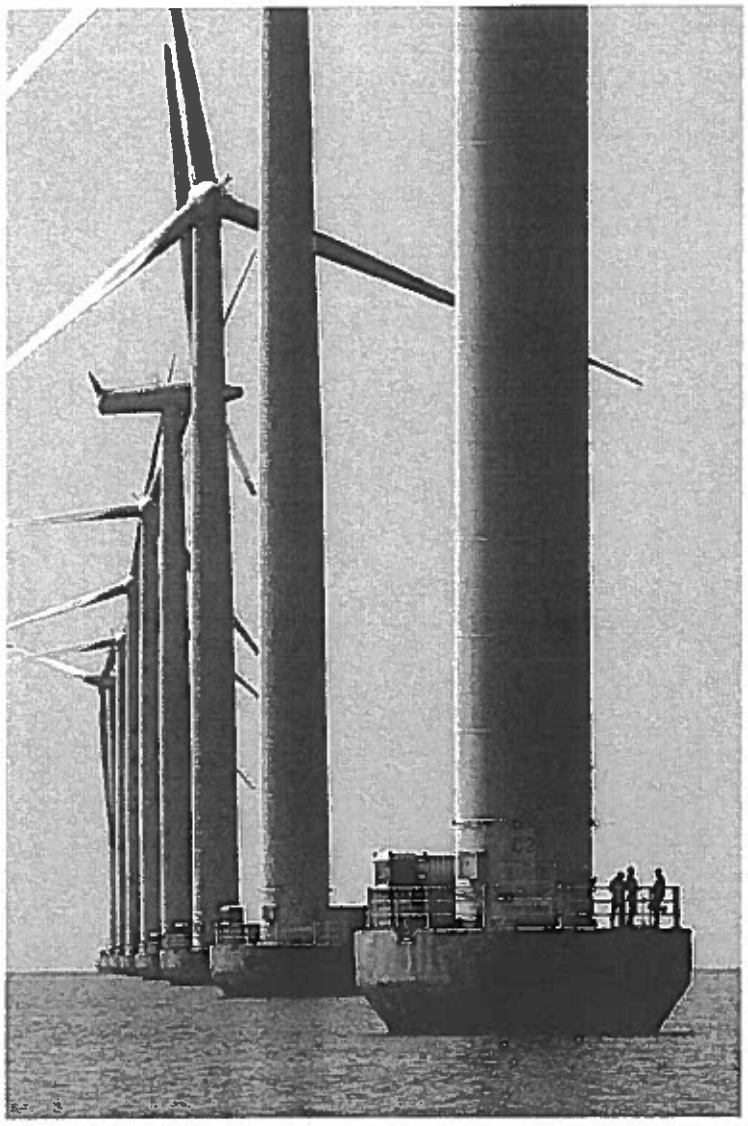

Fig. 1. Photograph showing as-built offshore wind turbines and ice-breaking cones (55° inverted cone), Nysted Offshore Wind Farm near Rødsand, Denmark.

and current data. The basic assumption is that loading is associated with impact from 2 km ice floes.

2. Verification of formulae for (inverse) conical structures.
3. Investigation of the effect of length of cone from actual water levels (risk of crushing against vertical cylinder); i.e. optimum size and angle for conical-shaped protective collar.
4. Evaluation of the likelihood and risk of confining broken ice pieces in front of structure (between cone and seabed).
5. Determining the dynamic amplification and risk of interlocking for different structural shapes and ice

conditions. This was to be investigated for both first-mode and second-mode vibration frequencies.
6. Determining the interaction from dynamic ice load on wind-induced tower oscillations (mainly for a monopile structure).
7. Determining the influence of the sharpness of a double-cone design with respect to ice loads and ice failure behaviour.

In order to address these issues, the study examined ice interaction with four conical structures and a cylindrical structure in ice conditions that were representative of Danish waters. The study also examined the effects of the ice loading with respect to the possible excitation of the first-mode and second-mode vibration frequencies of the wind turbine. The model test program provided information on all of the above items and the results are presented in this paper. The detailed application of the results is discussed in the accompanying paper (Gravesen et al., 2004).

2. Experimental process

2.1. Test facility

The tests were performed in the ice tank at the NRC Canadian Hydraulics Centre in Ottawa (Pratte and Timco, 1981). The tank, which is 21 m long by 7 m wide and 1.2 m deep, is housed in a large insulated room that can be cooled down to an air temperature of −20 °C. By varying the room's air temperature, ice sheets can be grown, tempered or melted. A carriage that can travel the length of the tank spans the tank. The carriage is driven through two helical-cut rack and pinion gears, and is designed for loads up to 50 kN with a speed range from 3 to 650 mm/s. A small service carriage also spans the tank and this was used in most tests to push the ice past the model being studied.

2.2. Modelling the structures

The model structures consisted of one or two parts—(1) a metal pipe that was closed at the bottom, and (2) a cone that was made of wood that could be slid along the pipe and clamped at the desired height. The wind turbine was modelled using five different structural shapes and two different dynamic characteristics:

- a cylindrical structure at the waterline,
- an inverted cone at the waterline with a cone angle of 55°,
- an inverted cone at the waterline with a cone angle of 65°,
- a double cone at the waterline with a cone angle of 55°,
- a double cone at the waterline with a cone angle of 55° and an edge rounded to a specified radius,
- a cylindrical structure with a system that had different dynamic characteristics (increased frequency and stiffness) corresponding to the second mode of a large offshore wind turbine,
- a double cone at the waterline with a cone angle of 55°, with the aforementioned second-mode dynamic system.

Fig. 2 shows these seven configurations as schematic illustrations with the model-scale characteristics of the structures and photographs of the models.

Choosing an appropriate geometric scale factor for the test is usually the first step of a model test program. For this, consideration must include the overall size and mass of the model structure, the scaled interaction rates, the capacity of the measuring equipment, and the appropriateness (or scalability) of the ice. The linear dimensions of the prototype (p) structure are reduced to model (m) scale by a geometric scale factor λ. For these tests, the inertial, gravitational (bending) and crushing forces are of particular importance, and so the scaling was performed using Froude and Cauchy scaling. The scaling laws are given in Table 1 (see Timco, 1984 for a review on ice modelling techniques). For the present tests, a scale factor of 1:26 was chosen (i.e. $\lambda=26$). The values presented in this paper are in model-scale.

2.3. Modelling the dynamic characteristics

Over the past several years, there has been a limited number of investigations of ice-induced vibrations on offshore and coastal structures. The tests have been of two different types. The first type uses a rigid structure and simulates the compliance of the foundation. Tests of this type investigated at the

CHC have included the bridge piers of the Great Belt Link in Denmark (Christensen et al., 1995; Timco et al., 1995) and the JZ-20 offshore platform in the Bohai Bay region of China (Timco et al., 1992). The second type of test models the full elasticity of the structure itself. This type of test is considerably more complicated than the first type. To date, the offshore structure Molikpaq has been modelled at the CHC using an elastic model (Cornett and Timco, 1997; Timco et al., 1997). In all cases, scaling of the test results to known full-scale behaviour and loads has yielded very good correlation. This study uses the first method of investigating the ice-induced vibrations.

The dynamic characteristics of the structure were modelled by assuming that the structure was compliant in the horizontal plane, but rigid in the vertical direction. With the present experimental arrangement, the structural compliance could be fully modelled in the horizontal plane, in the in-line (x-direction), transverse (y-direction) and rotational directions. The wind turbine structure is symmetrical

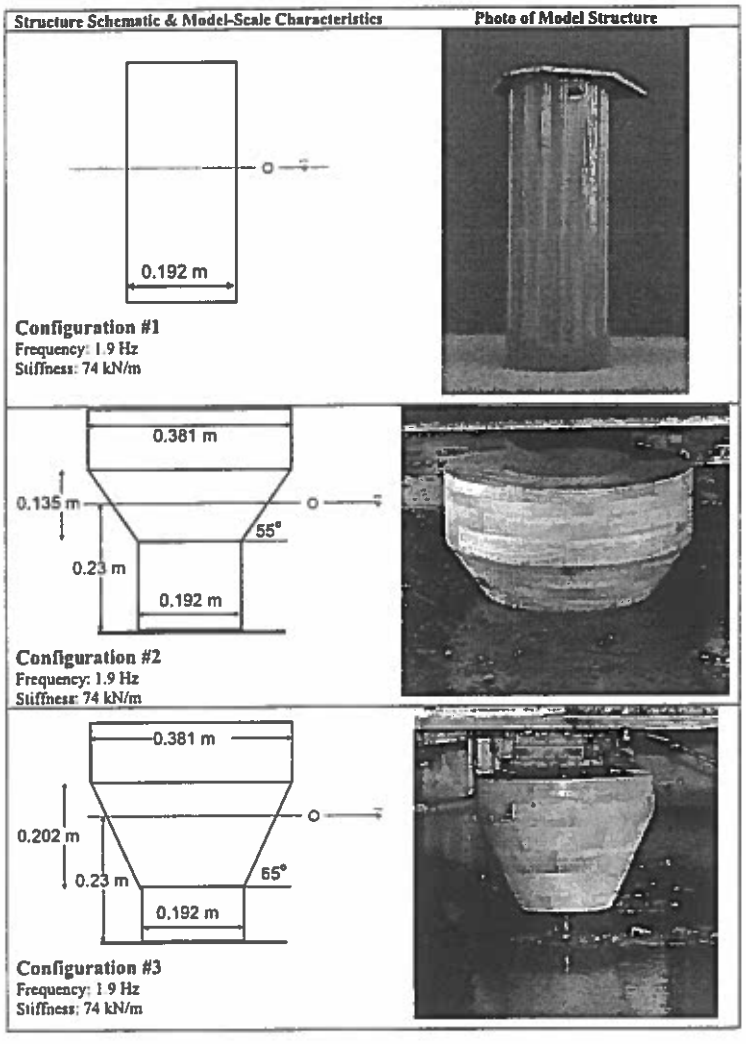

Fig. 2. Test structure schematics, characteristics and photographs.

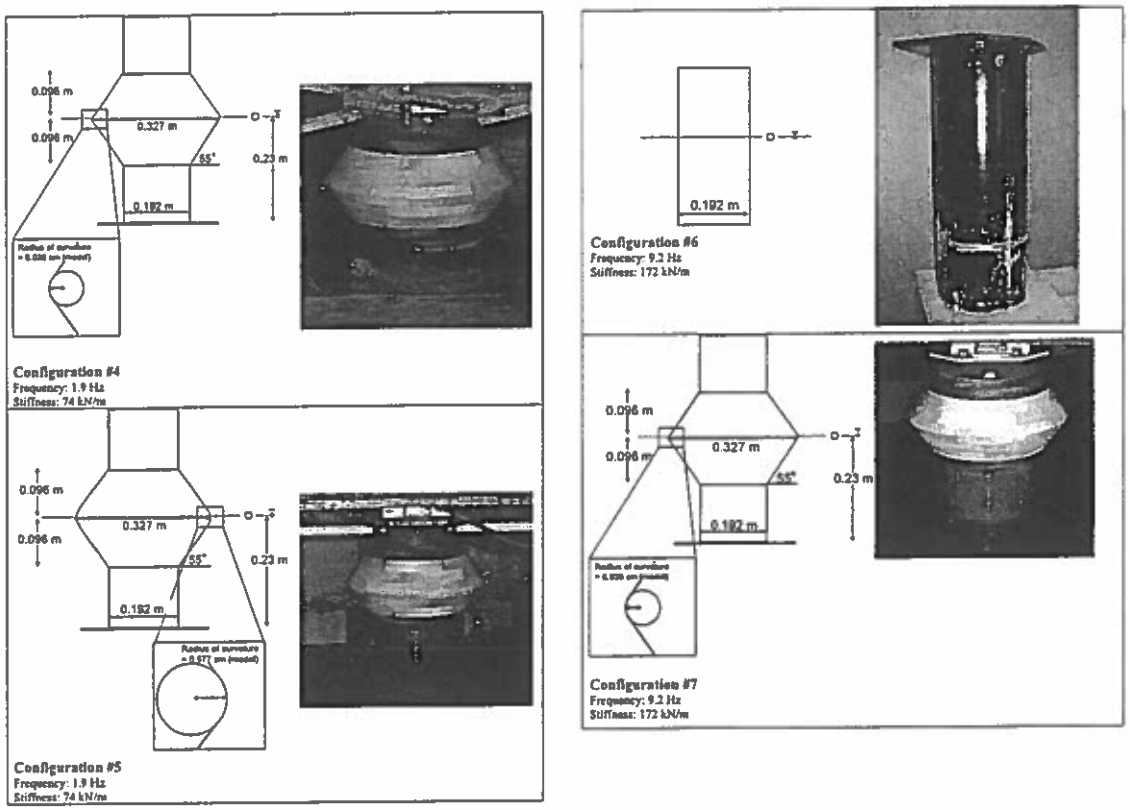

Fig. 2 (*continued*).

about the vertical axis; so, for the present situation, the rotational components were not of concern. It should be noted, however, that the structure characteristics in the transverse (y-) direction are the same as in the loading (x-) direction. The assumption that the structure is rigid in the vertical direction allows the placement of the "foundation" at the top with no loss in accuracy. This makes the experimental arrangement less complicated since the instrumentation does not have to be waterproof.

The model was mounted to a "compliance simulator" which simulated the flexibility of the foundation. This apparatus enables modelling of the structural characteristics over a wide range of values. The compliance simulator consists of a rigid upper frame to which a lower "floating table" is mounted at the four corners through four bars. These bars have universal joints at each end, thereby allowing complete freedom in the horizontal plane, but high rigidity in the vertical direction. The upper frame also supports a large steel plate that is drilled and tapped with numerous holes. This plate firmly supports two steel rods. The lower ends of the rods are mounted to the lower table through linear/spherical bearings. These two rods, therefore, provide a degree of constraint between the upper frame and the lower table. By correct selection of the bar length and diameter, the x-direction and y-direction stiffness can be adjusted to the desired value. Similarly, by adjusting the spacing between the two bars, the rotational stiffness can be adjusted over a certain range. Thus, the positioning of the bars gives control over the stiffness of the foundation support for the model. Further, by adjusting the total mass of the table, changes can be made to the natural frequency of the model.

Table 1
Modelling laws for the physical model tests

Property	Sale by	Property	Scale by
Length	λ	ice strength	λ
Time	$\lambda^{1/2}$	ice thickness	λ
Speed	$\lambda^{1/2}$	elastic modulus	λ
Acceleration	1	ice fracture toughness	$\lambda^{3/2}$
Mass	λ^3	ice–structure friction	1
Force	λ^3	ice–ice friction	1
Density	1		
In-line transverse			
Stiffness	λ^2		
Frequency	$\lambda^{-1/2}$		
Damping	1		
Mass	λ^3		

The upper frame of the compliance simulator was rigidly connected to the main carriage of the ice tank, and represented the "foundation". A turntable spacer and interface plate (a massive spacer with a large stiff plate) were suspended from the floating table. These were used to support the model and to provide additional mass (to get a lower frequency for the model). The floating table, turntable spacer, interface plate, weights, ice dynamometer, and the model structure represented the characteristics of the wind turbine structure. The rigid tests were performed by clamping the floating table to the upper frame, using a stiff, steel bracket. Examples of the typical test arrangement are shown in Figs. 3–5. The frame-of-reference for the tests is also shown in Fig. 3. It uses a Cartesian coordinate system using the right-hand rule with the x-direction in the direction of motion of the ice and the z-direction in the vertical direction.

The following instrumentation was used in this test program (see Figs. 3–5):

- An AMTI 6-component dynamometer (Model MC-6) with 5 kN capacity measured the applied ice loads. It was mounted onto machined pads on the underside of the interface plate for all but the last two configurations, where the dynamometer was mounted directly onto the lower portion of the compliance simulator. The output from this dynamometer gives information on the ice forcing loads on the structure at the waterline.
- Three accelerometers (Sundstrand QA-700 Q-Flex Servo) were mounted on the table of the compliance simulator. These accelerometers measured the model acceleration in the x, y and z directions.
- For two configurations, three more accelerometers (Jewell LCA-100 Inertial Sensors) were mounted on the upper frame of the compliance simulator to measure the vibrations of the carriage/upper frame assembly, so that these could be removed from the model vibration data.
- Three displacement gauges (Trans-Tek #0354-0000) measured the motion of the structure in the x and y directions.

The instrumentation was calibrated at the beginning of the test program to ensure reliable and accurate performance prior to installation in the model. The accelerometers were calibrated by inclining them at specific angles with respect to the earth's gravitational field. Calibration of the displacement gauges was achieved with the aid of precise electronic calipers. Factory calibration constants were used for the dynamometers since in situ calibration was not possible. However, these factory constants were verified by a number of static tests using a calibrated load cell, especially in the low load range for these tests.

The test arrangement described above was used for Configurations #1 to #5, which represented the first-mode vibration frequency of the structure and, accordingly, the overturning moment. The second mode, with less interaction with the tower vibration, was also considered to be important, at least to the design shear forces from the ice load. This was investigated in Configurations #6 and #7 of the program. For these configurations, the required dynamic characteristics were such that the total mass of the table could not be reduced enough to give the correct natural frequency. Therefore, a new floating table and model cylinder were built, constructed out of aluminum, in order to sufficiently reduce the total mass of the table.

A series of 'plucking tests' were conducted to define the dynamic characteristics of the model. In these tests, the model was subjected to a static displacement in a known direction and then suddenly released so that it would experience free vibrations. The response of the model in water (without ice) was

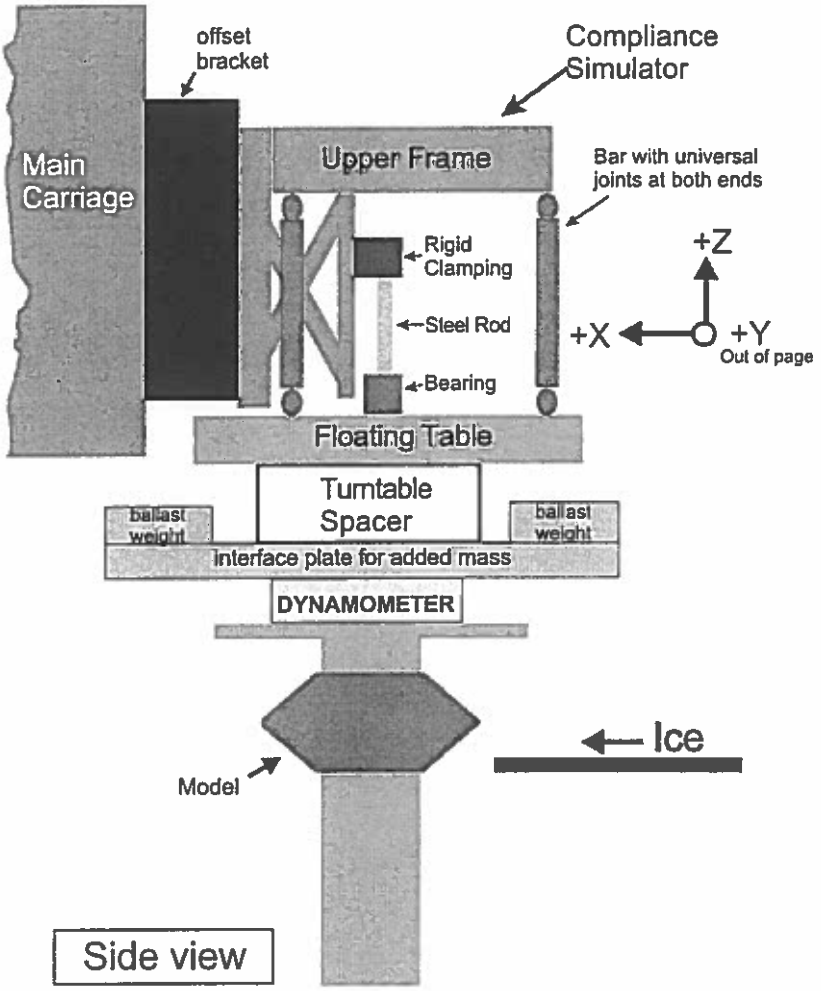

Fig. 3. Side view illustration showing the components of the test system. For Phase 2, the interface plate, ballast weights and turntable spacer were removed, and a new cylinder and floating table were constructed out of aluminum.

recorded. Frequency values were calculated from the analysis of the decaying time series from the results of the free vibration test. Information was obtained on both the natural frequency and damping, and this is indicated in Table 2.

The stiffness of the model in each response direction was determined from the static force/displacement relationship measured at the beginning of each plucking test. This was done by applying an increasing load and measuring the resulting deflection. The resulting load/deflection showed some variability, but in general, the response was linear over the measured region. The magnitude of static loading, p, was measured by a load cell and the resulting structural displacement, x, was recorded by a differential current displacement transducer (DCDT). The stiffness of the model, k, can be calculated according to

$$k = \frac{p}{x} \tag{1}$$

Representative ranges for the stiffness, natural frequency and damping were provided for the prototype system by SEAS, as shown in Table 2. The stiffness and frequency results from the plucking tests are also indicated.

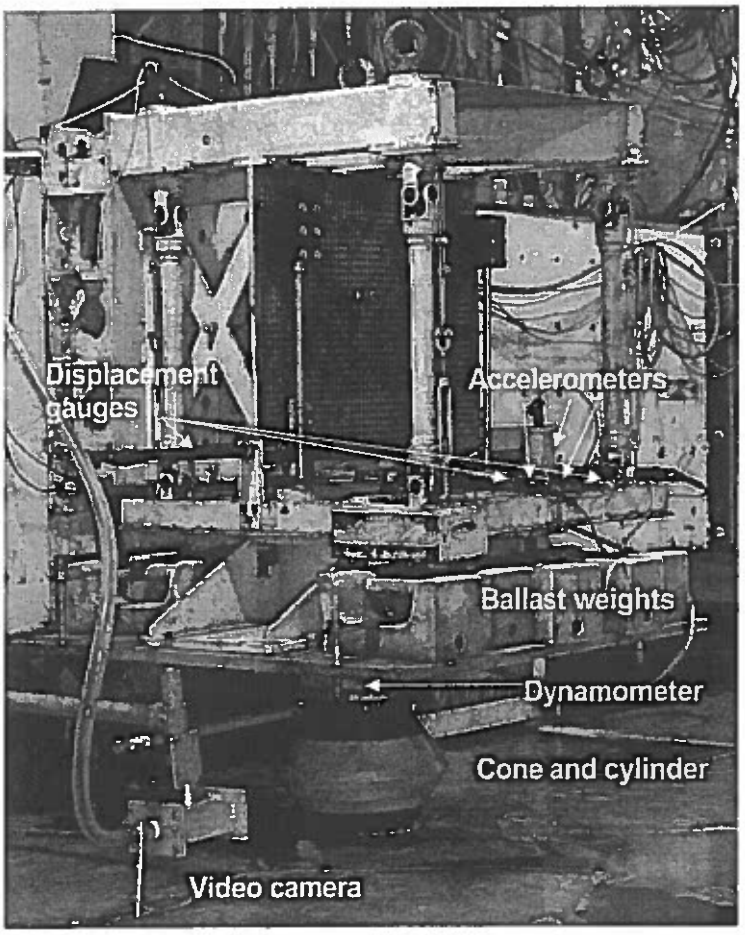

2.4. Ice properties

As the cones had inclined and/or vertical surfaces, the ice could fail in a variety of failure modes, including flexure (bending), buckling, crushing, or a combination of these modes (mixed mode). Thus, the correct scaling of the flexural strength, compressive strength and stiffness of the ice were required. This section will discuss the mechanical properties of the ice.

2.4.1. Full-scale characteristics

The general knowledge of ice properties in Danish waters is very limited, making it difficult to choose representative full-scale values. SEAS based the design bending and crushing strengths upon work by Christensen and Skourup (1991) and Tryde (1979). Further details may be found in the accompanying paper (Gravesen et al., 2004). The maximum full-scale ice thickness was assumed to be 0.6 m.

Four parameters directly affect the ice properties: the ice salinity, temperature, density, and grain structure. For this analysis, the following full-scale physical properties of the ice were used: salinity of 3–4 ppt, ice surface temperature of −11 °C, density of 0.90 Mg/m^3, and columnar grain structure. With the abovementioned properties, and

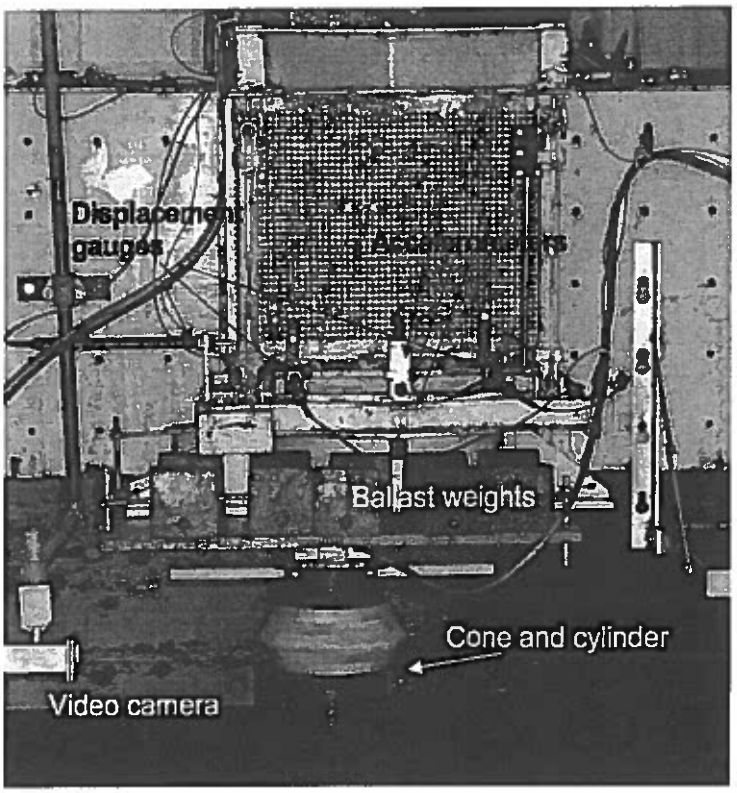

Fig. 5. Photograph showing a front view of the compliance simulator and one of the models.

using the flexural strength equation developed by Timco and O'Brien (1994), the flexural strength was calculated to range between 0.5 and 0.64 MPa.

To estimate the compressive strength of the ice, the relationships derived by Timco and Frederking (1990) were used. Using their approach and the ice properties discussed above, a compressive strength of 2.9 MPa was calculated for this ice. This strength value is appropriate for a loading strain rate of 10^{-4} s^{-1}, at the ductile to brittle transition. For the present tests, however, it was estimated that the strain rate is quite high (0.02–0.1 s^{-1}) and in the brittle range of ice failure. At these high strain rates, there are very few measured strengths of sea ice and those that have been made show very high scatter, with values less than that at the ductile–brittle transition. Therefore, for Danish waters, the compressive strength was estimated to be in the range of 1.9–2.9 MPa.

Thus, the full-scale ice strength properties used for the test series were:

ice flexural strength: 0.5–0.64 MPa
ice compressive strength: 1.9–2.9 MPa
ice thickness: 0.6 m (unless otherwise indicated)

2.4.2. model ice characteristics

As mentioned, SEAS supplied some information on the full-scale ice characteristics and these were scaled using the relationships described in Table 1. The model ice has certain characteristics of strength, thickness, and speed that must be modelled accurately for reliable test results. For this test series, PG/AD model ice was used. This is a state-of-the-art model ice, which is based on, and similar to, the EG/AD/S model ice developed at NRC in Ottawa (Timco, 1986). PG/AD model ice represents well, on a reduced scale, the flexural strength, uniaxial compressive strength, confined compressive strength and

Table 2
Conditions for tests; $\lambda = 26$

Configuration	1	2	3	4	5	6	7
Model structure	cylinder	55° cone and cylinder	65° cone and cylinder	55° sharp double cone and cylinder	55° rounded double cone and cylinder	aluminum cylinder	aluminum cylinder with 55° sharp double cone
Model mass (kg)	14	21	20	16	16	5	7
Full-scale frequency (Hz)	0.38	0.38	0.38	0.38	0.38	1.8	1.8
Model frequency (Hz)	1.9	1.9	1.9	1.9	1.9	9.2	9.2
Full-scale stiffness (MN/m)	50	50	50	50	50	120	120
Model stiffness (kN/m)	74	74	74	74	74	172	172
Full-scale damping (%)	not specified	not specified	not specified	not specified	not specified	not specified	not specified
Model damping (%)	5.9	5.9	3.8	5.9	5.9	8	8
Number of ice sheets	2	15	5	5	3	10	1

failure envelope of sea ice. In addition, there is reasonable scaling of the strain modulus, fracture toughness and density. The paper by Timco (1986) gives details of the mechanical properties of the model ice.

The thickness of the ice was adjusted by selecting an appropriate freezing time to produce the desired thickness. The strength of the ice was adjusted by altering the time allowed for warming-up the ice. The speed of the ice–structure interaction was accomplished by adjusting the speed of the carriage. Ice sheet growth was started using "wet-seeding" to nucleate the ice and produce uniform characteristics. The ice sheet was grown for 10.5 h at a temperature of -10 °C. This produced an ice sheet with an average thickness of 25 mm.

Table 3
Values of the flexural and compressive strength for PG/AD ice of 36 mm thickness and strain rate of 10^{-3} s^{-1}

Flexural strength (kPa)	Compressive strength (kPa)	Ratio (compressive/flexural)
20	65	3.2
30	75	2.5
40	90	2.3
50	110	2.2
60	125	2.1
70	150	2.1

Because the strength is related to the porosity and grain structure of the ice, the flexural strength and compressive strength are "tied-together" in the sense that one cannot independently control one strength without affecting the other strength. The ratio of the compressive/flexural strength is not linear. Table 3, which was derived from Timco's (1986) results, gives information on the flexural strength and uniaxial compressive strength (with horizontal loading) for model ice of 36 mm thickness. The values of the compressive strength represent the value at the peak of the compressive strength/loading rate relationship. These values represent average values since there was considerable scatter in the measured strength values (see Fig. 17, Timco, 1986). For the present tests, the minimum full-scale values used for 0.6-m-thick ice were 0.5 and 1.9 MPa for the flexural and compressive strength minimum values, respectively. At a scale factor of $\lambda = 26$, this gives a flexural strength of 19 kPa, and compressive strength of 73 kPa. From Table 3, the strength requirements are met if the tests are performed with a flexural strength in the range of 20–30 kPa. This strength range was targeted for the present tests.

The friction of the ice–model structure was measured for the conditions appropriate to this test program. The results showed that the static coefficient of friction was 0.11 on average, while the average friction coefficient of moving ice on the structure was 0.07.

2.5. Testing procedure

In the usual test procedure at the CHC ice tank, the structure is mounted through the compliance simulator to the front face of the main carriage and the carriage is driven along the tank, simulating the interaction process. In this case, however, it was found that this approach was not suitable. Preliminary tests showed that the (small) vibrations of the carriage caused inertial forces that were high compared to the ice loads. Therefore, a different approach was used for most of the tests. For Configurations #1 through #5, the main carriage (with the model) remained fixed during the whole test. The interaction process was simulated by pushing the ice sheet against the structure using the service carriage. For the four speeds that were used for the majority of the model tests (0.04, 0.08, 0.14 and 0.2 m/s), the speed of the interaction could be well controlled, and this proved to be a very good approach to study the interaction process. In Configurations #6 and #7, ramping velocity tests and tests with very low velocities were required. For these tests, it was too difficult to maintain the correct speed using the service carriage, so the main carriage was driven through the ice. Three additional accelerometers, mounted to the upper compliance simulator, were added in order to monitor the carriage vibrations.

The data acquisition system (DAS) recorded the analogue signals from the instrumentation. The signals were sampled and digitized by a NEFF Instruments System 100 data acquisition system. The data was sampled at a rate of 100 Hz. During sampling, an analogue low-pass filter with a cut-off frequency of 33 Hz was applied to prevent aliasing. The digitized signals were recorded on a Digital VAX AlphaStation computer as GEDAP data files (Miles, 1990). GEDAP is a software package developed at the CHC to facilitate experiment control, data acquisition, data analysis and the graphical presentation of time series data. Since the data acquisition system was always started before the ice was pushed towards the structure, segments were extracted from the longer time series to represent conditions when the structure was fully embedded in ice. These "time-selected" segments were analyzed to provide simple force statistics. The force–time series presented in this report are all interaction segments extracted from a longer data record.

Each test was conducted when the level ice reached the target strength. SEAS specified water elevations for testing to a range both below and above the water line. Before testing began, if a conical model was being studied, the cone was lowered to the correct water elevation and tightly fastened in place. For testing against the cylinder, the wooden model cone was lifted up and out of the water for experimental convenience, rather than removing the cone from the cylinder entirely. Offset values were taken for all instrumentation before each test with everything held stationary. When this was completed, the data acquisition system (DAS) was started, and the ice sheet was pushed towards the structure at the desired speed. With this approach, there were very low (zero) loads at the initial portion of each time series. These represent the loads during the time before the structure encounters the ice. After the carriage had travelled the appropriate length of the ice tank for the test, it was stopped along with the DAS system. The ice thickness was measured along the track of the test. Following this, the entire process was repeated for the next test.

2.6. Data analysis

The following measurements were made as a function of time for the tests:

- load on the structure due to the ice loading (x, y, z directions)
- displacement of the structure (x, y directions)
- velocity of the structure (x, y directions)
- acceleration of the structure (x, y directions)

Measurements of ice thickness, flexural strength and interaction speeds were also made.

The measured test data was analyzed using a standard procedure. The measured data file was demultiplexed to separate it into a number of discrete data files. The data collected from Configurations #1–#5 were filtered with a 15 Hz low-pass filter in post-processing. This filter removed high-frequency "noise" from the acquired data. For Configurations #6 and #7, the 15 Hz filter was too close to the

natural frequency of the model (9.8 Hz), so the low-pass filter was changed to 30 Hz. This provided more acceptable results, as the filter maintained information concerning the peaks.

The measured dynamometer forces were corrected to compensate for the (non-zero) inertial loads. The load measured by the dynamometer (F_{dyn}) is comprised of two different components—one due to the ice (F_{ice}) and the other due to the moving inertial mass of the model, calculated as

$$F_{dyn} = F_{ice} + m_{mod}\ddot{x} \quad (2)$$

where m_{mod} is the mass of the model (including added mass effects from the water and ice) and $\ddot{x}$ is the measured acceleration (in this case the acceleration of the floating table). If the mass of the model was zero, or there was no acceleration of the model, the inertial force would be zero and the dynamometer would measure the "true" ice force. However, this is not true here (nor for any experiment of this type). Since F_{dyn}, m_{mod} and $\ddot{x}$ are measured, it is possible to correct for the inertial mass and give the "true" ice force. For most of the tests, the chosen inertial mass is the mass of the cone and the cylinder being studied. An example of the output from this calculation is shown in Fig. 6.

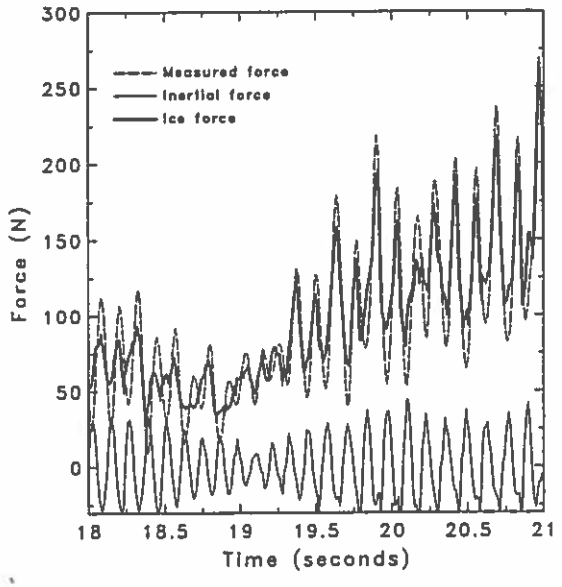

Fig. 6. Comparison of the load measured on the ice dynamometer with the load compensated for the inertial mass of the model. Note that the compensated load is the "true" ice load on the structure. The example shown is for a test from Configuration #6, where dynamic amplification of the structure occurred. In this case, the inertial force is much higher than the majority of tests, due to the acceleration of the model. Generally, the correction due to the inertial force was very small.

The displacement in the x-direction was determined by calculating the average displacement of the two gauges measuring displacement in the x-direction. The velocities were determined by differentiating the measured displacement signals. The acceleration of the model was calculated from the measured accelerations of the floating table. A portion of the time series was selected to provide a region in which both the test speed was constant and the model was fully immersed into the ice sheet. This region was used to define the "steady-state" region for the test and this portion was used for statistical analysis. The maximum measured values from the analysis are presented here.

The results were plotted in a standard format giving full information on the ice loads, displacements, velocities and accelerations. For the tests with the double cones and the aluminum cylinder, cameras in watertight housings were used to document the ice interaction process. Generally, one camera was placed underwater, directly behind the model and the second camera was placed perpendicular to the model, slightly above the water level.

3. Results

A total of 41 ice sheets were grown for the test program. The general results are given in this section. A comprehensive examination of the application of the results to the full-scale design is presented in the accompanying paper (Gravesen et al., 2004).

3.1. Failure modes

The ice failed in a number of different ways in this test program. The failure modes have been characterized by the size of the ice pieces and by the structural response of the structure. Three failure modes are

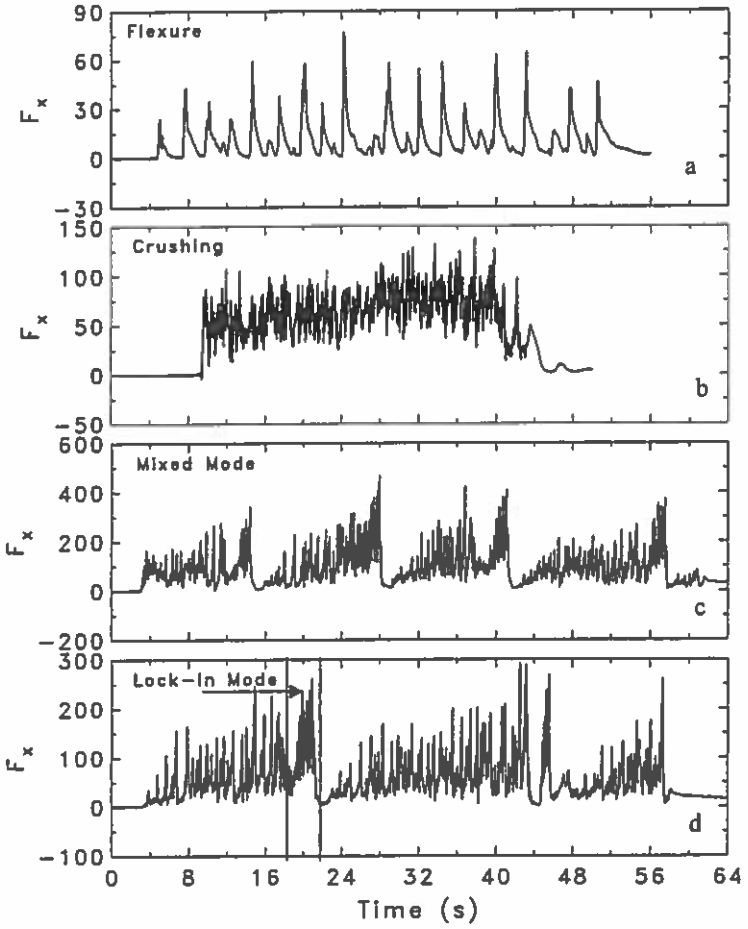

Fig. 7. Typical time series traces of the failure modes observed during testing. Note that the lock-in mode time series trace of the force is very similar to the mixed mode failure trace. It is not possible to assess lock-in solely from the measured forces.

discussed here with examples of their time series traces shown in Fig. 7.

3.1.1. Flexural failure

This failure mode was characterized by large ice pieces that failed at a distance of typically 5–10 times the ice thickness away from the structure. Flexural failure was the most predominant failure mode on the cone. This failure mode was characterized by progressive bending (flexure) failures of the ice sheet as it interacted with the model structure. This produced a series of large peaks in the time series trace with the load often dropping to zero after some loading events (see Fig. 7a). With the cylindrical (vertical) structure, the ice also often failed with large ice pieces but this appeared to be a mixed mode failure of the ice (crushing with a buckling component). This type of failure mode is described below.

3.1.2. Crushing failure

Continuous crushing events occurred throughout the test series, primarily for short durations. The ice in these crushing events was pulverized into very fine pieces, and the failure occurred at the ice–structure interface. However, few of these events could be considered "pure" crushing, as the observed events generally also included some flexural or buckling

failure. The forces observed in crushing events were generally very large compared to flexural failure mode forces. The time series traces showed a rapid variation in the force level with the force always remaining above zero (Fig. 7b).

3.1.3. Mixed mode failure

Mixed mode failure is a combination of different failure modes. Generally, the ice crushes locally against the structure for a short duration, then it reaches a point where the ice fails in large-scale behaviour. The process then began anew, with another crushing event in a fairly regular pattern (note that this was different from the crushing events where some flexural failures took place, as in those cases, the combination of crushing build-up followed by flexural failure did not occur regularly). The time series trace showed alternating regimes of crushing behaviour (rapid variation in the load) followed by a large drop in the load with zero (or near zero) loads for a short time following the large-scale ice failure ice (Fig. 7c). Previous experiments investigating ice failure behaviour have shown that this failure mode is a transition mode between crushing behaviour and large-scale buckling behaviour of the ice (Timco, 1987). In nature, buckling failure is usually only observed in thinner ice sheets (ice thickness typically less than about 0.5 m). The scaled thickness of the present tests was below this value. Thus, in scaling these results, it should be kept in mind that the buckling failure observed in the tests would probably not be as prevalent in nature as observed here. Buckling is a thin-plate phenomenon that is common in model tests, regardless of the type of model ice, since the tests use thin ice sheets. Nevertheless, observations of the time series traces showed that the crushing failure loads were generally comparable to the buckling loads so a load analysis based on this failure mode should give reasonable full-scale loads.

For tests observed in Configuration #6, this type of failure mode caused the ice to pile in front of

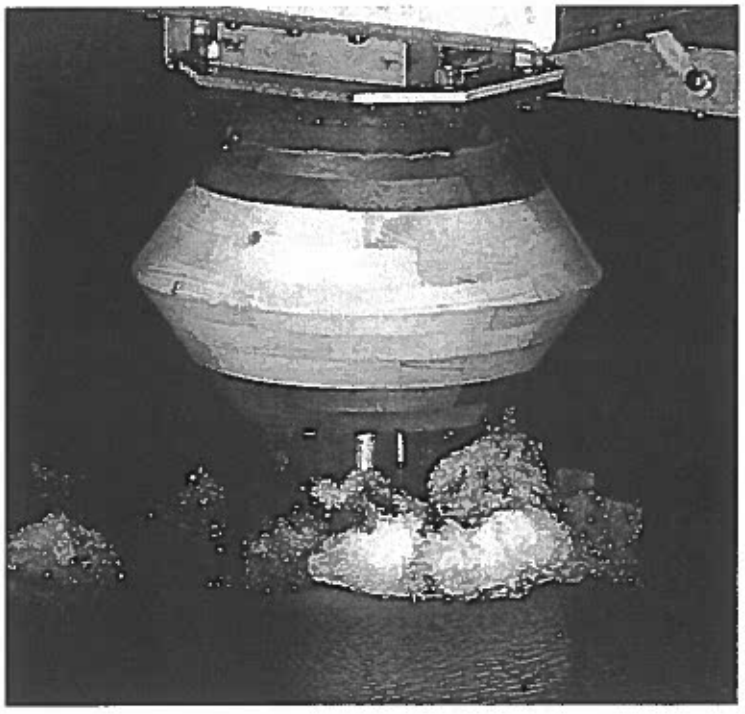

Fig. 8. Ice with a mixed failure mode crushing against cylinder during testing.

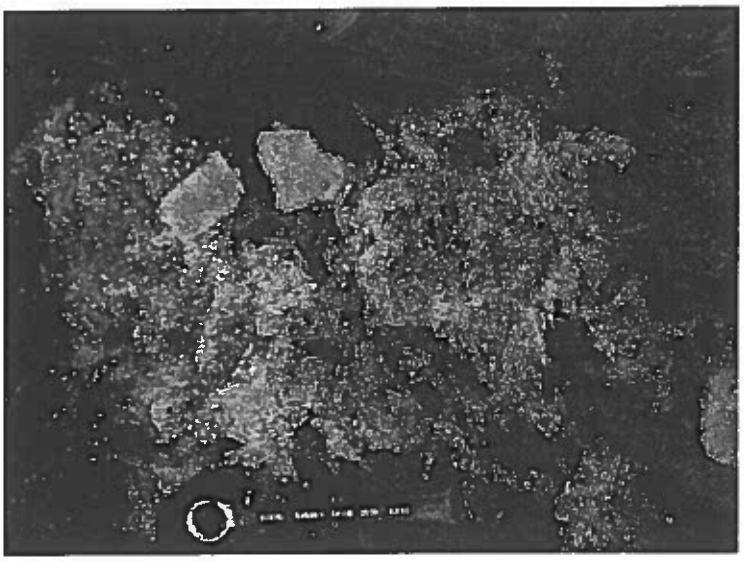

Fig. 9. Photograph of ice that had a mixed failure mode.

the structure, "spilling" backwards onto the oncoming ice. A photograph showing this occurring during a mixed mode event is shown in Fig. 8. Even with this behaviour, the ice cleared quickly around the structure for most of the tests. The exceptions were some tests at low velocities, where the ice remained at the upstream side of the structure for longer than usual. A close-up photograph of ice that had a mixed failure mode is shown in Fig. 9. The ice consisted of primarily smaller pieces of

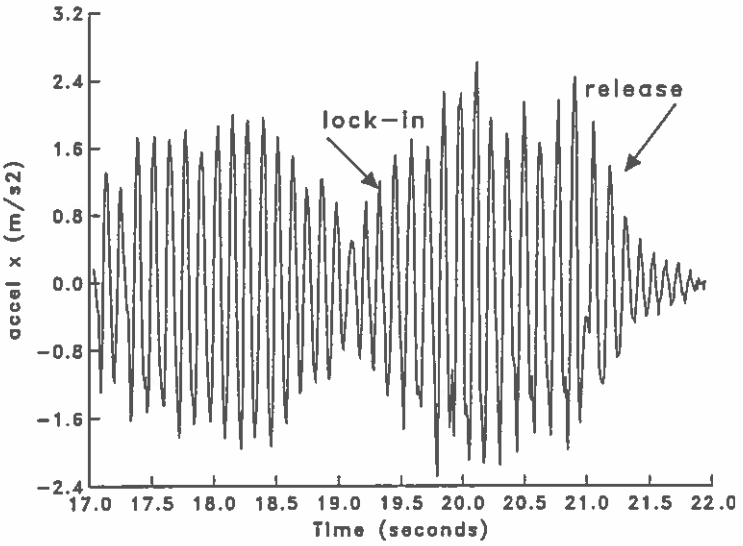

Fig. 10. Time series trace of measured acceleration in the x-direction, showing the occurrence of lock-in vibrations. Note that the figure also shows the structure releasing after the ice sheet has failed in flexure.

pulverized ice, typical of pure crushing. However, there were also large pieces of ice that indicated that the ice had a bending or buckling type of failure as well.

3.1.4. Lock-in

Lock-in occurred during a few of the tests. A detailed example of the time series traces for one such test is shown in Fig. 10. This figure shows lock-in occurring over a short duration. Lock-in, when viewed as a time series trace of the x-direction force, looks similar to the mixed mode failure plot (compare Fig. 7c–d). Only upon inspection of the acceleration and displacement time series traces and spectral analysis results does it become apparent that the failure mode of the ice has accelerated the model structure, causing structural vibrations at the resonant frequency. In these tests, lock-in causing dynamic amplification never occurred for a long period of time. Additionally, amplification occasionally occurred during a transitional stage from a crushing to a flexural failure mode. The effects of lock-in on the dynamic response of the structure are described in the Discussion.

3.2. Quantitative results

3.2.1. Configuration #1

Two ice sheets were used to investigate the conditions specified for Configuration #1. The basic cylinder was used for these tests. Tests used either a compliant or a rigid foundation. Most of the tests had crushing failures. For this and all other configurations, the ice did not jam around the structure below the waterline. Summaries of the test arrangements and results are shown in Table 4. In these accompanying results tables, a positive or negative full-scale water depth value indicates that the ice was interacting above or below the original waterline (as indicated in Fig. 2), respectively.

3.2.2. Configuration #2

A 55° inverted cone was used with the basic cylinder for Configuration #2. Fifteen ice sheets were used to study this configuration. The test results are shown in Table 5. As with Configuration #1, a combination of compliant and rigid tests were carried out. Failure modes for most of the tests were either crushing or flexure, with some tests, generally at lower velocities, switching between crushing and flexural failure.

3.2.3. Configuration #3

For Configuration #3, a 65° inverted cone wastested using five different ice sheets. Similar to the previous configuration, the model was tested with both compliant and rigid modes. The failure mode was primarily flexural. When compared with the 55° model, the loads for ice interacting at the same waterline were generally higher for the 65° model. Table 6 contains the test results.

3.2.4. Configuration #4

Five ice sheets were used in Configuration #4. The model had a 55° double-sided sharp edge. The ice failed either in flexure or by a combination of crush-

Table 4
Summary of test parameters and results for Configuration #1

Velocity (cm/s)	Ice thickness (mm)	Flexural strength (kPa)	Compressive strength (kPa)	Full-scale water depth (m)	Compliance	Max Fx (N)	Max Fy (N)	Max Fz (N)	Max accel (m/s^2)	Failure mode
4	22	21	66	−2.00	flexible	57.30	−21.68	14.09	0.11	crushing/flexure
8	22	21	66	−2.00	flexible	48.50	−19.01	11.27	0.07	crushing
14	22	21	66	−2.00	flexible	79.00	27.47	6.92	0.09	crushing
20	22	21	66	−2.00	flexible	100.14	26.90	11.77	0.1	crushing
4	25	22	67	−2.00	rigid	79.51	24.50	3.07		crushing
8	25	22	67	−2.00	rigid	104.01	28.40	1.48		crushing
14	25	22	67	−2.00	rigid	106.58	44.23	0.15		crushing
20	25	22	67	−2.00	rigid	145.01	45.52	0.5		crushing

Tests with cylinder, f_n = 1.9 Hz and stiffness of 74 kN/m.

Table 5
Summary of test parameters and results for Configuration #2

Velocity (cm/s)	Ice thickness (mm)	Flexural strength (kPa)	Compressive strength (kPa)	Full-scale water depth (m)	Compliance	Max Fx (N)	Max Fy (N)	Max Fz (N)	Max accel (m/s^2)	Failure mode
4	23	38	88	1.50	rigid	26.11	−13.66	46.5		flexure
8	23	38	88	1.50	rigid	26.31	−14.52	45.78		flexure
14	23	38	88	1.50	rigid	50.32	−14.26	58.68		flexure
20	23	38	88	1.50	rigid	46.63	17.71	63.22		flexure
4	23	65	137	−1.50	rigid	156.35	−56.00	27.64		crushing/flexure
8	23	65	137	−1.50	rigid	168.17	60.17	21.72		crushing
14	23	65	137	−1.50	rigid	176.71	77.83	21.91		crushing
20	23	65	137	−1.50	rigid	247.44	74.97	34.86		crushing
4	23	24	69	−1.50	rigid	47.13	22.36	10.94		crushing
8	23	24	69	−1.50	rigid	73.34	−27.57	17.79		crushing
14	23	24	69	−1.50	rigid	83.10	−35.26	15.31		crushing
20	23	24	69	−1.50	rigid	78.55	30.69	12.33		crushing
4	22	30	77	1.50	flexible	19.06	8.00	20.88	0.02	crushing/flexure
8	22	30	77	1.50	flexible	30.15	−16.99	35.65	0.06	flexure
14	22	30	77	1.50	flexible	26.91	15.97	46.55	0.04	flexure
20	22	30	77	1.50	flexible	35.11	15.93	51.81	0.13	flexure
4	20	32	79	−1.50	flexible	45.47	−17.08	11.45	0.07	crushing/flexure
8	20	32	79	−1.50	flexible	51.26	14.58	9.29	0.06	crushing
14	20	32	79	−1.50	flexible	55.10	−20.35	13.63	0.04	crushing
20	20	32	79	−1.50	flexible	57.47	−20.91	12.2	0.02	crushing
8	23	20	65	−1.25	flexible	125.62	−55.97	20.81	0.14	crushing
20	23	20	65	−1.25	flexible	111.75	−27.13	16.37	0.07	crushing
8	23	20	65	−1.00	flexible	106.77	73.92	24.12	0.19	flexure
20	23	20	65	−1.00	flexible	95.81	22.85	33.56	0.27	flexure
8	25	24	69	−0.50	flexible	24.38	13.26	20.46	0.09	flexure
20	25	24	69	−0.50	flexible	34.74	13.49	21.39	0.12	flexure
8	25	24	69	0.00	flexible	39.73	−14.43	22.63	0.07	flexure
20	25	24	69	0.00	flexible	60.89	−17.86	29.42	0.2	flexure
8	24	23	68	−1.25	rigid	87.88	−32.53	7.26		crushing
20	24	23	68	−1.25	rigid	104.85	−46.29	6.28		crushing
8	24	23	68	−1.00	rigid	87.80	−28.80	10.93		crushing
20	24	23	68	−1.00	rigid	82.34	−28.19	13.18		crushing
4	24	21	66	−1.00	rigid	26.82	8.20	9.91		flexure
14	24	21	66	−1.00	rigid	69.40	20.28	14.94		flexure
8	24	21	66	−1.00	rigid	63.34	19.09	13.75		crushing/flexure
8	24	27	73	−1.25	flexible	112.13	31.37	8.79	0.29	crushing
20	24	27	73	−1.25	flexible	123.30	31.56	10.26	0.1	crushing
8	24	27	73	−1.00	flexible	36.71	−16.57	15.77	0.06	crushing/flexure
20	24	27	73	−1.00	flexible	59.13	13.57	17.25	0.03	crushing/flexure
4	24	24	69	−0.75	flexible	30.32	8.22	11.38	0.03	crushing/flexure
8	24	24	69	−0.75	flexible	47.76	10.76	19.05	0.05	flexure
14	24	24	69	−0.75	flexible	55.22	8.61	23.26	0.06	flexure
20	24	24	69	−0.75	flexible	63.14	−15.72	31.65	0.1	flexure
4	25	23	68	−0.50	flexible	31.36	−12.76	22.42	0.04	crushing/flexure
8	25	23	68	−0.50	flexible	34.87	−12.53	16.83	0.04	flexure
14	25	23	68	−0.50	flexible	54.43	13.67	29.98	0.08	flexure
20	25	23	68	−0.50	flexible	51.42	13.49	34	0.1	flexure
4	24	18	63	0.00	flexible	10.25	−4.81	7.91	0.01	flexure
8	24	18	63	0.00	flexible	16.22	−5.33	11.08	0.03	flexure
14	24	18	63	0.00	flexible	23.82	−7.11	17.18	0.05	flexure

Table 5 (*continued*)

Velocity (cm/s)	Ice thickness (mm)	Flexural strength (kPa)	Compressive strength (kPa)	Full-scale water depth (m)	Compliance	Max Fx (N)	Max Fy (N)	Max Fz (N)	Max accel (m/s^2)	Failure mode
20	24	18	63	0.00	flexible	32.91	9.4	24.17	0.1	flexure
4	26	21	67	+1.50	flexible	15.91	−3.55	10.02	0.01	crushing/flexure
8	26	21	67	+1.50	flexible	15.03	−5.39	13.34	0.02	crushing/flexure
14	26	21	67	+1.50	flexible	18.29	−5.62	16.52	0.03	flexure
20	26	21	67	+1.50	flexible	35.13	−10.05	28.72	0.09	flexure
4	26	25	70	−0.75	flexible	30.30	−16.65	11.63	0.03	crushing/flexure
8	26	25	70	−0.75	flexible	35.17	−14.49	10.38	0.04	crushing/flexure
14	26	25	70	−0.75	flexible	40.48	6.12	15.55	0.5	flexure
20	26	25	70	−0.75	flexible	44.85	10.36	19.74	0.05	flexure

Tests with 55° inverted cone, $f_n = 1.9$ Hz and stiffness of 74 kN/m.

ing and flexure. The loads were generally larger than those previously observed, most noticeably, the forces in the *z*-direction acting downwards onto the cone. The test results are found in Table 7.

3.2.5. Configuration #5

The model for Configuration #5 had a rounded edge, with a curvature radius of 0.6 cm. The test results are shown in Table 8. As with the sharp cone, the rounded cone failed either in flexure or by a combination of crushing and flexure. The *x*-direction force on the structure appeared to be larger than the sharp-edged cone, particularly near the waterline, where the cone had been rounded. This could be the result of this section of the cone resembling a near-vertical section of the model.

3.2.6. Configuration #6

For Configurations #6 and #7, the model's dynamic characteristics were changed so that the compliance simulator was both stiffer and vibrated at a higher frequency, as indicated in Table 2. Ten ice sheets were grown for Configuration #6, which was the cylindrical structure. Parameters such as ice thickness and

Table 6
Summary of test parameters and results for Configuration #3

Ice velocity (cm/s)	Ice thickness (mm)	Flexural strength (kPa)	Compressive strength (kPa)	Full-scale water level (m)	Compliance	Max Fx (N)	Max Fy (N)	Max Fz (N)	Max accel (m/s^2)	Failure mode
4	26	24	69	+1.50	rigid	53.27	18.88	14.07		flexure
8	26	24	69	+1.50	rigid	32.41	−7.39	11.5		flexure
14	26	24	69	+1.50	rigid	56.84	−17.84	18.32		flexure
20	26	24	69	+1.50	rigid	96.31	−22.42	31.87		flexure
8	26	19	64	−2.00	rigid	38.25	12.95	10.11		crushing/flexure
20	26	19	64	−2.00	rigid	47.65	−15.92	15.68		flexure
8	26	25	70	−2.50	rigid	28.78	11.86	7.7		flexure
20	26	25	70	−2.50	rigid	78.54	−18.01	21.52		flexure
4	26	21	66	+1.50	flexible	42.67	16.66	12.82	0.04	crushing/flexure
8	26	21	66	+1.50	flexible	30.53	9.22	13.37	0.06	flexure
14	26	21	66	+1.50	flexible	45.54	−13.13	16.25	0.11	flexure
20	26	21	66	+1.50	flexible	69.58	−20.53	26.44	0.23	flexure
4	26	24	69	−2.50	flexible	39.02	−14.66	9.79	0.03	crushing/flexure
8	26	24	69	−2.50	flexible	26.69	−6.12	8.43	0.03	flexure
14	26	24	69	−2.50	flexible	41.18	−8.72	12.99	0.08	crushing/flexure
20	26	24	69	−2.50	flexible	64.41	−14.09	20.86	0.11	flexure

Tests with 65° inverted cone, $f_n = 1.9$ Hz and stiffness of 74 kN/m.

Table 7
Summary of test parameters and results for Configuration #4

Velocity (cm/s)	Ice thickness (cm)	Flexural strength (kPa)	Compressive strength (kPa)	Full-scale water depth (m)	Max F_x (N)	Max F_y (N)	Max F_z (N)	Max acceleration (m/s^2)	Failure mode
4	2.2	29	75	+0.27	47.23	−32.97	13.60	0.07	flexure
8	2.2	29	75	+0.27	77.68	−44.48	13.85	0.15	flexure
14	2.2	29	75	+0.27	84.73	−42.08	16.44	0.25	flexure
20	2.2	29	75	+0.27	98.08	−46.46	−22.33	0.43	flexure
4	2.5	27	73	+0.42	140.66	115.57	−36.70	0.15	crushing/flexure
8	2.5	27	73	+0.42	135.47	−53.52	−40.18	0.25	crushing/flexure
14	2.5	27	73	+0.42	134.46	71.17	−51.58	0.3	flexure
20	2.5	27	73	+0.42	131.38	64.14	−47.53	0.44	flexure
4	2.6	27	73	+0.12	46.01	−23.30	14.40	0.05	crushing/flexure
8	2.6	27	73	+0.12	36.61	−20.05	16.18	0.06	flexure
14	2.6	27	73	+0.12	78.86	−18.26	16.58	0.15	flexure
20	2.6	27	73	+0.12	95.42	−26.32	29.53	0.22	flexure
4	2.4	26	72	+0.80	47.75	15.23	−30.83	0.04	crushing/flexure
8	2.4	26	72	+0.80	40.80	−22.17	−33.95	0.07	crushing
14	2.4	26	72	+0.80	48.99	−19.26	−48.35	0.12	crushing
20	2.4	26	72	+0.80	55.13	20.06	−50.45	0.12	crushing
8	2.6	32	79	+0.27	91.98	−44.16	22.00	0.13	crushing/flexure
20	2.6	32	79	+0.27	140.76	−50.07	25.47	0.36	flexure
8	2.6	32	79	+0.42	135.96	57.02	−34.34	0.36	crushing/flexure
20	2.6	32	79	+0.42	166.23	−47.89	−60.83	0.63	flexure

Compliant tests with 55° double-sided sharp cone, $f_n = 1.9$ Hz and stiffness of 74 kN/m.

strength were varied for this phase of testing, and ramping velocity tests were also performed. For ramping tests, the velocity is listed as "ramp".

For most of the tests, the measured ice force against the structure was much higher than those in previous tests using a cone. For some of the ice sheets in this configuration, the carriage was moved through the ice. It was used to examine very low velocities, less than 8 cm/s, some of which would have not been possible to achieve by pushing the ice. The ice usually failed in a mixed mode except for the lowest velocity, where the ice crushed at the

Table 8
Summary of test parameters and results for Configuration #5

Velocity (cm/s)	Ice thickness (cm)	Flexural strength (kPa)	Compressive strength (kPa)	Full-scale water depth (m)	Max F_x (N)	Max F_y (N)	Max F_z (N)	Max acceleration (m/s^2)	Failure mode
8	2.4	28	74	+0.27	174.60	83.47	−43.52	0.42	flexure
20	2.4	28	74	+0.27	201.97	67.07	−49.29	0.91	flexure
8	2.4	28	74	+0.42	121.73	−58.27	−35.43	0.4	flexure
20	2.4	28	74	+0.42	169.86	52.48	−63.28	0.5	flexure
4	2.1	27	73	+1.75	18.73	−8.17	−14.87	0.02	crushing/flexure
8	2.1	27	73	+1.75	24.62	9.63	−17.68	0.04	crushing/flexure
14	2.1	27	73	+1.75	26.69	−11.01	−24.30	0.07	crushing/flexure
20	2.1	27	73	+1.75	47.54	−13.57	−40.29	0.11	crushing/flexure
8	2.2	27	73	+2.25	74.50	−24.95	−15.42	0.06	crushing/flexure
20	2.2	27	73	+2.25	64.71	14.62	−27.22	0.17	crushing/flexure
8	2.2	27	73	+2.00	41.53	−14.64	−23.33	0.05	crushing/flexure
20	2.2	27	73	+2.00	65.20	24.86	−43.02	0.13	crushing/flexure

Compliant tests with 55° double-sided rounded cone, $f_n = 1.9$ Hz and stiffness of 74 kN/m.

Table 9
Summary of test parameters and results for Configuration #6

Velocity (cm/s)	Ice thickness (cm)	Flexural strength (kPa)	Compressive strength (kPa)	Full-scale water depth (m)	Max F_x (N)	Max F_y (N)	Max F_z (N)	Max acceleration (m/s^2)	Failure mode	Lock-in observed?
4	1.55	19	64	n/a	136.08	64.55	−9.01	1.87	crushing/ flexure	transitional
8	1.55	19	64	n/a	101.53	−61.45	−8.74	1.30	crushing	no lock-in
14	1.55	19	64	n/a	137.51	−44.36	−10.34	1.48	crushing	no lock-in
20	1.55	19	64	n/a	198.24	73.92	−13.18	1.53	crushing	no lock-in
4	2.16	22	67	n/a	65.44	25.66	−6.23	0.48	crushing	transitional
8	2.16	22	67	n/a	62.22	−33.60	−6.87	0.94	crushing	no lock-in
14	2.16	22	67	n/a	102.77	−48.64	−8.41	1.60	crushing	no lock-in
20	2.16	22	67	n/a	109.59	−36.76	−9.01	1.24	crushing	no lock-in
Ramp	2.30	17	63	n/a	158.50	−164.68	−18.30	1.88	mixed mode	lock-in
Ramp	1.95	10	56	n/a	233.10	112.35	−12.46	1.87	crushing	lock-in
1	1.95	22	67	n/a	281.48	111.99	−28.46	2.57	crushing/ flexure	no lock-in
3	2.10	22	67	n/a	256.78	91.30	−23.88	1.78	mixed mode	lock-in
5	2.30	22	67	n/a	291.94	99.14	−32.63	3.02	mixed mode	lock-in
7	2.45	22	67	n/a	465.42	−183.92	−50.29	4.34	mixed mode	lock-in
2	2.20	26	72	n/a	270.09	107.50	−26.93	1.14	mixed mode	transitional
4	2.20	26	72	n/a	195.27	−89.40	−26.68	1.79	mixed mode	lock-in
6	2.20	26	72	n/a	371.66	128.19	−55.91	4.37	mixed mode	lock-in
8	2.20	26	72	n/a	346.69	−115.02	−44.70	3.69	mixed mode	lock-in
ramp	2.30	29	75	n/a	445.14	−277.84	−64.93	5.45	mixed mode	lock-in
ramp	1.80	21	66	n/a	389.63	−170.50	−33.07	3.45	mixed mode/ crushing	lock-in
4	1.85	24	69	n/a	125.39	95.35	−12.52	1.23	crushing/ flexure	transitional
8	1.85	24	69	n/a	131.91	−39.48	−15.88	0.93	crushing/ flexure	no lock-in
14	1.85	24	69	n/a	98.48	−28.41	−18.32	0.80	crushing	no lock-in
20	1.85	24	69	n/a	105.85	56.46	−14.90	1.53	crushing	transitional
14	2.20	25	71	n/a	288.93	128.38	−35.88	3.37	mixed mode	transitional
20	2.20	25	71	n/a	268.83	99.97	−33.67	2.50	mixed mode	transitional
14	2.20	25	71	n/a	339.52	131.37	−43.87	3.87	mixed mode	transitional
20	2.20	25	71	n/a	430.24	−164.54	−48.80	4.11	mixed mode	transitional

Compliant tests with aluminum cylinder, $f_n = 9.2$ Hz and stiffness of 172 kN/m.

beginning of the test, then switched to a buckling failure mode. Lock-in acceleration of the model occurred during a number of these tests at all but the lowest velocity. The test results may be found in Table 9.

3.2.7. Configuration #7

One ice sheet was used for Configuration #7, which used the aluminum cylinder with the sharp-edge double-sided cone. As this was a ramping velocity test, the main carriage was driven through the ice. As with the

Table 10
Summary of test parameters and results for Configuration #7

Velocity (cm/s)	Ice thickness (cm)	Flexural strength (kPa)	Compressive strength (kPa)	Full-scale water depth (m)	Max F_x (N)	Max F_y (N)	Max F_z (N)	Max acceleration (m/s^2)	Failure mode
Ramp	2.10	24	69	−0.42	35.79	−16.07	24.46	0.78	flexure

Compliant tests with aluminum cylinder and 55° double-sided sharp cone, $f_n = 9.2$ Hz and stiffness of 172 kN/m.

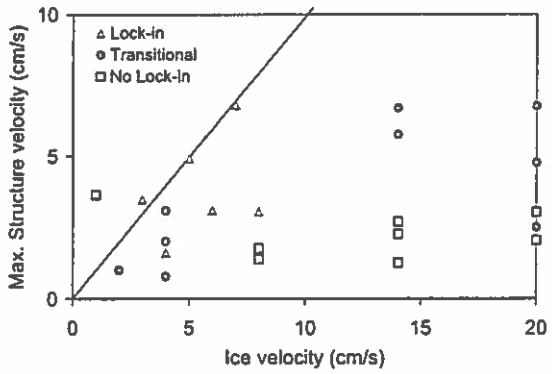

Fig. 11. Maximum measured structural velocity plotted against ice velocity for Configuration #6. Note that structural velocity during the tests where lock-in occurred was often similar to the ice velocity.

previous tests using a cone, there was no evidence of lock-in or ice pile-up. The ice failed in flexure. Table 10 shows the test results for this configuration.

4. Discussion

Some results were common to most of the configurations. In most cases, the ice failed by flexure. As the ice interacted with one of the conical structures, the ice bent, failed and cleared around the structure. The loads were generally large for the configurations when the ice interacted with the conical structure where the structure was closest to vertical; that is, near the bottom and the top of the model, at the transition to the cylindrical structure. The highest loads were often observed to occur when just the cylindrical structure was used. One of these configurations, Configuration #6, was also the only one to exhibit large dynamic amplification and lock-in as a result of the ice interaction. It should be noted that although lock-in was observed for tests with Configuration #6, the lock-in mode did not persist. It occurred for a relatively short duration. However, when lock-in did occur, there were large displacements and accelerations of the model structure. Some aspects of this lock-in behaviour are discussed in the next sections.

4.1. Dynamic response

Large dynamic amplification events were only observed to occur during Configuration #6. A brief analysis of the data was carried out to investigate the dynamic response of the structure to the second mode of vibration. A relationship between the structural velocity and the ice velocity has been discussed in Karna and Turunen (1990). Their analysis indicated that when a lock-in condition arises, the structure's velocity amplitude at the waterline is approximately the same as the ice velocity. Velocity results from Configuration #6 have been plotted in Fig. 11, with the structural velocity plotted against the ice velocity. In this plot, the test data has been put into three categories: tests where dynamic amplification was observed; tests where dynamic amplification occurred during a transitional phase as the ice changed failure modes; and tests where dynamic amplification was not observed. As shown in the plot, tests where the two velocities were similar generally coincided with those where dynamic amplification occurred. Most of the transitional tests had structural and ice velocities that were also similar. However, there were a few notable exceptions—tests that occurred at higher velocities, where conclusive lock-in was difficult to determine.

4.2. Damage zones

Sodhi and Morris (1984) performed a large series of tests investigating ice crushing on *rigid* vertical indentors in a laboratory. In these tests, it was noted

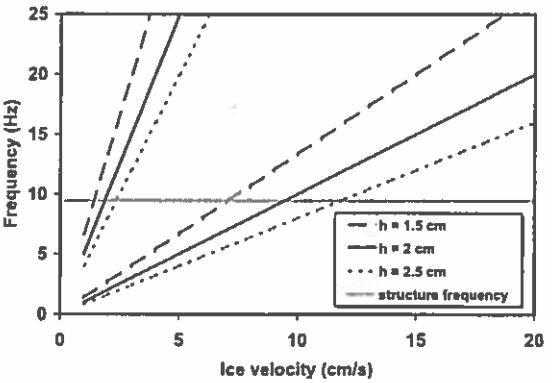

Fig. 12. Plot showing the zones of the ice crushing frequency on a rigid indentor as a function of ice velocity, for different ice thicknesses. Note that over a wide range of the test parameters, the ice crushing frequency is similar to the natural frequency of the structure for Configurations #6 and #7.

that the crushing frequency on the rigid indentor increased with increasing ice velocity, and decreased with increasing ice thickness. Sodhi and Morris related these facts by using the concept of a damage zone "Δ" which was defined as:

$$\Delta = \frac{v_i}{f_{cr} h_i} \tag{3}$$

where v_i is the ice velocity, f_{cr} is the characteristic frequency of the ice crushing process, and h_i is the ice thickness. From their experimental observations, they noted that the value of Δ varied from 0.1 to 0.5 (i.e. was one-tenth to one-half of the ice thickness for a constant velocity). With this equation as a basis, the question arises: can we anticipate excitement of a structure, based upon ice thickness and velocity, and the geometry of a structure?

For the present model tests, the velocity ranged from 1 to 20 cm/s, and the ice thickness was in the range of 1.5–2.5 cm. Eq. (3) can be used to define the limits of the crushing frequency as a function of ice velocity for different ice thicknesses, for a rigid structure. Working backwards, by assigning Δ values of 0.1 and 0.5, one can solve for f_{cr}, using a range of model-scale values for v_i and h_i. Fig. 12 shows the bounds for ice thickness values of 1.5, 2.0 and 2.5 cm. The natural frequency of the compliant structure is also indicated. The figure shows that over a wide velocity range (virtually over the whole test range) the frequency for ice crushing is close to the natural frequency of the structure. Even though the structure investigated was compliant, the equation derived from the rigid test observations does provide a means of quickly assessing whether there is a high potential for excitement of a structure. Based on this analysis, it is not surprising that there were significant dynamic events with the vertical-sided structure.

5. Summary

An extensive laboratory model study at the CHC investigated seven offshore wind turbine configurations with respect to ice forces interacting with these structures. Parameters that were studied included model structure design, structure stiffness and natural frequency, water level, ice speed, ice thickness and ice strength. Analysis of the data indicated that the ice most often failed in flexure. When the ice interacted with a cylindrical-type structure, the loads were much higher than when the ice interacted with a conical structure. For studies investigating the second mode of vibration, lock-in acceleration of the structure was frequently observed, accompanied with very large amplitude vibration. The model test results provide valuable information for the full-scale design of the offshore wind turbines (Gravesen et al., 2004).

Acknowledgements

The authors would like to thank SEAS for the permission to publish the results of this study, as well as Jean-Pierre Des Becquets and the staff of the CHC for their assistance in the manufacturing of the model and the test set-up.

References

Christensen, F.T., Skourup, J., 1991. Extreme ice properties. Journal of Cold Regions Engineering 5 (2), 51–68.

Christensen, F.T., Timco, G.W., Nwogu, O.G., 1995. Compliant model tests with the great belt west bridge piers in ice. Part 2: analyses of results. Cold Regions Science and Technology 23 (2), 165–182.

Cornett, A.M., Timco, G.W., 1997. Ice-induced vibrations of the Molikpaq. Proceedings 8th International Conference on the Behaviour of Offshore Structures, BOSS97, vol. 3, pp. 229–243. Delft, The Netherlands.

Gravesen, H., Vølund, P., Timco, G., Barker, A., 2004. Ice Loading on Danish Wind turbines. Part 2: Analyses of Results. Cold Regions Science and Technology 41, 25–47.

Karna, T., Turunen, R., 1990. A straightforward technique for analyzing structural response to dynamic ice action. Proceedings of the 9th Offshore Mechanics and Arctic Engineering Conference, Houston, USA, vol. 4, pp. 135–142.

Miles, M.D., 1990. The GEDAP Data Analysis Software Package. NRC Report TR-HY-030, Ottawa, Ont., Canada.

Pratte, B., Timco, G., 1981. A new model basin for the testing of ice–structure interactions. Proceedings POAC '81, vol. 2, pp. 857–866. Quebec City, Canada.

Sodhi, D.S., Morris, C.E., 1984. Ice forces on rigid, vertical cylindrical structures. US Army CRREL Report 84-33, Hanover, NH, USA.

Timco, G.W., 1984. Ice forces on structures: physical modelling techniques. 2nd IAHR State-of-the-Art Report on Ice Forces on Structures. Proceedings 7th International Association for Hy-

draulic Research Symposium on Ice, vol. IV, pp. 117–150. Hamburg, Germany.

Timco, G.W., 1986. EG/AD/S: a new type of model ice for refrigerated towing tanks. Cold Regions Science and Technology 12, 175–195.

Timco, G.W., 1987. Indentation and penetration of edge-loaded freshwater ice sheets in the brittle range. Journal of Offshore Mechanics and Arctic Engineering 109, 287–294.

Timco, G.W., Frederking, R.M.W., 1990. Compressive strength of sea ice sheets. Cold Regions Science and Technology 17, 227–240.

Timco, G.W., O'Brien, S., 1994. Flexural strength equation for sea ice. Cold Regions Science and Technology 22, 285–298.

Timco, G.W., Irani, M.B., Tseng, J., Liu, L.K., Zheng, C.B., 1992. Model tests of the dynamic ice loading on the Chinese JZ-20-2 jacket platform. Canadian Journal of Civil Engineering 19, 819–832.

Timco, G.W., Nwogu, O.G., Christensen, F.T., 1995. Compliant model tests with the great belt west bridge piers in ice. Part 1: Test methods and key results. Cold Regions Science and Technology 23 (2), 149–164.

Timco, G.W., Cornett, A.M., Singh, S.K., 1997. A Study of Ice-Induced Vibrations using a Segmented, Elastic Model of the Molikpaq. Proceedings 16th International Conference on Offshore Mechanics and Arctic Engineering, OMAE97, vol. 4, pp. 313–320. Yokohama, Japan.

Tryde, P., 1979. Flexural and uniaxial compression strength of sea ice in Danish waters. Proceedings POAC'79, vol. 1, pp. 633–641. Trondheim, Norway.

Available online at www.sciencedirect.com
SCIENCE DIRECT
Cold Regions Science and Technology 41 (2005) 25–47
cold regions science and technology
www.elsevier.com/locate/coldregions

Ice loading on Danish wind turbines: Part 2. Analyses of dynamic model test results

Helge Gravesen[a,*], Søren L. Sørensen[a], Per Vølund[b], Anne Barker[c], Garry Timco[c]

[a]*Carl Bro, Granskoven 8, DK 2600 Glostrup, Denmark*
[b]*SEAS, Slagterivej 25, DK 4690 Haslev, Denmark*
[c]*Canadian Hydraulics Centre, National Research Council of Canada, Ottawa, Ont., Canada K1A 0R6*

Received 14 July 2003; accepted 19 May 2004

Abstract

The present paper deals with ice loads on wind turbine foundations from large floating ice floes. Some newly developed procedures to estimate the extreme ice load and combined loads from wind with loads from ice are described. The procedures have been developed as a part of the design basis for two of the first large offshore wind farms in Denmark, and they have been further developed in a research project including ice model tests with cones and vertical cylinders at the National Research Council (NRC), Canada. The principles are included in the new "Danish Recommendation to Technical Approval of Offshore Wind Turbines". The design procedures are an integrated part of a selected design philosophy, which also includes a procedure for defining a consistent set of partial safety factors for the various extreme load cases. For a partial safety factor for wind loads of 1.4 to 1.5 (as defined in the Danish standards), the partial coefficients for ice load should be 2.0 to 2.5, depending on the determining ice load case.

Keywords: Wind turbine; Offshore; Foundation; Ice load; Cone; Combined loads; Safety; Partial safety factors

1. Introduction

Ice loads on wind turbine foundations from floating ice floes has been simulated by physical model tests in a scale of 1:26 performed at the National Research Council (NRC), Canada. The test conditions and the results are described in a companion paper (Barker et al., 2004). The present paper concentrates on methods for practical applications of the model-test results.

1.1. Ice model tests at NRC

The model tests were carried out for prototype ice design conditions valid for Danish waters during a 1/50-year event with ice thickness h=0.57 m, crushing

* Corresponding author.
E-mail addresses: HlG@carlbro.dk (H. Gravesen), SSo@carlbro.dk (S.L. Sørensen), pvl@e2.dk (P. Vølund), anne.barker@nrc-cnrc.gc.ca (A. Barker), garry.timco@nrc-cnrc.gc.ca (G. Timco).

0165-232X/$ - see front matter © 2004 Elsevier B.V. All rights reserved.
doi:10.1016/j.coldregions.2004.05.009

strength r_u=1.9 MPa and bending strength r_f=0.5 MPa (see Section 1.2). The model results were scaled by means of the Froude model scaling with a scale factor of λ=26. Full-scale values are used throughout the paper.

Fig. 1 shows the four test models, including inverted cones with a cone angle of, respectively, 55° and 65°, double-sided cones (both sharp and round) and vertical cylinders. For all tests, the basic vertical cylinder had a diameter of 5 m. Results were obtained for a stiff structure, a compliant structure corresponding to a typical first mode tower oscillation with resonance frequency of 0.38 Hz, a damping ratio of ζ=0.06 and a stiffness of 50 MN/m, and a compliant structure corresponding to a typical second mode tower oscillation with resonance frequency of 1.81 Hz, a damping ratio of ζ=0.08 and a stiffness of 116 MN/m. The coefficients of friction of the model structures at NRC were determined to be 0.11 and 0.07 for static and moving friction, respectively. Ice floe velocities were generally V_{ice}=0.2, 0.4, 0.7 and 1.0 m/s, but for the vertical cylinder, a few tests were also carried out at V_{ice}=0.05, 0.1, 0.15, 0.25, 0.30 and 0.35 m/s. In addition, some "ramping" tests with a continuously increasing V_{ice} from 0 to 1 m/s were carried out.

1.2. Ice characteristics in the Danish Straits

The estimated ice load scenario for floating ice floes in the Danish Straits and the corresponding ice properties are described below.

- The maximum size of the ice floe is assumed to be 2×2 km.
- The maximum ice velocities and distributions of ice velocities determined for the area, mainly based on the current velocity because limited correlation with the wind velocity is assumed. In connection with the wind farms at Middelgrunden and Nysted-Rødsand, $V_{ice,max}$=1.0 m/s is estimated. This is elaborated further in Section 3.
- From the Danish fixed link projects across the Great Belt and the Sound, the extreme ice properties have been estimated in Christensen and Skourup (1991) (see Table 1), and these values are also used here (Ottesen Hansen and Gravesen, 2001).

Table 1
Extreme ice properties in Danish Straits

Return period	5 years	10 years	50 years	100 years	1320 years
K_{max} (−°C 24 h)	170	245	410	480	744
r_u (MPa)	1.0	1.5	1.9	2.0	2.4
r_f (MPa)	0.25	0.39	0.50	0.53	0.64
h (m)	0.33	0.42	0.57	0.63	0.80

r_u=the crushing strength of the ice.
r_f=the bending strength of the ice.
h=thickness of the ice=$0.032(0.9K_{max}-50)^{0.5}$.
K_{max}=frost index=the sum of the 24-h average temperature (in °C) during the frost period (<0 °C).

1.3. Structural shapes

Five different structural shapes were evaluated in the model test program. There are a cylindrical structure, 55° and 65° inverted cones and double-sided cones with a sharp and a blunt transition between the cones.

1.4. Scaling to standard conditions

According to the Froude model scaling, the prototype time (t) and force (F) from a model

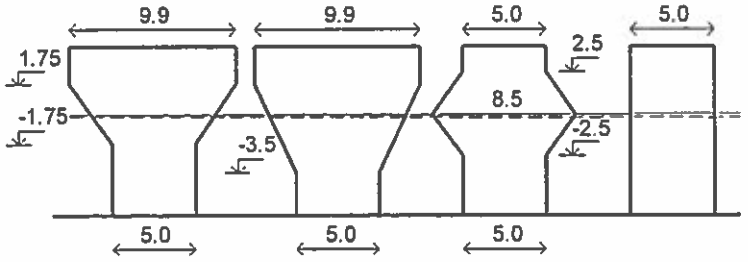

Fig. 1. Tested configurations, NRC tests.

test performed in a model scale of 1:λ is given by:

$$t_{\text{prototype}} = t_{\text{model}}\lambda^{0.5} \tag{1.1}$$

and

$$F_{\text{prototype}} = F_{\text{model}}\lambda^{3} \tag{1.2}$$

During the physical model tests, the actual ice thickness h_{model} and the bending strength $r_{\text{f,model}}$ were measured. The crushing strength $r_{\text{u,model}}$ was determined by a calibrated ratio to the bending strength. To obtain a given combination of thickness and strength is difficult, and a certain deviation from the previous mentioned target parameters has to be accepted.

The ice force has to be corrected for the deviations of the thickness and strength, and this correction depends on the failure mode. In connection with this scaling, a pure linear-elastic bending failure mode is assumed for the cone structures (cf. Sections 3 and 4) and a pure crushing mode is assumed for the vertical cylinder structures (cf. Section 2). In a linear-elastic bending failure, the force is proportional to the product of the bending strength and the thickness squared. In crushing failure, the force is proportional to the product of the crushing strength and the thickness. In buckling failure, the failure is proportional to the elastic modulus and the thickness cubed. For further information regarding the scaling of the elastic modelling of artificial ice, the reader is referred to Timco (1986). The corrections due to the deviations in thickness and strength are outlined in Table 2.

Table 2
Corrections of measured ice force due to deviations in ice thickness and strengths

	Cone structures	Vertical cylinder structures
Assumed failure mode	Linear-elastic bending	Crushing
Proportionality	$F \alpha r_f \cdot h^2$	$F \alpha r_u \cdot h$
Correction	$F = \frac{r_f}{r_{f,\text{meas}}}\left(\frac{h}{h_{\text{meas}}}\right)^2 F_{\text{meas}}$	$F = \frac{r_u}{r_{u,\text{meas}}}\frac{h}{h_{\text{meas}}} F_{\text{meas}}$

2. Vertical cylinder

At first, four tests were carried out corresponding to the typical first mode tower oscillations and four tests with a stiff structure. In these tests, forces up to 2.5 MN were experienced. The main part of the cylinder tests though, namely, 28 out of 36, were carried out for the cylinder corresponding to the typical second mode tower oscillations (f_n=1.8 Hz), as these gave more unexpected results. Out of these 28 tests, 24 were carried out with a constant ice velocity and 4 with ramping velocity.

Out of the 24 constant velocity tests with eigenfrequency f_n=1.8 Hz, 12 tests were conducted with a rather continuous crushing and a force level staying at typical 2 MN, with a large mean value (typically 1.4 MN). During the 12 other tests, a mixed-mode pattern with very nonstationary conditions occur, with peak force levels in the order of 5 MN. These two types of ice failure were experienced randomly in occurrence and even for the same test setup. In some tests, both types were experienced, but generally, when a certain failure mode has been initiated, the remaining time of the test tends to follow this failure mode. For crushing, there may appear some changes in the max and mean force during a test, and in a few of the tests, there appears to be a type of mixed failure mode.

2.1. Crushing failure

Fig. 2 shows a typical example of the force on the cylinder during a continuous crushing failure. The force spectrum has a nearly constant variance over all frequencies from 0 to 3 Hz. A minor peak may be seen in the force spectra at the resonance frequency of the system (1.8 Hz in water). In cases with crushing, a significant velocity dependence is experienced. This velocity dependency is observed in both the constant velocity (cf. Fig. 3) and the ramping tests (cf. Fig. 4).

2.2. Mixed-mode failure

Fig. 5 shows a typical example of the force on cylinders when mixed-mode failure occurs. The force spectrum has a dominant variance on frequencies below 0.5 Hz due to the nonstationary character of the

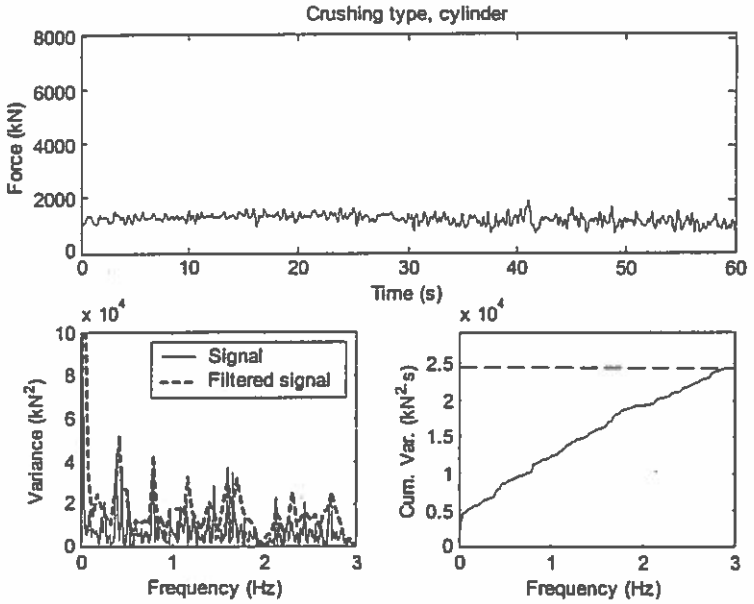

Fig. 2. Example of time series and spectra of 60 s of data when crushing occurs. Same test setup as in Fig. 5 is used. The ice velocity is 1 m/s.

force. The time series of the force seem to be composed of three more or less separate components:

- A buckling force component with a low frequency. This component has a length scale of approximately 5 (±1.2) times the diameter of the structure.
- An ice crushing component with frequencies about 10–20% lower than the eigenfrequency in water (1.8 Hz), which might be due to the additional added mass from ice during the buckling load. The crushing frequency was relatively independent of the velocity (in the range of about 0.4–1 m/s).
- A minor component with length scale of about 1–2 m.

The first two components are illustrated in Fig. 6, by applying a 0.27 Hz FFT filter to the force signal. There appears to be a certain correlation between the buckling component amplitude and the amplitude of

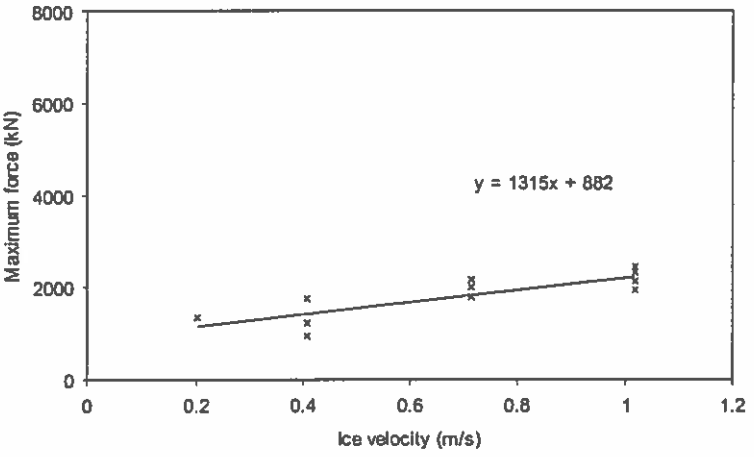

Fig. 3. Maximum force when crushing occurs.

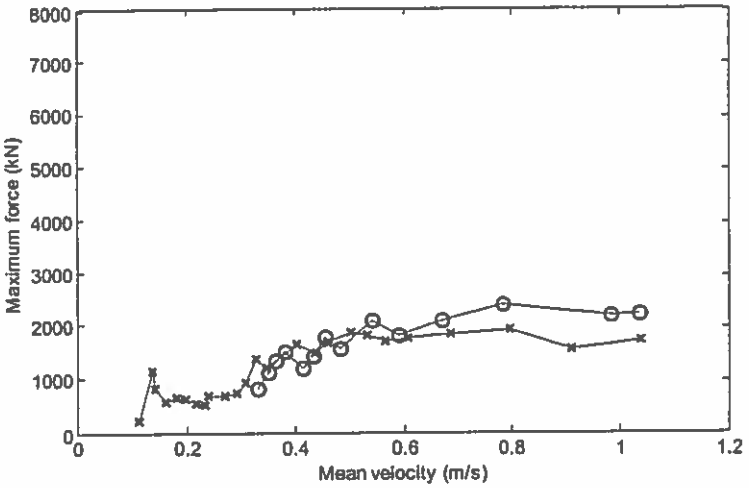

Fig. 4. Ramp results when crushing occurs. The figure shows two separate tests.

the crushing component in the sense that, close to the peak of the buckling component, the crushing component has a reasonable large value. But they are not correlated in the sense that the peaks are occurring at the exact same time. The phase of the crushing component seems to be rather random. The maximum high pass component is typically, say, 50% of the low pass component. No significant velocity dependence is experienced when the above-described mixed mode occurs (cf. Figs. 7 and 8).

2.3. Design time series

A simple method of extending the information obtained during the model test to a time series of 10-min duration will be presented. The method is

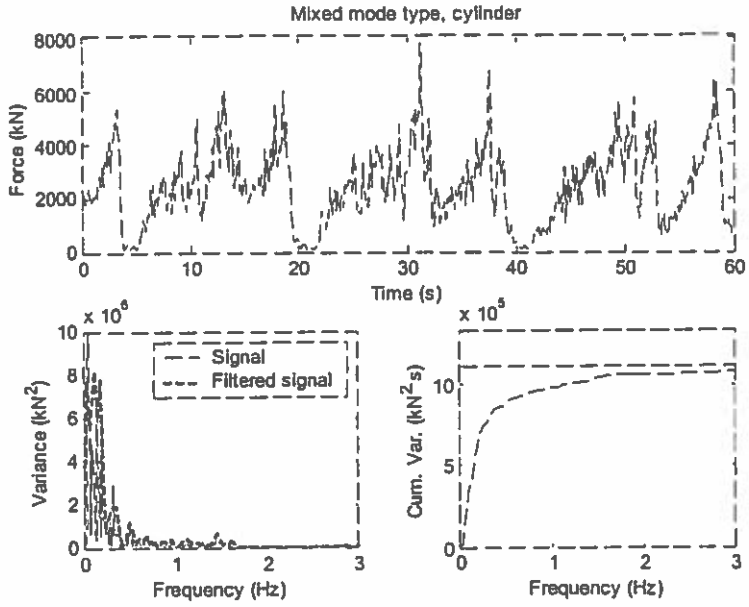

Fig. 5. Example of time series and spectra of 60 s of data when mixed-mode failure occurs. Same test setup as in Fig. 2 is used. The ice velocity is 1 m/s.

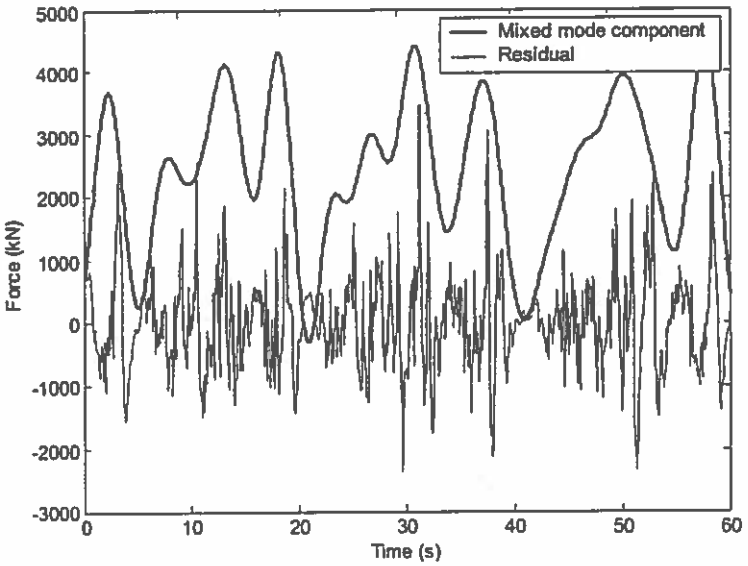

Fig. 6. Force components of time series from Fig. 5.

developed due to the need for examining the effect of the combination of loads from wind and ice on the structure. The mixed-mode failure is dominating the design, thus, only this case is considered. For $V_{ice}<0.2$ m/s, the momentum in even large ice floes is limited, thus, continuous ice loading may only occur in case of high wind or current velocities. This load case is left out in the present analysis.

The data are separated in two velocity ranges: $0.2\leq V_{ice}<0.5$ and $0.5\leq V_{ice}\leq 1.0$ m/s. For each of the two velocity ranges, the mixed-mode events are defined as illustrated in Fig. 9. The distribution type and parameters of the maximum forces of the mixed-mode events is determined (cf. Fig. 10). For each event, the time series is normalised relative to the maximum force. Connecting random-selected events, scaled randomly to fit the peak distribution, enables the generation of time series of 10-min duration. The time scale is not changed, thus, the variation in the length scale of the combined time series may be larger than in the original results. Note that this should not influence the lock-in component of the force.

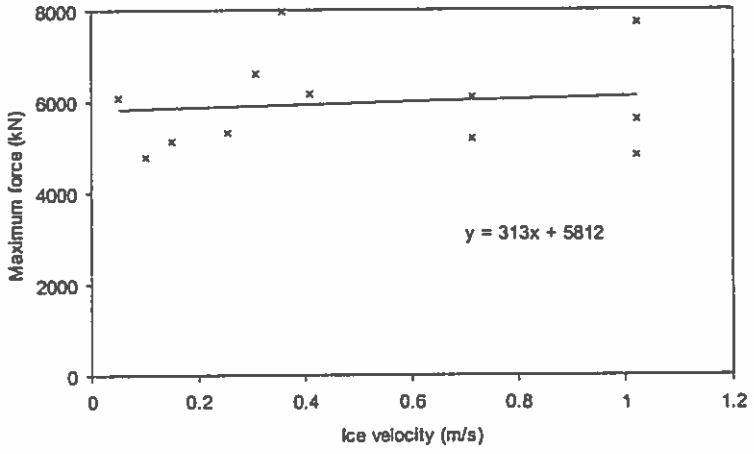

Fig. 7. Maximum force when mixed mode occurs.

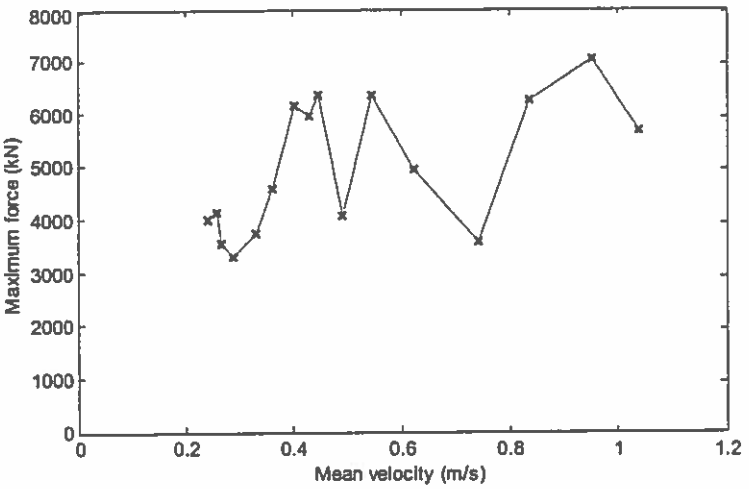

Fig. 8. Ramp results when mixed mode occurs.

2.3.1. Modifying results for other stiffness/eigenfrequency

In mixed mode, the eigenfrequency is very important for the ice load, as discussed above. If the model tests should be interpreted to apply for another eigenfrequency, care should be taken. It would be reasonable though to expect that the amplitudes of the ice force would not change considerably for eigenfrequencies (determined in water) in the range of $1.3<f_n<2.6$. It is important to scale the time to keep the ratio of structure eigenfrequency to lock-in frequency. The time should be scaled by a factor of $1.8/f_n$.

If the model tests should be interpreted to apply for another stiffness and mass, but the same eigenfrequency, the structure displacement is expected to be larger, but because more failure types are involved, one can only guess about the effect that this would have.

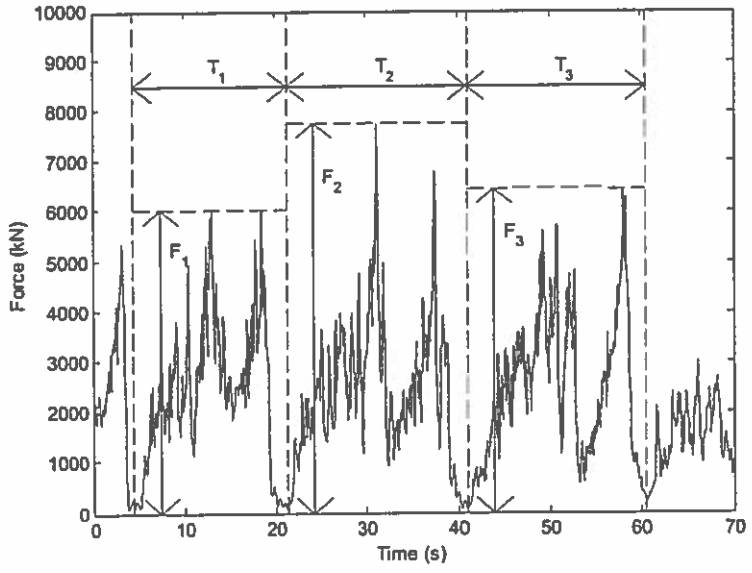

Fig. 9. Example of definition of parts in time series. Only mixed-mode events are used.

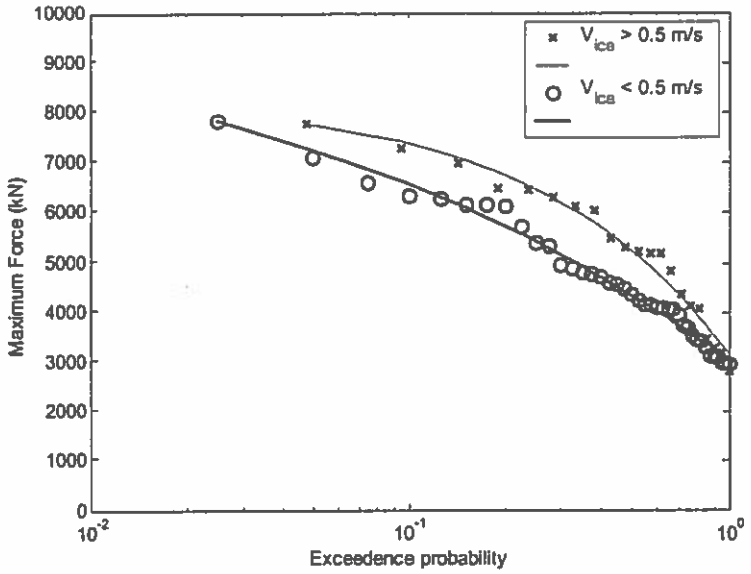

Fig. 10. Statistics of time-series parts.

2.3.2. Perturbation of mixed-mode events

Perturbation of the mixed-mode events in the extension method described above might be a method to test the sensitivity of the shape of these events. A method will be suggested and preliminary results presented. The basis of the method is the perturbation of the complex Fast Fourier Transform (FFT) spectrum of time-series parts by the use of a random number generator. Perturbed time series with approximately the same spectral property can then be formed by an Inverse Fast Fourier Transform (IFFT) of the perturbed spectrum.

All time series of the mixed-mode events are zero padded to a fixed length before the FFT analysis is

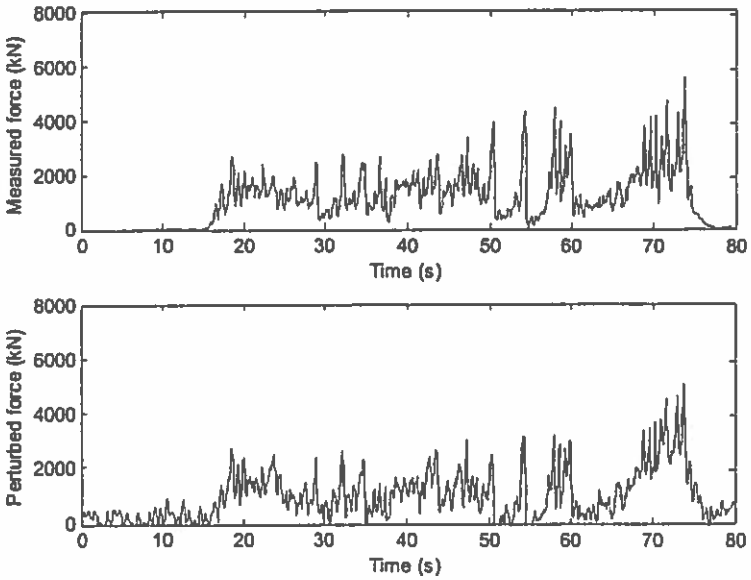

Fig. 11. Example of perturbation of mixed-mode events.

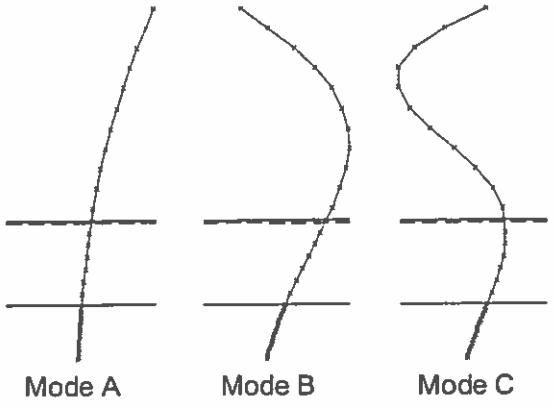

Fig. 12. Definition of mode shapes in GTSTRUDL calculations.

performed, to ensure that the spectra of all time-series parts are comparative.

Each number in the FFT amplitude spectrum, A_i, is given a small perturbation defined by

$$A_i' = A_i r_i \tag{2.1}$$

where r_i is randomly chosen and uniformly distributed in the interval

$$r_i \in [1 - k_{\text{meas},i};\ 1 + k_{\text{meas},i}] \tag{2.2}$$

where $k_{\text{meas},i}$ is a predefined constant defined from the statistics of all buckling event time series in the analysis. The minimum ($A_{i,\min}$), maximum ($A_{i,\max}$) and average ($A_{i,\text{mean}}$) of each number in the amplitude spectrum are determined, and $k_{\text{meas},i}$ is defined as

$$k_{\text{meas},i} = |(A_{i,\max} - A_{i,\min}) - A_{i,\text{mean}}|/A_{i,\text{mean}} \tag{2.3}$$

Each number in the FFT phase spectrum ϕ_i are given a small perturbation defined by

$$\phi_i' = q_{\phi,i} + \phi_i \tag{2.4}$$

Where $q_{\phi,i}$ is randomly distributed in the interval

$$q_{\phi,i} \in [-k_\phi; k_\phi] \tag{2.5}$$

Where k_ϕ is a predefined constant that is the same for all numbers in the phase spectrum. In the present example k_ϕ=60°.

An example of a time-series peak before and after perturbation is shown in Fig. 11. The perturbed time series are not independent of the original time series due to the induced restrictions to the amount of perturbation. On the other hand, it is necessary to maintain the basic physics in the results. The perturbation procedure, including a determination of the required limitation of perturbation (mainly to phase spectrum), has not yet been finalized and compared with the more simple composition procedure. One disadvantage is that the perturbed ice force

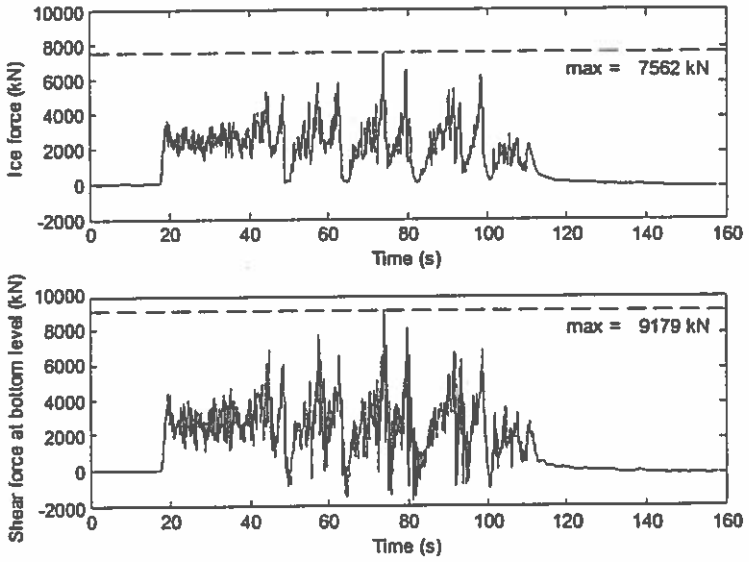

Fig. 13. Ice load contra shear force at bottom level. The maximum shear force is 1.2 times the maximum ice force.

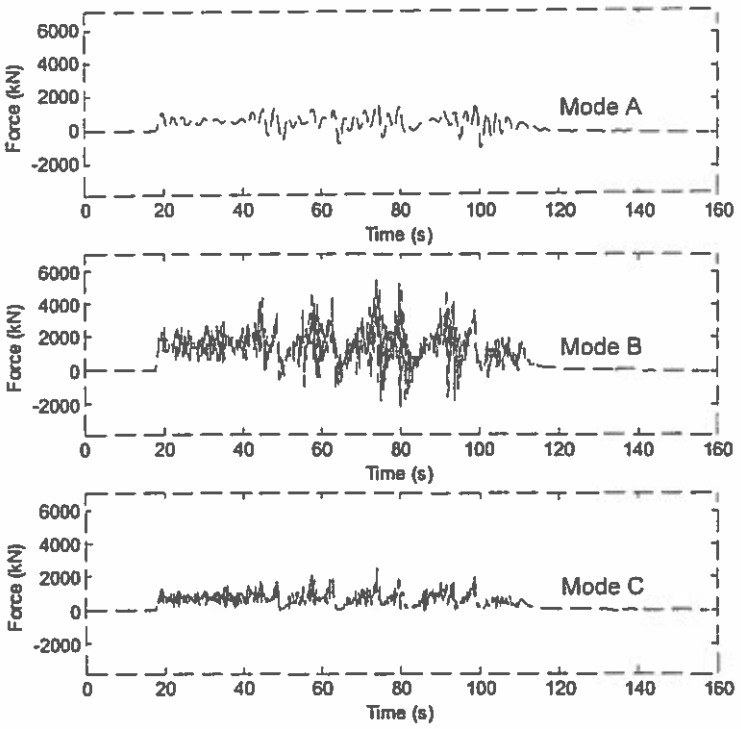

Fig. 14. Contributions to the shear force at bottom level using mode separation in GTSTRUDL. The mode shapes are shown in Fig. 12.

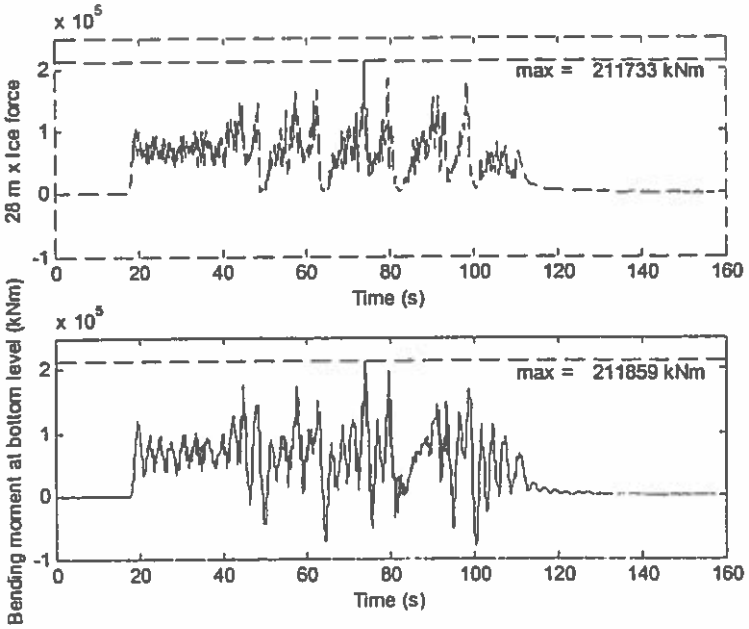

Fig. 15. Ice force multiplied by moment arm contra bending moment at bottom level. The maximum moments are the same.

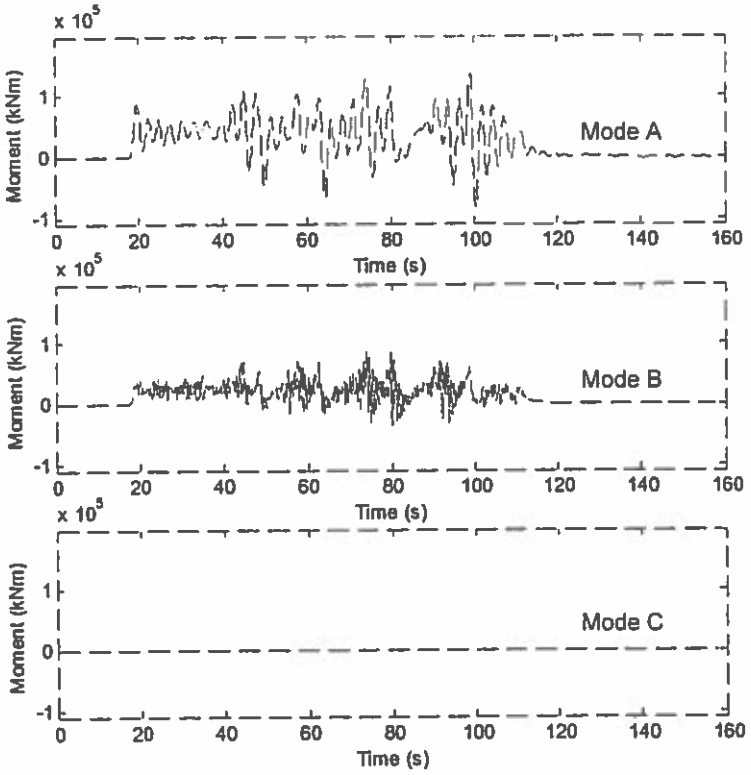

Fig. 16. Contributions to the bending moment at bottom level using mode separation in GTSTRUDL.

can experience negative ice forces, which does not correspond to the physics.

2.4. Multiple degrees of freedom

During the physical model tests, only two eigenfrequencies were examined because it was assumed that only two eigenmodes of a typical offshore wind turbine structure would be excited. To examine this more closely, a finite element model of the structure was developed using the commercial FEM program GTSTRUDL. The structure is a mono pile structure, with a reasonable geometry for large wind turbines on deep water and with a rather high damping (7%). One of the force time series with mixed-mode failure is applied at water level, and the response force and moment at the bottom level are examined. A high number of mode shapes are allowed during the calculations, of which the most interesting ones are shown in Fig. 12. The maximum shear force at the bottom level is approximately 20% higher than the maximum ice force (at water level; see Fig. 13). The shear force is distributed on all of the three modes shown in Fig. 12. The contributions from each mode to the shear force are shown in Fig. 14. The maximum bending moment at the bottom level is the same as the maximum ice force multiplied by the moment arm (see Fig. 15). The bending moment is only distributed on the first two modes, and contributions are shown in Fig. 16.

3. Inverted cones

The tested geometrical conditions are shown on Fig. 17.

Fig. 18 shows typical examples of forces to a cone with bending failure. Typical forces were in the range of 0.5–0.75 MN for the inverted cones. The force spectrum has a peak at the bending failure frequency. The typical breaking length is about 2.5 m (cf. Figs. 19 and 20). With an ice velocity of V_{ice}=1 m/s, the

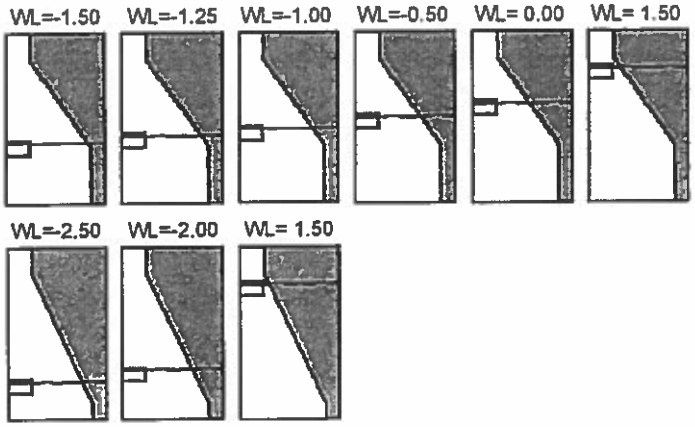

Fig. 17. Water level configurations for the down bending cone at the 55° and 65° slope angle.

peak frequency is, accordingly, about 0.4 Hz. For other velocities, the breaking failure frequency may be estimated from:

$$f \approx 0.4 V_{ice} \text{(in Hz when } V_{ice} \text{ is in m/s)} \quad (3.1)$$

3.1. Effective damping

During the physical model tests, the displacement, velocity, acceleration and force are measured as time series, and the mass, stiffness and the viscous damping in water are also determined. Because the physical model tests represent a single degree of freedom oscillation, the equation of motion is:

$$F(t) = m\ddot{x} + c\dot{x} + kx \quad (3.2)$$

where F is the ice force, m is the mass, c is the damping, k is the stiffness, and x is the displacement. The damping is assumed to be viscous damping, and the amount of damping is expressed in terms of the

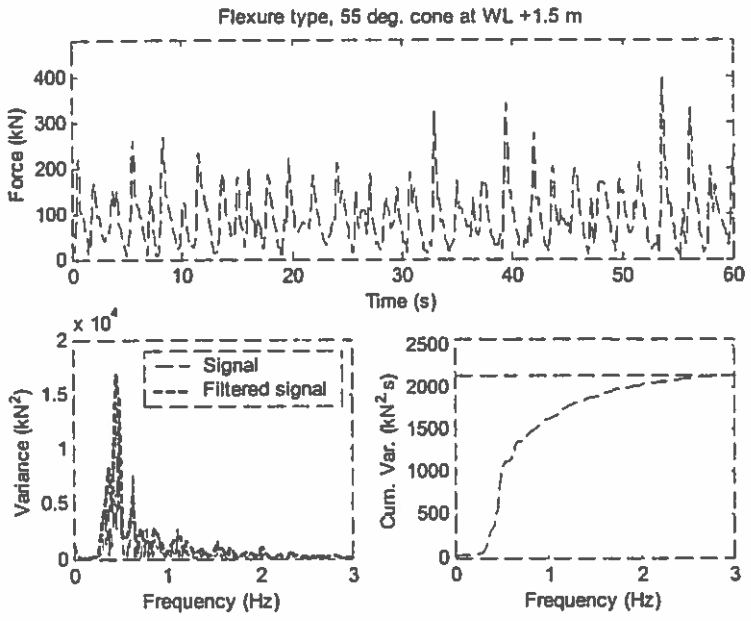

Fig. 18. Example of time-series and spectra of 60 seconds of data, inverted cones.

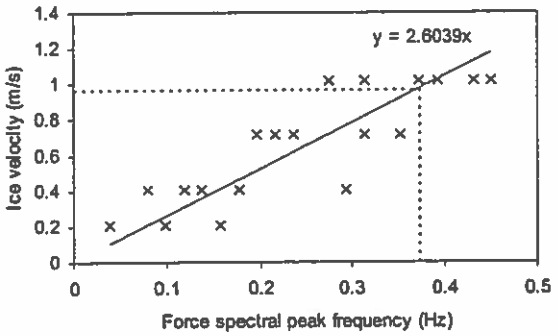

Fig. 19. Spectral peak frequency for the 55° cone.

damping ratio ζ that is the percent of the value required for critical damping, i.e.,

$$\zeta = \frac{c}{4\pi m f_n}. \tag{3.3}$$

When the structure moves in ice-covered water instead of pure water, the ice induces some extra damping. By solving the equation of motion, this extra damping has been determined to be about 6%, which is a considerable amount of damping. A wind turbine structure is usually considered to have a damping ratio in the order of 1%. This ice-related damping value of 6% is only relevant to the specific mode of oscillation considered here, which was the second mode for the vertical structure.

3.2. Compliance sensitivity

There is no evidence that the forces determined during stiff tests differ from the forces during compliant tests. A minor deviation cannot be identified due to the relative large scatter between results from different tests. This, on the other hand, confirms the intuitive feeling that minimal interaction between the force and the structural response should occur for a cone structure.

3.3. Water level sensitivity

The ice model tests show quite a large scatter of the same magnitude as for field measurements. During some tests, changes in the breaking mode and pattern appeared, and the statistical properties changed. Due to the relatively large scatter, it has not been possible to determine the relation between ice load and the actual cone diameter at the waterline. For this reason, results with varying diameters have been combined.

A major concern in the cone design is the required cone height. In the past, rather conservative requirements have been specified by various researchers, although this has not been reflected in the API (1995). The requirement of a large cone height could rapidly become a killing assumption to wind turbine foundations, as this would result in a large cone with associated increased wave loads and construction costs. Basically, the cone geometry should make sure that no crushing of ice takes place on the vertical cylinder. With 0.6-m-thick ice, the failure mode is dominated by bending failure at water levels larger than WL≥ -0.75 m when the cone ends in elevation -1.75 m (c.f. Fig. 21). From this, it may be concluded that a distance of 0.5 m from the bottom of the ice to the intersection point with the vertical structure should be sufficient for the given ice thickness of 0.6 m. When the failure mode is dominated by bending, minor velocity dependency is present. The combined dependence upon water level and ice velocity is illustrated on Fig. 22 for water levels dominated by bending failure. For water levels below WL<0.75, the ice failure is dominated by crushing, and for the largest water levels, only bending takes place. In between these ranges, a mixed breaking/crushing failure is observed, which can be detected by the angle of force resultant (see Fig. 23). Hence, in this range of water levels, the tendency is that the force decreases

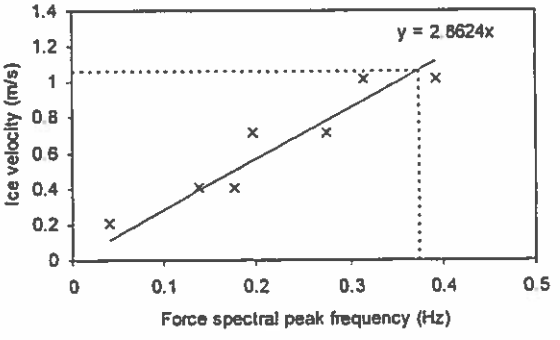

Fig. 20. Spectral peak frequency for the 65° cone.

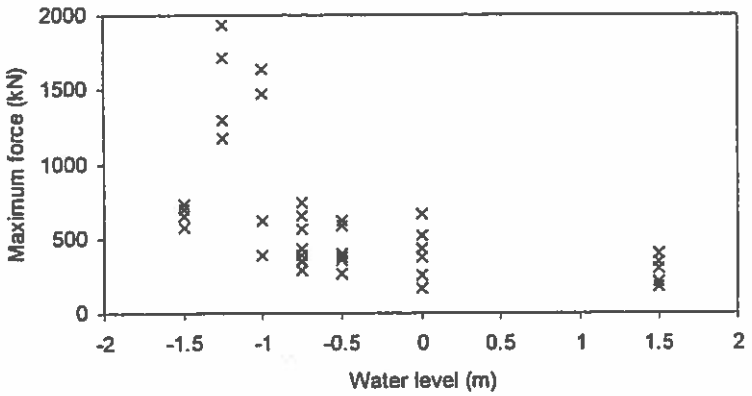

Fig. 21. Water level sensitivity. All water levels and all velocities.

for increased water level, although the effective diameter increases with the water level. The general conclusion is that, for an inadequate cone length, the design should be based on forces in the 2-MN range. The exact water level where conditions equal those of a pure vertical cylinder and associated forces in the range of 5 MN has not yet been determined.

3.4. Comparison with the Ralston formula

The main results are presented in Table 3. The model tests show consistent results compared with previous model tests and field measurements, resulting in values less than, but very close to, predictions by the Ralston (Ref) formula (0.075 for measured results, compared with 0.1 for Ralston formula). Due to resonance, a certain increase in the oscillations in the first mode (0.38 Hz) of the tower does occur for the larger ice velocities (around V_{ice}=1 m/s).

3.5. Correction for velocity variation

In general, the loads on the cones were increasing with increasing ice velocity, V_{ice}. To produce a maximum number of independent time series, the time series and max events were corrected to ice velocity V_{ice}=1 m/s by means of linear regression of

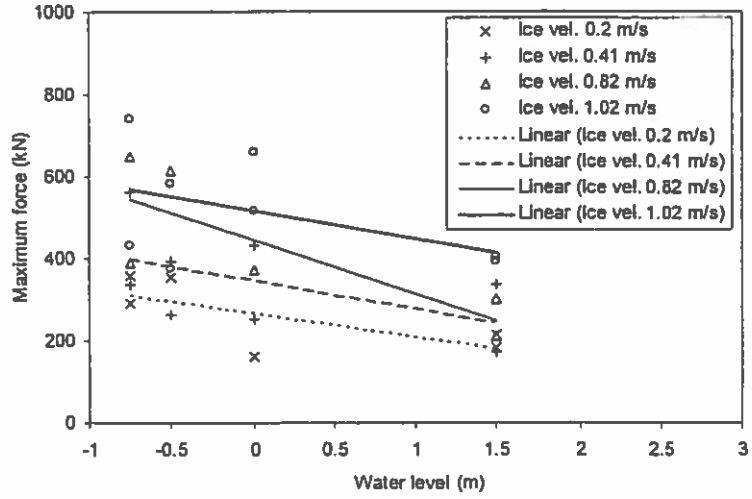

Fig. 22. Water level sensitivity separated in ice velocities for water levels above WL≥ −0.75 m.

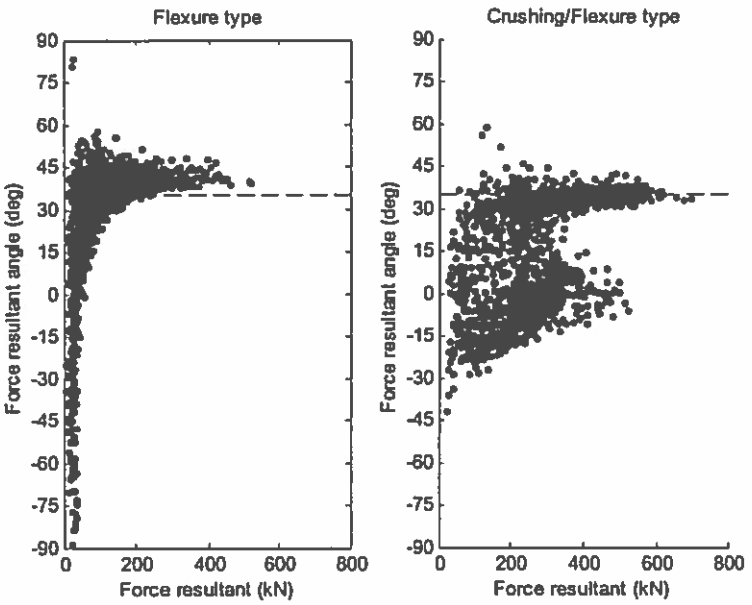

Fig. 23. Two examples of force resultants, with flexure and crushing/flexure type, respectively.

the mean and the standard deviation as function of the ice velocity.

The ice force statistics and the regressions lines are shown in Fig. 24. The slope of the regression curve for the mean is termed A_{mean}, and the slope of the regression curve for the standard deviation is termed A_σ. To correct the mean and standard deviation, the measured values are moved parallel to these regressions lines. Hence, the mean value at the design velocity, $F_{mean}(V_{design})$, and the standard deviation at the design velocity, $F_{rms}(V_{design})$, are calculated from:

$$F_{mean}(V_{design}) = F_{mean,meas} + A_{mean}(V_{design} - V_{meas}) \tag{3.4}$$

$$F_{rms}(V_{design}) = F_{rms,meas} + A_\sigma(V_{design} - V_{meas}) \tag{3.5}$$

Hence, the force at any time is corrected by:

$$F_{final}(t) = F_{mean}(V_{design}) + (F_{meas}(t) - F_{mean,meas}) \cdot \frac{F_{rms}(V_{design})}{F_{rms_{meas}}} \tag{3.6}$$

Table 3
Comparison of results from model tests for inverted cone with Ralston's formula [D_{WL}=9.5 m (at water level), D_t=4.3 m (at bottom of cone), t=0.57 m, r_f=0.5 MPa, $\mu_{cone\text{-}ice}$=0.1/0.2]

Cone angle		F_x (MN)		F_z (MN)	
		Max	σ	Max	σ
55°	Model tests $\mu \approx 0.1$	0.54 (0.50[a])	0.13	0.37 (0.36[a])	0.11
	Ralston μ=0.1/0.2	0.54/0.70	–	0.38/0.38	–
65°	Model tests $\mu \approx 0.1$	0.63 (0.75[a])	0.14	0.22 (0.24[a])	0.05
	Ralston μ=0.1/0.2	0.88/1.26		0.39/0.39	

[a] Average for only tests at V=1 m/s.

3.6. Statistical velocity analysis

An attempt to generalize the force distribution from several ice tests is demonstrated below. The time, t, is corrected by:

$$t_{final} = \frac{V_{meas}}{V_{design}} t_{meas} \tag{3.7}$$

After this correction and the previous mentioned corrections, all the time series of each velocity are

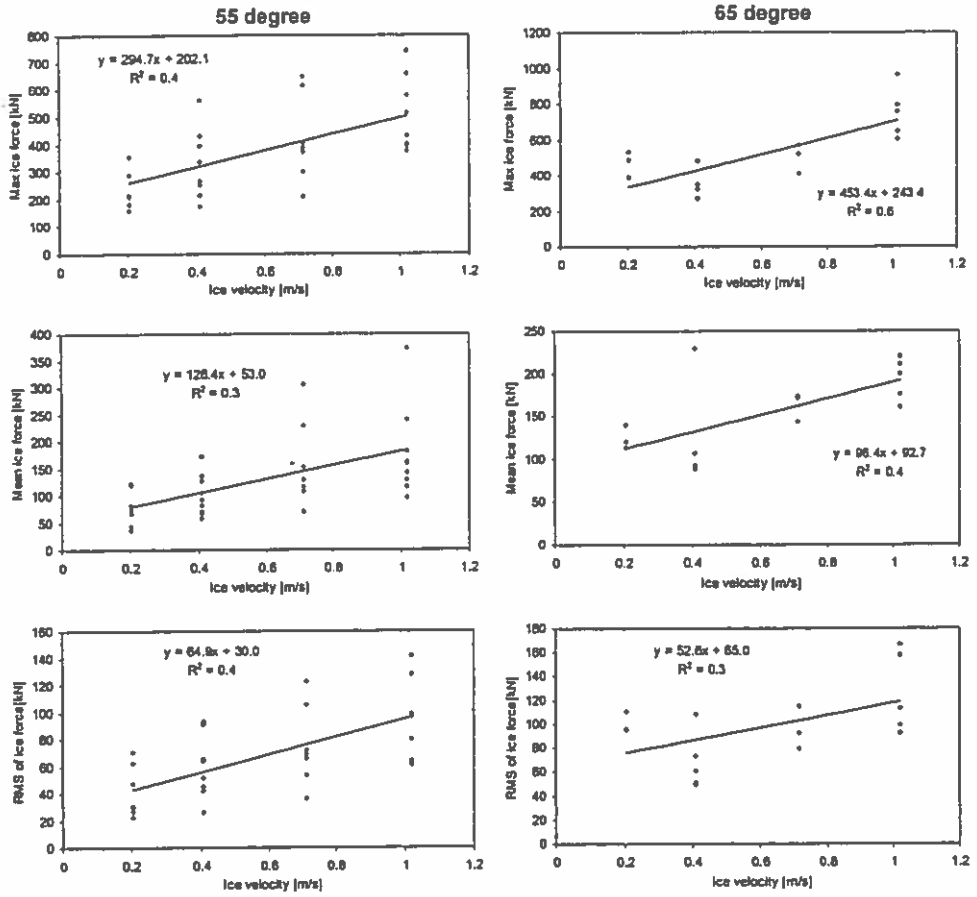

Fig. 24. Ice velocity dependency of statistical values of the ice force.

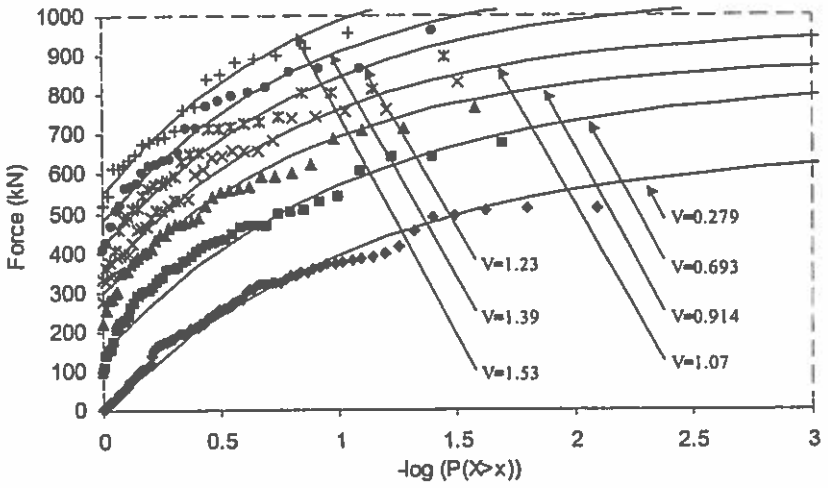

Fig. 25. Determination of general exponential functions after splitting up in 1 min time series. Results from relevant ice velocities, V, are shown.

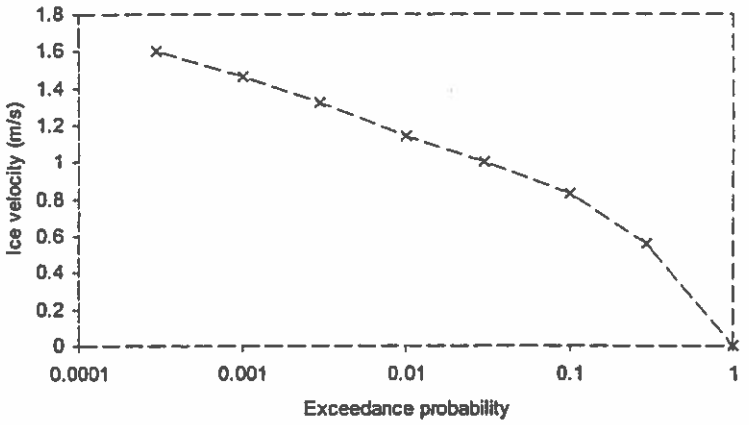

Fig. 26. Ice velocity statistics.

assumed representative for the same load case. Hence, all time series can be put after each other. The time series of each velocity are then split up in 1-min time series, and the maximum values are extracted. Exceedance curves are fitted to the maximum values from a general exponential distribution given by:

$$F = A + k\left(\frac{1 - e^{-\alpha y}}{\alpha}\right) \tag{3.8}$$

in which A, k and α are arbitrary coefficients and y is the base 10 logarithm of the exceedance frequency (see Fig. 25).

By applying the velocity distribution (Fig. 26), the weighted ice statistics may be determined (Fig. 27; Table 4).

3.7. Design time series

Below is described potential methodologies for extrapolating a short time series from a model test to a design time series of 10-min prototype time used in connection with combined ice/wind load analysis. The time series from wind and ice are assumed uncorrelated.

Table 4
Ice velocity statistics

Probability	Velocity (m/s)	Mean velocity (m/s)	Probability interval size
1	0	0.279	0.7
0.3	0.558	0.693	0.2
0.1	0.8280	0.914	0.07
0.03	1.0000	1.07	0.02
0.01	1.1400	1.23	0.007
0.003	1.3200	1.39	0.002
0.001	1.4600	1.53	0.0007
0.0003	1.6000		

3.7.1. Simple extension

Initially, a method was used equivalent to that used for the cylinder case (cf. Section 2.4). Ice bending failure events are determined from a zero-up crossing analysis relative to the mean value (cf. Fig. 28). Connecting these events randomly enables the generation of 10-min time series.

3.7.2. Statistical extension

From the above-described failure events, the force peak heights F and periods T are determined, and the normal distributions of T and F are determined (cf. Fig. 29). The time series of the force during the failure events are stored in a database (cf. Fig. 30). Connecting failure events chosen randomly and scaled to F and T values randomly chosen to fit the distributions enables the generation of 10-min time series. An example is given in Fig. 31.

4. Double-sided cones

The influence of the water level of a double-sided cone has been investigated for seven water levels, as illustrated in Fig. 32.

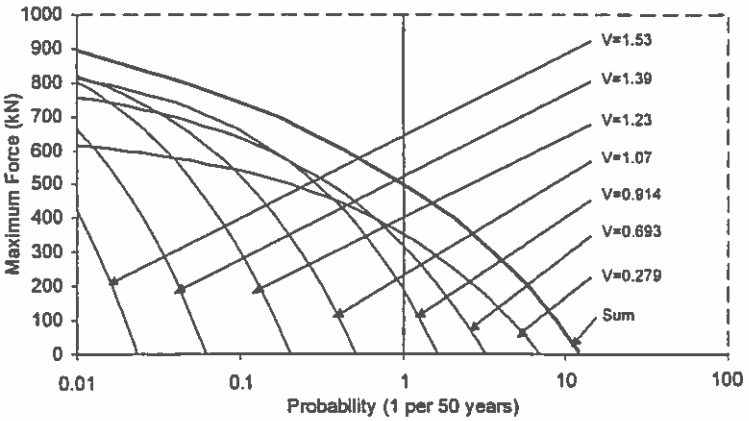

Fig. 27. Statistical summation of ice load over velocities (max force/relative probability).

The two main questions to be solved through the ice model tests are:

- the influence of the water level and the rounded corner when the undisturbed level of the ice coincides with the level of the corner;
- the influence of the water level when the ice approaches the upper corner of the ice cone.

In total, 32 experiments were performed to investigate these effects. The maximum force of each test is shown in Fig. 33.

The experiments with sharp corner (r=0.01 m) have a maximum at the water level 0.42 m, where the centre of the ice floe is slightly above the corner, which might be due to the fact that the friction force from a given volume of accumulated ice above the

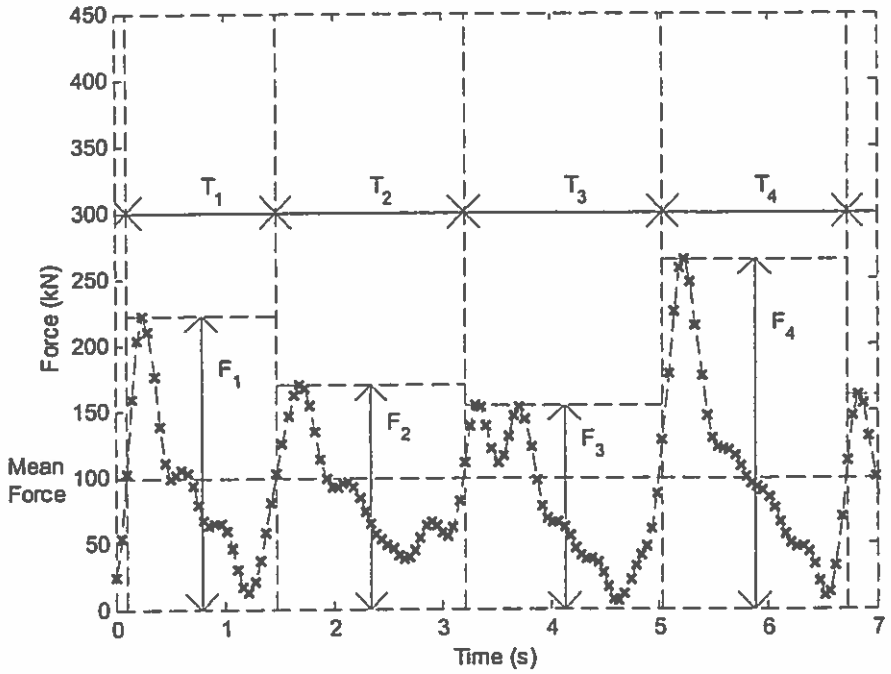

Fig. 28. Example of determination of time series parts for artificial generation of time series.

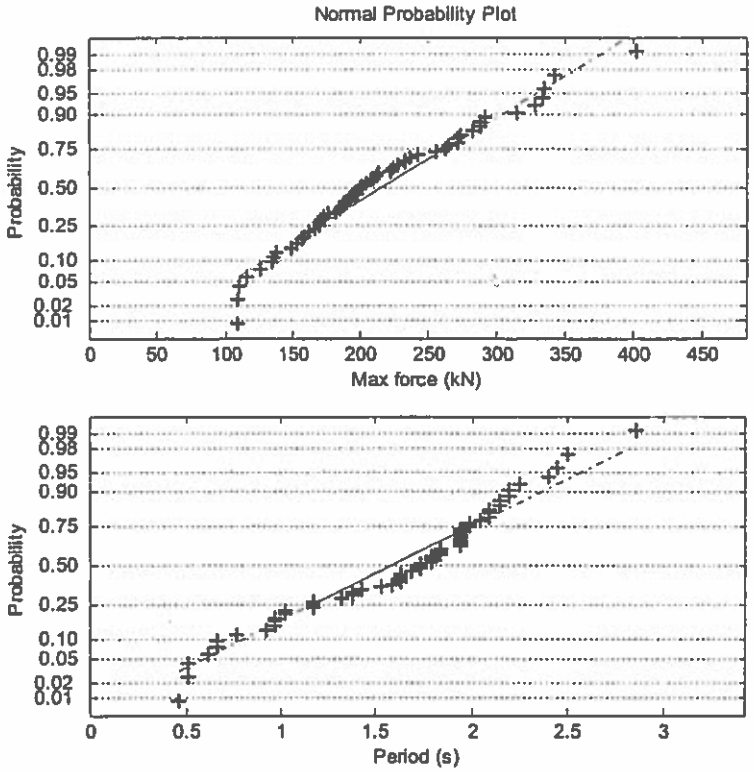

Fig. 29. Normal distribution plots of max force and periods for the time series parts as shown in Fig. 28. Only the results of one of the measured time series are shown.

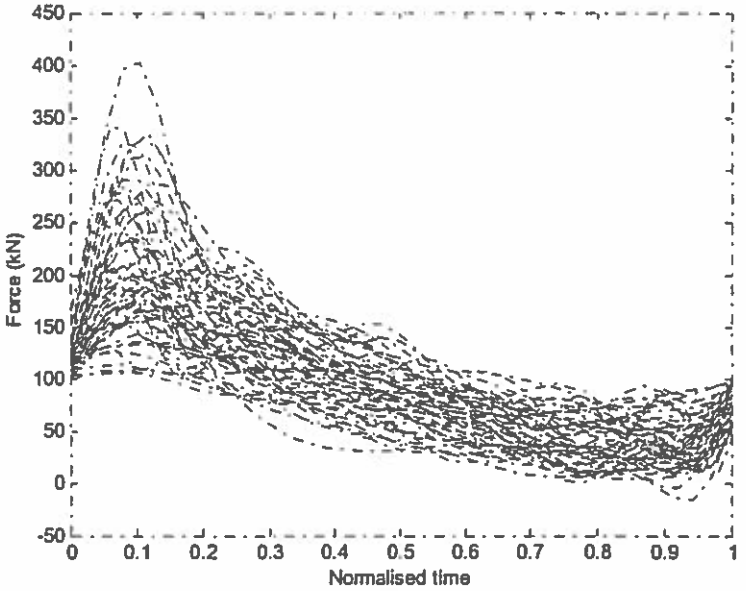

Fig. 30. Example of form database for time-series parts.

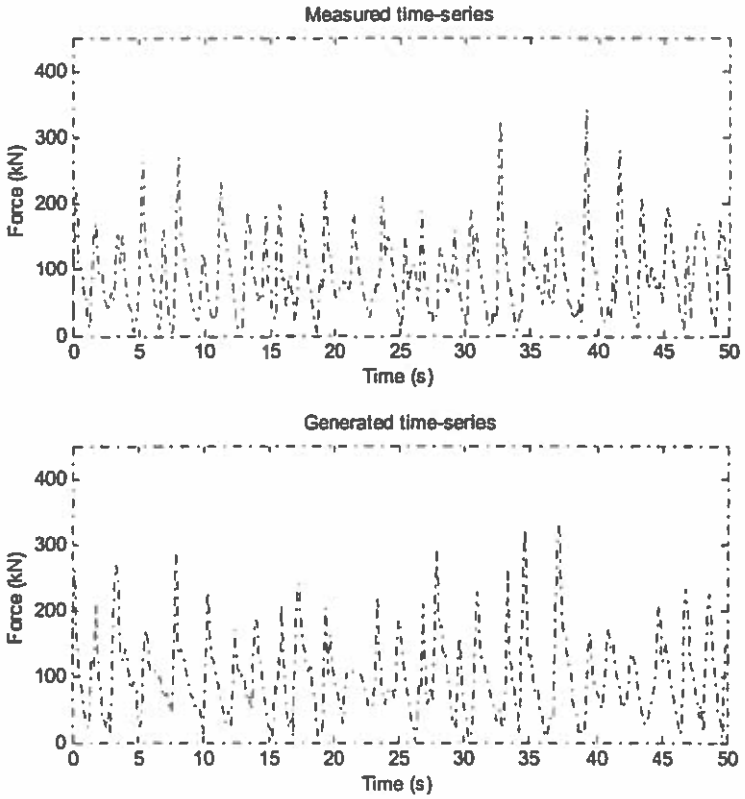

Fig. 31. Example of generated time series.

water surface is about nine times the friction force of the same volume of accumulated ice below the water surface (assuming that the friction coefficients above and below the water surface are the same). The maximum of all results are 1.35 MN (Table 5).

The introduction of the round corner (r=0.15 m) causes quite dramatic changes to the maximum ice force. The maximum force of all measurements increases by 50% relative to the sharp corner results to a level of 2.0 MN, and the maximum force is no longer observed at the water level 0.42 m. Although no experiments were performed at this water level, the maximum force at water level 0.12 m is expected to give smaller force than for 0.27 m because the centre of the ice is below the corner for this water level.

Regarding the experiments with water levels 1.75, 2.0 and 2.25 m, the maximum force shows a tendency to increase with the water level despite that the area of attack decreases. This indicates that, if the distance from top of the ice to the upper intersection point of ice cone and cylinder is less than about 0.5 m, crushing (at least partial) against the cylinder could

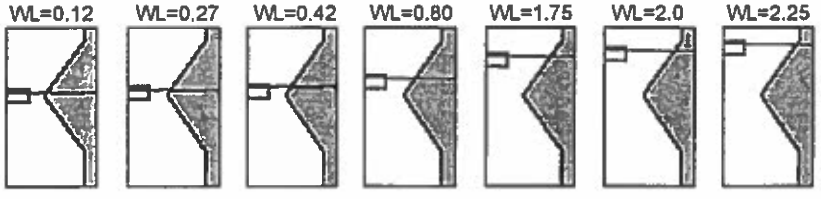

Fig. 32. Water level configurations for tests with double-sided cones.

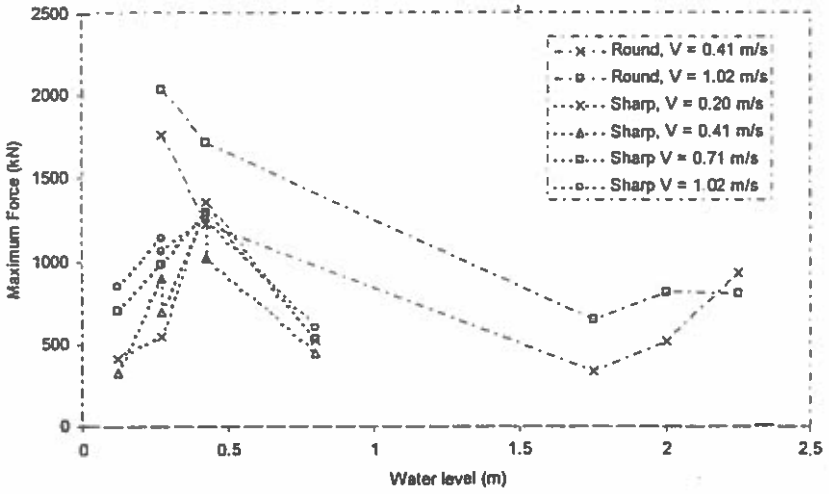

Fig. 33. Water level sensitivity for double-sided cones. Comparisons between round and sharp cones are shown.

occur. This distance between the ice and the intersection point is the same, as for the previously investigated down-bending cone (see Section 3).

5. Design example

For the first large offshore wind farms in Denmark, it has been required to develop procedures to combine loads from wind with loads from ice. The principles are in a generalized form included in the new "Danish Recommendation to Technical Approval of Offshore Wind Turbines" (DEA/Risø, 2001). The procedure includes a method for defining a consistent set of partial safety factors for the various extreme load cases. The partial safety factor for wind loads is defined in the Danish standards to be 1.4 to 1.5. The safety factors are different for the other environmental loads. To reach an equivalent safety level at once per 1320 years, the partial safety factor for waves, which includes little statistical uncertainty, will be typically 1.1–1.2, whereas the partial safety factor for ice load will be typically 2.0–2.5, due to a larger statistical uncertainty. The combined load cases need to include a consistent weighted average of the different partial safety factors.

For some wind turbines, the wind loads during operation (before shutdown at a mean wind velocity of 25 m/s) may be of the same order of magnitude as the extreme wind load for parked conditions. In these cases, the determining load case for wind combined with ice is a situation with maximum operational wind load, which may be at a mean wind velocity equal to 23–25 m/s for a stall controlled turbine and approximately 14 m/s for a pitch controlled turbine in operation.

The combined load time series at the foundation level may be calculated based on wind and ice load

Table 5
Example of maximum of combined extreme ice force with operational wind force for an inverted cone with a cone angle of 55°

Frequency	Wind load (maximum)			Ice load (maximum)			Wind+ice load					
	F_{xv} (mean-max)	M_{yv} (mean-max)	V_v	F_{xi} (mean-max)	M_{yi} (mean-max)	V_i	F_x (mean-max)	M_y (mean-max)	$1+kV_{Fx}$	$1+kV_{My}$	F_x (max)	M_y (max)
Per year	MN	MNm	–	MN	MNm	–	MN	MNm	–	–	MN	MNm
2×10^{-2} year^{-1}	0.63	43.6	0.23	0.50	9.2	0.30	1.00	47.9	1.62	1.39	1.30	55.2
2×10^{-3} year^{-1}	0.63	43.6	0.23	0.85	15.6	0.30	1.36	52.4	1.64	1.40	1.83	61.0
7.6×10^{-4} year^{-1}	0.63	43.6	0.23	1.00	18.4	0.30	1.52	54.6	1.65	1.41	2.07	63.8

The number of events are n=100 each of 10 min.

time series. Based on the combined load time series, the average of the maxima, as well as the coefficient of variation, can be determined. In case of the operational wind load being a part of the load case, the load situation (10-min duration by definition) may occur numerous times during the lifetime. For this case, the peak distributions of the combined load relative to the average maximum combined load per 10 min are estimated. The present work only describes the result for a relatively stiff foundation with limited dynamic interaction between the wind and the ice loads.

This section presents an approximated easy-to-use method to combine wind loads with wave/ice loads, as well as approximated methods to include the effect of the number of repeated design events when the operational wind loads dominate the load cases. The improved design principles can be used to reduce considerably the cost of offshore wind turbine foundations (Gravesen et al., 2001).

5.1. Design considerations with many repeated load cases during operational conditions

The accumulated force distribution of combined wind and ice force is assumed to fit a Gumbel distribution for loads dominated by wind load (overturning moment at foundation level, M_y) and a Normal distribution for loads dominated by the ice load (horizontal force, F_x). A safe estimate for the composition of the maximum force and moment and a variation coefficient is determined from numerical simulations. The number of events during the design scenario is safely estimated.

Below, an example of the procedure to predict the characteristic mean of the maxima values for wind and ice loads and to predict the combined maximum values is described. The prediction is valid for 100 events, each of 10 min (operational conditions).

The formulas presented below have been revised relative to the versions given in Gravesen et al. (2002). The effect of high-frequency contents in the ice force is accounted for by a 15% increase in the dynamic part of the ice force instead of an empirical increase in the mean value, as used in the previous version. It is assumed that $F_{ice,mean}=0.30F_{ice,max}$ and $F_{wind,mean}=0.60F_{wind,max}$, corresponding to a specific site. The example includes realistic estimates of the characteristic loads for a modern 2-MW wind turbine installed offshore in Denmark.

$$F_x = 0.60\cdot F_{x,wind} + 0.30\cdot F_{x,ice} + \left(\left(0.40\cdot F_{x,wind}\right)^2 + \left(1.15\cdot 0.7\cdot F_{x,ice}\right)^2\right)^{0.5} \tag{4.1}$$

$$M_y = 0.60\cdot M_{y,wind} + 0.30\cdot M_{y,ice} + \left(\left(0.40\cdot M_{y,wind}\right)^2 + \left(1.15\cdot 0.7\cdot M_{y,ice}\right)^2\right)^{0.5} \tag{4.2}$$

$$F_x(\max) - F_x(\text{mean}) = \left(F_x(\text{mean of max}) - F_x(\text{mean})\right)\cdot\left(1 + k\cdot V_{Fx}\right), \tag{4.3}$$

$$M_y(\max) - M_y(\text{mean}) = \left(M_y(\text{mean of max}) - M_y(\text{mean})\right)\cdot\left(1 + k\cdot V_{My}\right) \tag{4.4}$$

Where k is determined by the number of events and the type of distribution [k=1.56 at n=100 for the Gumbel distribution (F_x) and k=2.3 at n=100 for the Normal distribution (M_y)].

The coefficient of variation, V, is determined for the value exceeding the average value:

$$V_{Fx} = \left(V_{wind}\cdot\left(0.4F_{x,wind}\right) + V_{ice}\cdot\left(0.7F_{x,ice}\right)\right)/\left(0.4F_{x,wind} + 0.7F_{x,ice}\right) \tag{4.5}$$

$$V_{My} = \left(V_{wind}\cdot\left(0.4M_{y,wind}\right) + V_{ice}\cdot\left(0.7M_{y,ice}\right)\right)/\left(0.4M_{y,wind} + 0.7M_{y,ice}\right) \tag{4.6}$$

6. Summary and conclusions

The physical model tests carried out at the NRC in Ottawa and their subsequent analysis by Carl Bro and SEAS has provided great insight into the loads and loading behaviour that might be expected on Danish offshore wind turbines. The results presented in this paper represent a direct conversion of the model

results to prototype conditions, following a Froude model law, assuming that the model is a correct representation of the prototype. The tests and analysis showed that, for the structural and ice conditions described in this paper:

(1) Typical maximum loads of 0.54 (55°) and 0.63 MN (65°) are predicted for a down-bending cone with the ice failing in flexure mode.
(2) Significantly high loads, in the order of 5 MN, are experienced for the cylindrical structure in about half of the experiments. For this structure, note that the test series represents a limited set of investigations on a vertical structure, concentrating on the risk for dynamic interaction between the ice and the second mode of structure oscillation. This limits the generalization of these specific test results.
(3) The tests show that flexure failure predominates for the conical structure as long as the ice loading is fully on cone structure. If the ice interacts with the cylindrical part of the structure, the failure mode can change to crushing or mixed mode, with significantly higher loads. This information was used to design the size of the cone.
(4) An analysis has been presented that illustrates a methodology for combining the time series of short laboratory tests to produce long ice-load history that can be combined with wind loading. This provides direct information on the combined ice/wind loads on the wind turbine structure.
(5) Tests with the double-sided cone showed a considerable increase in the load with a blunt (rounded) transition between the upper and lower cones. The blunt edge induced a crushing failure of the ice.

References

API, 1995. Recommended Practice for Planning, Designing, and Constructing Structures and Pipelines for Arctic Conditions (2nd ed).

Barker, A., Timco, G., Gravesen, H., Vølund, P., 2004. Ice loading on a Danish wind turbines: Part 1. Dynamic model tests. Cold Regions Science and Technology 41, 1–23 (this volume).

Christensen, F.T., Skourup, J., 1991. Extreme ice properties. Journal of Cold Regions Engineering 5 (2), 51–68 (ASCE).

Danish Energy Agency/Risø, 2001. Danish Recommendation for Technical Approval of Offshore Wind Turbines.

Gravesen, H., Tarp-Johansen, N.J., Vølund, P., 2001. Combined loads from wind, waves and ice on offshore wind turbine foundations. 2001 European Wind Energy Conference. P.G5.6, Copenhagen, Denmark.

Gravesen, H., Sørensen, S.L., Vølund, P., 2002. Extreme ice and wind loads to foundations (of offshore wind turbines). 2002 World Wind Energy Conference, Berlin, Paper PD 2.4.

Ottesen Hansen, N.-E., Gravesen, H., 2001. Engineering practice for ice load design in Denmark. POAC'01, Ottawa, Canada, Paper No. 135.

Timco, G.W., 1986. EG/AD/S: a new type of model ice for refrigerated towing tanks. Cold Regions Science and Technology 12, 175–195.

Kärnä, T. and Nykänen, E. 2004. An approach for ridge load determination in probabilistic design. Proc. 17th International Symposium on Ice. Int. Ass. Hydr. Eng. Res. St.Petersburg, Vol 2, pp. 42-50.

AN APPROACH FOR RIDGE LOAD DETERMINATION IN PROBABILISTIC DESIGN

Tuomo Kärnä[1] and Esa Nykänen[1]

ABSTRACT

This paper addresses the methods of determining ice loads caused by first-year ice ridges in connection with a probabilistic analysis of the ice loads. A typical probabilistic analysis is done using the Monte Carlo simulation technique. While using this method, the ice loading formulas should not require extensive computations. Two solutions are proposed to evaluate the keel force component of the ridge load with a very small computational effort. First, an advanced ridge model is used to teach a neural network to provide the same results as the basic model. Second, the same advanced model is used to derive small modifications to the Dolgopolov's keel force model. After these modifications this model can be considered as a reliable method to provide an upper bound value for the keel load.

INTRODUCTION AND OBJECTIVES

The determination of forces caused by keels of first-year ice ridges is one of the current problems in ice engineering. Timco et al. (1999) evaluated twelve different models that have been proposed for the determination of forces caused by ridge keels. The methods are different variants of the passive-earth-pressure theory (Tsytovich, 1986 and Bowles, 1988 and). Timco et al. (1999) found that the ice forces predicted by different methods vary greatly, and recommend more efforts in new numerical techniques that should provide realistic ice force predictions. Using classical concepts of soil mechanics, Kärnä et al. (1996, 2001) and Croasdale (1999) have proposed such numerical models for the determination of the keel load. Based on extensive field measurements, Heinonen (2004) has developed a more advanced material model for first-year ridges, to be used in numerical FE models.

[1] VTT Technical Research Centre of Finland, P.O. Box 1805, FIN-02044

Recent field observations on first-year ice conditions have shown (Timco et al, 2000; Kärnä and Jochmann, 2003) that the structure does not penetrate a first-year ice ridge in its strongest area. Instead, a dodging behaviour will occur in one of several possible variants. These include spine failure, shear fracture, failure behind or stopping and a subsequent failure by creep buckling. These failure modes were illustrated and further discussed by Wright and Timco (2001). The ice floe may also rotate so that the penetration can continue along a weak zone of the ridge field. The area of the ridge sail is a potential weak zone. Field observations (Kärnä and Jochmann, 2003) show several conditions where the penetration of a ridged ice area occurs for a along distance along the ridge sail or along the boundary between an area of rafted ice and level ice. An obvious explanation of the observed dodging behaviour is based on the large-scale behaviour of the drifting ice fields. The first-year ice cover always has several weak zones. Therefore, ridge failure behaviour is very complicated. Large-scale deformations and rotation of the ice field can occur owing to the interaction forces caused by the bottom-founded structure.

The dodging behaviour of the ice ridges is a force limiting mechanism. Unfortunately, it is difficult to construct models that would consider all the failure mechanisms that have been observed. Therefore, there is still a need to make use of models where the structure is assumed to directly penetrate the ice ridge. These models will yield upper bounds for the realistic ice forces.

The objective of this paper is to derive an approach of ridge load determination for the probabilistic design. The paper will address only forces caused by the ridge keel. While using the Monte Carlo simulation technique, there is a need to obtain values of the keel force with a minimum computational effort. Numerical tools that are available for the deterministic estimation of the ridge forces appear to consume too much computing time. As a first solution to this problem we will apply a neural network. An advanced passive failure model is used to teach a neural network to provide the same results as the basic model. As a second option, we will compare the advanced failure model with the Dolgopolov's formula and show how this formula can be used to yield realistic values for the keel force component.

AN ADVANCED RIDGE MODEL

Kärnä et al. (1996, 2001) derived a passive failure model for the ridge keel. This model considers ice ridges having a cross section depicted in Fig. 1. The figure shows the geometrical characteristics of the ice feature in an initial condition of ridge penetration. The model simulates the ridge penetration as a sequence of discrete failure events. Figure 2 illustrates the assumed failure mechanism with an inclined and two vertical failure planes. Depending on the amount of penetration and the internal strength properties of the ridge, an individual failure event can be characterised either as a local failure or as a plug failure (Brown et al. 1996, Croasdale, 1999). The model considers

the evolution of the ice ridge by redistributing the failed ice rubble below and behind the original keel profile. Accordingly, the model considers the surcharge effect that arises while the keel height increases during the interaction.

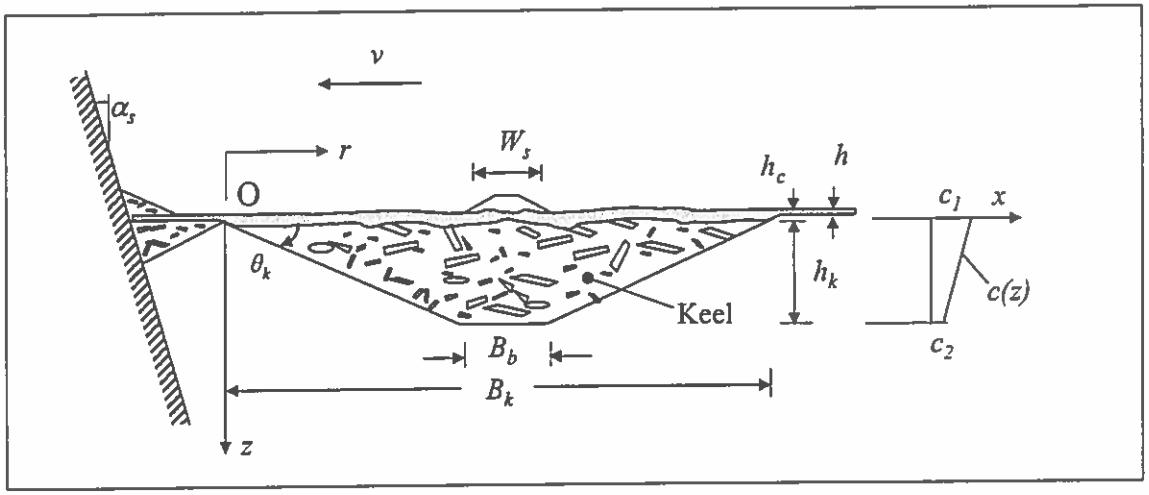

Figure 1. Cross section and parameters of a first-year ice ridge. The parameter $c(z)$ shows the distribution of the cohesion strength

The shape of the ice ridges has been a subject of active research (e.g. Timco and Burden, 1997). Parametric studies carried out with the present model indicate that the maximum keel force depends on the initial volume of the ridge keel. The keel profile is of less importance.

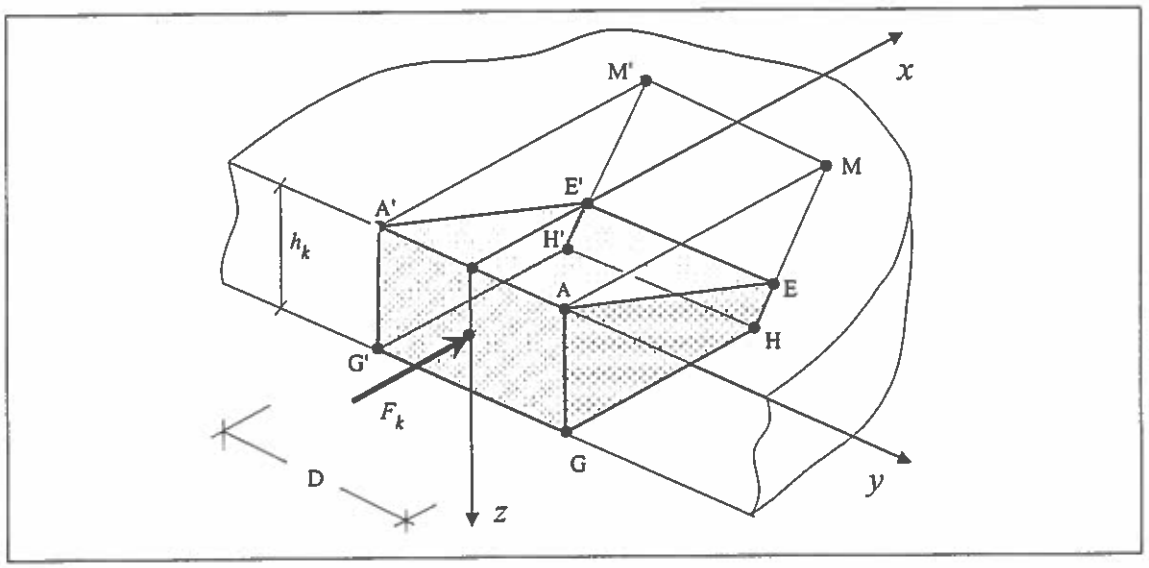

Figure 2. Assumed failure mechanism with an inclined and two vertical slip planes.

Figures 2 and 3 illustrate a typical step in the numerical simulation. The forces acting on the inclined slip plane AEE'A' and vertical slip planes AEHG, A'E'H'G' are evaluated based on the stress conditions at the Mohr-Coulomb failure envelope. The reactive force S is then solved from an equation of equilibrium where also the volume force Q and

friction at the ice-structure contact are considered. This calculation is repeated for several tentative slip planes that are kinetically possible. The horizontal component of S is defined as the keel force F_k. The minimum value of F_k found at each step is defined as the actual keel force.

The original passive failure model described by Kärnä et al. (1996, 2001) was upgraded for this paper. First, the stress state within the keel was assumed to consist of three components (σ_x, σ_y, σ_z) where σ_z is the main stress component arising directly from the buoyancy forces. The lateral stresses σ_x and σ_y arise due to the lateral confinement provided by the keel material (Tsytovicy, 1986, Sect. 2.1). Second, the cohesion strength $c(z)$ of the ridge keel was assumed to vary linearly within the keel as shown in Fig. 1. This assumption takes account of the fact that the keel strength is higher in the upper keel layers than in the keel bottom (Blanchet 1998). It was assumed in all subsequent calculations that the cohesion vanishes at the keel bottom ($c_2 = 0$).

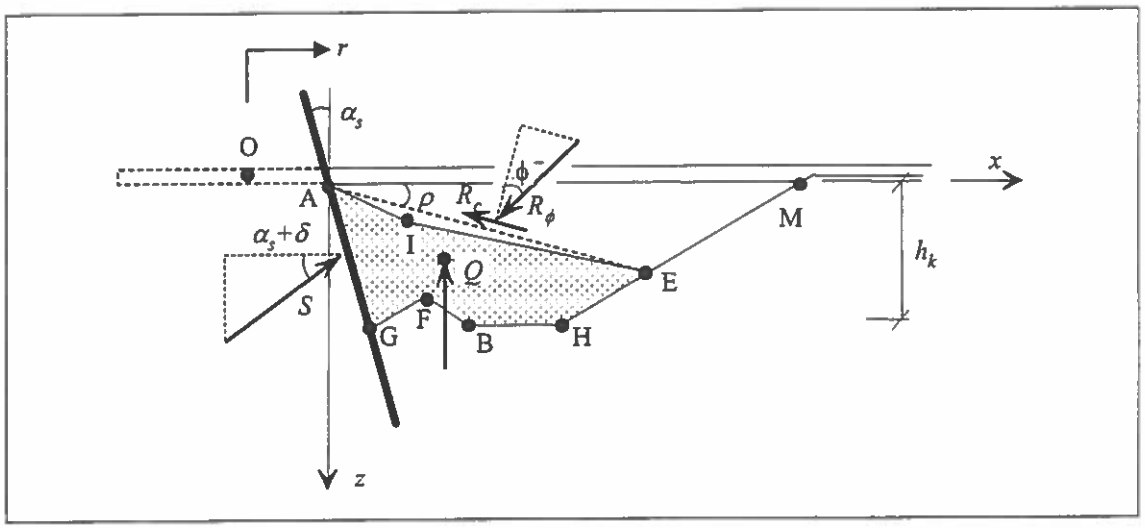

Figure 3. Forces acting on the failing rubble volume. The parameters δ and ϕ are the angle of friction at the contact surface and the internal friction, respectively.

The frictional and cohesion forces of the Mohr-Coulomb theory can not be mobilized simultaneously in full extent. Corresponding to the concepts of soil mechanics (Tsytovich, 1986, p. 52), the cohesion is considered to consist of two components. One of them is a structural rigid cohesion due to refrozen bonds between the ice blocks. The second component is a plastic cohesion, which arises during large slippage at the failure plains, as large ice fragments rotate and experience damage. The rigid cohesion is mobilized in an initial phase while the failure planes are forming. We assume that this component is not acting simultaneously with the internal friction, which attains its maximum level only after a relatively large deformation (Ramiah and Chickanagappa, 1990 and Bowles, 1988, Fig. 11-3). Quantitative data on the rigid and plastic cohesion is not available at present. Therefore, we assume that an estimate of the total cohesion is

used as input to the advanced ridge model. Then, this total cohesion is reduced slightly (by 25%) to consider the non-simultaneous mobilization of the cohesion and friction.

Bowles (1988) recognises that a passive-pressure theory, which assumes linear failure planes consistently overestimate the actual passive pressure. In a more advanced application to the theory of plasticity, non-planar failure surfaces can be assumed. Therefore, the inclined failure plane AEE'A' depicted in Fig. 2 is likely to be slightly curved when the actual failure occurs. The advanced model of the present paper considers this by using a bi-linear failure plane. This is shown in the cross-sectional presentation of Fig. 3 by the line AIE.

In the advanced passive failure model, frictional and cohesion forces are active both in the inclined and in the two vertical failure planes. Figure 3 shows the resultant forces R_ϕ and R_c on the inclined failure surface. Corresponding force resultants act on the vertical failure planes AEHG and A'E'H'G' shown in Fig. 2. Both the internal stresses and the cohesion strength vary in accordance with the parameter z. Therefore, the internal force resultants are evaluated by integration over the failure surfaces concerned.

A NEURAL NETWORK APPROXIMATION

As a next step of this study, a trained Neural Network was developed to allow a much faster force evaluation than while using the advanced ridge model. In order to train the Neural Network, the advanced ridge model was first used to create a wide set of data on keel forces. The input variables of this calculation were selected as

- D is the width of the structure (m)
- h_k keel depth (m)
- α_s angle of inclination of the structure (deg)
- δ friction angle at the ice-structure contact (deg)
- ϕ internal friction angel of the keel material (deg)
- c_1 cohesion at the upper part of the ridge keel (kPa)

A total of 4143 combinations of these parameters were selected and the horizontal keel force component F_k was evaluated for each combination of the input. The results were then transformed to a line load $Q_k = F_k/D$, which was used to train the neural network. The NeuroShell 2 ® software was used to develop the neural network. The network was designed so that 80 % (3315) randomly selected data lines were used as the training set and 20 % of the data was used for testing.

The method used for training was GRNN (General Regression Neural Network) with the type *Ward* net that has 3 three hidden layers with totally 67 neurons. The trained net provides a value of the line load Q_k for any combination of the six input parameters within the trained range.

As shown in Fig. 4, the Neural network has learned quite well the data. At present, there are still some high individual absolute errors when comparing the "net" value to the "actual" value. This problem can be solved by using further data and improving the training process.

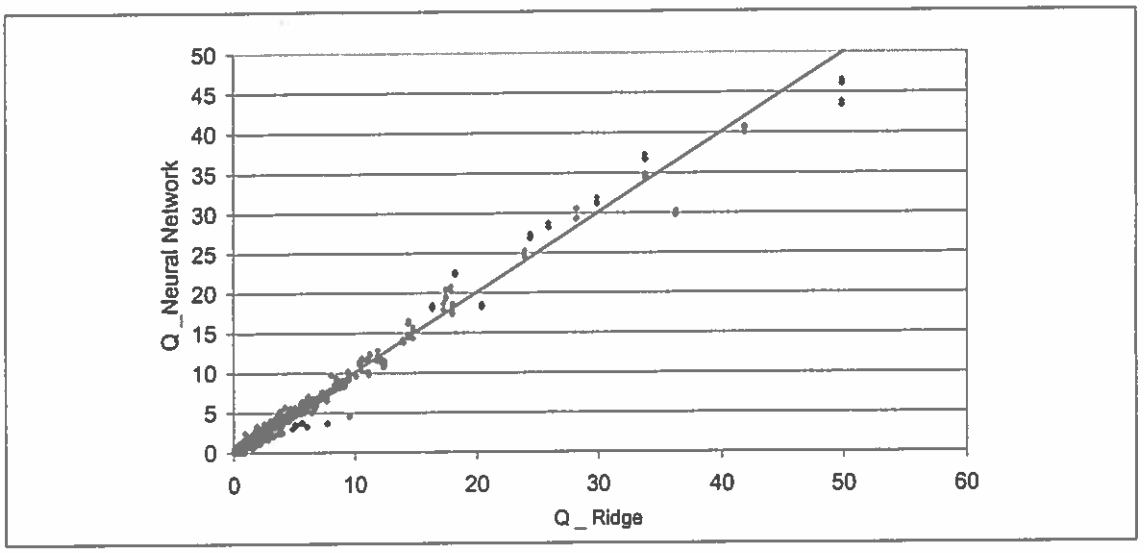

Figure 4. The keel resistance values Q_k obtained by the advanced ridge model vs the corresponding values provided by the trained neural network.

NeuroShell 2 provides a possibility to create different runtime versions based on the trained net. In this case, the most potential possibility is to create DLL (dynamic linked library) files to be called directly from a main program.

COMPARISONS WITH DOLGOPOLOV'S MODEL

Timco et al. (1999) recognise that the model proposed by Dolgopolov et al. (1975) considers most of those essential parameters that influence the keel forces. Using the notation of the present paper, Dolgopolov's formula for the keel load is given by

$$F_k = \mu\, h_e\, D\left(\frac{h_e\, \mu\, \gamma_e}{2} + 2c\right)\left(1 + \frac{2\, W_s}{3\, D}\right) \tag{1}$$

where $\mu = \tan\left(45^0 + \frac{\phi}{2}\right)$, ϕ is the angle of internal friction, c is the apparent cohesion, D is the width of the structure, h_e is an effective keel depth, W_s is the width of the ridge sail and γ_e is the effective buoyancy given by

$$\gamma_e = (1-n)(\rho_w - \rho_{ice})\, g \tag{2}$$

Here, n is the keel porosity, g is the acceleration due to gravity and ρ_w, ρ_{ice} are water and ice densities, respectively. The shape factor $q = \left(1 + \frac{2}{3}\frac{W_s}{D}\right)$ of Eq. (1) contains a parameter W_s, which in Dolgopolov's original paper was defined as a the width of the ridge sail (Fig. 1) and was related to the keel depth h_k by an assumption that h_k is equal

to four to five times W_s. It is of interest to notice that Dolgopolov et al. (1975, Fig.1) used the character H for the width of the ridge sail. Apparently due to this special notation, most subsequent discussions on Dolgopolv's model show Eq. (1) in a form where the sail width W_s is replaced by the keel depth h_k. This leads to an approach where Eq. (1) yields significantly higher keel force estimates than the original formula.

The effective keel depth h_e considers the surcharge effect that arises during the ridge penetration. Dolgopolv et al. (1975) assume that $h_e \leq h_k + D/2$ but provide no exact definition for this parameter.

A parametric study was conducted to compare the keel forces predicted by the advanced ridge model and the Dolgopolv's model. The aim of this effort was to clarify the influence of the parameters q and h_e. For these comparisons, it was tentatively assumed that the advanced ridge model yields "correct" keel forces and can be used to tune Eq. (1). It should be appreciated that Eq. (1) does not consider the effects of the inclination angle α_s and friction angle δ at the contact surface Therefore, the initial comparisons were made for vertical structures (α_s =0) assuming that the friction between the keel rubble is defined by δ=0°. The keel geometry was defined by assuming θ_k = 30° and $B_b = \frac{1}{2}\, h_k \cot\theta_k$ (see Fig. 1). The keel porosity was set as n = 0.30.

First parametric studies were made by assuming that the surcharge effect in Eq. (1) varies with the structure width as $h_e = h_k + D/10$. The results showed that the keel force predicted by Eq. (1) becomes excessive for wide structures. Therefore, further studies were made with $h_e = h_k$. The influence of the shape factor q was then studied assuming that in the equation of q, the parameter W_s is either replaced by the keel depth h_k or is given in its original form by $W_s = h_k/5$ or $W_s = h_k/4$. Parameters that influence the keel resistance were varied as ϕ = 10° to 50° and c = 1 kPa to 20 kPa. The geometrical parameters were varied as D = 2 m to 60 m and h_k = 2 m to 40 m. This study showed that the best fit with the Dolgopolov's formula and the advanced ridge model arises when Eq. (1) is used in its original form with $W_s = h_k/4$.

One of the differences between the advanced ridge model and Eq. (1) is that the advanced model considers the keel resistance arising in the inclined and two vertical failure planes. Eq. (1) considers explicitly only the resultant forces R_ϕ and R_c on the inclined failure surface AEE'A' (Figs 2 and 3). Numerical comparisons between the two models show that the factor q successfully compensates the deficiency that arises while Eq. (1) ignores the effects of the vertical failure planes AEHG and A'E'H'G' (Fig. 2). The resistance provided by these vertical planes is important for narrow structures.

As a final step of the comparisons, the influences of the contact friction and the cohesion were studied. First, the input value of the cohesion was reduced in computations by 25% on both models. Second, while using the advanced ridge model, the

friction angle δ was varied from 0° to 20° (kinetic friction coefficient $\mu_k = \tan(\delta)$). It was found that the outputs from the advanced ridge model are close to each other while Eq. (1) is used with $h_e = h_k$ and $W_s = h_k/4$ and when the friction angle is assumed as $\delta = 10^0$.

As a result of these comparisons, it is proposed that the Eq. (1) is modified to

$$F_k = \mu\, h_k\, D\left(\frac{h_k\, \mu\, \gamma_e}{2} + 2c\right)\left(1 + \frac{h_k}{6\, D}\right) \tag{3}$$

PARAMETRIC STUDIES

A parametric study was conducted to examine how the three models developed above compare with each other. Table 1 shows values of the input parameters in six cases that were studied. The results are shown in Figs. 5 to 7. The keel force was plotted in terms of the global keel pressure defined by $p_k = F_k/(D\, h_k)$

Table 1. Input parameters for the sample calculations.

	Case1	Case2	Case3	Case4	Case5	Case6
D (m)	varied	60	30	30	30	30
h_k (m)	20	varied	20	20	20	20
α_s (deg)	0	0	varied	0	0	varied
δ (deg)	10	10	10	10	varied	10
ϕ (deg)	30	30	30	30	30	30
c_1 (kPa)	5	5	5	varied	5	5

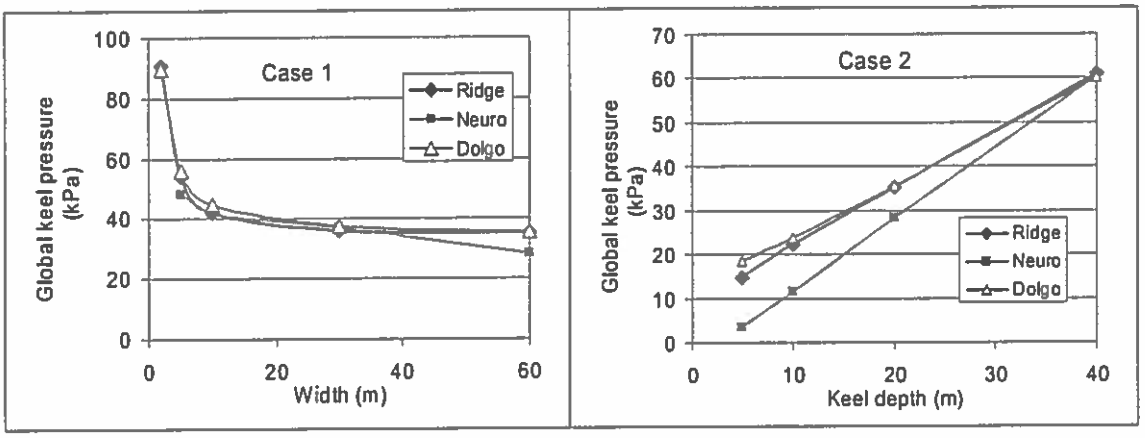

Figure 5. Influence of the structure width and the keel depth on the pressure p_k.

The results in Figs. 5 and 6 concern a vertical structure where the kinetic friction coefficient is about 0.18 (δ = 10°). In these conditions, the slightly modified Dolgopolov's formula (3) ("Dolgo") gives a keel force that is mostly very close to the value predicted by the advanced model denoted in the figures as "Ridge". While varying the contact parameters α_s and δ (Fig. 7), the Dolgopolov's model provides a constant value that can be significantly different from the prediction of the advanced ridge model. This problem can be solved by replacing in Eq. (3) the term μ by a passive

pressure coefficient that considers the two contact parameters α_s and δ. Bowles (1988, Sect. 11-4) show the necessary derivations in the case of the Coulomb earth pressure theory. This modification is not done in this paper.

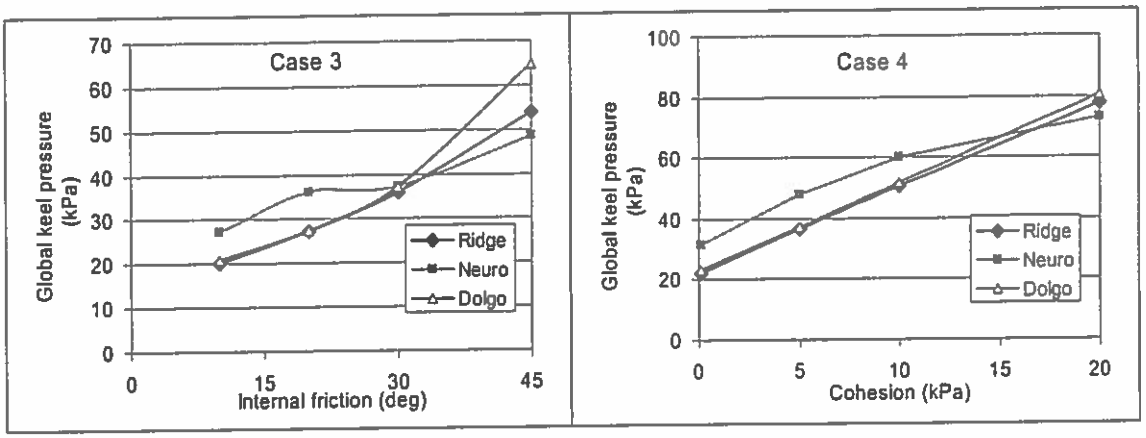

Figure 6. Influence of the internal friction and the cohesion on the pressure p_k.

Figures 5 to 7 show that the neural network solution derived in this paper shows in all conditions the same trends as the advanced ridge model. Occasionally, excessive errors are found in the neural network solutions. This problem could be solved by improving the training process.

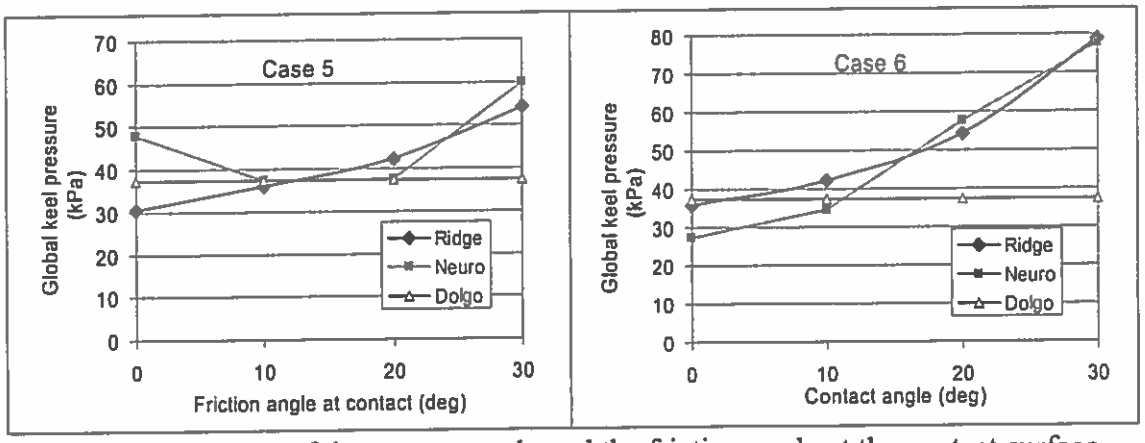

Figure 7. Influence of the contact angle and the friction angle at the contact surface.

SUMMARY

An advanced model on ridge keel forces was upgraded. This model was then used to develop a neural network application for the same problem. As a further effort, Dolgopolov's model for keel forces was studied. It was found that while using this model in a special way, the advanced model and the Dolgopolov's model provide practically the same results for vertical structures where the frictional forces at the ice-structure contact surface are within a specified range. The paper also refers to a possibility to extend the validity of Dolgopolov's model.

ACKNOWLEDGMENTS

The main part of this work was done as an internal development activity at VTT. The final computations and studies on the Dolgopolov's model were supported by the EU funded project STANDICE. The authors acknowledge the support received. Discussions with Dr. Jaakko Heinonen are also appreciated.

REFERENCES

Blanchet, D. Ice load from first-year ice ridges and rubble fields. *Can. J. Civ. Eng.* 25: 206-219 (1998).

Bowles, J. E. Foundation Analysis and Design. McGraw-Hill Civil Engineering Series. 4th Ed. New York (1988) 1004p.

Brown, T., Croasdale, K. and Wright B. Ice loads on the Northumberland straight Bridge Piers - An approach. Proc. 6th Int. Offshore and Polar Eng. Conf., Los Angeles. Vol. II, 367 - 372 (1996).

Croasdale, K. A study of ice loads due to ridge keels. Proc. 4th Int. Conf. Development of Russian Arctic. St. Petersburg, 268-274 (1999).

Dolgopolov, Y., Afanasiev, V., Korenkof, V and Panfilov, D. Effect of hummocked ice on the piers of marine hydraulic structures. Proc. 3rd IAHR Ice Symp., Hanover, NH. 463-477 (1975)

Heinonen, J. 2004. Constitutive modelling of ice rubble in first-year ridge keel. VTT Publications. Dissertation for the degree of Doctor of Technology. (in review).

Kärnä, T & Rim, C.W., Model for global first-year ice loads. VTT Building Technology, Internal Report RTE39-IR-9/1996. 43 p.

Kärnä, T., Chae W. R. and Shkhinek, K. Global loads due to first-year ice ridges. Proc. 16th Int. Conf. Port and Ocean Eng. under Arctic Cond., Ottawa, Canada, August 12-17. Vol 2, 627-638 (2001).

Kärnä, T and Jochmann, P. Field observations on ice failure modes. Proc. 17th Int. Conf. Port and Ocean Eng. under Arctic Cond., Trondheim, Norway, June 16-19, Vol 2, 839-848 (2003).

Ramiah, B and Chickanagappa, L. Soil Mechanics and Foundation Engineering. 2nd ed. Balkema, Rotterdam (1990), pp. 168-179.

Tsytovich, N. Soil Mechanics (Concise Cource). English Tranlation, Mir Publishers 1986, Moscow. 176p.

Timco, G., Frederking, B., Kamesaki, K. and Tada, H. Comparison of ice load calculation algorithms for first-year ridges. Proc. Int. Workshop on Rational Evaluation of Ice Forces on Structures, REIFS99. Mombetsu, Japan, February 2-4, 1999. 88-102 (1999).

Timco, G., Croasdale, K. and Wright, B. 2000. An overview of first-year ice ridges. Canadian Hydraulics Centre, Technical report HYD-TR-047. PERD/CHC Report 5-112. (2000) 159p.

Timco, G. and Burden, R. An analysis of the shapes of sea ice ridges. *Cold Regions Science Technology* 25(1997) 65-77.

Wright, B and Timco, G. First-year ridge interaction with the Molikpaq in the Beaufort Sea. *Cold Regions Science Technology* 32(2001) 27-44.

ICE STANDARDS AND RECENT DEVELOPMENTS IN ICE ENGINEERING

Tuomo Kärnä
VTT Tecnical Research Centre of Finland
(ISO TC67 SC7 WG8_Technical Panel TP2b on ice actions)

New understanding on ice actions obtained in full scale structures:

Lighthouse in the Baltic Sea

Conical Structure at JZ20-2

Content

- The forthcoming ISO 19906 "Arctic Offshore Structures"
- Notes on the size effect
- Notes on ice ridges
- Notes on dynamic ice actions

Old Standards on ice forces

- API Recommend Practice 2N (RP-2N), 1995
- Canadian Standards Association. S471-92.
- SNiP 2.06.04-82* Loads and influences on marine structures (from waves, ice and vessels)
- VSN-41.88. Design of fixed ice strengthened platforms

New Standards on ice forces

- API will not be updated
- Canadian Standards Association. S471-04. (confidential, will not be published?)
- **ISO 19906. Arctic Offshore structures** (to be published in 2009)

ISO 19906-1; Actions and Action Effects

Basic structure of the instructions:

- Physical and mechancial properties
- Gravity actions due to ice
- Ice Action Scenarios
- Propabilistic Methods
- Limit-Stress global Ice Actions
- Limit-Energy Ice Actions
- Limit-Force Ice Actions
- Local Ice Actions

Notes on the Size effect

Conventional approach: *p = p(Area)*

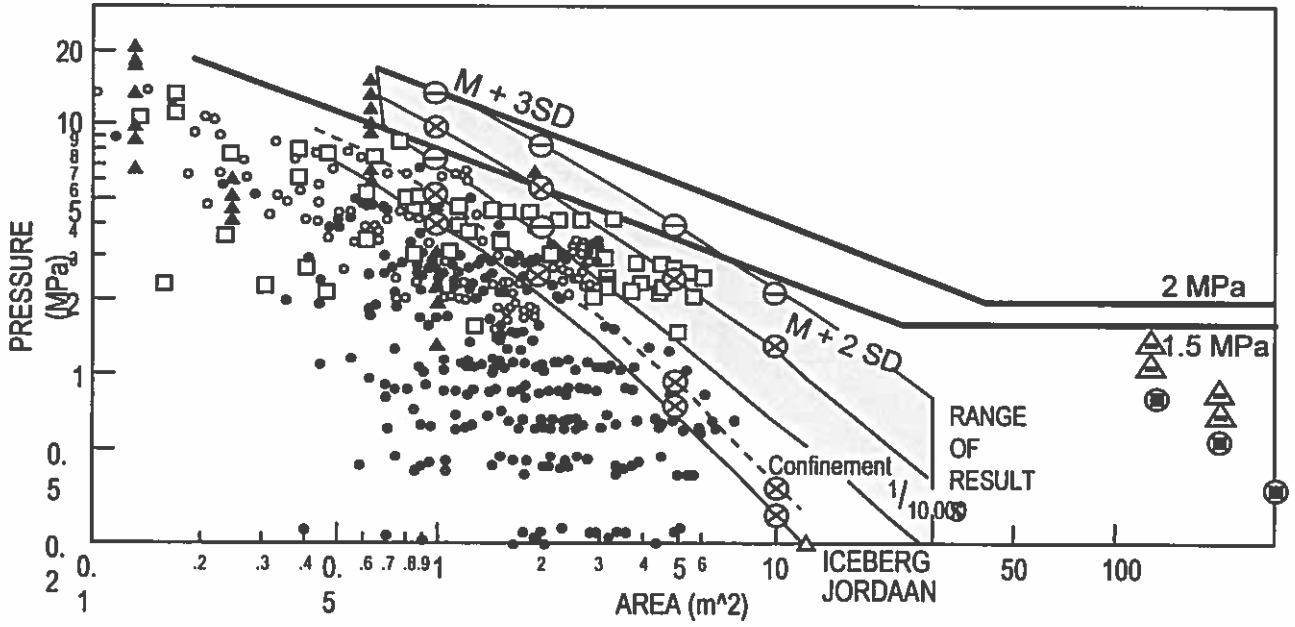

Data is being analysed at VTT to find a more accurate relationship *p = p(w,h)*

Data analysis on the size effect

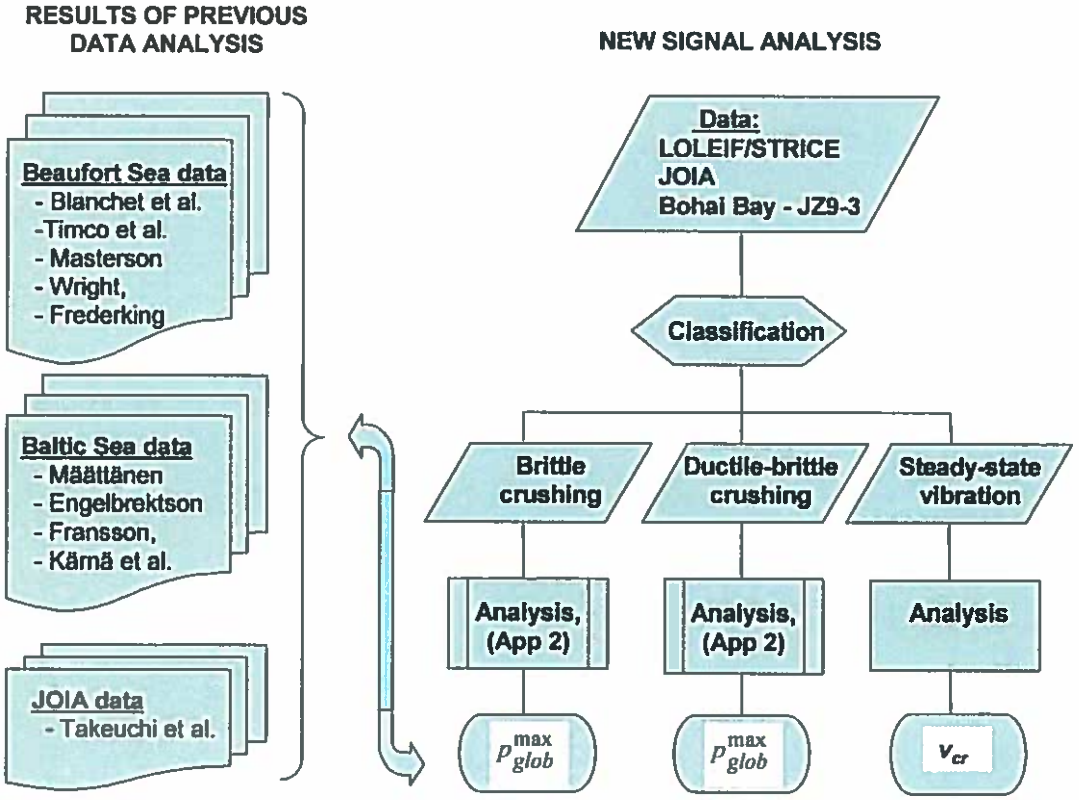

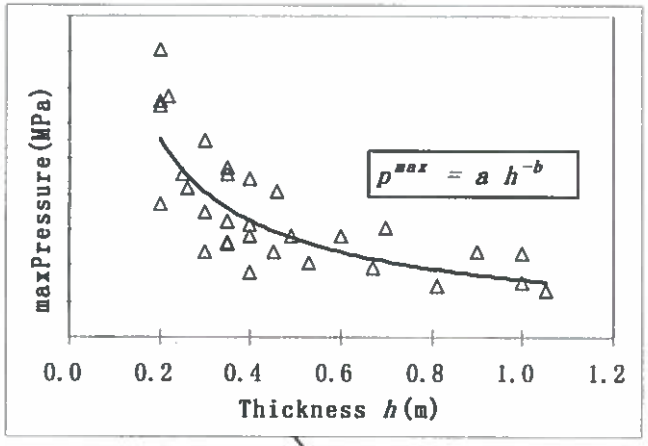

Thickness effect has been confirmed for brittle crushing. Global pressure to be defined as:

$$p^{\max} = A\,h^{C}\,(w/h)^{D}$$

Notes on ice ridges

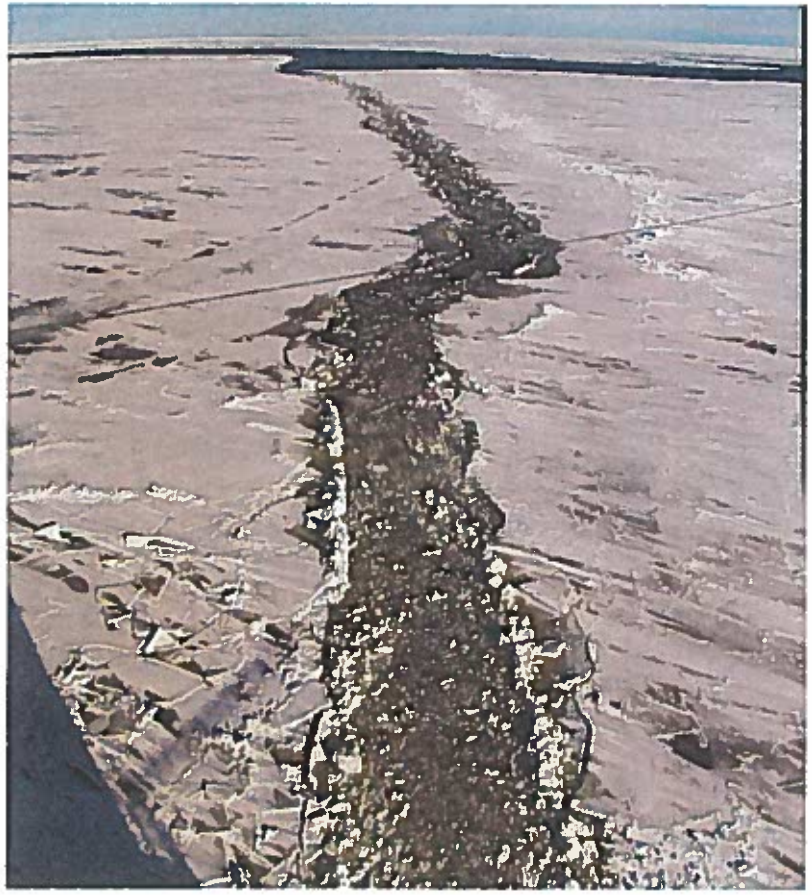

Force limiting mechanisms

- crushing along the level ice/rafted ice boundary
- crushing along the sail
- spine failure
- failure behind
- splitting
- rotation of the floe

- Force limiting mechanisms determine the ridge load
- Classical methods needed to provide upper bound values

Calculating upper bounds for ridge forces.

Dolgopolov's model found to yield appropriate results for vertical structures

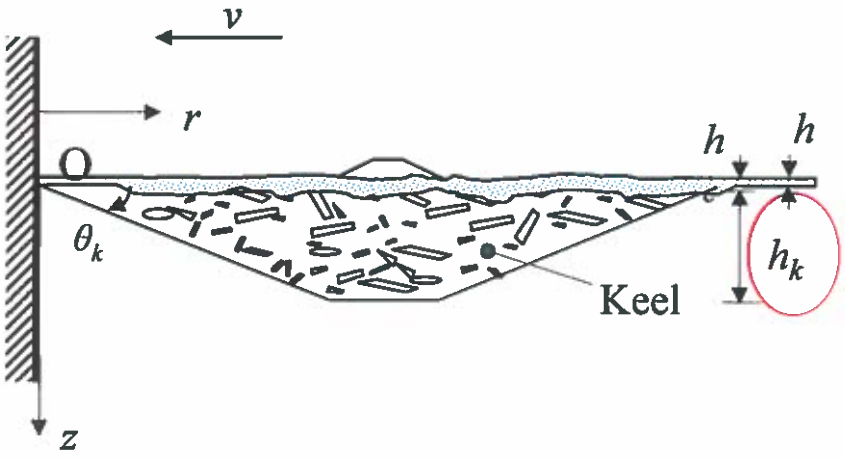

$$F_k = \mu\, h_k\, D\left(\frac{h_k\, \mu\, \gamma_e}{2} + 2c\right)\left(1 + \frac{h_k}{6\, D}\right)$$

3D effect (edge effect)

Note: Dolgopolovs formula has practially always been missunderstood (Kärnä & Nykänen IAHR`04)

Notes on dynamic ice actions

(A) Vertical structures - Actions by sheet ice

1. **Random excitation due to brittle ice crushing**
2. **Frequency-locked vibrations** (Self-excited vibration)
3. **Response to ductile-brittle crushing**

(B) Conical structures - Actions by sheet ice

Narrow-band random excitation

Random excitation due to ductile brittle crushing

Vertical stuctures; Ice velocities v > 0.10 m/s

Force in time domain

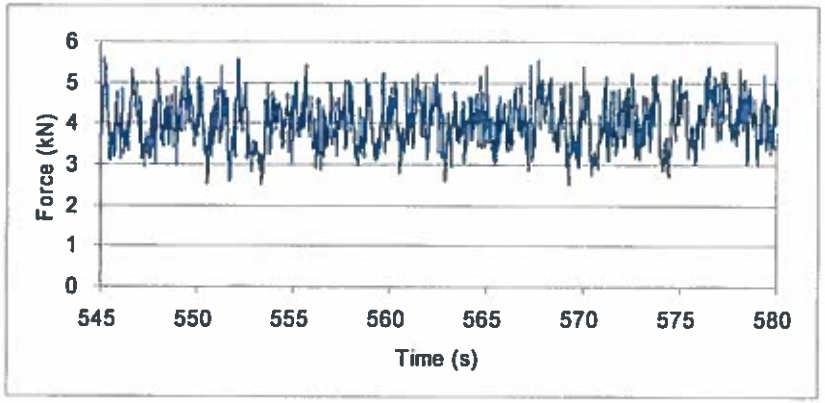

Dynamic force component in frequency domain

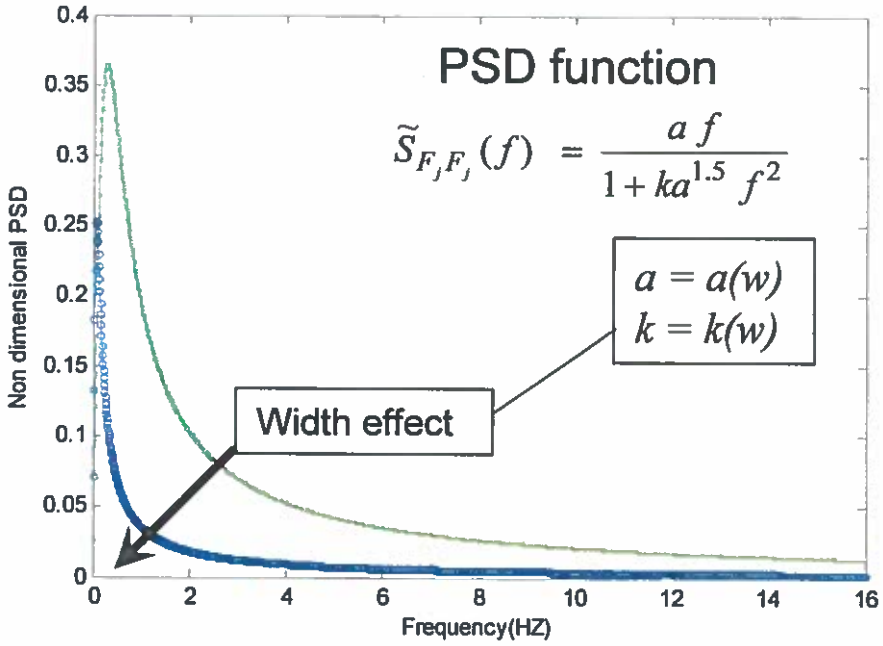

Use a FEM program to obtain:

Response to mean level of the time-varying ice force

\+ Response to the wide-band random ice force

Relevant for fatique + serviceability limit states

Self-Induced vibration

Narrow & vertical structures, $0.02 < v < 0.07$ m/s

Monopode at Bohai Bay

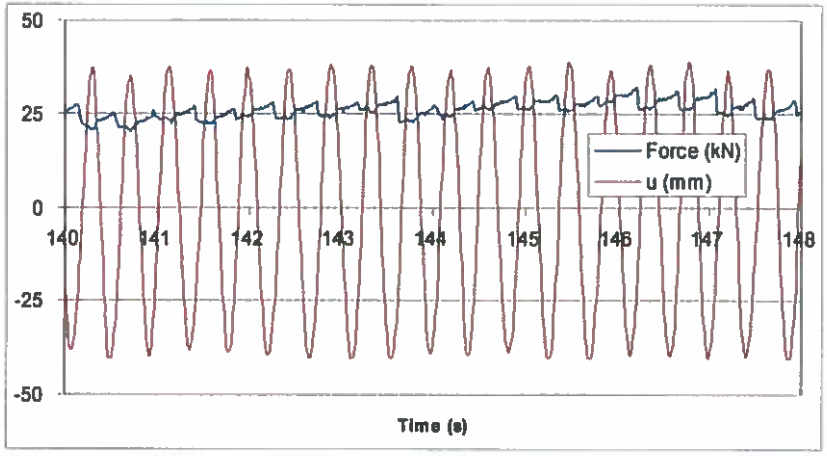

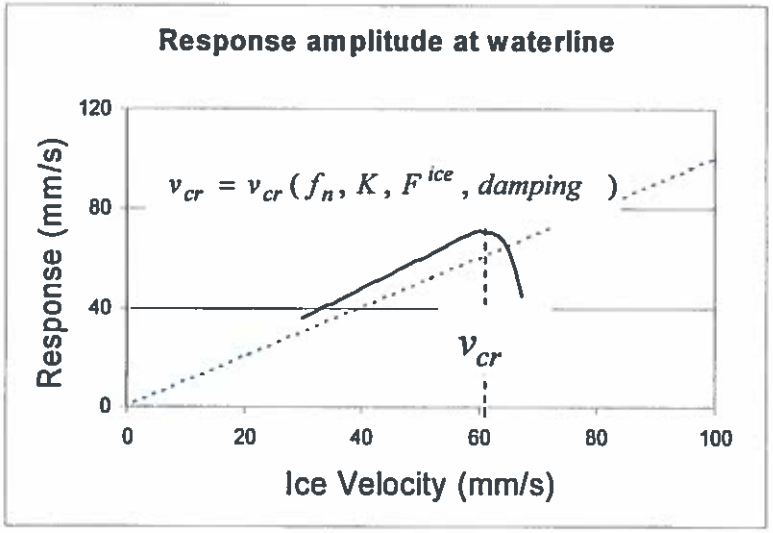

$$\text{Response amplitude} = \frac{\beta\, v}{2\,\pi\, f_n} \qquad \beta = 1.2 \text{ to } 1.4$$

Use a FEM program:

- Harmonic displacement-controlled excitation at waterline
- Maximum response at v_{cr}

v_{cr} higher than the velocity for ductile-brittle transition

Relevant for ultimate limit state design, including fatigue

Response to ductile-brittle crushing

$v < 0.05$ m/s

Construct a time-varying force function

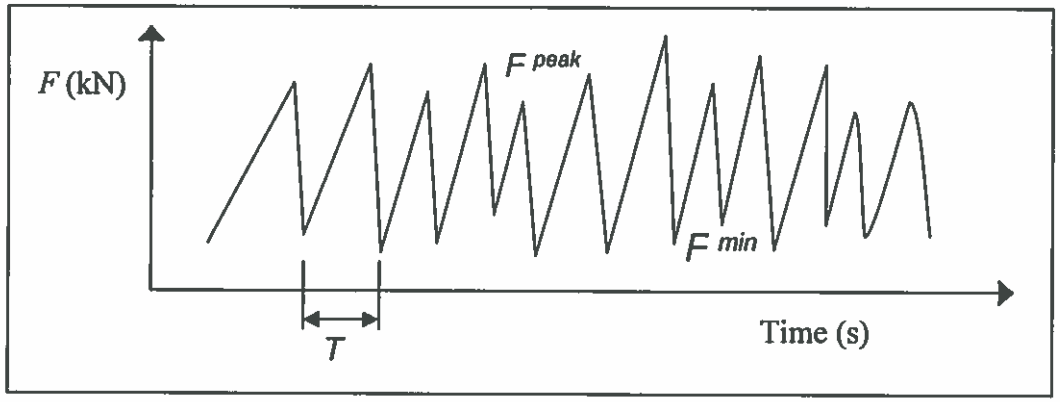

$F^{min} = F^{min}(K,v)$

$T = T(\text{Stiffness, velocity, } F^{peak})$

$F^{peak} = F^{peak}(h, w/h)$; Randomly distributed

Use a FEM program to obtain the response

Relevant for ultimate limit state design, including fatigue

Vibration of conical structures

(Model deveoped by Prof. Yue Qianjin et al.)

JZ20-2 Structure at Bohai Bay

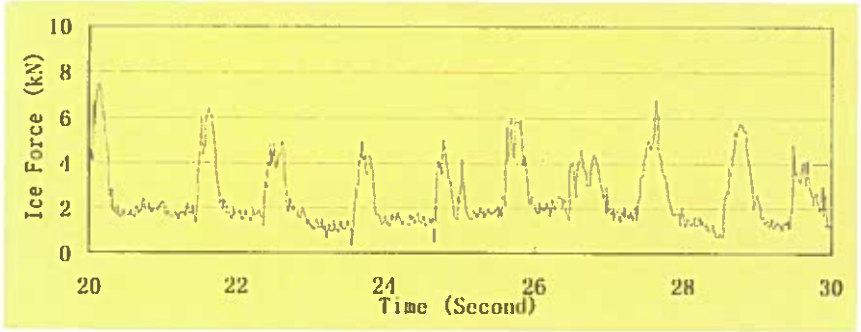

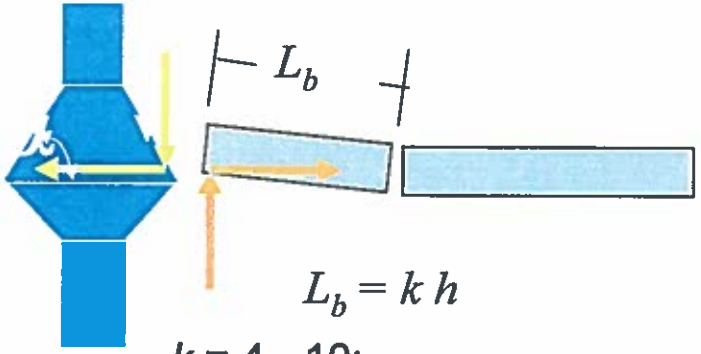

k = 4 - 10;
log normally distributed

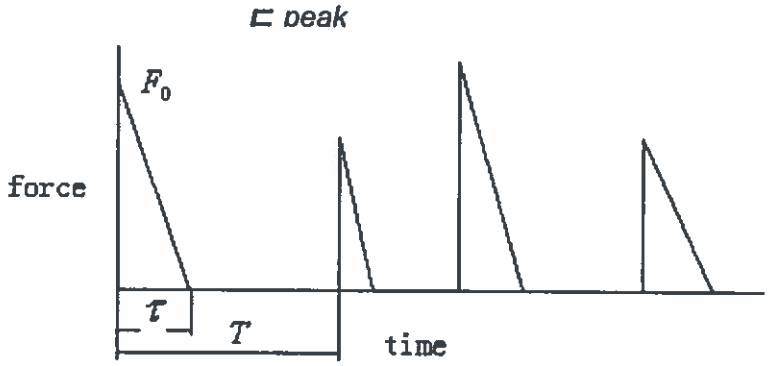

Use a static model to obtain F^{peak}; Assume normal distribution (Qu et al. POAC'03)

$$T = \frac{L_b}{V} = \frac{kh}{V}$$

Constract a random force function and use a FEM program to obtain the response

Relevant for serviceability limit state design + fatigue

Conclusions on dynamic ice actions

Simplified models for dynamic actions due to level ice are available (will be constructed / updated) for:

- **Random excitation on vertical structures**
- **Self-excited vibration of vertical structures**
- **Excitation due to ductile-brittle crushing; vertical structures**
- **Narrow-band excitation on conical structures**

CONCLUSIONS

- Full-scale data is preferred while deriving new instructions for ice load determination

- Recent full-scale data helps in clarifying and simplifying formulas for ice load determination:
  - size effect
  - ridge loads
  - dynamic actions

- The forthcoming ISO 19906-1 will include formulas that can be used for wind turbines. However, appropriate load combination rules will not be included